A STUDY OF THE MAGNITUDES OF FAINT GALAXIES

GILLIAN ELIZABETH PICKUP

Doctor of Philosophy

University of Edinburgh

1979

A C K N O W L E D G E M E N T S

I should like to thank Professor V.C. Reddish for suggesting this project, and for his help and encouragement. I am grateful to Dr H.T. MacGillivray for providing useful suggestions, and to Mr H.G. Corwin, Jr. for letting me use his step scale magnitude calibration. I wish to thank Professor G. de Vaucouleurs for his advice on galaxy photometry. I should also like to thank the UKSTU for supplying the photographic plates, the COSMOS staff who carried out the plate measurements, and Mrs J. Shand for typing the manuscript.

This project was supported by a University of Edinburgh Vans Dunlop Scholarship.

A B S T R A C T

A method is developed for calculating integrated magnitudes of faint galaxies using COSMOS mapping mode measurements of UKSTU Schmidt photographs. The intensity calibration is provided by the step filters and the zero point of the magnitude scale is taken from the photoelectric sky brightness at the time of the exposure. Tests carried out on both star and galaxy images are described. The galaxy magnitudes are isophotal, the limiting isophote being about 28 mag arcsec^{-2}. The errors range from $\pm 0^{m}.08$ at the bright limit of m = 18 to $\pm 0^{m}.43$ at the faint limit of m = 22.

The magnitudes from several hundred galaxies calculated from COSMOS mapping measurements are calibrated against the logarithm of the image area obtained from COSMOS coarse measurements. Using this calibration the magnitudes of galaxies in three areas near the south galactic pole are calculated. The total area of the survey is about 11 arcdeg^{2} and there are some 83,000 galaxies. The limits of the sample are discussed in detail.

The log N(m) relation is compared with standard Friedman cosmological models. Some of these models are modified to take account of selection effects. An excess of observed faint galaxies is found which can be attributed to the effects of evolution or inhomogeneity of the universe.

The effect of galaxy evolution is investigated assuming that the luminosity decreases linearly with time. The observations can be explained if, on average, the intrinsic luminosity of a galaxy decreases at the rate of about one magnitude per 10^{10} yr.

C O N T E N T S

INTRODUCTION

Many astronomers have measured and studied the magnitudes of distant galaxies because they are distance indicators and can be used to study the large scale structure of the universe. The N(m) relation describes the numbers of galaxies recorded out to successive magnitude limits. Assuming a uniform space distribution of galaxies, and that all galaxies have the same luminosities, the numbers represent the volumes, V, contained within different radii, r, and the V(r) relation gives the curvature of the universe. However, if a model is used to describe the shape of the universe,any departure of the observed N(m) relation from the calculated one shows how the numbers of galaxies in the universe have changed with time,or how the magnitudes of galaxies have evolved. Thus magnitude limited counts play an important part in cosmology.

Modern cosmology began in the 1920s when the first definite proof was given for the existence of galaxies other than our own. Hubble (1925), using photographs from the Mt Wilson 100-inch reflector, showed that NGC6822 consisted of faint stars. By observing cepheid variables in the galaxy and using the period-luminosity relation, he was able to estimate its distance and prove that this was an external galaxy. Later, Hubble (1929) showed that the light from galaxies is redshifted by amounts proportional to their distances. These observations have provided the basis for cosmological theories, together with the assumption that the universe is homogeneous and isotropic.

By the time Hubble had made these discoveries, Einstein had put forward his theory of general relativity, and theoreticians used

general relativity to develop a variety of cosmological models which had not been considered using Newtonian physics. In particular, Friedman (1922) investigated expanding models of the universe, and these have been developed by many astronomers, since the redshift of galaxies found by Hubble is usually assumed to be caused by the expansion of the universe.

There are two types of model which give rise to an expanding universe. The exploding, or 'big bang'model (Gamow 1956) assumes that the universe originated as a singularity, whereas the steady state model (Bondi & Gold 1948, Hoyle 1948) supposes that the universe remains unchanged throughout time and as the expansion takes place new matter is created to maintain the density. At present the 'big bang' model is favoured because it can easily explain the existence of the $2.7^{o}K$ background radiation. This is the only model considered here.

Robertson (1955) and Hoyle & Sandage (1956) introduced the terms H and q to describe the expansion of the universe and its rate of change. If R is the 'radius' of the universe, which is a function of time, then

$$H \equiv \frac{\dot{R}}{R} \quad \text{and} \quad q = \frac{-R\ddot{R}}{\dot{R}^2}$$

H is Hubble's 'constant', the constant of proportionality in the velocity-distance relation (Hubble 1929), and q is called the deceleration parameter. Since R, H, and q vary with time, the subscript zero is used to denote the present-day value, e.g.

$$H_o = \frac{\dot{R}o}{Ro} \quad .$$

According to general relativity, space is curved in the presence of matter, and matter and energy are equivalent. This leads to the hypothesis that the large scale curvature of space is determined by the energy content of the universe. From the observational point of view, this means that if the curvature of the universe is measured, for example using the N(m) relation, information can be obtained about the energy of the universe. In the absence of any intrinsic curvature of space, i.e. assuming that space is not curved if there is no matter in the universe, it is possible to derive relations between the curvature, k, and the deceleration parameter q_o. The universe will either expand forever,or the expansion will gradually halt and the universe will start to collapse. In the first case there is not enough matter in the universe to stop the expansion. The universe is said to be 'open' and the curvature, $k = -1$, with $0 \leq q_o < \frac{1}{2}$. ($q_o = 0$ is the lower limit for exploding models.) If there is sufficient matter to make the universe contract again, the universe is said to be 'closed' and $k = +1$, $q > \frac{1}{2}$. The intermediate case when $k = 0$, $q = \frac{1}{2}$ arises when the universe just stops expanding after an infinite time. The universe is also 'open' in this case. If $k = 1$, the volume within radius r is less than $4/3\pi r^3$, if $k = 0$ it equals $4/3\pi r^3$ (Euclidian space),and if $k = -1$, it is greater than $4/3\pi r^3$.

The magnitude-redshift relation and the number-magnitude relation have been calculated by Mattig (1958,1959) in terms of H_o and q_o. The derivation of these formulae is given in Appendix I. Using Mattig's formula it is possible to estimate the value of q_o from magnitude limited counts, in order to determine whether the universe is open or closed.

Sandage (1961) found that the N(m) relation is insensitive to the value of q_o, unless galaxies can be observed out to very large redshifts of $z = d\lambda/\lambda \sim 5$. However, the magnitude-redshift relation should be able to distinguish between values of q_o using observations of galaxies out to $z \sim 0.5$. Brown and Tinsley (1974) showed that the N(m) relation is no more sensitive to the cosmological model than it is to the effects of luminosity evolution of the galaxies, or intergalactic extinction if it is present. In fact, the determination of q_o by any method is complicated because the travel time for light emitted by distant galaxies may be several thousand million years, and the effects of evolution which have altered the properties of galaxies since then must be taken into account. It is therefore impossible to determine q_o by one method alone. A variety of observations are required to assess the size of the effects such as evolution in luminosity. In this respect magnitude limited counts are of value in the investigation of the luminosity evolution of galaxies.

A survey of the methods used for galaxy photometry is given in chapter 1, part 1, and the results obtained so far in observational cosmology are discussed in chapter 1, part 2. Chapter 2 describes the method for photometry used in this project and the tests carried out on the magnitudes. Chapter 3 is concerned with the determination of the N(m) relation for galaxies in three fields near the south galactic pole, and finally, in chapter 4, the results are analysed using cosmological models.

1. A SURVEY OF THE LITERATURE

Part 1. Methods for Galaxy Photometry

The determination of galaxy magnitudes is difficult because of the wide range of surface brightnesses within a galaxy. The nucleus is very bright with a steep gradient in intensity, while the outer parts of the galaxy are of low intensity and fade gradually and assymptotically into the sky background, so that at large distances from the nucleus the intensity is below the threshold of detection. Due to their great extent, the outer regions of a galaxy contribute significantly to the total luminosity,and so the total luminosity cannot be measured directly. Instead the magnitude may be derived from the luminosity of the galaxy within a given intensity isophote, producing an isophotal magnitude. If the magnitudes within successively fainter isophotes are found, the relationship between the magnitudes and the intensities of the isophotes,or the areas contained within the isophotes can be determined. The magnitudes decrease assymptotically as the areas increase and therefore the relation can be extrapolated to give an assymptotic magnitude, which should be a good approximation to the total magnitude.

Stellar photometry is much more simple because stars are unresolved and the intensity distribution in the images is the same for all stars, (Moffat 1969). Because of this, stellar magnitudes can be measured photoelectrically using one aperture for stars of all luminosities, since the same fraction of the total luminosity is measured each time. In photographic photometry star magnitudes can be found quickly by comparing their images with those of stars with known magnitudes using,

for example, a Becker iris diaphragm photometer. Neither of these methods can be applied to galaxies because they form images of different shapes and sizes, unless they are unresolved.

The extended images of galaxies also produce problems in linking their magnitudes with the photometric systems set up for stars. Because of these difficulties,many different methods for measuring galaxy magnitudes have been tried using photographic or photoelectric photometry.

1.1 Photographic Photometry

In photographic photometry the density of developed grains in the emulsion is measured at intervals over the plate and a calibration is used to convert the density to intensity. The density measurements are made with a microphotometer or a microdensitometer. In a microphotometer the plate is illuminated by a narrow beam of light from a stabilised source, and the light transmitted by the plate at that point is detected. The transmission,T,gives an indication of the number of developed grains, because the higher the number density of grains, the lower the transmission. A microdensitometer works on the same principle, except that the quantity output is the optical density. This is defined as $\log_{10}(1/T)$ and is also related to the number density of grains. In both machines the plate usually rests on a moveable carriage, so that the transmission or density is scanned as the plate moves across the light beam. The results are recorded on graph paper using a pen recorder, or, more recently on paper tape or magnetic tape. For example, in the Joyce Loebl microdensitometer,the plate transmission is compared with that of a wedge which has a uniform density

gradient and the wedge is moved along by a servo mechanism until the transmissions are equal. A recording pen moves with wedge, and as the plate is moved the pen traces a curve,the height of which is proportional to the density of the plate.

If the transmitted light is detected over a very small solid angle by passing it through a narrow aperture before detection, the density is termed specular density. However,if the light from a wide solid angle reaches the detector so that scattered light as well as transmitted light is detected, the density is said to be diffuse. (There is actually a range of density measurements between these two extremes.) The relationship between the different types of density is non-linear.

The calibration is usually made by recording on a photographic plate a series of spots or squares which have known relative intensities. A tube sensitometer is commonly used,in which diffuse light passes through a set of tubes to the photographic plate. The apertures at the entrance to the tubes are of different sizes,and the light intensity transmitted through the tube is proportional to the aperture size area. At the other end of the tubes the apertures are of equal sizes so that the spots formed on the plate are all the same size. The advantage of the tube sensitometer is that it produces spots of uniform intensity except at the edges. Spot or step sensitometers use a set of neutral filters of different densities to provide spots of different intensities. In this type of sensitometer care has to be taken to ensure that the densities of the filters are uniform,and that the filters are completely neutral. The zero point of the calibration has to be obtained from photoelectric measurements.

The reduction of microphotometer scans of galaxies may be time consuming. A variety of methods have been devised which are more suitable for finding the magnitudes of a large sample, and enable the galaxy images to be compared more easily with star images. These will be discussed first.

a) Visual Estimates of Magnitudes

The simplest method was used by Shapley & Ames (1932) in the Harvard survey of magnitudes of galaxies. Small-scale photographic plates were used and the galaxies were compared visually with stars of known magnitude. This method was necessarily quick because the whole sky was covered down to thirteenth magnitude. However, there are large errors in the results depending on the surface brightness of the galaxies, which arise because stars and galaxies do not have the same light distributions.

b) Out of Focus Photometry

Several astronomers have used out of focus photography to blur star and galaxy images to make them similar so that they can be compared. Keenan (1935) and Seyfert (1935) both used this method. Seyfert tested 82 of the galaxies measured by Shapley & Ames in the Coma and Virgo clusters using plates which were taken slightly out of focus with small scale telescopes, with apertures of 4-inches and 1½-inches. The images were measured with a Schilt photometer, the whole of the image being included in the diaphragm. The internal errors were slightly larger that $0^m.1$ and for galaxies fainter than $m_{pg} = 11$, there was good agreement with Shapley & Ames' results. Galaxies brighter than this produced images which were too large to be measured. Keenan tried two

methods. In the first the galaxy and star images were spread over an area of two to three times that of the galaxy so that the surface brightness of the image, except at the edges, was proportional to the total luminosity of the source. A diaphragm which was smaller than the extra-focal disk was therefore used in the photometer. It was found that the exposure times required for this method were too long, and so a second method was used in which the telescope was only a small distance out of focus to smooth out the irregularities of the galaxies. This time the size of the photometer diaphragm was set slightly larger than the images. The mean error for the galaxies of $m_{pg} = 13$ was about 0.06. In Seyfert's and Keenan's second method there is the disadvantage that the outer parts of the galaxy are not measured, and the magnitudes are not 'total' ones.

Redman (1936) used out of focus images of stars to obtain the zero point for galaxy magnitudes. Two exposures were made on the same plate: an in focus one of the galaxy and an out of focus one of the stars. Both types of images were measured by taking microphotometer reading in a rectangular grid. Redman's method was therefore more precise than the other methods described above, and will be discussed in more detail later. Holmberg (1950, 1958) also used this method for calibration.

More recently, the out of focus method has been revived by Abell & Mihalas (1966). A series of out of focus plates, each one more out of focus than the previous one were required. A standard formula for the intensity distribution (which in this case was a modified Hubble formula, Hubble (1930), was used to calculate the total magnitudes of elliptical galaxies. The method is quick and is useful for studying

the magnitudes of the numerous elliptical galaxies occurring in rich clusters. However, this method cannot be applied to spiral or to irregular galaxies, the intensity distributions of which are not so easily described analytically.

On the out of focus plates, the galaxies appear as disks which are blurred at the edges. The centre of the disk contains light from the outer parts of the galaxy and as the telescope is put more out of focus, the light from regions further from the nucleus is included in the disk. It is possible to calculate the fraction of the total luminosity in the disk using the standard intensity distribution and to find the correction to total magnitude as a function of the size of the extra-focal disk. The densities of the disks were estimated visually by comparing them with spots of known density. These were converted into magnitudes using the densities of the extra-focal disks of stars of known magnitude as a calibration. A graph of magnitude measured vs. the size of the disk was drawn for each galaxy and compared with the theoretical curve to give the correction to total magnitude. Tests were carried out on galaxies in the Coma cluster, of magnitudes $m_{pg} = 13$ to $m_{pg} = 15$. The results obtained by four different observers agreed to within $\pm 0^m.2$, and most were within $\pm 0^m.1$. This method is therefore not as accurate as photoelectric photometry or detailed photographic photometry,but it can be applied to large numbers of galaxies to produce enough data for statistical studies.

c) The Schraffierkassette

Another method which enables a comparison to be made between star and galaxy images directly is that of the schraffierkassette, or jiggle

camera. While the exposure is taking place, the photographic plate is moved in a rectangular pattern so that the images are in the form of squares of uniform density. Provided the squares are large enough the images of galaxies and stars are identical. The densities of the images of galaxies can be found by comparing them with squares of known density and the calibration of density in terms of magnitude can be obtained from the star images, as in the extra-focal method.

Hubble (1936c) used this method to obtain the magnitudes of small faint galaxies to determine the limiting magnitudes of plates used in a number-magnitude survey of galaxies. The plates were taken on the 100-inch reflector at Mt Wilson and the images were spread out to 1mm squares.

The magnitudes of galaxies in distant clusters were measured by Sandage, (Humason, Mayall & Sandage,1956), using the schraffierkassette method on the 200-inch reflector at Mt Palomar. The images were squares of sizes 1, 2, or 4 mm. Tests on the accuracy of this method were carried out on stars of known magnitude in globular clusters, and the mean residual was $0^m.1$. Galaxy magnitudes were found to $m_{pg} = 18$ in this way. The results were used for examining the redshift-magnitude relationship for the brightest galaxies in rich clusters.

Zwicky has also used the schraffierkassette method. He determined the magnitudes of galaxies to $m_{pg} = 15.7$ for the 'Catalogue of Galaxies and Clusters of Galaxies'. An 18-inch Schmidt telescope was used with exposure time of 23 to 26 minutes. The images were squares of size corresponding to 1 arcmin. A correction had to be made for a systematic error according to the size of the galaxy because, in the case of large

galaxies, their sizes were comparable to the size of the schraffier-kassette squares. At the bright end, $m_{pg} = 10$ to $m_{pg} = 13$ the results were altered so that on average they agreed with those of Shapley & Ames.

This method is unfortunately affected by the intermittency effect in the photographic emulsion. A continuous exposure of a given intensity for a given length of time produces a higher density of developed grains than a series of exposures of the same intensity making up the same total time. Any point in the square formed from a star is exposed intermittently whereas for a galaxy which is an extended object the exposure is continuous.

d) The Fabry Lens Method

Bigay (1951) used a Fabry lens to obtain magnitudes of 175 galaxies between $m_{pg} = 9$ and $m_{pg} = 13$. In this method a Fabry lens, inserted behind the primary focal plane, focusses the entrance aperture onto the photographic plate. Each object observed forms an image of the same size, the image of the objective,which has a uniform surface brightness proportional to the total brightness of the object. In addition to the exposure of the galaxy an exposure of equal length is required of the night sky, and one or two exposures of comparison stars. Calibration spots were subsequently added to the plate in the laboratory. Bigay found that his magnitudes agreed with those of Seyfert and Keenan, who used out of focus photometry, Stebbins & Whitford (1937) who used photoelectric photometry, and Redman & Shirley (1938) who used photographic photometry with microphotometer measurements. However there was a systematic difference from the magnitudes of Shapley & Ames, especially

at the bright end. This was due to errors arising in the visual method. The internal errors of Bigay's method were about $0^m.1$.

This method is fairly slow and suffers from all the disadvantages of photoelectric photometry which are discussed later.

e) Microphotometer Scans

Photographic photometry enables detailed examinations of the light distribution in a galaxy to be carried out if the density is measured over a range of points in the image and then converted into relative intensities using a calibration. The total magnitude of the galaxy can subsequently be found by extrapolating the distribution to zero intensity and then integrating.

Surface photometry was first carried out by Reynolds (1914) who examined the light curve along the major axis of the Andromeda Galaxy, M31, using a 28-inch reflector. Reynolds measured the density of the plate at intervals of 1mm (69 arcsec) along the major axis with a Hartmann photometer in which the density at each point was compared with a standard set of densities. The intensity calibration was fairly crude. It was made on a different plate from that of the galaxy exposure, which was cut into several pieces. Each piece was exposed at a different distance from the lamp. The intensity distribution of the galaxy was found to be of the form

$$I \propto \frac{1}{(1 + x)^2}$$

where I = intensity

x = distance from the centre of the galaxy.

Reynolds noticed that the light was very intense in the nucleus and thought that there must be a star in the centre, therefore rejecting the hypothesis that M31 is a distant galaxy of stars.

Hubble (1930) examined the luminosity distributions in 15 elliptical galaxies. The plates were taken on the 100-inch reflector at Mt Wilson and the transmissions in the images were measured on a Koch registering photometer. The intensity calibration was made on plates exposed to sunlight in the laboratory. Hubble found that the light distributions in the galaxies were similar and fitted the same kind of formula to the data as Reynolds had done,

$$I = \frac{I_o}{(1 + \frac{r}{a})^2}$$

where I_o is the central intensity, r is the distance from the centre, and a is a parameter which is equal to the distance at which the intensity has fallen to a quarter of I_o. This formula has become known as the Hubble formula.

Hubble discovered that if longer exposures were taken of a galaxy, the size of the image increased, and the boundary of the galaxy was not reached even at $r/a > 35$.

In the late 1930s Redman (1936) and Redman & Shirley (1938) carried out photometry on elliptical galaxies using a 36-inch Newtonian reflector. As mentioned previously, the zero point was obtained from an out of focus exposure of stars on the same plate. The plates were measured by a microphotometer in a grid of 0.1 mm using a spot of size 0.07 mm square, and the calibration was obtained from a tube sensitometer.

Redman realised that the main source of error was due to under exposure of the outer parts of the galaxy. However, with longer exposures, the nucleus becomes saturated. To overcome the problem of the large range in intensity within a galaxy (more than 10000:1), he used a series of plates with a range of exposure times to build up the luminosity curve. The luminosity was calculated by assuming that the isophotes are elliptical, the major and minor axes of the n th isophote of intensity I_n being represented by a_n and b_n respectively. Then, the formula for the luminosity within the m th isophote is:

$$L_m = \sum_{n=1}^{m} \pi(a_{n+1} b_{n+1} - a_n b_n)\tfrac{1}{2}(I_{n+1} + I_n).$$

I_m is the intensity of the limiting isophote.
A graph of the contributions to the luminosity between the last few isophotes was drawn and extrapolated to $I = \frac{1}{2}I_m$ to give the contribution between $I = 0$ and $I = I_m$, hence the total luminosity was found. The magnitudes calculated by this method ranged from $m_{pg} = 8$ to $m_{pg} = 13$, and the internal errors were about $0^m.1$.

One mistake which Redman made was to superimpose the extra-focal star exposure on the galaxy exposure,and also to superimpose the sensitometer spots on the sky fog. This technique is incorrect since the photographic emulsion records non-linearly and this leads to an inaccurate calibration.

De Vaucouleurs started studying the photometry of galaxies in the 1940s, and in his paper on 'Recherches sur les Nebuleuses Extra-galactique' (1948a) he discusses in detail the errors which may arise

in the photometry of galaxies. His observational work was carried out on the 0.8 m telescope at Haute Provence.

There are many factors affecting the accuracy of magnitudes, starting with the effects which arise in the atmosphere, such as absorption, refraction and turbulence. Refraction can be ignored, and so can absorption, provided the standard stars used for obtaining the zero point for the calibration are observed at the same zenith distance. Turbulence, which spreads out the light has a negligible effect on nearby galaxies. De Vaucouleurs counts the brightness of the night sky as a more important factor because it affects the measurements of the outer parts of the galaxy which have to be made out to 1% or less of the sky brightness. In the telescope, errors arise from diffraction, aberrations, imprecise focussing, imprecise guiding, extra reflections, and vignetting. Care must be taken when observing to keep these down to a minimum.

There are several sources of error in the photographic plate. Firstly, each point of light impinging on the plate becomes a diffuse patch of density which is dark in the centre and decreases exponentially to the edges. This could affect the luminosity gradient at the nucleus, which would be measured to be less than its true value. De Vaucouleurs thinks that this effect may occur in the nucleus of NGC3115, but concludes that the effect is negligible. The graininess of the emulsion produces small scale fluctuations in the density of a uniform exposure. This affects the determination of the sky background intensity, and also the detection of the faintest isophotes of the galaxy.

The way in which the plate is developed can affect the results. Varying the kind of developer and the length of the development can alter the plate contrast, i.e. the slope of the straight part of the characteristic curve, D vs. log I. De Vaucouleurs suggests that for the best results the two plates of the galaxy, a short exposure for the nucleus and a long exposure for the outer regions, should be developed in different kinds of developer for different time intervals to give a contrast of 1 to 1.5 for the nucleus, and 2 to 3 for the other exposure.

Adjacency effects occur in regions where there is a sharp contrast in the light intensity and the developed image does not represent the true intensity distribution of the source. During development, at the edge of a region exposed to intense light there is extra developer available from adjacent regions and so this part of the image becomes extra dense. The reaction products in the neighbouring, little-exposed region, hinder development there giving rise to a region of lower density. De Vaucouleurs found that these effects were unimportant in galaxy images.

The measured intensity distribution of light in a galaxy does, however, have to be corrected for local errors. These are the large-scale variations in the density of a region of uniform exposure, (over distances of at least 1 mm), such as the sky surrounding the galaxy. De Vaucouleurs (1944, 1948b) carried out a thorough survey of local errors. He found that for intermediate densities, the local errors are caused by variations arising during the development of the plate. They should have a negligible effect on the density-intensity

calibration except for a change in zero point. Because of this, the errors can be taken into account by supposing that there is a gradual variation in the sky intensity. Interpolation between the intensities surrounding the galaxy can be used to calculate the sky intensity superimposed at each point in the galaxy. The errors in correcting the galaxy intensities by this method are estimated at about 1% at the centre of the galaxy, and a few thousandths at the edges.

Errors can also arise in the photographic calibration. De Vaucouleurs used a tube sensitometer to obtain the calibration. It produced 12 spots, each of 5 mm in diameter, which covered an interval of 4 magnitudes. The spots were situated in a circle round the field and were in random order to cut down local errors. The areas of the apertures of the tubes were measured carefully so that the errors in the light intensities of the spots were only 1 to 2%.

The light from the lamp of the tube sensitometer was filtered to make the spectrum as similar as possible to the light from the galaxies. The conditions for the calibration and galaxy exposures were made as similar as possible. Both exposures were of equal duration, and were taken under similar conditions of temperature and humidity, the calibration exposure being taken as soon after the galaxy exposure as possible. In this way the characteristic curves of the two exposures were as identical as possible.

De Vaucouleurs measured the galaxy images by making tracings through the centres of the galaxies with a microphotometer. Errors can arise in several ways during the measurement of the plates. The size of the microphotometer spot should be chosen carefully so that it

is small enough to resolve the detail but large enough to smooth the noise due to the granularity. De Vaucouleurs used two sizes of spot: one of 50 x 100 μm^2 (0.8 x 1.7 arcsec) to measure the nucleus where there is a steep luminosity gradient, and the other of 125 x 750 μm^2 to measure the outer parts of the galaxy. Scattered light in the microphotometer can affect the results when measuring small images surrounded by a low density background. However, in practice, de Vaucouleurs found that this did not affect his results. Other sources of error were the instability of the photoelectric photometer and the inertia of the galvanometer.

Finally, more errors occur during the reduction of the results. It is most important to calculate the sky intensity carefully, since an error in the sky intensity will affect the distribution calculated for the galaxy and will produce an error in the luminosity calculated by integrating the light distribution. De Vaucouleurs estimated the sky intensity by examining the tracings visually. This is difficult because the light of the galaxy decreases very slowly at the outer edge. It is also complicated by the effect of local errors on the sky bakcground. He found that errors could be reduced if two tracings were made at different optical magnifications in the microphotometer and the results compared.

In the reduction of the calibration measurements, de Vaucouleurs, like Hubble, found that it was best to draw the characteristic curve as δ/Δ vs. magnitude, where δ is the density relative to the plate fog and Δ is the relative density of the sky. In this form, the curve is linear in the range of densities used in galaxy photometry.

Using the results of this study, de Vaucouleurs analysed the light distributions of four galaxies, NGC3115, NGC3379, NGC4649 and NGC4594. He adopted Redman's method to determine the total luminosity, and used the quantity $k_i = L_i/L_T$ to describe the ratio of the luminosity within the i th isophote to the total luminosity. He then defined the luminosity where $k = \frac{1}{2}$ as the equivalent luminosity, and used the major and minor axes of the galaxy within this isophote as a measure of the size of the galaxy, calling them the effective axes, a_e and b_e.

The estimated errors for the intensity profiles ranged from 1% near the nucleus to 6% near the edge, and the errors in the total magnitudes were $\pm 0^m.1$. De Vaucouleurs found that his data for elliptical galaxies fitted the formula:

$$\log B = -3.25(\alpha^{\frac{1}{4}} - 1)$$

where B is the surface brightness and α is the distance along the major axis. These quantities are in units of the effective surface brightness and the effective major axis respectively. This formula fits the intensity distribution at greater distances from the nucleus than Hubble's formula, and does not give an infinite value when integrated.

Holmberg (1950, 1958) has measured the magnitudes of many galaxies using photographic photometry in the international photographic (pg) and photovisual (pv) system. In 1950 he examined 39 nearby galaxies in the Local Group and the M81 and M101 groups in order to determine the luminosity function of galaxies and to find the relationship between galaxy magnitudes and the magnitudes of the brightest stars in a galaxy. The photographic plates were mainly taken at the Mt Wilson

Observatory. Galaxy exposures were made on one half of the plate and an out of focus exposure of the N.P.S. was made on the other. Sometimes a shorter exposure of the nucleus of the galaxy was included. The intensity calibration was obtained from the densities of the star images; no sensitometer measurements were made. Both the star and galaxy images were traced using a microphotometer with a slit of size corresponding to 3 x 8 arcsec^2. In the case of the galaxies, tracings were made through at least twelve cross sections of the galaxy. The clear plate density was subtracted from the density measurements and the intensity calibration was found as a function of log (1-d) which is a linear relationship.

Total magnitudes were calculated by numerical integrations. The results ranged from $m_{pg} = 4$ to $m_{pg} = 13$ and had a mean internal error of $0^m.056$. Several possible sources of error were discussed. Firstly, too low a value of the sky background may have been found because the sky fog increased towards the centre of the plate. To reduce this error, the background was measured over large areas of the plates and care was taken in determining the sky intensity over the galaxy region. Errors arising due to different values of the sky fog in the galaxy and in the N.P.S. were investigated and were found to be negligible. If the microphotometer slit was made too wide it was found that there were systematic errors in the intensity distribution, especially where the intensity gradient was steep. Tests were also carried out to see if the total luminosity measured for a galaxy increased with the limiting star magnitude of the exposure. There was a slight increase but it was negligible. The resulting magnitudes were in good agreement with those of Whitford (1936).

Holmberg carried out a further study of 300 galaxies, mainly brighter than the 12th magnitude, in 1958. The pg and pv magnitudes were found from plates taken on the Mt Wilton 60-inch and 100-inch telescopes, the reduction being carried out in a similar manner to those in the previous paper. This time, however, the magnitudes were given within a limiting isophote of 26.5 mag arcsec^{-2} in the photographic band, and 26.0 mag arcsec^{-2} in the photovisual band.

Until the 1950s very little galaxy photometry had been carried out in the southern hemisphere. The Harvard 'Survey of Bright Galaxies' (Shapley & Ames, 1932) extends into the southern hemisphere but the coverage is not good. Evans (1951, 1952) studied the light distribution of several elliptical galaxies at the Radcliffe Observatory in South Africa. De Vaucouleurs (1956) used the 30-inch Reynolds reflector at Mt Stromlo to photograph many bright galaxies in the southern hemisphere under photometrically standard conditions. Later detailed isophotometry and magnitudes were published by de Vaucouleurs for five galaxies, mainly spirals in the southern hemisphere, which were photographed using the 30-inch and 74-inch reflectors at Mt Stromlo between 1952 and 1956, (de Vaucouleurs 1961, de Vaucouleurs & Page 1962, de Vaucouleurs 1963a,b, 1964). The calibrations were made with a tube sensitometer which produced fifteen spots and the zero point was obtained from the sky brightness. Initially the plates were reduced by scanning along the major and minor axes using a microphotometer, but later, at Harvard, a microdensitometer was used to obtain a more detailed density distribution of the image. For each galaxy the average radial intensity was found, defining $r^* = \sqrt{A/\pi}$ as the equivalent radius. As in the case of M31 (de Vaucouleurs 1958a), it was found that the

light from spiral galaxies can be split into two components: a spheroidal component consisting of the nucleus which has a light distribution similar to that of ellipticals i.e. log I follows the $r^{\frac{1}{4}}$ law, and a flat component corresponding to the disk in which log I decreases linearly with radius. Many parameters describing the galaxy were also given, such as the effective major and minor axes and the effective surface brightness.

De Vaucouleurs also summarised his results on galaxy photometry at the I.A.U. Symposium in 1962. If the surface brightness and the distance along the major axis are expressed in terms of the effective quantities, then the luminosity law for ellipticals is:

$$\log \beta = -3.33 \, (\alpha^{\frac{1}{4}} - 1) \qquad (1.1)$$

where $\beta = B/B_e$ and $\alpha = a/a_e$. B_e is the surface brightness at the equivalent radius. In this case the total luminosity is $L_T = 7.268 \, B_e r_e^2$. For the disk of spiral galaxies and for irregular galaxies, the law is:

$$\log \beta = 0.7290 \, (\rho^* - 1) \qquad (1.2)$$

where $\rho^* = r^*/r_e^*$. Then the total luminosity is given by $L_T = 3.803 \, B_e r_e^{*2}$.

In early type spirals, Sa and Sb, the spheroidal component contains much of the luminosity, but this decreases relative to the disk component going to later type spirals, Sc and Sd.

Sersic (1968) also contributed to galaxy photometry in the southern hemisphere in the 'Atlas de Galaxias Australes'. He found the intensity distributions and magnitudes of 67 galaxies down to $m_{pg} = 11$ observing with the 60-inch reflector in Argentina. He used a step sensitometer to obtain the calibration and the magnitude zero point came

from the sky brightness. Microphotometer scans through the centre of each galaxy were made at various different position angles to enable an isophotal map to be drawn. Sersic reduced his results in a slightly different manner from de Vaucouleurs. He defined S(m) as the area within the isophote of magnitude m.

Then $L_T = \int_0^\infty 10^{-0.4m} dS,$

or integrating by parts, $$L_T = 0.921 \int_{m''}^{\infty} 10^{-0.4m} S(m)\, dm \qquad (1.3)$$

where $S(m'') = 0$.

A formula of the form $S(m) = K\,(m - m'')^n$ was fitted to the light distribution of each galaxy. K and n are parameters, K depending on the size of the galaxy, and n depending on the morphological type. For elliptical galaxies n = 8 and the formula is equivalent to de Vaucouleurs' $r^{\frac{1}{4}}$ law, while for irregular galaxies n = 2 which is equivalent to de Vaucouleurs' law for the disks of galaxies. The total luminosity was then calculated by integrating equation (1.3).

$$L_T = 10^{-0.4m''} K \frac{n!}{(0.921)^n}$$

There was a mean difference between Sersic's and de Vaucouleurs' (1963a and b) magnitudes of $0^m.1$. However there was good agreement with Sandage's (Humason, Mayall & Sandage 1956) magnitudes. The random error in the magnitudes was about $0^m.05$.

During the last ten years there has been an increase in the use of computers to reduce the photographic measurements, allowing more detailed analyses of the light distributions in galaxies to be carried

out. Jones, Obitts, Gallet & de Vaucouleurs (1967) describe a model for deriving the intensity distribution of a galaxy using numerical mapping techniques, and provide copies of the necessary computer programs. As an example, the reduction is shown for the measurements of the spiral galaxy NGC1448 which was photographed by de Vaucouleurs using the 30-inch telescope at Mt Stromlo.

A microphotometer was used to measure the transmission at intervals in a rectangular region of the plate, the transmission measurements being output onto paper tape along with the coordinates at each point. The field measured was divided into two parts, the inner field containing the galaxy and the outer one consisting of the sky background. The background region consisted of a continuous, slowly varying component caused by the effect of local errors on the uniform sky, and a discreet component due to stars and occasionally to pinhole defects in the emulsion. First the discreet component was removed. A low-order, two-dimensional polynomial was fitted to the transmissions in the background region, rejecting all the points with residuals greater than the standard deviation multiplied by a factor, β. (The value of β was between 2 and 3). This process was repeated several times until there were no more points to be rejected. Afterwards a higher order polynomial was fitted to the remaining points. This could be used to calculate the transmission due to the sky intensity only in the galaxy region.

A polynomial was also used to represent the intensity calibration from the tube sensitometer. At each point in the galaxy, the intensity was calculated by subtracting the calculated intensity due to the sky from the observed intensity due to the sky and galaxy. The

intensities were expressed in units of the sky intensity. There were several star images superimposed on the galaxy image. They could not be removed by the computer by the same method as that used for the stars in the outer field, because star images are similar to the nucleus, or to HII regions. The star positions were therefore found visually from a map of the galaxy and the intensity due to a star was replaced by the mean of the surrounding points. At low intensities the data was smoothed using a weighted function to obtain isophotes down to 1% of the night sky. The mean radial intensity distribution could then be calculated and integrated numerically to give the luminosities within different radii. This relation was extrapolated to give the total luminosity.

Several astronomers have used methods similar to those of de Vaucouleurs or Holmberg to obtain the light distributions in galaxies, (especially for elliptical galaxies). They include Liller (1960, 1966), Van Houten (1961), Rood & Baum (1968) and Oemler (1976). However, a different approach to the subject was made by Kormendy (1973) who calibrated the intensity profile of M31 using (in focus) star profiles.

King & Hinrichs (1967) have used a standard profile (in the form of magnitude as a function of radial distance) derived from a few stars to find the relative magnitudes of many more. They state that stars have the same intensity profiles, provided that the aperture of the microphotometer is much smaller than the image so that at any time the spot does not include regions of very different density, otherwise a systematic error will arise because of the non-linearity

of the density-intensity relation. Moffat (1969) also finds that star intensity profiles are all the same shape. Kormendy (1973) used plates taken on the 48-inch Schmidt telescope at Mt Palomar, which were calibrated with a spot sensitometer. Using images covering a range in magnitude he built up the stellar intensity profile. Then on a separate plate of M31, he found the density profile of one star, and from the standard stellar intensity profile derived the density-intensity relation. This calibration was used to find the intensity distribution along the major axis of M31. The zero point of the magnitude scale was determined from photoelectric measurements of the night sky during the plate exposure. A comparison with de Vaucouleurs' (1958a) results showed that the magnitudes in the distribution were accurate to within $\pm 0^{m}.1$.

1.2 Photoelectric Photometry

a) Photoelectric Photometry using Integrated Light of the Galaxy

In photoelectric photometry of galaxies, as in stellar photometry, the object is centred on the aperture of a diaphragm at the focus, and the light from the entrance aperture of the telescope is focussed onto the detector by a Fabry lens. Because of the extended size of galaxies larger apertures are used, of up to 20 mm or more, and an equally large comparison region of the sky is observed. The comparison sky region is chosen carefully, with reference to photographic plates, to ensure that there are no stars. Several measurements are made of the galaxy and the sky alternately, in order to take account of the variations in the sky brightness. Frequently stars are superimposed on the galaxy being studied, and these have to be measured separately with

small apertures so that their light can be subtracted.

As in photographic photometry, the total magnitude of a galaxy can only be found by extrapolation. The larger the aperture used, the larger the measured luminosity becomes as a greater fraction of the light of the galaxy is detected. This strong dependence of the luminosity, or magnitude on the aperture size has been called the 'aperture effect'. Since the apertures are usually circular, the magnitudes measured are not isophotal ones, unless the galaxy is circular, (i.e. face on).

There are advantages and disadvantages in photoelectric photometry when compared with photographic photometry. In photoelectric photometry, only one galaxy can be measured at a time, whereas on a photographic plate many galaxies may be recorded. Photographic emulsions only cover a small range in intensities (a ratio of 100:1), and the results are affected by graininess and larger scale density fluctuations (local errors). A density-intensity calibration has to be made, and the reductions of the data may be time consuming. In photoelectric photometry, these particular drawbacks do not arise. The magnitude, within a certain aperture, of a galaxy can be obtained directly by comparison with measurements of standard stars. However, corrections are required to convert the magnitudes of the 'natural' system of the photometer to a standard one such as the UBV system. Errors in photoelectric photometry can arise from the Fabry lens not being positioned properly, or from the size of the aperture not being measured correctly.

Photoelectric photometry of galaxies was first carried out by

Stebbins and Whitford. Whitford (1936) measured the 11 brightest galaxies with a Cooke 10-inch refractor. The aperture was selected to be at least as large as the diameter measured by Shapley & Ames (1932), the largest aperture being 10 mm diameter corresponding to 30 arcmin. A special case had to be made for M31 because of its large angular size. A $3\frac{1}{2}$-inch lens was used and the aperture was 15 mm in diameter, corresponding to 128 arcmin. (An aperture larger than this would have included several bright stars.)

A relationship was found, from stellar observations, between the photoelectric magnitudes and those measured on the international photographic system. Then, Whitford's calculated magnitudes were compared with the Shapley & Ames (1932) magnitudes and Hopman's (1921) magnitudes based on Holetschek's (1907) visual estimates. In general, Whitford's magnitudes were brighter than the other magnitudes, and there were large random errors of about $0^m.5$.

Stebbins & Whitford (1937) published the magnitudes of 165 galaxies down to magnitude 15 and the colours of 112 galaxies. They were the results of a survey started in 1930 by Stebbins. The observations were made on the 60-inch and 100-inch telescopes at Mt Wilson, and the aperture sizes ranged from 42 arcsec to 163 arcsec, a 64 arcsec aperture being used to obtain the colours. The estimated mean errors in the photoelectric magnitudes were $\pm 0^m.15$.

Later, Stebbins & Whitford (1948, 1952) published data on 6-colour photometry of bright galaxies and 2-colour photometry of fainter galaxies down to $m_{pg} = 18$. The two colour photometry was reduced to the international pg and pv system. Larger aperture sizes were used,

ranging up to 8.6 arcmin on the 60-inch telescope. However even this was not enough to include the whole of the brightest galaxies. They investigated the variation in colour with redshift for elliptical galaxies in clusters and found that the galaxies became redder with increasing redshift.

Pettit (1954) also made photoelectric observations of galaxies in the international photographic and photovisual system on the 60-inch and 100-inch telescopes at Mt Wilson. He used the same aperture sizes as those of Stebbins & Whitford. 558 galaxies were observed altogether with magnitudes ranging from $8^{m}.5$ to $15^{m}.5$. The mean internal error obtained from repeated observations was $\pm 0^{m}.07$. However, large differences were found when comparing the results with those of Shapley & Ames (1932) and Bigay (1951). There was better agreement with the results of Stebbins & Whitford.

Humason, Mayall & Sandage (1956) used the results obtained by Pettit and by Stebbins & Whitford to study the magnitude-redshift relation for field galaxies. The magnitudes were corrected for the aperture effect by reducing them to a standard isophote of 25 mag arcsec^{-2}. This was carried out using the profile of the elliptical galaxy NGC3379, which had been measured by Dennison (1954) out to a distance of r/a = 50, (a is the parameter in Hubble's formula). The diameter D_s of each galaxy was measured on the Palomar Observatory Sky Survey photographs. This diameter is the size of the galaxy out to the isophote of 22.6 mag arcsec^{-2}. $2.5D_s$ was used as the standard diameter, corresponding to the isophote of 25 mag arcsec^{-2}. From the profile of NGC3379, the magnitude correction, Δm, was found as a

function of $D_p/2.5D_s$, where D_p is the aperture diameter for galaxies of different ellipticities. This correction was used for all types of galaxies, the justification being that in spirals there is an underlying population of old stars which has an elliptical distribution. The errors in the magnitudes were assessed by comparing Stebbins & Whitford's, and Pettit's magnitudes with each other, and with Holmberg's photographic magnitudes. It was found that:

$$m_{SW} - m_P = 0^m.026 \qquad \sigma = \pm 0^m.190$$

$$m_H - m_P = 0^m.040 \qquad \sigma = \pm 0^m.189$$

$$m_H - m_{SW} = 0^m.014 \qquad \sigma = \pm 0^m.100$$

Pettit's magnitudes were therefore less accurate than those of Stebbins & Whitford and those of Holmberg.

De Vaucouleurs (1959a) measured the magnitudes of 124 galaxies in the UBV system. He observed on the 21-inch reflector at the Lowell Observatory, with the photometer used by Johnson in defining the system (Johnson & Morgan, 1953). The apertures used were 4 or 5.5 mm in diameter corresponding to 100 arcsec and 137.5 arcsec respectively. For the brightest galaxies 1 to 3 measurements were made and 2 to 4 sky measurements, while for the faint galaxies 3 to 5 measurements were made and 4 of the sky. The galaxy and the sky were observed alternately and the sky was measured to the north, south, east and west of the galaxy. The probable errors depend on the magnitude and the colour. In the V they range from $\pm 0^m.02$ at V = 9, to $\pm 0^m.11$ at V = 14, but the errors in the B and the U bands were slightly higher.

The results, combined with observations by Tifft (1958) and Johnson (1959) were used by de Vaucouleurs (1961) to study the colours of galaxies. First the effects of internal extinction in galaxies were investigated by plotting graphs of colour, e.g. (U - V), against d/D the ratio of the observed minor and major axes. If $(U-V)_o = (U-V) - \Delta(U-V)$ where $(U-V)_o$ is the face-on colour, then the relationship is of the form $(U-V) = \gamma(1 - d/D)$ where γ is a constant. It was found that

$$\frac{\Delta(U-B)}{\Delta(U-V)} = \frac{3}{5} \quad \text{and} \quad \frac{\Delta(B-V)}{\Delta(U-V)} = \frac{2}{5}$$

The variation in colour with aperture width was found for different types of galaxy. Early type galaxies are redder in the centre, especially for Sa types, and late type galaxies (irregulars) are slightly bluer in the centre.

Tifft (1961) carried out multicolour photometry of bright galaxies on the Mt Wilson 60-inch and 100-inch reflectors. There were four bands in the visible at effective reciprocal wavelengths of 2.66, 2.39, 2.07 and 1.68 μm^{-1}, and in addition a few galaxies were measured in the red and infrared at effective reciprocal wavelengths of 1.55, 1.26, 1.14 and 1.00 μm^{-1}. 57 galaxies and 52 stars were observed. There were five aperture sizes, ranging from 0.365 arcmin to 3.177 arcmin on the 60-inch and 0.216 arcmin to 1.874 arcmin on the 100-inch, and in general each galaxy was measured with three apertures. The internal random error for the measurement of one galaxy or star was estimated to be about $0^m.02$, and the tie-in systematic errors between different galaxies or galaxies and stars, or between different nights were about

$0^m.03$ to $0^m.04$

The results (Tifft 1963) were used to investigate the colours of galaxies in a similar way to the investigation by de Vaucouleurs (1961). Also discussed was the possibility of observing galaxies through apertures inversely proportional to their distances, and so observing the same volume of space round each galaxy. The size of the aperture could be chosen from the inverse redshift.

Tifft (1969) published extra results on 4-colour photometry of 64 galaxies mainly in the Virgo Cluster. The aperture sizes used by Tifft were smaller than those used by other astronomers, such as de Vaucouleurs (1961), in order to study the radial variation of colour in galaxies with a view to investigating their structure.

Hodge (1963) measured the magnitudes of 60 galaxies, mainly early types, in the UBV system at Mt Wilson. The position of galaxies in the colour-colour diagram was found to be shifted slightly to the blue in (B - V) in comparison with the relation found by de Vaucouleurs.

Shobbrook (1966) measured the magnitudes of 53 southern galaxies in groups and clusters using UBV photometry. The observations were carried out on the 26-inch reflector at the Mt Bingar Field Station of the Mt Stromlo Observatory, and on the 50-inch reflector at Mt Stromlo. There were four aperture sizes used on the 26-inch ranging in size from 0.26 arcmin to 1.75 arcmin in diameter, and on the 50-inch one aperture was used of 0.493 arcmin in diameter. At least two sky regions beside each galaxy were chosen which had a faint star density similar to that superimposed on the galaxy, using charts from the Uppsala 20-inch Schmidt telescope or the Mt Stromlo

74-inch telescope. It was found to be impractical to obtain total magnitudes of large, bright galaxies by photoelectric photometry because such large apertures were necessary. Instead, the results were reduced to what would have been observed through an aperture equal to a standard diameter of the galaxy. The diameter used was the corrected face-on diameter defined by de Vaucouleurs (1959b) using the diameters from the Heidelberg Survey (Reinmuth 1926). de Vaucouleurs found that the relationship:

$$\log D(0) = \log D + 0.4 \log d/D$$

holds for all galaxies, where D and d are the major and minor axes out to a certain isophote, and D(0) is the face-on diameter, where d/D = 1. Knowing D and d/D for any galaxy, D(0) can be found. D(0) decreases towards the plane of the galaxy due to interstellar extinction, (de Vaucouleurs 1959b). The results were therefore corrected to $D(0)_c$, the face-on diameter which would be observed from the galactic poles.

Graphs of B magnitude vs. $A/D(0)_c$, where A is the diameter of the aperture, were drawn for different types of galaxy, using Shobbrook's data and some diameter measurements from de Vaucouleurs. The B magnitudes were found in the form $(B - B_1)$ where B_1 is the magnitude at $A/D(0)_c = 1$. Using these graphs, the magnitude B_1 was calculated for all galaxies, the results ranging from $B = 10^m.0$ to $B = 14^m.0$. The internal magnitude errors were $\pm 0^m.02$ in V and (B - V) at $V = 10^m.0$ increasing to $\pm 0^m.05$ at $V = 13^m.0$. In (U - B) the errors ranged from $\pm 0^m.03$ to $\pm 0^m.09$. After the galaxy colours had been corrected for interstellar extinction to the face-on values, colour-colour diagrams were drawn and were compared with those of de Vaucouleurs

and Hodge, showing good agreement.

Westerlund & Wall (1969) measured the UBV magnitudes of southern Q.S.O.s, radio galaxies and normal galaxies using the 24-inch and 40-inch telescopes at the Siding Spring Observatory. All the objects fainter than V = 14 were observed on the 40-inch. For objects fainter than V = $15^{m}.5$, their positions were found by offsetting. An aperture size of 18 arcsec in diameter was used for the Q.S.O.s and N galaxies, and for the radio and normal galaxies, the aperture size ranged from 18 arcsec to 180 arcsec. The probable errors were $\pm 0^{m}.02$ in (B - V) and $\pm 0^{m}.04$ in (U - B) for objects brighter than V = 14. However, the faintest objects at about V = 18 probably have errors of $\pm 0^{m}.1$.

G. & A. de Vaucouleurs (1972) published the results of UBV photometry of 461 galaxies north of declination -50^{o}. Most of the observations were carried out between 1960 and 1968 using the 91 cm reflector at the McDonald Observatory. The galaxy magnitudes ranged from about V = $10^{m}.0$ to V = $14^{m}.0$, and the mean internal errors were $\pm 0^{m}.04$ in V, $\pm 0^{m}.03$ in (B - V), and $\pm 0^{m}.045$ in (U - B). Corrections were applied to the colours for galactic extinction, redshift, aperture and inclination effects, the values of the corrections being determined statistically from the data. A discussion of these corrections, which have to be applied before comparing the magnitudes of galaxies will be given in section 1.5.

Sandage carried out a program of photoelectric photometry of faint galaxies, including first ranked cluster galaxies, radio galaxies, N galaxies and Q.S.O.s, in the 1960s, using the 60-inch

and 100-inch telescopes at Mt Wilson and the 200-inch at Mt Palomar. The results were published in a series of papers on the redshift-distance relation (Sandage 1972a,b,c, 1973a,b,c, 1975, Sandage & Hardy 1973). Several of the galaxies measured were fainter than V = 18. A method of aperture correction different from that described by Humason, Mayall & Sandage (1956) was employed because, as Stock & Scheuking (1957) pointed out, the isophotal sizes of galaxies do not correspond to their metric sizes in an expanding universe. Since the objects, especially the Q.S.O.s, observed by Sandage have large redshifts, it was necessary to take this effect into account. The new aperture correction used the relation between metric diameter Θ_m, and redshift z, for the Friedman cosmological model with $q_o = 1$, which is

$$\Theta_m = \text{const.} \frac{(1 + z)^2}{z}$$

For first ranked cluster galaxies, a graph of magnitude vs. $\frac{\Theta_p z}{(1 + z)^2}$ was drawn, where Θ_p is the angular diameter of the photometer aperture. The resulting curve was used to derive magnitude corrections to a standard diameter which is equal to $4.1\Theta_s$ in Humason, Mayall & Sandage (1956), and in the limit of z = 0, corresponded to an isophotal diameter at V = 26 mag arcsec^{-2}. In paper VI (1973a), the errors in the photometry were given from a comparison of two sets of measurements. The standard errors in V were $\pm 0^m.09$, and in B were $\pm 0^m.12$.

Paper VIII (Sandage 1975) describes photometry carried out in the southern hemisphere. UBVR magnitudes of 74 galaxies in the Shapley-Ames catalogue (1932), south of $\delta = -30^o$, were measured using

the Siding Spring 1 m reflector. The magnitudes ranged from V = 10 to V = 14, and the internal random errors were $\pm 0^{m}.03$. The external errors, found by comparing the results with those of Shobbrook (1966) were of the same order.

Finally, Alcaino (1974) also measured the UBV magnitudes of the galaxies in the southern hemisphere using photoelectric photometry. 38 galaxies of different morphological types, between V = 10 and V = 14 were studied. The observations were made on the 1 m reflector at the European Southern Observatory, and the galaxies were all measured with a 21 arcsec aperture. The photoelectric errors were about $\pm 0^{m}.06$ in the first observing run, and $\pm 0^{m}.08$ in the second.

b) Photoelectric Scans

Integral magnitudes can be calculated directly from photoelectric photometry using apertures which include a large proportion of the light of the galaxy. However, this method is impracticable for large nearby galaxies because the apertures required are too large. Instead the light distribution may be found by scanning photoelectrically across the galaxy with a small aperture, and the distribution can be integrated to give the total magnitude. This technique is particularly useful for galaxies in the Local Group, the images of which are too large to be measured on a photographic plate. Photoelectric scans can also be used for calibrating photographic plates.

Van Houten, Oort & Hiltner (1954) made photoelectric scans of nine bright galaxies on the 82-inch telescope at the McDonald Observatory, using a synchrous motor to move the diaphragm in the Cassegrain

focal plane in an arbitrary direction. Tracings were made along the major and minor axes of the galaxies. The main cause of error in the faint outer parts of the galaxy was in the subtraction of the sky background. Near the nucleus, where there is a high intensity gradient, the intensities in the scans were too faint, compared with single measurements of the nucleus. This was probably due to too high a scanning speed.

Eggen & de Vaucouleurs (1956) carried out low resolution photometry of the Large Magellanic Cloud in blue and yellow band-widths. 42 measurements were made in a rectangular grid covering a region from $04^h\,00^m$ to $06^h\,30^m$ in right ascension and from -62^o to -77^o in declination, using an aperture of 2.42 arcdeg in diameter. Corrections were applied for the night sky and for field stars. The intensity distributions were calculated and then integrated to give the total magnitude and colour.

De Vaucouleurs (1958a) measured the UBV magnitudes of M31 using photoelectric scans over the whole galaxy at intervals of 10 arcmin in declination. The measurements were made on the 21-inch reflector at the Lowell Observatory. An aperture of 137.5 arcsec was used. The total magnitude (excluding the companions), was found to be B = 4.36. De Vaucouleurs (1957b) measured the magnitude of M33 by the same method.

The outer corona of M87 was measured by de Vaucouleurs (1969) using photoelectric scans from N-S and E-W across the galaxy. The observations were made with the 36-inch reflector at the McDonald Observatory. At the limiting surface brightness of $\mu_B = 27.3$ mag arcsec^{-2},

the diameter of the corona was more than 1 arcdegree. The intensity due to the corona was found to decrease exponentially. G. & A. de Vaucouleurs (1970) measured the intergalactic light in the centre of the Coma Cluster using photoelectric scans. They found that the light could be accounted for by the overlapping coronas of the two giant galaxies NGC4874 and NGC4889.

1.3 Other Methods for Galaxy Photometry

Recently there has been the development of new types of imaging devices, such as electronographic cameras, image tubes, and television-type detectors. They combine the high quantum efficiency of the photoelectric detectors with the imaging properties of the photographic plate. Although most of the work carried out so far with these systems has been of an experimental nature, several astronomers have tried galaxy photometry with these new methods, and the results have been quite promising.

Ables & Ables (1972) used a Kron electronographic camera on the 40-inch telescope at the Flagstaff Station of the U.S. Naval Observatory to find the luminosity distribution and magnitude of NGC4881. The Kron electronographic camera consists of a photocathode from which the photoelectrons are accelerated in a vacuum on to nuclear emulsion. It has the advantage of a linear density-intensity relation. The results were calibrated from their own photoelectric photometry and from photoelectric photometry by Rood & Baum (1968) and de Vaucouleurs & de Vaucouleurs (1964). The small scatter of $\pm 0^{m}.01$ in the constants required to convert the electronic magnitudes to the standard B and V magnitudes shows that the electronographic photometry was quite accurate.

Hoffman & Crane (1977) have used an SEC vidicon to measure the magnitudes of galaxies in six distant clusters. The vidicon is a television-type detector, which has a high quantum efficiency, although there is a low dynamic range. Corrections had to be made for the varying gain over different parts of the system, and for a non-linear response at high intensities. Both metric and isophotal magnitudes were calculated; the metric magnitudes were from an area within a metric diameter of 20.3 kpc, and the isophotal magnitudes were within the isophote of 23 mag arcsec^{-2}. Corrections to the magnitudes were made for atmospheric seeing effects, assuming that the intensity profiles for all galaxies followed the Hubble formula, and that the seeing spread function was gaussian. The passband was to the red of the V band and the magnitudes ranged from m = 16 to m = 19. Internal errors were $\pm 0^m.07$ at M = 16, increasing to $\pm 0^m.3$ at m = 19.

1.4 The Reduction of Galaxy Magnitudes to a Standard System

Due to the difficulty involved in galaxy photometry, astronomers have used their own individual photometric systems for galaxy magnitudes. Some have found total magnitudes, such as Redman (1936) while others, like Humason, Mayall & Sandage (1956), have found isophotal magnitudes. Early magnitude determinations were in the photographic and photovisual colourbands (Seares 1922), but since the 1950s many observations have been made in the UBV system (Johnson & Morgan 1953).

De Vaucouleurs & de Vaucouleurs (1964) collected information on galaxies, such as magnitudes, diameters and redshifts, from many sources,

and reduced the data to standard systems. The magnitudes were given in the form of B(0) which is the integrated Johnson B magnitude within a circular field aperture of diameter A, equal to the face-on diameter D(0). The D(0) diameter was defined by de Vaucouleurs (1959b). This catalogue is an enlarged and improved version of the Harvard 'Survey of Galaxies Brighter than Thirteenth Magnitude' by Shapley & Ames (1932). The Harvard magnitudes, m_H, and m_c, their values corrected to the B(0) system are listed, along with the B(0) magnitudes derived from photoelectric photometry and modern photographic photometry for over 800 galaxies brighter than 15th magnitude. The B(0) magnitudes come from the photometry of many astronomers, including Stebbins and Whitford, Bigay, Pettit, Holmberg, Tifft, and de Vaucouleurs.

In the 'Second Reference Catalogue of Bright Galaxies' (de Vaucouleurs, de Vaucouleurs & Corwin, 1976) the total, or assymptotic B_T magnitudes are given for more than 1500 galaxies brighter than 16th magnitude. A standard system of $B_T(S)$ magnitudes was set up from the detailed photographic photometry of galaxies by Ables (1971), Ables & Ables (1972), Bertola (1966, 1967), Bernacca and Bertola (1969), Fraser (1977), and de Vaucouleurs (various references already given). Standard luminosity curves for different morphological types were found, and these were used to calculate $B_T(A)$ total magnitudes from multi-aperture photoelectric photometry. The estimated mean errors were $0^m.14$ for the $B_T(S)$ and $0^m.1$ to $0^m.2$ for the $B_T(A)$.

De Vaucouleurs et al (1977), in a series of papers entitled 'Contributions to Galaxy Photometry' describe in more detail the

reduction of magnitudes to the B_T system, and give more accurate lists of magnitudes.

1.5 The Corrections for Galactic Extinction, Internal Extinction and Redshift

Galaxy magnitudes are affected by several features which make the magnitudes of identical galaxies appear different. In order to use the magnitudes as distance indicators they have to be corrected so that they are a measure of the same quantity for each galaxy. Corrections are required for the extinction of light in the Galaxy, internal extinction in galaxies, and for redshift (the K-correction).

a) Galactic Extinction

It has been known for a long time that galaxies seem to 'avoid' the plane of the Milky Way and are more numerous at high galactic latitudes (Hinks 1911). Hubble (1934) analysed the distribution of galaxies, assuming that the 'zone of avoidance' was due to obscuring clouds in the galactic plane. He found that the numbers of galaxies, N, followed the relation:

$$\log N = 2.115 - 0.15 \operatorname{cosec} b$$

from $b = 90^{\circ}$ to $b = 15^{\circ}$. (b is galactic latitude.)

This formula is consistent with the model of a uniform absorbing layer in the galactic plane. There is little variation of the numbers with galactic longitude, except at low galactic latitudes, where there is more obscuration in the direction of the galactic centre. Using the relation $\frac{d \log N}{dm} = 0.6$, which ignores the effect of redshift on

magnitude, Hubble found that the galactic extinction was:

$$A_{pg} = 0.25 \text{ cosec } b.$$

Holmberg (1958) obtained the relation $A_{pg} = 0.26$ cosec b for galactic extinction from an examination of the dependence on galactic latitude of the surface brightness of spiral galaxies. The effect of galactic latitude on the colour, $C = m_{pg} - m_{pv}$, was:

$$C = \overline{C}_o + 0.062 \text{ (cosec } b - 1)$$

where $\overline{C}_o$ is the average colour of galaxies at the north galactic pole.

Shane & Wirtanen (1967) examined the effects of galactic extinction using galaxy counts from the Lick Observatory survey plates. They found that log N = 1.95 - 0.242 cosec b, and used $\frac{d \log N}{d m} = 0.47$, which was calculated taking the effects of redshift on magnitude into account. This gives a value of $0^m.51$ for the optical half-thickness, τ, of the Galaxy, which is about twice the value obtained by Hubble (1934). (The optical half-thickness is the amount of extinction for a galaxy seen in the direction of the galactic pole. The light from such a galaxy has travelled through half the thickness of the absorbing layer in the plane of the galaxy, assuming that the Sun is in the centre of the layer.)

A reanalysis of Hubble's counts was carried out by de Vaucouleurs & Malik (1969). They showed that the difference between the results of the two surveys was due to a bias introduced in the early survey data. Hubble had omitted the zero-count fields at low latitudes which led to an underestimate of the galactic extinction, and he had ignored the dependence on longitude, so that the counts at low latitudes were

dominated by the transparent regions in the direction of the galactic anticentre. At low latitudes the obscuration is caused by nearby clouds which are not distributed symmetrically about the galactic plane. The angle b_o, which is a function of longitude, was introduced to describe the plane of symmetry of the absorbing layer. Because the Sun is displaced to the north of the absorbing layer, the corrections are not exactly the same for the two hemispheres. The formula found for the variation of log N was:

$$\log N = 2.14 + B\,|C|$$

where $C = \operatorname{cosec}(b - b_o(1)) = \operatorname{cosec}(b + 0.25 - 1.7 \sin 1 - 1.0 \cos 31)$

$$-B_N = 0.193 + 0.031 \cos 1 + 0.019 \cos 31$$

$$-B_S = 0.217 + 0.037 \cos 1 - 0.003 \cos 31$$

and where suffices N and S denote north and south.

With $\frac{d \log N}{d m} = 0.44$ at the limiting magnitude of 19.4 for the Hubble counts, $\tau_B = 0^m.47 \pm 0.2$, which agrees well with the value obtained by Shane and Wirtanen.

However, this large value for the optical half-thickness contradicted the small values for the selective extinction, E_{B-V} found at the galactic poles by several astronomers. Peterson (1970) observed the redshift, V magnitude and V-r colour of the first-ranked galaxy in each of 48 clusters and 7 groups. (The r band was that defined by Sandage & Smith 1963). The absolute magnitude was calculated using the redshift-distance relation. Assuming that the absolute magnitude for the first-ranked cluster galaxy is constant, any observed variation in the absolute magnitude will be due to galactic

extinction. After correction for selection effects, Peterson found that the extinction at the galactic poles was $A_V = 0^m.06$, and $E_{V-r} = 0^m.023$, corresponding to $E_{B-V} = 0^m.027$.

An analysis of the distribution of magnitudes of faint galaxies by Sandage (1937b) showed that either the ratio of galactic extinction/selective extinction is very high, or that the extinction below $b = 30^o$ is not connected with the extinction at higher galactic latitudes. Assuming that the former is incorrect,

$$A_B = 0.132 \text{ (cosec } b - 1) \qquad |b| \leq 50^o$$

$$A_B = 0.0 \qquad |b| \geq 50^o$$

$$A_V = 0.75\ A_B.$$

Knapp & Kerr (1974) suggested that the absorption coefficient evaluated from galaxy counts was over-estimated. The detection of a galaxy depends on its surface brightness, and not on its total magnitude. Since the surface brightness is independent of the distance (ignoring the effects of redshift), the extinction coefficient is the same as that in the log N relation. This means that the optical half-thickness should be 0.15 from Hubble's galaxy counts, and 0.24 for Shane & Wirtanen's results.

De Vaucouleurs and de Vaucouleurs & Corwin (1976) reanalysed the Lick and Mt Wilson galaxy counts to obtain a more accurate value of the correction. They found that

$$A_B = 0.19\ (1 + S_N \cos b) \qquad |C| \qquad b > 0$$

$$A_B = 0.21\ (1 + S_S \cos b) \qquad |C| \qquad b < 0$$

where $C = \text{cosec}\ (b - b_o(l)) = \text{cosec}\ (b - 0.25 - 1.7 \sin l - 1.0 \cos 3l)$, and S_N and S_S are factors depending on galactic longitude for the northern and southern hemispheres.

b) Internal Extinction

The observed magnitude and colour of a spiral galaxy, of a certain morphological type and luminosity class, and at a given distance, depend on the inclination of the plane of the galaxy to the line of sight. It is usually assumed that the disk of the galaxy is in the form of an oblate spheroid. If i is the angle between the plane of the galaxy and the line of sight, then

$$\sin^2 i = \frac{(b/a)^2 - q^2}{1 - q}$$

where b/a is the ratio of the apparent minor and major axes, and q is the ratio of the smallest to the largest axis of the spheroid.

There are in fact two effects which alter the appearance of a galaxy. Looking across the plane of the galaxy there is a greater optical path, and therefore the surface brightness of the galaxy is increased and also the diameter out to a certain isophote will be larger for edge-on galaxies. However, in the plane of the galaxy, there is an increased amount of dust which absorbs the light, tending to make the galaxy fainter.

Reynolds (1920) found that there appeared to be an excess of spirals viewed edge-on. The cause of this, as suggested by Opik (1923), was that the surface brightness increased with inclination of the galaxy leading to an increase in the isophotal diameter, so that in a survey of galaxies the edge-on spirals were included from a larger

volume of space than other spirals. Holmberg (1946) examined the variation of galaxy diameters with inclination and found that the major axis increases as $(a/b)^{1/6}$ for a model in which the intensity distribution is of the form $I \propto r^{-3}$. However, Holmberg (1958) omitted this effect when calculating the corrections to the magnitude for the tilt effect. He examined the dependence of the average surface brightness, S_o, of galaxies on the axis ratio, b/a, where

$$S_o = m_o + 5 \log a$$

where m_o is the integrated magnitude reduced to galactic latitude 90^o. It was assumed that the major axis, a, was independent of inclination, and that the variation of the surface brightness would show the effect of inclination on magnitude. The relation was found to be of the form

$$S_o - \overline{S}'_o = \Delta A = \alpha(\text{cosec } i - 1), \text{ for } i \geqslant 13^o$$

where $\overline{S}'_o$ is the average value of S_o for $i = 90^o$. The mean value of the parameter α was $0^m.28$ for S_c^- and S_c^+ galaxies, and $0^m.43$ for types S_o, S_b^- and S_b^+. The colour $C_o = m_{pg} - m_{pv}$, corrected for galactic extinction, varied with the observed axial ratio in the form

$$C_o - \overline{C}'_o = \Delta C = \beta(1 - b/a)$$

where $\overline{C}'_o$ is the average colour for face-on galaxies. β depends on the type of spiral, being largest for S_a and S_b^- with a value of $0^m.25$.

De Vaucouleurs (1959b) studied the variation of apparent diameter of the major axis, D, with the axial ratio R = D/d for galaxies with magnitudes between 11 and 12. He found that for all

galaxy types

$$\log D(0) = \log D - 0.4 \log R$$

where D(0) is the face-on diameter. This has been criticised by Tully (1968) who claims that there is no dependence of diameter on axial ratio.

Heidmann, Heidmann & de Vaucouleurs (1972) carried out a thorough study of inclination effects using both optical data and radio observations of the hydrogen 21 cm line. They concluded that there was an effect on the apparent major diameter of galaxies, but that it was not as large as that found by de Vaucouleurs (1959), and was given by

$$\log D(0) = \log D - 0.2 \log R$$

The coefficient of log R has a small dependence on the amount of hydrogen self-absorption assumed, but the value of 0.2 agrees with the value calculated from galaxy models. If this increase in the observed diameter with axial ratio is included, the magnitude corrections as found by Holmberg (1958) are too large. However, Tully (1972) again gives evidence to show that there is no variation in the diameter with inclination, and states that Holmberg's magnitude corrections are correct. There are obviously selection effects in the data producing these contradictory results.

De Vaucouleurs, de Vaucouleurs & Corwin (1976) used diameters within the isophote of $\mu_B = 25$ mag arcsec^{-2} and calculated the diameter-axis ratio relation by two different methods to give:

$$\log D(0) = \log D_{25} - 0.235 \log R_{25}$$

They found the magnitude correction, A(i) in the form

$$A(i) = \alpha(T) \log R_{25}$$

where T is the number given by de Vaucouleurs to the Hubble morphological types (de Vaucouleurs 1962b).

$$\begin{aligned} \alpha(T) &= 0 && T \leq -4 \\ &= 0.2\,(T + 4) && -3 \leq T \leq -1 \\ &= 0.7 && T = 0 \\ &= 0.8 && 1 - T \leq 8 \\ &= 0.1\,T && T \geq 8 \end{aligned}$$

c) The K-correction

If a galaxy is redshifted, the light observed by a detector of a certain bandwidth comes from a bluer region of the spectrum. The k-correction reduces the magnitude of the galaxy to that which would be observed in the same wavelength band in the rest frame of the galaxy.

Hubble (1936c) found that the numbers of galaxies observed out to different limiting magnitudes departed from the theoretical relation for a stationary, Euclidean universe. (In this case the numbers of galaxies out to limiting magnitudes indicate the volumes contained by different radii.

$$N \propto 4/3\,\pi r^3$$

$$m = 2.5 \log r^2 + \text{const}$$

$$\log N = 0.6\,m \times \text{const})$$

He explained the departure of the observed relation from the theoretical

one in terms of corrections to the magnitudes for redshift, considering that the redshift was due either to a velocity (Doppler) shift, or to some unknown mechanism causing photons to lose energy. There are two effects caused by redshift on the magnitudes of a galaxy. The 'number effect' which applies only to velocity shifts is that the rate of photons reaching the observer from the galxy is reduced due to the expansion of the universe. If the true wavelength is λ, and the observed wavelength is $\lambda + d\lambda$, the change in magnitude due to this effect is

$$\Delta m = 2.5 \log (1 + d\lambda/\lambda)$$

The 'energy effect' is caused by the reduction in energy of each photon due to the redshift. $E_o = hc/\lambda$, (where h is Planck's constant and c is the speed of light), is the energy emitted at λ by the galaxy, and $E_1 = hc/(\lambda + d\lambda)$ is the energy detected. This effect also alters the bolometric magnitude by

$$\Delta m = 2.5 \log (1 + d\lambda/\lambda)$$

However, because the energy spectrum of the source is altered, there is another term in this correction, denoted by K which depends on the atmospheric transmission function, the spectral sensitivity of the telescope mirror, and the photographic plate. The total correction to the magnitude for redshift is:

$$\Delta m = 5 \log (1 + z) + K \quad \text{for velocity redshifts}$$

$$\text{or } \Delta m = 2.5 \log (1 + z) + K \text{ for non-velocity redshifts,}$$

where $z = d\lambda/\lambda$.

It is usually assumed that the redshifts are due to the velocity of recession of the galaxies although this has not been proved decisively.

The K-correction is therefore not the total correction to a magnitude for redshift, but it is the difference between the bolometric correction for a galaxy at redshift z, and the bolometric correction for a galaxy at zero redshift, (Humason, Mayall & Sandage 1956). The other effects of redshift on magnitude are usually accounted for in the theoretical equations. Hubble & Tolman (1935) give a formula for the K-correction. If $I_o(\lambda_o)$ is the spectrum of an unredshifted source, $I(\lambda)$ the spectrum of a redshifted galaxy, $a(\lambda)$ the spectral response of the atmosphere and $p(\lambda)$ the spectral response of the photographic plate, then:

$$K = 2.5 \log \left\{ \frac{\int_o^\infty I(\lambda)\, d\lambda}{\int_o^\infty I_o(\lambda_o)\, d\lambda_o} \cdot \frac{\int_o^\infty I_o(\lambda_o) a(\lambda_o) p(\lambda_o)\, d\lambda_o}{\int_o^\infty I(\lambda) a(\lambda) p(\lambda)\, d\lambda} \right\}$$

The K-correction can be calculated as a function of redshift of $I_o(\lambda_o)$ is known as well as $a(\lambda)$ and $p(\lambda)$. Hubble & Tolman assumed that galaxies had a black body spectrum with $T = 6000^o K$.

The first measurement of the K-correction was made by Stebbins & Whitford (1948) who used broad band 6-colour photometry to find the intrinsic energy distribution of M32 which has a redshift of approximately zero. They found that the predicted change in colour of more distant galaxies due to redshift did not equal the observed change, and this difference was called the Stebbins-Whitford effect. It was thought to be due to a change in the colour of galaxies with time.

Oke & Sandage (1968) determined K-corrections out to z = 0.28 using spectrophotometry of giant E and SO galaxies, as well as M31 and M32. They define the K-correction in the same way as Hubble & Tolman (1935) and Humason, Mayall & Sandage (1956), but regard it from a slightly different point of view. The spectrum of a galaxy is denoted by $F(\lambda)$, and $S(\lambda)$ is the combined spectral response of the filters and the detector. Each observed wavelength, λ, originated at a wavelength of $\lambda/(1 + z)$ for a galaxy at redshift z. There are two components to the K-correction. The first arises if the spectrum is not flat, so that the flux detected by the photometer at wavelength from a redshifted galaxy, which is $F(\lambda/(1 + z))$. Secondly, the bandwidth observed for a redshifted galaxy is smaller by a factor of $(1 + z)$ than for a non-redshifted galaxy. The second effect is independent of the spectrum, $F(\lambda)$. For passband i, the K-correction in magnitudes is:

$$K_i = 2.5 \log (1 + z) + 2.5 \log \frac{\int_o^\infty F(\lambda) S_i(\lambda)\, d\lambda}{\int_o^\infty F(\lambda/1+z) S_i(\lambda)\, d\lambda}$$

The bolometric magnitude is then given as:

$$m_{bol} = m_i - K_i + \Delta m_{bol}(i)$$

where m_i is the observed magnitude through passband i, and $m_{bol}(i)$ is the bolometric correction. $m_{i\,corr}$, the magnitude of all galaxies seen through the same passband, is given by:

$$m_{i\,corr} = m_i - K_i$$

The values of $F(\lambda)$ were found from the spectrum of the galaxies which had been observed. In the ultraviolet, the spectrum of M32 was

different from that of the average giant elliptical galaxy. This explains the so-called Stebbins & Whitford effect, since the K-corrections derived from M32 had previously been applied to giant elliptical galaxies. When the K-corrections calculated from the giant ellipticals were used, the Stebbins-Whitford effect disappeared.

Several astronomers have found K-corrections in a similar way, such as Whitford (1971) and Schild & Oke (1971). More recently Pence (1976) has calculated the K-corrections for five different types of galaxy, E-SO, Sab, Sbc, Scd, Sdm-Im, out to redshifts of 1.00 for K_U, 1.40 for K_B, and 2.18 for K_V. The spectral energy distributions were obtained from the OAO-2 satellite observations for wavelenghts from 1500 Å to 3500 Å, from Wells (1972) between wavelengths 3500 Å and 5500 Å, and from Oke & Sandage (1968) for 5500 Å to 8000 Å. Two values of the K-correction are given. The first ignores galactic extinction, following Sandage (1973b) and Knapp (1975) who claim there is almost no extinction at the galactic poles, and secondly assuming $A_B = 0^m.23$ at the north galactic pole, which was the value provided by de Vaucouleurs from a revision of de Vaucouleurs & Malik (1969).

Part 2. Application of Galaxy Magnitudes to Cosmology

1.6 Observational Cosmology

Since Hubble's (1929) discovery that the light of galaxies is redshifted, many attempts have been made to measure the Hubble constant $H_o = \frac{\dot{R}_o}{R_o}$, and later the deceleration parameter, $q_o = \frac{-\ddot{R}_o R_o}{\dot{R}_o^2}$, which describes the rate of change of redshift with distance. (R_o is the

present distance scale of the ~~scale of the~~ universe.) The results obtained over the years have had widely ranging values. In 1929 Hubble calculated H_o to be 500 km s^{-1} Mpc^{-1}, but there was an error in the zero point of the period-luminosity relation of the cepheid variables used as distance indicators, and since then most determinations have given answers of between 50 and 100 km s^{-1} Mpc^{-1}. The value of q_o was first determined by Humason, Mayall & Sandage (1956) as 2.6, which means that the universe is closed. However, more recently values closer to zero have been obtained, indicating an open universe. It is now clear that q_o cannot be determined accurately using galaxy magnitudes until the evolution of galaxies is understood in more detail.

In the 1930s Hubble surveyed large areas of the sky down to faint limits using the 60-inch and 100-inch telescopes at Mt Wilson. Five sets of photographic plates were taken with different exposure times, for which the average limiting magnitudes were m_{pg} = 18.47, 19.0, 19.4, 20.0 and 21.03. The numbers of galaxies on each plate were counted and were reduced to standard conditions of a certain exposure time taken under good conditions at the zenith. The limiting magnitudes were found using a schraffierkassette or out-of-focus photometry of faint galaxies. With the results of the first two surveys (with magnitude limits of 19.4 and 20.0), Hubble (1934) examined the distribution of galaxies over the sky and investigated the effects of galactic extinction. He also carried out a preliminary survey into the distribution in depth of the galaxies, by comparing the numbers of galaxies in the two surveys.

In 1936 he published the results of the magnitude-limited counts using the five surveys (Hubble 1936c). It was found that the log N vs. m relation departed from the calculated one for a uniform distribution of galaxies, (neglecting the effects of curvature of the universe), which is

$$\log N = 0.6\,m + \text{const.}$$

The deviation was accounted for by the effect of redshift on magnitude. Hubble supposed that the magnitude correction, Δm, depended on distance, so that

$$\log \Delta m = 0.2\,(m - \Delta m) + b.$$

Then $$\log N = 0.6\,(m - 10^{0.2\,(m - \Delta m) + b}) + C.$$

b and C are constants which were found to be -4.239 and -9.052. Earlier, Hubble (1936b) had found the redshift-magnitude relation, which was

$$\log z = 0.2\,(m - \Delta m) - 4.707.$$

These two equations gave the magnitude correction as a function of redshift,

$$\Delta m = 2.94\,z.$$

Hubble used this relation to test whether or not the redshifts were velocity shifts. (The formulae for the effects of redshift on magnitude are given in section 1.5.) He assumed that the spectrum of a galaxy can be descrived by a black body of temperature $T = 6000^{\circ}K$, and calculated that $\Delta m \doteqdot 4z$ for an expanding universe and $\Delta m \doteqdot 3z$ for a universe which is stationary with the redshift being caused by some other effect. The observations fit the relation for a stationary

universe well, but disagree with the relation for an expanding universe, unless the magnitudes are affected by the curvature of space. Hubble calculated that, in the latter case, the universe must be small and closed with a density of 10^{-26} gm cm^{-3}. However, it is now known that T = 6000^{o}K is too high for the black body temperature of E galaxies, and in any case the spectrum cannot be approximated adequately by a black body (Oke & Sandage 1968). The K-corrections calculated by Hubble were therefore in error.

Another method of distinguishing between velocity and non-velocity redshifts was discussed by Hubble & Tolman (1935), namely the variation of the average surface brightness of galaxies with redshift. For a stationary universe in the absence of redshift, the surface brightness should be constant, because both the luminosity and the area decrease by a factor of $1/r^2$. When redshift is included, the surface brightness decreases by a factor of $1/(1 + z)$ due to the decrease in the bolometric luminosity by this factor (Hubble's 'energy effect'). However, if the universe is expanding, the bolometric luminosity decreases by a factor of $1/(1 + z)^2$ due to the number and energy effects, and also the solid angle subtended by a galaxy is larger than in the stationary case by a factor of $(1 + z)^2$, because since the light was emitted by the galaxy, the universe has expanded by a factor of $(1 + z)$. Therefore the surface brightness decreases by a factor of $1/(1 + z)^4$. The relationship between redshift and the parameter a in the Hubble formula for the light distribution in elliptical galaxies also depends on whether the redshift is a velocity redshift or not. Hubble & Tolman however did not have enough data to distinguish between the two kinds of redshift.

Since then it has nearly always been assumed that the redshifts are due to the expansion of the universe, and the observations discussed below have all been compared with the Friedman exploding model.

Humason, Mayall & Sandage (1956) investigated the redshift vs. magnitude relation for all types of field galaxies, the brightest galaxies in isolated groups, and for galaxies in rich clusters. The redshift data came from redshift surveys which had been carried out at the Mt Wilson and Mt Palomar Observatories, and at the Lick Observatory. The magnitudes were measured by Stebbins & Whitford (1952) and Pettit (1954) and they were corrected for the aperture effect as described in section 1.2. For different types of field galaxies graphs of bolometric magnitude vs. log cz were drawn, and a linear relation was fitted. To first order, the theoretical relation is

$$m_{bol} = 5 \log cz + (M - 5 - 5 \log H).$$

The coefficient relating m_{bol} and log cz was found to be approximately 5, and the constant term varied with the type of galaxy, depending on the absolute magnitude. However these magnitude vs. redshift diagrams had a large scatter due to the variation in absolute magnitude of the galaxies, the random motion of galaxies, selection effects favouring nearby intrinsically faint galaxies, and observational errors in m and z. It was found that the scatter could be reduced by observing the brightest galaxies in isolated groups, or the brightest cluster galaxies. In this case the absolute magnitudes are similar and, if the average redshift of the cluster or group is found,

the effect of random motion is removed leaving only the effects of the random motion of the cluster as a whole and the expansion of the universe.

The magnitudes of the 1st, 3rd, 5th and 10th ranked galaxies in clusters were used to study the m(z) relation in more detail, since observations of the brightest cluster galaxies probe the universe to greater depths. The mean differences were found between the magnitude of the 1st ranked galaxy and those of the 3rd, 5th and 10th ranked galaxies, and then all the magnitudes were reduced to those of the first ranked galaxies by adding the average differences. q_o was estimated using the formula by Robertson (1955):

$$m_{bol} = 5 \log cz + 1.086 (1 + q_o - 2\mu) z + \text{const.}$$

The parameter μ depends on the rate of change of the bolometric magnitude, $\dot{M}$, the rate of change of colour (i.e. the rate of change of the K-correction), $\dot{K}$, and the effects of intergalactic extinction $F(\lambda)$. $\dot{M}$ was calculated from theories of stellar evolution to be 0.3 mag/10^9yr. The colour evolution was estimated as $\dot{K}_{pv}$ = 0.0 mag/10^9yr, and $\dot{K}_{pg}$ = 0.3 mag/10^9yr. The value of H used was 180 km s^{-1} Mpc^{-1} which was calculated using revised distances to the galaxies. With no intergalactic extinction, the average value of q_o found from the photographic and photovisual bands was 2.6. If F_{pg} = 0.3 mag/$10^9$1 yr, q_o = 5. From these results it was concluded that the universe must be closed.

Another attempt to measure q_o was made by Baum (1957) using multicolour photoelectric photometry to find the energy distribution $E(\lambda)$. The redshift was calculated from the displacement of the $E(\lambda)$ curve, and the bolometric magnitudes were found by integrating under

the $E(\lambda)$ curve. No K-corrections were needed. The results gave $q_o = +1 \pm \frac{1}{2}$. This determination is more reliable than that of Humason, Mayall & Sandage because the spectrum of M32 measured by Stebbins & Whitford (1948) which was used to calculate the K-corrections gave rise to errors due to the poor resolution of 6-colour photometry and the abnormally blue colour of M32.

Sandage (1961) discusses the possibility of distinguishing between different cosmological models using the 200-inch reflector at Mt Palomar. Four separate tests are discussed. 1) The magnitude-redshift relation, 2) the number-magnitude relation, 3) the angular diameter-redshift relation, and 4) the age of the universe. He shows that it should be possible to distinguish between an open and a closed universe using the m(z) relation, but not using the N(m) relation. The angular diameter-redshift relation can be used, but this test is complicated by the fact that on a photographic plate isophotal diameters are measured and not metric ones. The relationship between isophotal diameter and redshift involves the variation of surface brightness with redshift (which is $1/(1 + z)^4$ for expanding models) and the intensity distribution law for the galaxies, such as the Hubble distribution. The age t_o of the universe can be calculated in terms of H_o and q_o alone. This value for the age can be compared with other estimates, such as the age of the oldest stars, as a check on the values of H_o and q_o, or on the validity of the model. Sandage used the value of $q_o = 1$ and $H_o = 75$ km s^{-1} Mpc^{-1} (Sandage 1958) to give $t_o = 7.4 \times 10^9$ yr, which was in contradiction with the ages of the oldest stars, estimated to be 20×10^9 yr old.

Recently, Sandage has investigated the redshift-distance relation to try to find q_o (Sandage 1972a,b,c, 1973a,b,c, 1975, Sandage & Hardy 1973), and along with Tamman he has tried to determine H_o (Sandage & Tamman 1974a,b,c,d, 1975a,b, 1976). In order to measure H_o, the distances to galaxies had to be carefully calibrated, and their redshifts found. Sandage & Tamman used three sets of distance indicators. For the nearest galaxies the magnitudes of the brightest stars were used to calculate their distances. Then, once the distances to the nearby galaxies were known, the size of the largest HII regions in galaxies were found as a function of absolute galaxy magnitude to enable the distances of more distant galaxies to be calculated. Finally, the luminosity classes of Sc galaxies were calibrated in terms of absolute magnitude, and ScI galaxies were used to extend the distance measurements even further. (Van den Bergh (1960) had discovered that the absolute luminosity of spiral galaxies could be estimated by the degree of development of the spiral arms and he assigned luminosity classes to spirals, the brightest being type I). Sandage & Tamman found that the velocity of expansion for nearby galaxies is regular, linear and isotropic, and they estimated H_o to be 57 km s^{-1} Mpc^{-1}.

This result was checked using the correlation discovered by Tully & Fisher (1977) between the width of the 21 cm line of hydrogen and the absolute B magnitude of a galaxy. The value obtained by this method was $H_o = 50$ km s^{-1} Mpc^{-1}.

Although the different estimates of H_o made by Sandage & Tamman are in good agreement and the errors quoted are of the order of ± 4 km s^{-1} Mpc^{-1}, they differ considerably from the value found by van den Bergh (1975) of 93 ± 7 km s^{-1} Mpc^{-1} by averaging the results of

twelve different methods. Kirshner & Kwan (1974), however, found $H_o = 60 \pm 15$ km s^{-1} Mpc^{-1} using the rate of expansion of type II supernovae. This method is independent of the distances measured to stars in the Galaxy or the Local Group. Branch (1977) used observations of type I supernovae and also obtained a low value for $H_o = 49 \pm 9$ km s^{-1} Mpc^{-1}. At present it seems likely that H_o lies between 50 and 100 km s^{-1} Mpc^{-1}, but the value cannot yet be determined more accurately.

While trying to determine q_o, Sandage examined the redshift-magnitude relation for the first-ranked cluster galaxies, radio, Seyfert galaxies and N galaxies, and Q.S.O.s. He found no evidence for non-cosmological redshifts in N galaxies or Q.S.O.s such as those found by Arp who claims that in certain groups of galaxies (e.g. Stephan's Quintet) one galaxy may have an excessive redshift (Field, Arp & Bahcall 1973). The Q.S.O.s in the Hubble diagram (the graph of log cz vs. magnitude) lie above the mean line for radio galaxies and Seyfert galaxies and Sandage assumes that this is because the Q.S.O.s are more luminous than the other galaxies. This is consistent with the theory that the light from Seyfert and N galaxies and Q.S.O.s is a combination of a normal galaxy and a non-thermal quasi-stellar source, the non-thermal source dominating in the case of quasars (Rowan-Robinson 1976).

The dispersion in the Hubble diagram for the first-ranked cluster galaxies is small, and Sandage shows that it can be mainly attributed to the scatter in absolute magnitude. The magnitude residuals were compared with the Bautz-Morgan type of the cluster and the cluster population. Bautz & Morgan (1970) had categorised clusters

according to the contrast in magnitude between the brightest galaxy and the next few brightest, type I clusters being dominated by a super giant cD galaxy, and type III having no galaxies significantly brighter than the other bright galaxies. Sandage found that the first-ranked galaxies were brighter in clusters of Bautz-Morgan type I. Having corrected the magnitudes for B-M types, the remaining residuals from the mean redshift-magnitude relation were examined according to the population N_c^{48} of the cluster or group. N_c^{48} is the number of galaxies counted on the 48-inch Palomar Observatory Sky Survey plates within 2 Mpc from the cluster centre, (using H_o = 54 km s^{-1} Mpc^{-1}), and within $2\overset{m}{.}5$ of the third brightest galaxy, corrected for background galaxies. It was found that there was a definite increase in the absolute luminosity with N_c^{48} for groups and small clusters, but only a slight increase for rich clusters.

The variation of colour with redshift was examined to test for colour evolution in galaxies. However the observed (B - V) and (V - R) colour changes agreed well with the predicted change from redshift only, so colour evolution does not affect the m(z) relation out to z = 0.5.

Mattig's (1958) formula was used to calculate the theoretical m(z) relation for a variety of values of q_o, and the value which minimised the residuals of the theoretical relation from the observed one was found. It was assumed that the cosmological constant, Λ, which measures the intrinsic curvature of space was equal to zero. The best value of q_o was 0.96, i.e. $q_o \doteq 1$, ignoring the effects of evolution. Tinsley (1972a) pointed out that q_o found using the m(z) relation for giant elliptical galaxies could be overestimated by at

least 0.5, because in these galaxies there is an initial burst of star formation, making them brighter in the past. Sandage estimated that the value of q_o could be reduced to zero if the luminosity evolution is $\dot{M} = 0.09$ mag/10^9 yr.

Finally, Sandage estimated the value of q_o from perturbations in the local velocity field. He used the redshifts of nearby groups and clusters in the southern hemisphere and the magnitudes of the brightest galaxies in each group to investigate the dependence of deviations from the Hubble diagram on direction or distance. The gravitational field of the Local Supercluster should slow down the rate of expansion of the surrounding galaxies so that the value of H_o obtained in the direction of the centre of the Supercluster (the Virgo Cluster) is above average for galaxies between our own Galaxy and the Virgo Cluster, and below average for galaxies beyond the Virgo Cluster. This perturbation in H_o can be used to find the local value of q_o, which is greater than the global value, giving an upper limit to the global value of q_o.

De Vaucouleurs (1958b) analysed the radial velocities of nearby galaxies and found that there was a rotation round the Virgo Cluster and that the rate of expansion near the dense central regions of the Supercluster was slower. Rubin, Ford & Rubin (1975) examined the velocities of ScI galaxies with $14 \leq m_{pg} \leq 15$ and found that the Hubble constant was greater in one half of the sky than in the other. Further evidence for this anisotropy has been given by Rubin & Ford (1975), who suggest that the Galaxy may have a velocity of 700 ± 200 km/s in the direction $l \doteqdot 200^o, b \doteqdot 5^o$. Sandage found that there was an

insignificant difference in H_o in the two Rubin, Ford & Rubin regions, and neither did he find evidence for the large motion of the Galaxy. However, Guthrie (1976) made an independent study of the Hubble relation using the brightest galaxies in the velocity range $4000 < V < 25000$ km/s, (a larger range than that used by Rubin, Ford & Rubin, and by Sandage) and his results agree with Rubin, Ford & Rubin. According to Gross (1977) this anistropy could be caused by patchy intergalactic extinction.

Sandage found no variation in H_o with supergalactic longitude (i.e. in the plane of the Supercluster), and the maximum variation in H_o in the centre-anticentre directions of the Supercluster as found from E galaxies gives

$$< \frac{dH}{H} > = 0.08$$

However, this result was given low weight, since the galaxies are mainly beyond the Virgo Cluster. The upper limits to the perturbation in H_o from ScI galaxies with distances less than 20 Mpc is

$$< \frac{dH}{H} > = 0.28$$

Silk (1974) calculated the relation between the density contrast and the velocity perturbation for different values of q_o. The density enhancement due to the Local Supercluster was calculated by comparing counts of galaxies in the direction of the centre and anticentre and was found to be $\delta\rho = 2.4$. This gives a value of $q_o = 0.02 \pm 0.02$ for $<\frac{dH}{H}> = 0.08$, or $q_o = 0.15 \pm 0.09$ for $<\frac{dH}{H}> = 0.28$. The upper limit on q_o was set at 0.28.

Sandage compared the values of q_o with values obtained by different methods.

1) The value of q_o detemined from the age of the universe is $q_o = 0.03 \pm 0.03$, assuming that $H_o = 50$ km s^{-1} Mpc^{-1}, and that the age of the universe is 4×10^9 yr more than the age of the galactic globular clusters. (Sandage & Tamman 1975b).

2) Gunn & Gott (1972) find $q_o < 0.1$ by considering the infall of matter in clusters to produce the observed X-ray luminosity.

3) A comparison of the observed deuterium abundance with the amount calculated to have been formed from the 'big bang' gives $q_o \lesssim 0.025$, (Rogerson & York 1973, Peimbert & Torres-peimbert 1974).

4) $q_o = 0.03$ from a calculation of the lower limit of the density of the universe by estimating the luminosity density of galaxies and the mass to luminosity ratio (Tamman 1973, Gott et al 1974).

Other attempts habe been made to find q_o using clusters of galaxies. Abell (1962) found that there is a break in the luminosity function of galaxies in clusters. (See section 1.7.) The magnitudes at this break can be used as a distance indicator (Bautz & Abell 1973) and it produces much less scatter in the Hubble diagram than the magnitude of the brightest cluster member. Bautz & Abell also calibrated the difference between the magnitude $m_{pv}(1)$ of the first-ranked galaxy and the magnitude at the break, m^*_{pv} as a function of Bautz-Morgan type and cluster richness. Their data are consistent with $q_o = 0$, although no evolutionary corrections are applied.

Austin, Godwin & Peach (1975) have also used m^*_v and agree that

it is a better distance indicator than the magnitude of the brightest cluster member. They found that the relation between redshift and m_v^* (corrected for galactic extinction and K-dimming) fits the line for $q_o = 1$. The same value for q_o was found by Austin & Peach (1974) using the radii of clusters as distance indicators.

Other estimates of q_o have been made recently by Gunn & Oke (1975) and by Hawkins & Martin (1977).

Gunn & Oke (1975) used spectrophotometry to find the monochromatic magnitudes and redshifts of galaxies in distant clusters out to $z = 0.6$. As in Baum's (1957) method, no K-corrections are needed. The value of q_o which gave the best fit to the Friedman model was

$$q_o = 0.31 \pm 0.68$$

$$\text{or } q_o = -0.15 \pm 0.57 \text{ omitting 3C295}$$

When evolution was considered, the value of q_o was

$$q_o = -0.43 \pm 0.54$$

$$\text{or } q_o = -1.27 \pm 0.62 \text{ omitting 3C295}$$

These negative values of q_o, if they are real, suggest that the cosmological constant, Λ, is non-zero, i.e. space has intrinsic curvature. It is usually assumed that $\Lambda = 0$, because there are too many uncertainties to enable H_o, q_o and Λ to be calculated from the observations. However, Peach (1970) estimated that $|\Lambda| \leq 2 \times 10^{-55} \text{ cm}^{-2}$. Another explanation of this low value of q_o is that it may be wrong to assume that the brightest elliptical galaxies in clusters become fainter with time.

Ostriker & Tremaine (1975) suggest that giant galaxies may accrete neighbouring galaxies by the process of dynamic friction, and this may result in an increase in the brightness (Gunn & Tinsley 1976).

Hawkins & Martin (1977) used the number-magnitude relation of faint galaxies on a UK Schmidt plate to calculate q_o. They examined the log N vs. log Area graph for the galaxy images, and used an empirical relation between magnitude and log A, which was linear. It was found that the log N vs. log A relation changed slope at about log A = 1.5 (A was in units of $(8\mu m)^2$ equal to about $(\frac{1}{2}$ arcsec$)^2$). This change in slope was assumed to be due to the fact that there is a decrease in the flux from galaxies at 4000 Å, and this part of the spectrum was being redshifted into the band pass of the 098 emulsion and the Schott 630 filter. Theoretical models, using Mattig's (1959) formula were fitted to the data, and the best value of q_o was 0.8 ± 0.3. This value is higher than most recent estimates, but evolution was not considered.

Baldwin et al (1978) also obtained a high value of q_o from the m(z) relation for quasars. They calculated continuum magnitudes using correlations between the equivalent widths of the emission lines C(IV)λ1946 and Mg(II)λ2800 and the continuum luminosities. The best fitting values of q_o were between 1 and 2, and $q \sim 0$ was ruled out at the 99% confidence level.

Combining the results from the determinations of q_o, it seems likely that q_o lies between 0 and 1. This means that we cannot yet distinguish between an open and a closed universe.

1.7 The Luminosity Function of Galaxies

The luminosity function describes the relative numbers of galaxies of different absolute luminosities. It is necessary to know the luminosity function when studying field galaxies because the sample will contain galaxies of different intrinsic luminosities and the apparent galaxy magnitude cannot be used accurately as a distance indicator. If the entire range of absolute magnitudes of galaxies (i.e. from M = -10 to M = -25) could be observed at each distance, the luminosity function would only enter into the number-magnitude relation as a constant factor. In practice, however, samples are chosen according to apparent magnitude and at different distances a different range of absolute luminosities is observed.

There are two types of luminosity function. The differential luminosity function $\phi(L)dL$ is the number of galaxies per unit volume with luminosities in the range L to L + dL, and the integrated luminosity function N(L) is the number of galaxies per unit volume brighter than L. The luminosity function is often determined in terms of the absolute magnitude of galaxies, i.e. $\phi(M_V)dM_V$ is the number of galaxies per unit volume with absolute magnitudes between M_V and $M_V + dM_V$.

Early determinations of the luminosity function for field galaxies were made by Hubble (1936a,b). First he used the distribution of absolute magnitudes of galaxies for which he had resolved the brightest stars, and then he examined the magnitude residuals in the redshift-magnitude relation. In both cases he found that the dispersion in absolute magnitude could be described by a normal distribution curve. Zwicky (1957) examined the luminosity function of galaxies in clusters and found that the numbers of galaxies increased exponentially

with decreasing luminosity, $\phi(M) = 10^{0.2M}$. This disagreement was cleared by Kiang (1961), who showed that Hubble's results were wrong because he obtained the luminosity function directly from the observed distribution of absolute magnitudes of a magnitude-limited sample, thereby introducing selection effects. However, Kiang's results did not agree completely with Zwicky's luminosity function. He found that the luminosity function could only be described by an exponential function in the faintest two-thirds of the magnitude range. For brighter galaxies the luminosity function increases more steeply with decreasing luminosity and Kiang fitted a power law with exponent 3. Van den Bergh (1961) also found that the luminosity function increases more rapidly at the bright end.

Abell (1962, 1975) has studied the luminosity function in several clusters of galaxies. He found that the differential luminosity function does not increase monotonically with decreasing luminosity and that there is a peak at about 2 magnitudes fainter than the brightest cluster galaxy, which gives rise to a change in slope of the logarithmic integrated luminosity function. If the magnitude at the change of slope is denoted by m^*, then the luminosity function has the form

$$\begin{aligned} \log N(m) &= K_1 + s_1 m \qquad m \leq m^* \\ &= K_2 + s_2 m \qquad m > m^* \end{aligned}$$

$$s_1 \doteq 0.75 \qquad s_2 \doteq 0.25.$$

m^* can be used as a distance indicator, producing a scatter with a standard deviation of only $0^m.1$ in the Hubble diagram. This is smaller than the scatter of almost $0^m.3$ using the brightest cluster galaxy

(Sandage & Hardy 1973). Austin, Godwin & Peach obtained $M_V^* = -21.0$ from the luminosity function of the cluster A1930 (assuming $H_o = 50\,km\,s^{-1}\,Mpc^{-1}$).

Arakelyan & Kalloglyan (1970) and Christensen (1975) have determined the luminosity function for field galaxies, which agree qualitatively with the results of Kiang and Abell. They found a change in the slope of log N(M), but not a peak in $\phi(M)$. Abell (1975) suggests that this peak may be formed from galaxies in the cores of clusters. Christensen used data from the 'Reference Catalogue of Bright Galaxies' (de Vaucouleurs & de Vaucouleurs 1964), and found the luminosity function for eight different morphological types: Irr, E, SA0-0/a, SAa-bc, SAc-m, SB0-0a, SBa-bc, SBc-m. He found that:

1) There was no difference between the luminosity function for barred (SB) and unbarred (SA) spirals.

2) There were hardly any faint early spirals of $M_B > -18$.

3) The ratio of late to early spirals increases with decreasing luminosity.

4) There were no elliptical galaxies with $-16 > M_B > -18$, suggesting there are two types of ellipticals, giants with $M_B < -18$, and dwarfs with $M_B > -16$.

5) There is a wide range in the magnitudes of irregular galaxies, although none are found as bright as the brightest galaxies.

Schechter (1976) derived an analytical function which fits the observed distributions of field galaxies and cluster galaxies. It is

in the form:

$$\phi(L)dL = \phi^*(L/L^*)^{\alpha} \exp(-L/L^*)\, d(L/L^*)$$

where ϕ^*, L^* and α are parameters. ϕ^* is the number of galaxies per unit volume, and L^* is a characteristic luminosity, like Abell's m^*. The values of the parameters were found to be similar for field and cluster galaxies, using data from the 'Reference Catalogue of Bright Galaxies' (de Vaucouleurs & de Vaucouleurs 1964), and Oemler's (1974) observations of cluster galaxies.

$$\alpha = -5/4$$

$$M^*_{B(0)} = -20.6 + 5 \log(H_o/5)$$

$$\phi^* = 0.005\,(H_o/50)^3\ \mathrm{Mpc}^{-3}$$

($M^*_{B(0)}$ is the face-on B magnitude corresponding to L^*.)

Turner and Gott (1976) have compared the combined luminosity functions of 63 groups of galaxies with Schechter's formula. The data fit the expression quite well between $M_{pg} = -23$ and $M_{pg} = -16$. If α is set to 1, $M_{pg}^* = -20.85$. This provides evidence that Schechter's luminosity function can be used as a 'universal' luminosity function.

1.8 Evolution of Galaxies

As stated in the previous sections, it is necessary to know how evolution has affected the luminosity of galaxies before the magnitudes can be used as distance indicators in the study of cosmology. It is usually assumed that all types of galaxies have about the same ages, because the spheroidal components of galaxies contain only old stars and observations suggest that spheroidal systems are relaxed (Sandage, Freeman & Stokes 1970). Most of the evidence for the ages of galaxies

comes from studying the metal abundances of stars, assuming that heavy elements are synthesised in stars and are then ejected into the interstellar medium. This gas is subsequently incorporated in the next generation of stars which show a higher metal abundance. Van den Bergh (1974) has shown that the metal abundances within a galaxy are highest in the densest parts of the galaxy, and explains this by suggesting that dense regions favour the formation of massive stars which evolve rapidly producing heavy elements. He also finds evidence from the globular clusters in the Galaxy, M31, and the Magellanic Clouds, that M31 is older than our Galaxy by 10^9 yr and that the Magellanic Clouds are younger by 10^9 yr.

Galaxy formation and evolution can be considered from two points of view. Firstly there is the theoretical study of irregularities in the universe which collapse to form protogalaxies (or protoclusters which fragment to form galaxies). There are two main theories which are discussed by Peebles (1974). The first is the theory of gravitational instability in which perturbations grow out of statistical fluctuations in the gas density. This was first considered by Jeans (1928) who calculated the criterion for the collapse of density perturbations. Arguments against this theory are that galaxies may form too slowly and that it cannot explain the rotation of galaxies. Peebles (1968) suggested that the angular momentum of galaxies could arise through tidal interaction. An alternative theory, first put forward by Weizacker (1951), is that galaxies may form from turbulent gas clouds. This theory has been revived using 'big bang' models of the universe. During the early stages of the universe, when the temperature was higher, matter and radiation interacted, and under these conditions

turbulent eddy motions are found to grow. This theory can explain the rotation of galaxies and the observed rotation and alignment of galaxies in superclusters (Ozernoy 1974).

The second method for forming models of galaxy evolution is to synthesise the properties of galaxies we see now, such as integrated luminosities, colours, mass to light ratios, ratios of the mass of gas to the mass of stars, and the metal abundances of stars. The models are generally based on two other pieces of evidence. Eggen, Lynden-Bell & Sandage (1962) observed dwarf stars in our Galaxy and found a correlation of the eccentricity of their orbits and their space velocities with their ultra-violet excesses. An ultra-violet excess indicates metal deficiency, and it was concluded that the first stars formed during the collapse of the protogalaxy. Schmidt (1963) showed that the rate of formation of stars was greater in the past and also that relatively more bright stars were formed in the past. This indicates that galaxies were brighter in the past.

Larson (1974, 1975, 1976) considered models for elliptical and spiral galaxies forming from the collapse of protogalaxies. The models involve specifying the mechanism for energy loss in the gas, the rates of star formation and of stellar mass loss, and the rate of heavy element production. The rate of star formation used by Larson in most models depends on a power of the gas density, which was in the form suggested by Schmidt (1959), although it was shown by Reddish (1968) that it is the mass of gas which determines the rate of star formation, not its density. The initial mass function for stars was assumed to be given by $\frac{dN}{dm} \propto m^{-(1+x)}$ between upper and lower limits, where x is a free parameter. If x = 1.35, this gives the relation

discovered by Salpeter (1955) from an analysis of observational data.

For protogalaxies which are rotating, turbulent viscosity is required to transfer angular momentum outwards and allow the protogalaxy to contract. In elliptical galaxies, there is a high initial rate of star formation and the galaxy is very luminous. If a spiral galaxy is to form, some mechanism is required to slow down star formation until the gas has condensed into a disk. It was found that if there was not enough viscosity, or a high angular momentum, a small disk was formed. The formation of late type galaxies with a small bulge:disk ratio requires the star formation to be inhibited by tidal forces from the surrounding gas. Larson concludes that there are two stages in the star formation in spiral galaxies. The first is the rapid development of the spheroidal component, similar to the formation of elliptical galaxies, and then there is a slower phase of star formation in which the gas settles into a disk, before forming stars.

Gott (1973) assumes that a large fraction of the stars have formed before the elliptical galaxy collapses, although Larson argues that this does not form a dense enough nucleus. Gott & Thuan (1976) suggest that the key factor in determining whether a galaxy is elliptical or spiral is the amount of gas remaining at the time of maximum collapse. This depends on the ratio of the time scale for star formation to the time scale for collapse, τ_s/τ_c, which is large in elliptical galaxies and small for spirals. They conclude that ellipticals form out of more dense protogalaxies than spirals. Their theory also explains why there is a higher percentage of elliptical galaxies in clusters, where the gas is likely to be dense.

Tinsley (1972b) has formed models of galaxies using the evolutionary tracks of stars on the H-R diagram to deduce the evolution in luminosity, colour and metal abundance. She also considers analytical functions for the luminosity evolution (Tinsley 1973) and shows how different parameters used in star formation can affect the results. For elliptical galaxies, the stars in which are old, the 'initial burst' approximation for star formation may be used to synthesise the red colours observed now. In the case of spirals, the stars in which are bluer, continuous star formation becomes important in later types, and in irregulars. Larson & Tinsley (1974) examined the predicted colours and luminosities of Larson's (1974) model for a spheroidal galaxy with no rotation. The photometric properties depend mainly on the total rate of star formation as a function of time, and to a lesser extent on the initial mass function for stars. Models in which nearly all the star formation took place within 2×10^9 yr have colours and M/L ratios similar to elliptical galaxies.

In some of Larson's models (those with expanding boundaries) star formation continued and the colours and M/L ratio are similar to spirals. Galaxy colours are found to become redder with time, and the results fit reasonably with Oke & Sandage's (1968) observation that (B - V) does not change by more than $0^m.3$ for redshifts up to z = 0.2. For elliptical galaxies the rate of change of absolute magnitude is greater than for spirals, and using the Salpeter initial mass function, is given by

$$\frac{dM_v}{d\ln t} = 0.87 .$$

Reddish (1975) has considered galaxy evolution on the basis of arguments that star formation takes place due to fragmentation caused by hydrogen molecules forming on interstellar grains. This model contains no free parameters as do the other models. In gas clouds hydrogen atoms are adsorbed on to the surface of grains, where they combine to form molecules. The rate at which this process takes place depends critically on the temperature of the grains, which, it is argued, varies throughout the cloud on scales of about one optical depth. In the cooler parts of the cloud, hydrogen molecules form faster, decreasing the internal pressure and causing the cloud to fragment into protostars. The sizes of the fragments vary inversely with the density so that only below a certain density do the fragments have enough gravitational self attraction to contract to become stars. However, radiation from these stars dissociates the hydrogen molecules, causing an increase in pressure, and producing a shock wave which compresses the smaller fragments at the centre of the cloud, enabling them to collapse to form stars of lower mass. This model fits the observations of associations of OB stars surrounding dense T-associations. Also, the calculated initial mass function is similar in form to that observed by Salpeter.

The rate of star formation depends on the rate of formation of the hydrogen molecules which is governed by the grain temperature. Since the grain temperature depends mainly on the radiation field, the rate of star formation is also controlled by the radiation field. This gives rise to a negative feedback loop which regulates star formation. The grains cool, hydrogen molecules form, star formation takes place, and the grains heat up. The star formation rate therefore

decreases resulting in the grains cooling down again. If this negative feedback loop operates on cosmological scales, the star formation rate will depend on the cosmic radiation field which consists of the combined radiation of galaxies and the cosmic background radiation. The cosmic radiation field is detected as the universe expands, so that the rate of star formation will ultimately depend on the rate of cosmic expansion, i.e. on the Hubble constant, H. The current rate of star formation can be calculated from the rate of condensation of mass into stars required to maintain the cosmic star density. This gives a rate slightly higher than the observed rate in the Local Group, but the data on cosmic expansion and the cosmic radiation field are still inaccurate.

Models of galaxies are considered starting with the ratio of the number density of grains to that of hydrogen of $n_g/n_H = 10^{-15}$. First supermassive objects of $10^{10} M_\odot$ form producing a large amount of helium and some metals which increase the number density of grains. As the protogalaxy contracts, the density increases and smaller fragments producing stars of masses 30 to $10^3 M_\odot$, similar to the masses of type II supernovae. These stars eject large amounts of heavy elements, and as the density increases large numbers of dwarf stars form. Subsequently, as the number density of grains increases, star formation continues and the average stellar mass gradually increases.

This model agrees well with the observations that there was a rapid initial rise in the helium abundance in the Galaxy and then an outburst of heavy element production followed by the formation of many

dwarf stars. After a period of 10^{10} yr since formation, the model also has a similar M/L ratio and M_{gas}/M ratio as the Galaxy, and the metal abundance agrees with that of the Sun. These properties for elliptical galaxies can be produced by assuming that there is an overshoot in the rate of star formation. This is caused by a delay of about 10^{6} yr between the formation of H_2 molecules and the time when stars output radiation. The effects of this delay in the negative feedback loop will be greater in a cloud of lower than average temperature. Thus, the Hubble sequence of galaxies arises from a range in initial temperatures of the protogalactic gas clouds. The cooler the cloud, the larger the bulge:disk ratio.

All of the theories of galaxy evolution discussed can produce the observed properties of galaxies at the present. However, some models depend on assigning values to free parameters, such as the rate of star formation, in order to simulate the properties, and so the validity of these models at the early stages of evolution is uncertain. All models agree that there was an early burst of star formation in ellipticals while in later types of galaxies star formation has continued to the present day. The initial conditions determining which type of galaxy will form may be a combination of those suggested by Larson, Gott and Thuan, and Reddish. For example, elliptical galaxies may form in cool clouds which are dense and viscous. Nevertheless, observations of young galaxies, i.e. distant galaxies are required to confirm that this picture of galaxy evolution is correct, and also to try to establish the time of galaxy formation.

In most cases the correct cosmological model must be known in

order to determine the effects of evolution unambiguously. However the variation of surface brightness with redshift is insensitive to the cosmological model and this ought to show how the luminosity of a galaxy has evolved. (It is assumed that the redshift of galaxies is due to the velocity of recession, in which case without evolution the surface brightness is $\propto 1/(1+z)^4$, otherwise if the redshift is due to some other cause, the surface brightness is $\propto 1/(1+z)$). Gudehus (1975) suggested that the variation of central surface brightness B(0) with redshift could be used to test for luminosity evolution. This may be difficult from the observational point of view. Petrosian (1976) proposed that the surface brightness defined within an isophotal diameter could be used. However Tinsley (1976) has shown that the tests suggested by Petrosian are not as sensitive to evolution as expected. This is because both the luminosity within a given isophote, and the angular size within the isophote are affected by evolution and the two effects almost cancel. The only way of using this test is to carry out detailed surface photometry of galaxies to calculate the surface brightness within radius r defined such that the ratio of surface brightness within r to the surface brightness at r is a constant value for galaxies at different redshifts.

Tinsley (1977a) estimated the effects of evolution on the colour-redshift relation, the distribution of redshifts at a given apparent magnitude, the number-magnitude relation, and the intensity of cosmic light. All these relations are more sensitive to evolution than to the cosmological model. A model was used to calculate the luminosities and spectral energy distributions of galaxies at all times. The initial properties of a galaxy, i.e. a primeval galaxy,

were taken from a model by Meier (1976). In the case of older galaxies the UBVr magnitudes were calculated relative to the present day observations, assuming a star formation rate found from models mainly by Larson & Tinsley (1974). At intermediate stages in the development of the galaxy the properties were found by interpolation. Five different Hubble types of galaxies were considered, E, Sab, Sbc, Scd, and Sdm. The present spectral energy distributions were taken from Pence (1976) and the luminosity function was of the form proposed by Schechter (1976). Friedman cosmological models were used with $\Lambda = 0$ and $q_o = 0.02$ or 1.0 and $H_o = 50$ or 75 km s^{-1} Mpc^{-1}. The time of formation t_F or the redshift of formation z_F and the present ages of galaxies $t_o - t_F$ were varied.

The quantitative results of the models are uncertain but should give an idea of the qualitative effects of evolution. Galaxies are expected to appear slightly bluer at high redshifts ($z > 0.5$) with evolution, especially in the case of elliptical galaxies. Colours are sensitive to the redshift of formation of galaxies and become bluer at redshifts greater than 0.5 as z_F is decreased from 6.2 to 1.92. Observational evidence of this is perhaps given by the faint blue clustered galaxies found by Hawkins and Reddish (1975).

The distribution of redshifts N(z) for galaxies of a given apparent magnitude should be smooth, but if evolution is included and z_F is low ($\leqslant 3.5$) then the numbers may start to increase at redshifts of $z > 0.5$. The log N(m) relation was compared with that for a stationary Euclidian universe (the numbers for this being denoted by N_o). With evolution the numbers are greater by a factor

of three or more for magnitudes greater than 20. There is also a maximum in the log $N/N_o(m)$ relation which increases with decreasing z_F. If t_F, the time of galaxy formation, is known there is a large difference between the relation for models with $q_o = 1$ and $q_o = 0.02$. A rough value for q_o may be obtained by fitting observations to this relation, provided the time of galaxy formation can be established. These results could be altered if young galaxies are not detected either because they are unresolved and mistaken for stars, or because there is high internal extinction by dust. The intensity of cosmic light is also affected and should be brighter with evolution, unless galaxies are hidden by dust.

Ellis, Fong & Philipps (1977) have examined angular diameter counts on the UK Schmidt telescope photographs to find the selection function $\phi(z)$ defined as the probability of detecting a galaxy at redshift z. If the number of galaxies observed at redshift z is n(z) then

$$n(z) = \phi(z) \frac{dV_p}{dz} \rho_p$$

where dV_p is the proper volume element and ρ_p is the proper number density of galaxies. They found that it was necessary to include Tinsley's luminosity evolutionary corrections to account for the slope in the angular distribution curve at large angular diameters.

Several attempts have been made to detect primeval galaxies assuming their properties from theories of galaxy formation. These are defined as galaxies with an initial high rate of star formation which makes them much more luminous than galaxies are now. If star formation occurs before the collapse has taken place these objects

will be extended. Partridge (1974) and Davis & Wilkinson (1974) searched for extended objects at high redshifts. However they had no success. Kaufmann & Thuan (1977) attribute this to the fact that young galactic halos are too faint to have been detected by them. Meier (1976) detected two objects at high redshifts of $z = 3.4$ and $z = 2.9$ which he has put forward as candidates for primeval galaxies. He suggested that primeval galaxies at their maximum luminosity are much smaller than the objects considered by Partridge, and that they will appear as red quasi-stellar objects.

Quasars have also been considered as representing stages in the formation of galaxies. This was first suggested by Field (1964) who showed that the simultaneous formation of large numbers of massive stars in the dense centre of a collapsing cloud could account for the high luminosities of quasars. Kristian (1973) has photographed quasars on the 200-inch telescope at Mt Palomar to look for underlying galaxies. He detected galaxies round low redshift quasars, but not round the high redshift ones, because presumably they were too distant to be resolved. This provides evidence that quasars occur in the nuclei of galaxies and also confirms that the redshifts of quasars are at least largely cosmological. Larson (1974) discussed quasars as a stage in the formation of elliptical galaxies. In later stages for formation the remaining gas will be drawn into the centre of the galaxy to form a dense nucleus. This may give rise to the formation of massive stars which produce supernovae, and/or a black hole, which is required by many theories to explain the large amounts of non-thermal radiation output by quasars.

Quasars have been observed with redshifts of $z = 3$, which overlaps with the expected redshift of $2 < z < 5$ for the formation of galaxies. However quasars and similar objects like N galaxies and Seyfert galaxies are also observed with low, almost zero redshifts, which either indicates that galaxy formation is still continuing, or that quasar activity may occur in later stages of evolution of a galaxy. This activity may be triggered by a remnant of the initial gas cloud, or an intergalactic gas cloud falling into the nucleus of the galaxy. Weedman (1976) finds that the upper limit for quasar luminosities of 5×10^{47} ergs/s is independent of redshift for $z > 0.1$ if $q_o = 0$, otherwise q_o must be negative. This observation could indicate that quasars form at all redshifts.

However, Lang, Lord, Johanson & Savage (1975) have examined the Hubble diagram for normal galaxies, radio galaxies and quasars. The scatter in the diagram is similar for all three classes of object, and the slope of the least squares fitted straight line is compatible, within errors, with that for a homogeneous isotropic expanding universe in each case. The three types of object occupy different parts of the diagram. The quasars are intrinsically the brightest and have the highest redshifts, the normal galaxies are the least bright, having low redshifts, while the radio galaxies have intermediate properties. This suggests that the Hubble diagram shows an evolutionary sequence of galaxies from bright young quasars through less bright radio galaxies to fainter normal galaxies.

1.9 Other Factors affecting the N(m) Relation

The N(m) relation will be affected if the total number of galaxies does not remain constant with time. As mentioned in

section 1.6, Ostriker & Tremaine (1975) suggested that large galaxies may accrete smaller galaxies by dynamical friction. This process will affect mainly the galaxies in the centres of clusters. On the other hand Vorontsov-Vel'yaminov (1976) has concluded that satellite galaxies are formed from within parent galaxies and gradually separate. However the satellite galaxies may not be detected because they are too faint, or because they are not resolved from the main galaxy. If the numbers of galaxies per unit volume increase with time, the value of q_o obtained from N(m) counts will be too low, and if the value of q_o is assumed from another source, the amount of luminosity evolution deduced from log N(m) will be underestimated.

A greater effect on the N(m) relation may be due to the irregular distributions of galaxies. In most models it is assumed (mainly for convenience) that the universe is homogeneous and isotropic. However the universe is certainly not homogeneous, unless the numbers are averaged over large scales, because of the existence of clusters and superclusters of galaxies. Shane & Wirtanen (1954) discovered clouds (superclusters) of galaxies in a preliminary analysis of the Lick Survey. The existence of superclusters was confirmed by Abell (1961) who studied 17 superclusters on the Palomar Observatory Sky Survey photographs, and found that they have an average diameter of about 50 Mpc (using H_o = 75 km s^{-1} Mpc^{-1}) or 37.5 Mpc (using H_o = 100 km s^{-1} Mpc^{-1}). Shane (1974) discusses larger scale inhomogeneities of 200 Mpc in size (using H_o = 100 km s^{-1} Mpc^{-1}) found by Shapley. If such large scale irregularities exist, the results of the N(m) relation

may vary depending on the direction in the sky, and the depth of the survey.

The light from galaxies may be dimmed by the presence of intergalactic dust. De Vaucouleurs, de Vaucouleurs & Corwin (1972) detected an excess reddening of galaxies in the plane of the Local Supercluster. They estimated that the total optical depth through the centre of the Supercluster is $B = 0^m.2$ to $0^m.3$. Dodd et al (1975) searched for clouds of obscuring matter in a study of 3000 faint galaxies. An analysis of the distribution of nearer galaxies showed that there were blank regions which could not be account for by a random distribution. However, these could not be due to intergalactic clouds, because more distant galaxies were visible in these regions. It was concluded that the blank areas were due to clustering rather than intergalactic matter.

Chitre & Narlikar (1976) tried to account for the cosmic background radiation without the 'big bang' theory, by supposing that there is an intergalactic medium of needle-shaped graphite grains. These absorb the radiation from galaxies and re-emit it at millimeter wavelengths. The decrease in magnitude caused by this effect will produce an underestimated value of q_o. Chitre & Narlikar estimate that the change in q_o will be of the same magnitude as the evolutionary effect, but in the opposite direction.

The conclusions drawn from N(m) counts depend on the validity of the cosmological model. Many assumptions are made in choosing a Friedman model with zero cosmological constant. If an inappropriate model is chosen, the value of q_o will not represent the deceleration

of the expansion of the universe. This will lead to the wrong value being found for the rate of evolution. If a value of q_o lower than the true value is found, the amount of luminosity evolution will be underestimated, and vice-versa.

The Friedman cosmological model assumes that the universe is expanding. However it is possible that the redshift of galaxies is caused by some mechanism other than a velocity shift. Krat & Gerlovin (1974) have suggested that the vacuum of space is filled with proton-antiproton pairs, and that radiation interacts with these particles, losing energy of an amount proportional to the distance travelled. If the universe is really stationary, the cosmological constant must equal the critical value found by Einstein of Λ_c to prevent the universe collapsing under gravity. The type of redshift proposed by Krat & Gerlovin will change the bolometric magnitude of a galaxy by a factor of $1/(1 + z)$ instead of $1/(1 + z)^2$. If a Friedman model is applied to a universe which is really stationary, the luminosity distance will be overestimated and q_o will be found to be negative.

It is possible that the redshift of galaxies is caused partly by the expansion of the universe, and partly by some other effect. Arp has put forward evidence to show that some galaxies have peculiar redshifts, while other astonomers such as Bahcall disagree, (Field, Arp & Bahcall 1973). Since the majority of galaxies obey the Hubble relation, the discrepant redshifts should not affect the results of a survey.

The effect of a non-zero cosmological constant in expanding models must also be examined. If $\Lambda > 0$, there is an extra repulsive

force, and if $\Lambda < 0$ there is an extra attractive force. Therefore for $\Lambda > 0$, q_o will be calculated to be too small. If q_o is found to be negative, then Λ must be positive. Models with $\Lambda > \Lambda_c$ can be ruled out, however, because in these models the expansion of the universe is almost zero at one epoch, producing observational properties different from other Friedman models (Tinsley 1977b).

Finally, it is normally assumed that the physical constants do not vary with time. Baum & Florentin-Nielsen (1976) have shown that the atomic constants h (Planck's constant), c (the velocity of light) and m (the mass of a proton) are constant to within observational errors. However, the gravitational constant G may vary. Van Flandern (1975) analysed data on lunar occultations to find that $\dot{G}/G = (8 \pm 5) \times 10^{-11}$ yr^{-1}. Several cosmologies have been developed with a decreasing gravitational constant, such as that of Hoyle & Narlikar (1972). A larger value of G in the past would mean that galaxies were brighter in the past, and would lead to a large value of q_o being found. Barnothy & Tinsley (1973), however, argue that Hoyle & Narlikar's theory predicts that distant galaxies will be brighter and bluer than those observed.

2. THE METHOD FOR CALCULATING GALAXY MAGNITUDES

2.1 The Schmidt Plates

The photographic plates used in this project were all taken with the 1.2 m aperture UK Schmidt telescope at Siding Spring in Australia. They were provided by the Schmidt Telescope Unit, some being plates rejected from the Southern Sky Survey, although they were not of poor quality. Kodak IIIaJ emulsion was used, which is fine grained and produces a high contrast in the developed plates. Before exposing, the plates were sensitised by soaking in nitrogen and then hydrogen. The exposures were taken with a Schott GG395 filter, which, with the IIIaJ emulsion produces a passband similar to the Johnson B band, but extending further into the yellow to about 540 nm. The magnitudes determined using this passband will be denoted by m_j.

The plates are 356 mm square and cover an area of 6.6 degrees square on the sky, giving a plate scale of 67.2 arcsec/mm. For exposure times of about one hour, the limiting stellar magnitude is B = 23, (Reddish, Corben & Sim 1974). The number density of images detected on each plate depends on galactic latitude. Most of the plates used in this project were taken at high galactic latitudes, where there are on average 2 to 5 images mm^{-2}. Each plate has two step wedge exposures for calibration purposes, one on the north side and the other on the east. The exposure for the step wedge is made at the same time as the sky exposure, so that they are taken under the same conditions in order to obtain a true calibration.

2.2 The COSMOS Measuring Machine

The plates were measured on the COSMOS measuring machine at the Royal Observatory, Edinburgh. COSMOS (Co-ordinates, Size, Magnitudes, Orientation and Shape), was designed for use with the UK Schmidt plates to give fast and accurate measurements of the thousands of images (galaxies and stars) photographed, (Pratt et al 1975).

In the machine the plate rests on a horizontal carriage which is moveable in the X and Y directions, the position being measured to an accuracy of $\pm\frac{1}{2}$ μm using moiré gratings. The light source is a micro-spot cathode ray tube the beam from which is focussed onto the photographic emulsion. A photomultiplier is situated below the plate to detect the transmitted light, which is measured to an accuracy of 1%. The resulting voltage, proportional to the plate transmission, is converted into relative transmission values in integers, ranging from 0 - 127 using an analogue-to-digital convertor. Two different modes of operation of COSMOS were used: mapping and coarse.

In the mapping mode the transmission is measured every 8 μm. The measurements are carried out in lanes 1024 μm wide, (128 x 8 μm units), which are scanned in a raster fashion. The rows are scanned by moving the spot from the cathode tube, and the movement along each lane is provided by the Y-motion of the carriage. The data is output on magnetic tape in blocks of 1024 transmission values, i.e. 8 rows at a time.

The coarse measurement mode has the same scanning system but uses an on-line computer to detect images, by finding the points with transmissions below a certain threshold level. The parameters output for each image are the x and y coordinates of the centre of the image and the x and y extents, all of which are in units of 0.1 μm, the minimum transmission in COSMOS transmission levels, and the area of the image at the threshold level in units of $(8\ \mu m)^2$. The threshold is set at any chosen level, in this case, three standard deviations below the mean transmission level of the sky, and is altered automatically to take account of the variation in the average background transmission across the plate.

2.3 A General Description of the Method

The magnitudes were calculated using mapping and coarse measurement data from COSMOS. An area of between 4 and 5 cm^2 on the plate was used since this size of region could be mapped onto one magnetic tape. There are usually 500 to 1000 images in an area of this size. The coarse measurement data was used to locate the images and to separate stars from galaxies, while the mapping measurements were used to calculate the magnitudes. The calibration from transmission to intensities was determined from mapping measurements of one of the step wedges, and the zero point was obtained from photoelectric measurements of the night sky.

All the COSMOS measurements were carried out by the COSMOS staff. The computer programs required to reduce the data were run on the ICL 1906A computer at the Atlas Computing Laboratory.

In the processing of the mapping measurements, the reduction of the step wedge data was carried out first. Each step wedge consists of 7 steps of approximate size 6 mm x 3 mm. The ratios of intensities between the steps are given in table 2.1. Only one step wedge could be measured at a time by COSMOS without altering the position of the plate in the plate holder. Therefore, the step wedge nearer to the region of interest was used.

There are not enough transmission levels on COSMOS to cover the range from clear plate with a density of D = 0.2 to the density of the densest step of the step wedge, of D = 3.0, so the step wedge had to be measured twice: once with the photomultiplier E.H.T. voltage on COSMOS set at the same level as that used for measuring the galaxy region, and a second time with the E.H.T. voltage lowered so that clear plate could be measured. The second set of measurements were scaled to the first set.

The minimum transmission number output by COSMOS is never lower than 2 or 3 arbitrary transmission units, even for a completely opaque object which should have T = 0. Before the measurements could be scaled therefore, the zero points had to be subtracted. The transmission values for the steps were converted to Baker densities, Δ, using the formula:

$$\Delta = \log_{10} \left(\frac{T_f - T_o}{T - T_o} - 1 \right)$$

TABLE 2.1

The Relative Intensities of the Steps on the Calibration Wedge

Step	Relative Intensity	Log(Relative Intensity)
1	72	0.858
2	115	2.061
3	185	2.268
4	285	2.455
5	437	2.640
6	676	2.830
7	1000	3.000

where T = transmission value

T_f = transmission of plate fog (clear plate)

T_o = zero point, i.e. the transmission measured on COSMOS for an opaque object.

Baker density is so called because it was first noticed by Baker (1949) that this quantity gives an almost linear relation with log intensity over a range of transmission from 0.002 to 1.000.

The transmissions of the steps were found using a combination of two methods. First, the average transmission of each block of mapping was found and plotted on a graph of transmission vs. number of blocks along the wedge, (which is distance in units of 128 μm). The steps at low transmissions can be seen clearly in this way, but the steps at high transmissions are affected by noise. To overcome this, a histogram of transmissions in the region was also plotted, which contains peaks at the transmissions corresponding to the steps. The average transmissions of the steps were found from the centres of the peaks. Examples of the two graphs are given in figures 2.1 and 2.2.

Once the transmissions of each step were found, they were converted to Baker densities using the formula given above. The relation between Baker density and log intensity was found by fitting a straight line using the least squares method. This relation, inverted, gives the calibration for intensity in terms of transmissions

FIGURE 2.1 TRANSMISSIONS ALONG THE EAST STEP WEDGE, PLATE 2520.

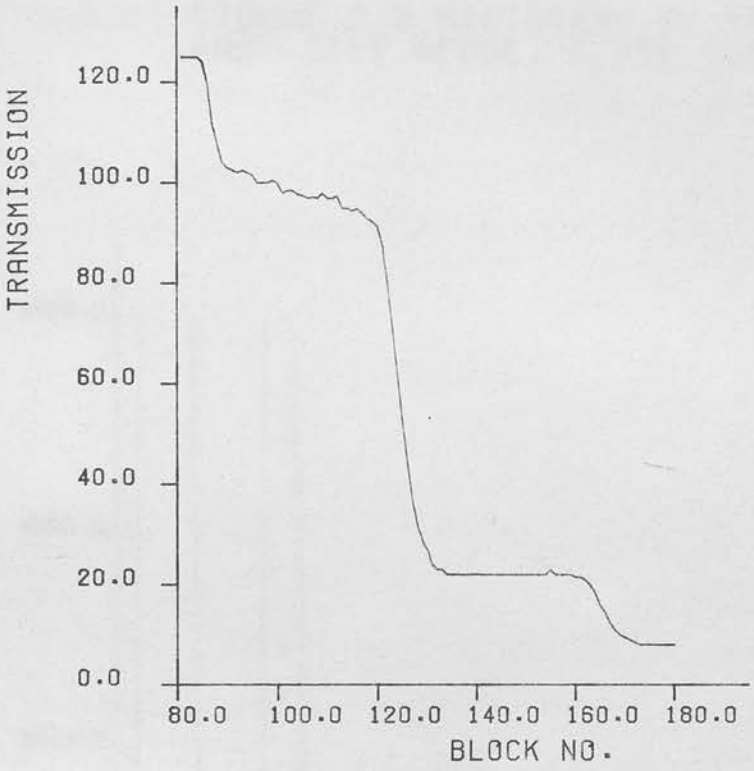

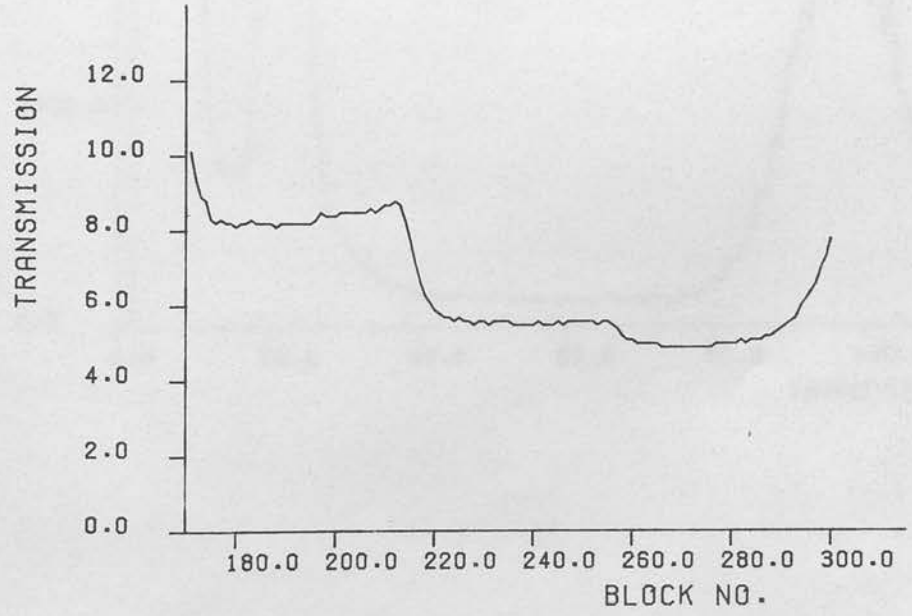

FIGURE 2.2 HISTOGRAM OF TRANSMISSIONS IN THE EAST STEP WEDGE, PLATE 2520.

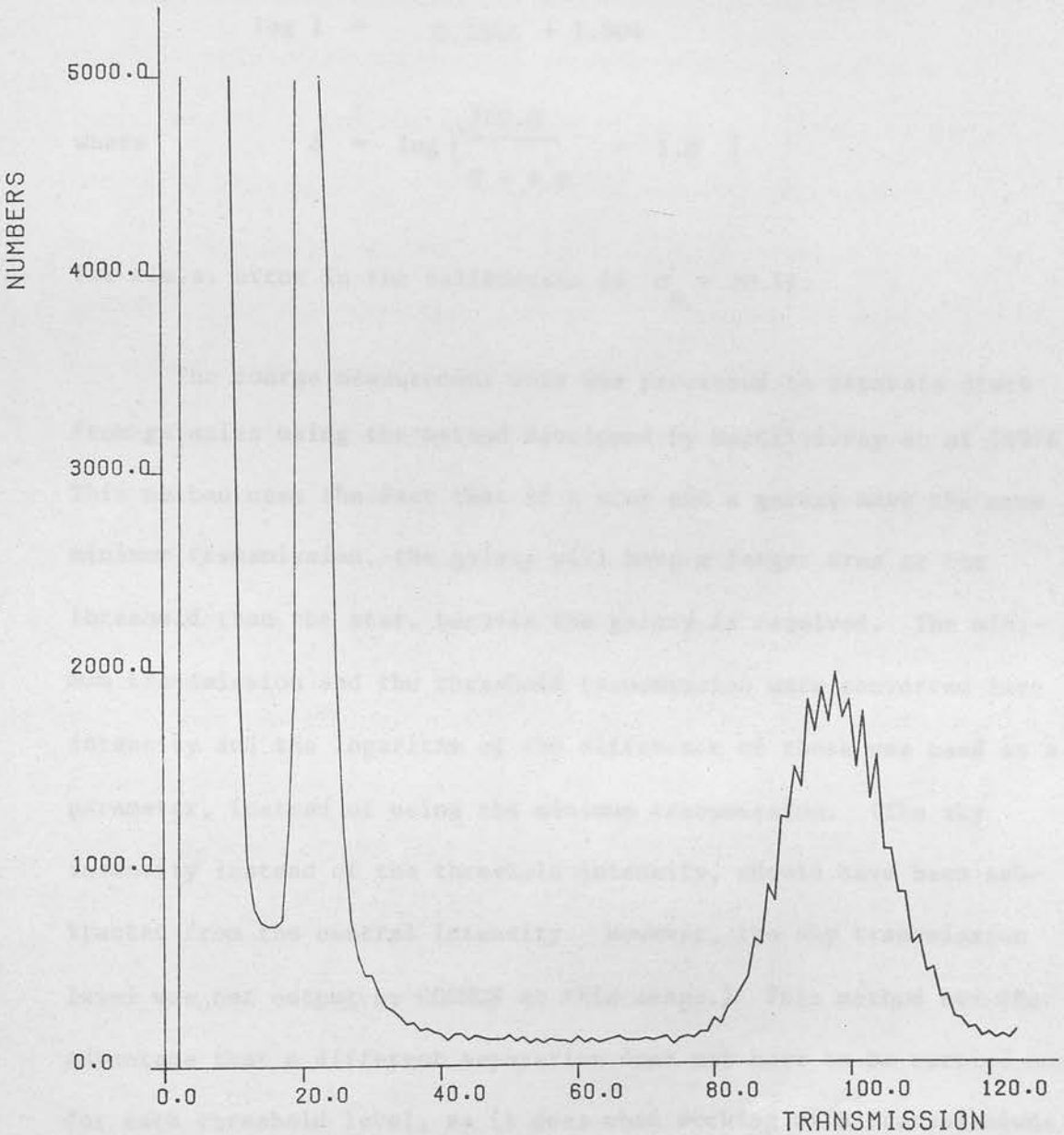

which was stored in a computer file in the form of an array of intensities corresponding to transmissions between the limits of the step wedge. As an example, the step wedge calibration for plate 2520 is:

$$\log I = 0.354\Delta + 1.904$$

where $$\Delta = \log\left[\frac{760.0}{T - 4.0} - 1.0\right]$$

The r.m.s. error in the calibration is $\sigma_\Delta = \pm 0.13$.

The coarse measurement data was processed to separate stars from galaxies using the method developed by MacGillivray et al (1976). This method uses the fact that if a star and a galaxy have the same minimum transmission, the galaxy will have a larger area at the threshold than the star, because the galaxy is resolved. The minimum transmission and the threshold transmission were converted into intensity and the logarithm of the difference of these was used as a parameter, instead of using the minimum transmission. (The sky intensity instead of the threshold intensity, should have been subtracted from the central intensity. However, the sky transmission level was not output by COSMOS at this stage.) This method has the advantage that a different separation does not have to be carried out for each threshold level, as it does when working with transmissions. The other parameter used was the logarithm of the area. (Logarithmic quantities were chosen because they gave a convenient range of values.)

A small region of the plate was examined under a microscope to separate about a hundred stars and galaxies by eye. A graph of $\log (I_{max} - I_{thr})$ vs. $\log A$ shows that the stars lie mainly above and to the left of the galaxies. The equation of the curve forming the upper boundary of the stars was found, (the dashed line on the graph). This curve was moved a certain perpendicular distance corresponding to the scatter of the stars on the graph, to give a new curve which formed the boundary between the stars and the galaxies of the sample examined by eye, (shown by a solid line on the graph). This curve was then used as the boundary for separating all the other images measured. It was estimated that stars and galaxies can be separated using this method down to about one magnitude above the plate limit. However, at the faint end it becomes very difficult to distinguish stars and galaxies, because the galaxy images are smaller and the stars are no longer dense in the centre.

Once the separation had been carried out, the coordinates, extents, area, central intensity, threshold intensity and type of each image were stored in a computer file for later use.

The computer program to calculate the magnitudes used the magnetic tape of mapping data, the file of coarse measurement data, and the file containing the step wedge calibration. A whole magnetic tape containing several hundred galaxy images, of sizes ranging from about 2 arcsec to 1 arcmin in diameter, could be processed in one run of the program. Using the coordinates of a galaxy from the file of

FIGURE 2.3 LOG(I-I_{TH}) VS. LOG A FOR STARS AND GALAXIES, PLATE 149

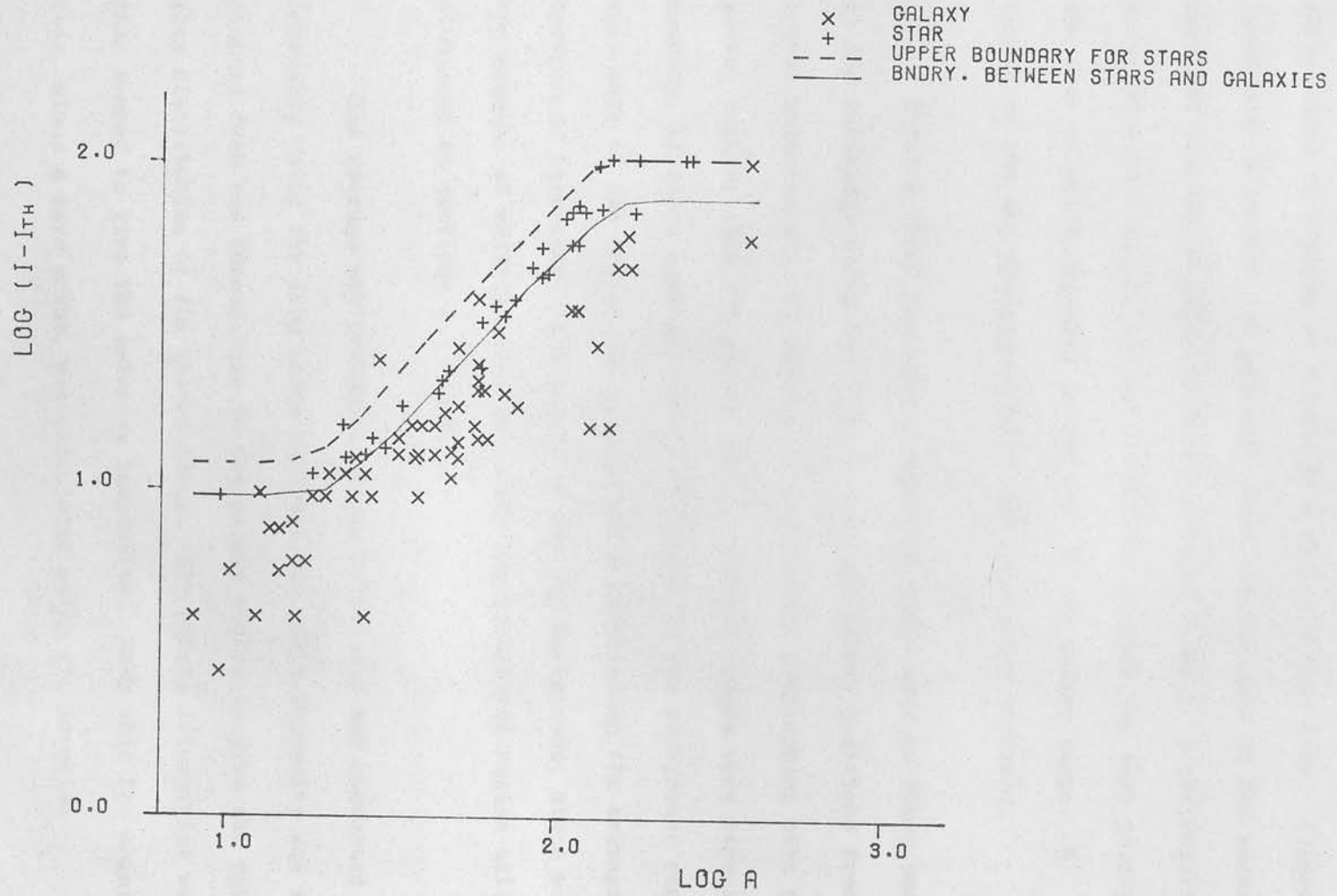

coarse measurement data, the mapped region corresponding to this galaxy was found. The technique used was to store the data from three lanes of mapping at a time in a direct access file. (Three lanes made allowance for galaxies whose centres were in the second lane but overlapped into the first or third lanes.) A rectangular array of transmissions was accessed from the disk for each galaxy, the size of which depended on the size of the galaxy image. A region of the sky background round the galaxy was included.

First a check was made to see that there were no other images in the vicinity, using the file of star and galaxy positions from coarse measurement. If there were any objects overlapping with the galaxy region, then the galaxy and those other images were rejected. However, if there were any objects situated in the background region, this part of the region was ignored while calculating the average background intensity. The nature of the sky background, along with the removal of objects situated in the sky background region will be discussed in sections 2.4 and 2.5.

The average sky transmission was calculated and converted into intensity using the step wedge calibration. This intensity was subtracted from the intensities in the galaxy region to give the intensity distribution of the galaxy alone. The galaxy intensities were then summed to give the relative luminosity. From this the magnitude, minus a zero point, was calculated using the formula:

$$m = -2.5 \log L.$$

The night sky brightness was used to give the zero point. While each plate was being exposed, the B sky magnitude at the south pole was measured in units of mag arcsec^{-2}. Since the unit of measurement on COSMOS is 8 μm, which corresponds to 0.5376 arcsec on the sky, the sky magnitude was converted to the magnitude falling on an area of 64 μm^2 on the plate. The galaxy magnitude could then be found from the formula:

$$m = m_{sky} - 2.5 \log (L/I_{ave})$$

where m_{sky} is the sky magnitude and I_{ave} is the average sky background intensity.

This method of determining the magnitude zero point worked well, as can be seen from the results in section 2.12, despite the fact that the brightness of the night sky (which is caused by aurora, zodiacal light and galactic light) varies across the sky and may be different at the south pole from the region where the plate was exposed, (Elvey & Roach 1937). However, the plate exposures were always taken under good weather conditions, and corrections to the sky brightness were found to be unnecessary.

The method for calculating the magnitudes was developed and tested using several Schmidt plates. Initially two regions were chosen and three plates of each region were measured, so that the results from different plates could be compared. Further tests were carried out on three fields near the south galactic pole, which were later used for studying the N(m) relation. Details of all the plates

used are given in table 2.2. The COSMOS measurements of plates 92, 149, 204, 329, 330 and 950 were carried out in March and May 1976, and those of plates 1915 and 1920 in August 1978.

The first region, near the south galactic pole, covered an area of 2 cm square, i.e. about 20 min square. It contained several hundred images, most of which were galaxies, as can be seen from figure 2.4. This region was chosen because it was not too crowded and was similar to the other regions near the S.G.P. used for the number-magnitude counts.

Since this method is applicable to stars as well as to galaxies, measurements were also made of NGC121, a globular cluster in the Small Magellanic Cloud, where a sequence of stars has been measured photoelectrically by Tifft (1963) down to magnitude 21. This region is 1 cm square in size and contained about 1000 images, mainly stars, (see figure 2.5). It therefore provided a test for the method on plates where there is a high number density of images. Table 2.3 gives the photoelectric magnitudes corresponding to the bandwidth of the IIIaJ emulsion and the GG395 filter, referred to as m_j magnitudes. The colour equation for the j band in terms of B and V was determined for stars near the S.M.C. by Kontizas (unpublished) and is

$$j = B - 0.2\,(B - V).$$

In the next three sections a fuller description will be given of some parts of the method which were developed using these measurements. The tests carried out on COSMOS will be discussed in later sections.

TABLE 2.2

Summary of Plate Details

Plate No	Survey Field No	R.A.(1950)	Dec.(195))	Date of Exposure	Exposure Time (mins)
92	416	$02^h\ 41^m$	$-30^o\ 00^m$	2. 8.73	90
149	416	$02^h\ 41^m$	$-30^o\ 00^m$	3. 9.73	120
204	416	$02^h\ 41^m$	$-30^o\ 00^m$	25. 9.73	60
329	SMC	$00^h\ 55^m$	$-73^o\ 00^m$	17.11.73	120
330	SMC	$00^h\ 55^m$	$-73^o\ 00^m$	17.11.73	60
950	SMC	$00^h\ 55^m$	$-73^o\ 00^m$	11.10.74	20
1915	474	$00^h\ 44^m$	$-25^o\ 00^m$	24.11.75	60
1920	412	$01^h\ 09^m$	$-30^o\ 00^m$	25.11.75	60
2520	237	$22^h\ 00^m$	$-50^o\ 00^m$	18. 8.76	60
3192	N10	$15^h\ 19^m$	$+02^o\ 16^m$	21. 5.77	60

FIGURE 2.4 MAP OF REGION 1, PLATE 92.

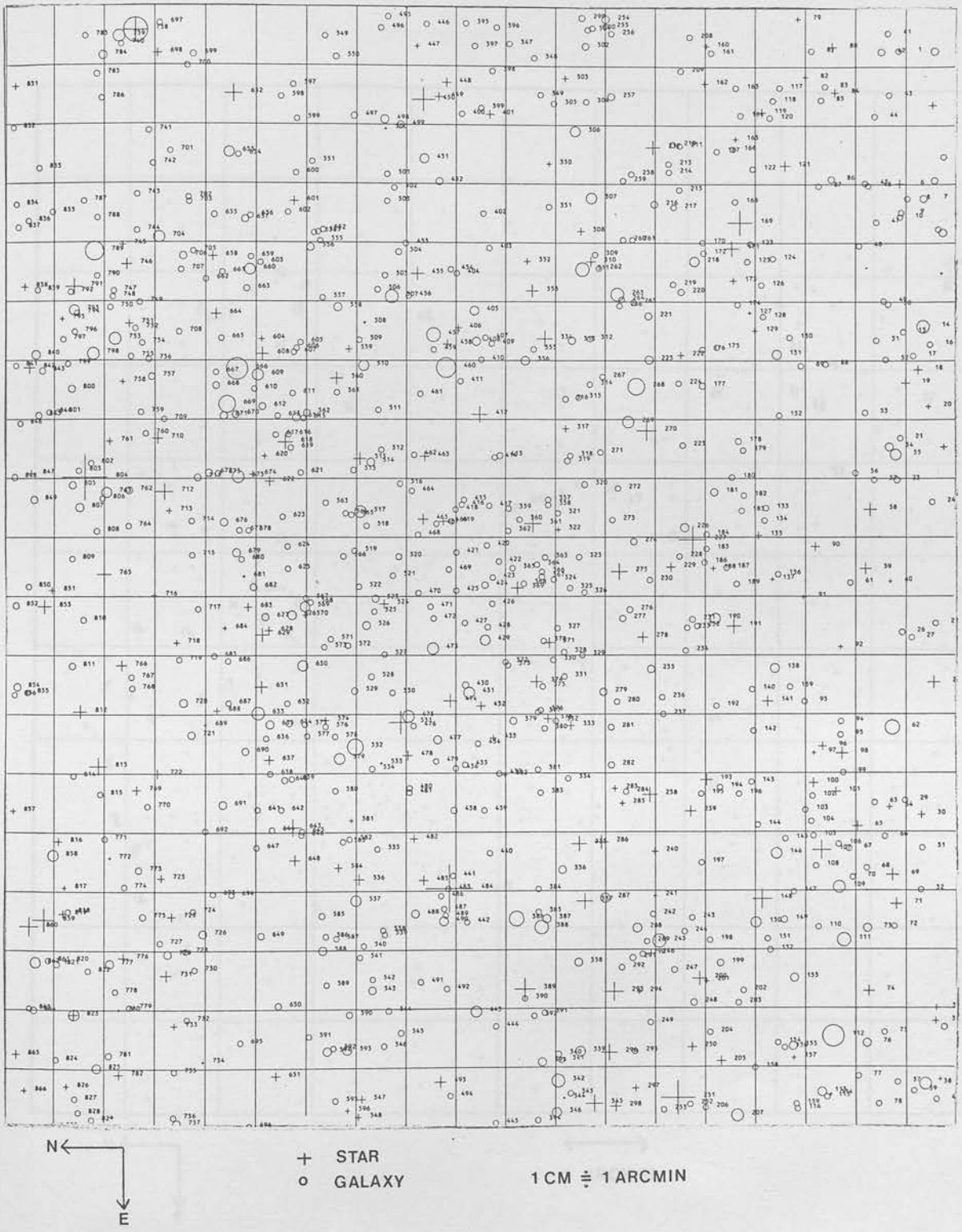

FIGURE 2.5 MAP OF NGC121, PLATE 950.

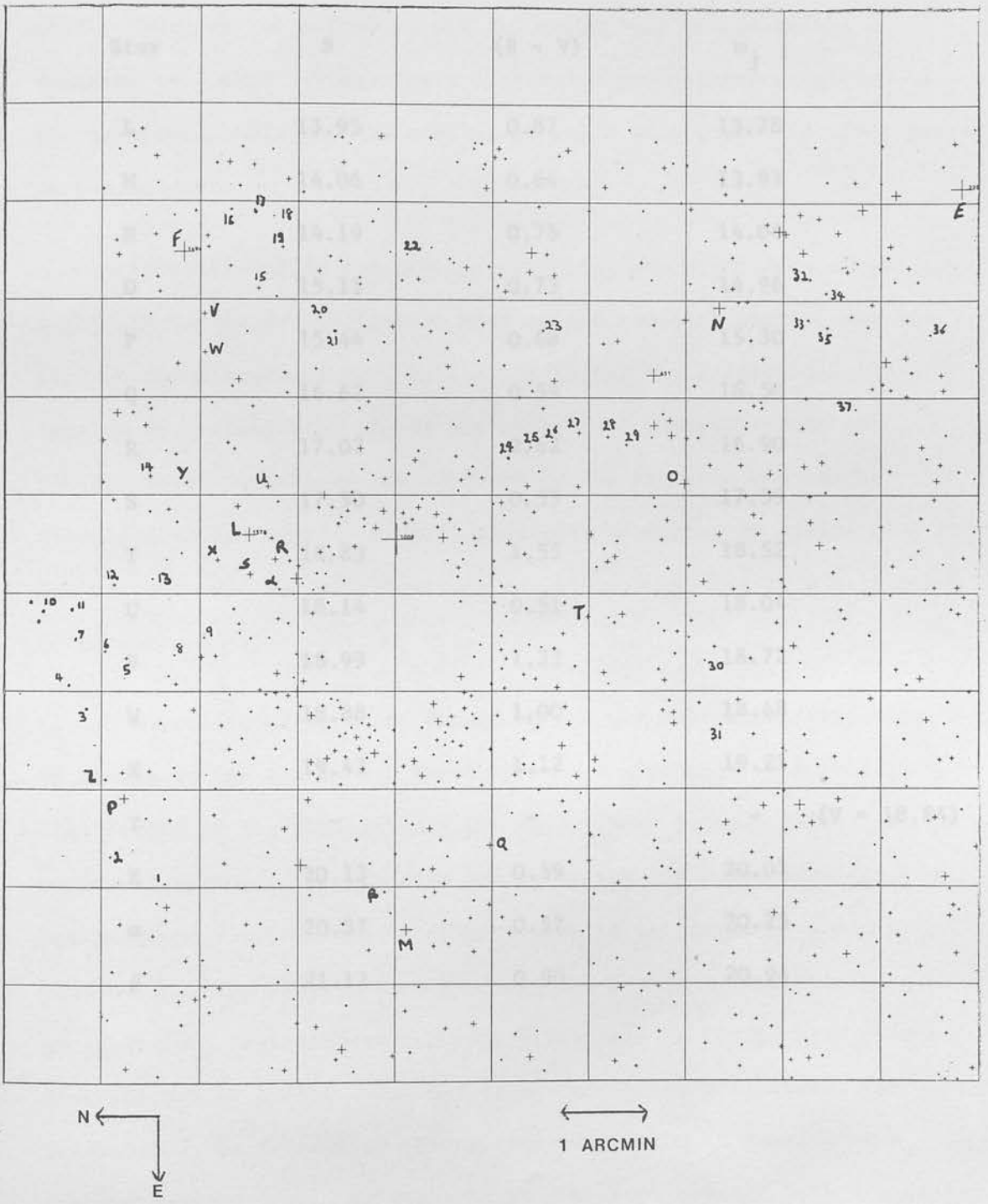

TABLE 2.3

Magnitudes of Stars in the j Band from Photoelectric Photometry by Tifft in NGC121

Star	B	(B - V)	m_j	
L	13.95	0.87	13.78	
M	14.06	0.64	13.93	
N	14.19	0.75	14.04	
O	15.11	0.73	14.96	
P	15.44	0.68	15.30	
Q	16.62	0.59	16.50	
R	17.02	0.62	16.90	
S	17.50	0.53	17.39	
T	18.83	1.55	18.52	
U	18.14	0.51	18.04	
V	18.99	1.33	18.72	
W	18.88	1.00	18.68	
X	19.43	1.12	19.21	
Y	-	-	-	(V = 18.84)
Z	20.13	0.59	20.01	
α	20.37	0.57	20.25	
β	21.12	0.90	20.94	

2.4 The Determination of the Sky Background Intensity

When calculating the luminosity or magnitude of a galaxy, it is important to determine the sky intensity accurately. Before deciding on the best method of calculating it, several tests were made to examine the nature of the sky background transmissions as measured by COSMOS. These tests involved a general investigation of the developed emulsion, the results of which were useful in other parts of the project.

As mentioned in the previous section, the brightness of the night sky varies due to factors such as the zodiacal light. However, even in the absence of real variations in the sky brightness, the density or transmission of the sky background changes across the plate. These variations are produced by the emulsion and can be divided into two types: microfluctuations occurring on scales of a few microns, and macrofluctuations occurring on scales of a millimetre or larger.

Microfluctuations are caused by the non-uniform distribution of grains in the emulsion. These have been discussed in detail in 'The Theory of the Photographic Process', (Mees & James 1966). A uniformly exposed plate appears grainy to the eye under magnification, and produces fluctuations in density when it is traced by a microphotometer. The distribution of densities has an approximately gaussian form, which shows that the graininess is caused by a random distribution of grains. One way of measuring the graininess, the granularity, is defined as the standard deviation in density at a certain density level, as measured by a microphotometer with a scanning

aperture of a certain area. For a gaussian distribution, the standard deviation is inversely proportional to the square root of the size of the measuring sample, and so the granularity should be inversely proportional to the square root of the area of the microphotometer scanning aperture. Because of this, Selwyn (1935) used

$$G = (2a)^{\frac{1}{2}} \sigma_D$$

as a measure of the graininess of a given photograph, where a is the area of the measuring aperture and σ_D is the standard deviation in density. G is known as the Selwyn granularity and should be constant for different sizes of aperture. In practice, however, it is found to increase for large aperture sizes because of the effect of large scale variations in density.

COSMOS outputs results directly in transmissions, and so tests on the graininess were carried out in transmission. It was found that the distribution of transmissions of the sky background in the many regions tested is also approximately gaussian, as can be seen in figure 2.6, showing the distribution of transmission values determined from a region of 0.86 mm square on plate 149, sampled at intervals of 8 μm. This is because the range in density or transmission covered by the sky background is small, so the non-linearity between these two quantities is not noticed. The standard deviation in transmission at a certain transmission level can therefore be used as a measure of graininess.

Granularity, the standard deviation in density, increases with density (Mees & James 1966). Since

$$D = -\log T, \text{ and } \frac{dD}{dT} = \frac{-1}{T},$$

FIGURE 2.6 HISTOGRAM OF SKY TRANSMISSIONS, PLATE 149

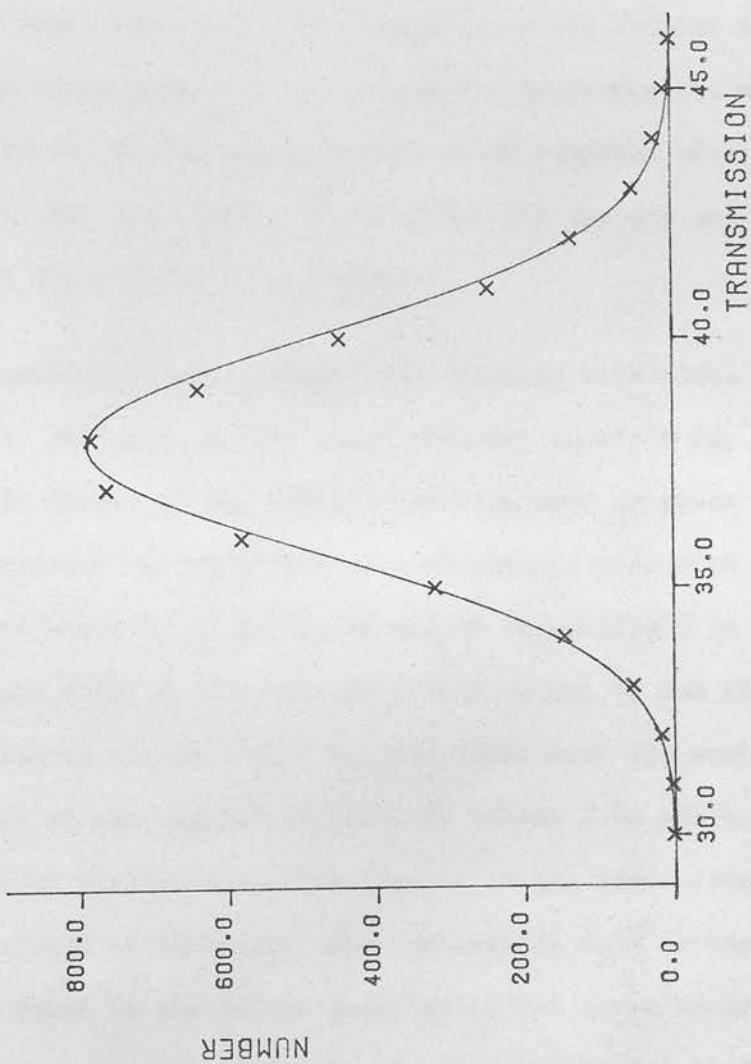

the relation between the standard deviation in density and the standard deviation in transmission is

$$\sigma_D = \frac{\sigma_T}{T}$$

σ_T/T was found for the steps of the wedge on plate 2520, and the variation of σ_T/T with T is shown in figure 2.7.

Two regions on plate 149 were used to examine the randomness of the distribution of the grains. One region was of the sky background at a point where there were no images visible, and the other was part of the step wedge where the transmission was similar to that of the sky. The measurements in the step wedge correspond to measurements of a region of uniform exposure and can be compared with the sky region to ensure that the results obtained for the sky are not due to the inclusion of faint galaxies or stars.

The transmissions were averaged over squares with sides of sizes 1, 2, 4, 8, 16 and 32 units, where one unit equals 8 μm. Since the width at half height of the COSMOS measuring spot is about 25 μm, the results correspond approximately to measurements made with square scanning spots of sizes 3, 4, 6, 10, 18 and 34 respectively in units of 8 μm. For each area, A, the average transmission, $\overline{T}$, and the standard deviation in transmission, σ_T, was found over the whole region. A sample of the results is given in tables 2.4a and b. For a completely random distribution, the figures in the last column of the two tables should be constant. The increase in $\sigma_T\sqrt{A}$ is the same as the increase found in the Selwyn granularity for large areas of the microphotometer aperture, which has been accounted for by the

FIGURE 2.7 THE VARIATION OF σ_T/T WITH TRANSMISSION FOR THE STEP WEDGE, PLATE 2520.

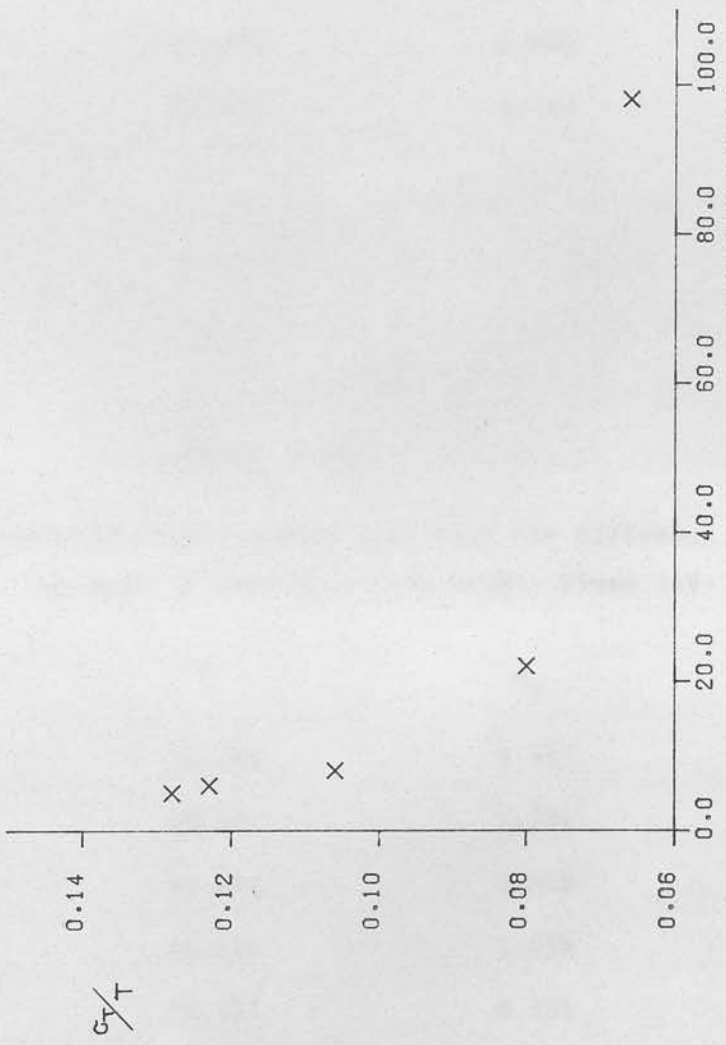

TABLE 2.4a

Average Transmission and Standard Deviation for Different Sample Areas in the Region of Sky Background, Plate 149

A^*	$\overline{T}$	σ_T	$\sigma_T\sqrt{A}$
9.77	37.369	2.265	7.078
17.02	37.369	1.700	7.013
37.52	37.369	1.345	8.238
102.52	37.369	0.997	10.095
328.52	37.369	0.666	12.071
1164.52	37.369	0.442	15.083

TABLE 2.4b

Average Transmission and Standard Deviation for Different Sample Areas in part of the North Step Wedge, Plate 149

A	$\overline{T}$	σ_T	$\sigma_T\sqrt{A}$
9.77	16.184	2.497	7.803
17.02	16.184	2.284	9.422
37.52	16.184	2.078	12.728
102.52	16.184	1.456	14.742
328.52	16.184	0.951	17.237
1164.52	16.184	0.559	19.076

* Areas are given in units of $(8\ \mu m)^2$

presence of larger scale variations. $\sigma_T\sqrt{A}$ increases steadily which indicates that there is no cellular structure in the emulsion.

Macrofluctuations, also known as local errors, have been studied in detail by de Vaucouleurs (1944). They are usually accounted for by variations in the emulsion thickness and variations occurring during the development and drying of the plate. De Vaucouleurs found that the density of a uniformly exposed plate varies smoothly over large scales and that the density of any point can be determined by interpolation between points of known density.

One theory, due to Eberhard (1931), is that the main cause of local errors is that the glass of the plate is not completely smooth, so that the emulsion, when it is poured on, flows and fills the 'valleys' in the glass, giving rise to variations in the thickness. Subsequently it is assumed that the density of uniformly exposed plate is greater in parts where the emulsion is thicker. However, de Vaucouleurs (1948b) tested these two hypotheses and found that firstly the depth of the emulsion was not correlated with the depth of the glass, and secondly the density variations were only correlated with emulsion thickness for plate fog and at very high densities. The latter is due to the fact that for exposures producing densities up to about 1.5, the developed grains are concentrated at the surface of the emulsion and therefore the number of developed grains cannot depend on the emulsion thickness. For the plate fog, the developed grains are distributed uniformly through the thickness of the emulsion, and also at high densities the number density of developed grains tends to become uniform through the thickness of the emulsion. De Vaucouleurs

found that for densities between 0.2 to 0.3 and 1.2 to 1.3, in the range where the characteristic curve, D vs. log E, is linear, the local errors were independent of density and that at these densities the local errors were mainly due to plate processing effects arising during development and drying. Therefore within this range of densities the relative intensity calibration is unaffected by local errors. Using this property, and the fact that local errors produce a continuous variation in density, de Vaucouleurs devised a method for correcting for local errors in the photometry of galaxies, using the variation of the density of the sky background surrounding the galaxy. As described by Jones, Obitts, Gallet and de Vaucouleurs (1967), a polynomial is fitted to the sky background transmissions. Interpolation is then used to calculate the transmission due to the sky only in the galaxy region. These are converted into intensities and subtracted from the total intensities to give the intensity distribution of the galaxy.

The large scale variations in the average transmission across a Schmidt plate can be seen in the data from the coarse measurement mode of COSMOS. The transmissions of the background are continuously monitored in this mode, and the threshold level for image detection is altered to take account of the macrofluctuations. The level is set at three standard deviations below the mean transmission which for a gaussian distribution means that there is a 99% certainty that a transmission below this level is in an image. In this way the threshold level is made to correspond to approximately the same isophote in intensity so that the images are detected uniformly across the plate. A change in the average transmission gives rise to an equal

change in the threshold transmission and so the threshold levels, which are output on the magnetic tape with the rest of the coarse measurement data, can be used to examine the large scale variations in the average transmission.

The threshold values of coarse measurement data on plate 149 vary from 25 to 31, the average distance between the different levels being at least 100 x 8 μm (see figure 2.8). Since the total region size used for a galaxy and the background is usually less than 100 units, the average transmission does not appear to vary significantly over the areas required. However, some tests were carried out to find the effect of fitting a polynomial to the sky transmissions. A first order polynomial will produce approximately the same luminosity as simply averaging the transmissions. A second order two dimensional polynomial was used. However, the fit was not a good one, since the standard deviation of the observed points from those of the polynomial were only slightly less than the standard deviations of the points from the average background transmission. (See table 2.5).

It was decided that local errors are not important over the size of region used, and the sky intensity was calculated by averaging the transmissions over the background region, and converting the resulting transmission to intensity.

2.5 The Removal of Images Present in the Background Region

One problem which often occurred was the presence of images in the region to be used to determine the sky intensity. Images in the background increase the calculated sky intensity and therefore decrease

FIGURE 2.8 CONTOUR PLOT OF COARSE MEASUREMENT THRESHOLD TRANSMISSIONS, PLATE 149.

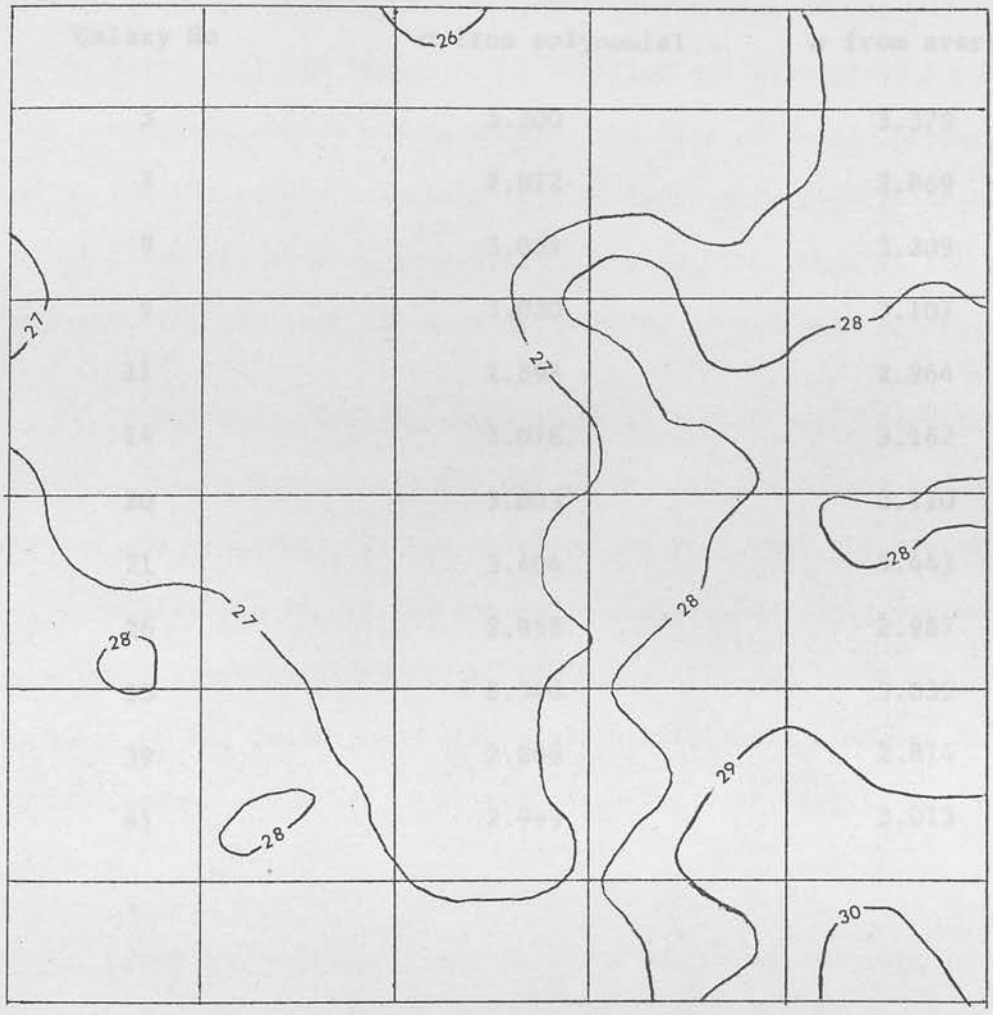

TABLE 2.5

Comparison of the Standard Deviation of Background Transmissions from a Fitted Two Dimensional, Second Order Polynomial with the Standard Deviation from the Average Background Transmission.

Galaxy No	σ from polynomial	σ from average
3	3.300	3.379
7	2.822	2.869
8	3.069	3.209
9	3.020	3.107
11	2.895	2.964
14	3.076	3.162
20	3.003	3.110
21	3.404	3.443
26	2.958	2.987
35	2.948	3.035
39	2.808	2.874
41	2.999	3.013

the luminosity of the galaxy, so that it is important that they are detected and removed. Different methods for doing this were applied to regions 1 and 2.

In the case of region 1, the south galactic pole region, the number density of images was low, and coarse measurement was relied on to detect all the images. The position and size of an image in the background region was known from the file of coarse measurement data, and the points belonging to that image were omitted when calculating the average transmission value. The whole of the image was removed, not just the area detected by coarse measurement.

In region 2, NGC121, where there is a high number density of images, coarse measurement did not detect all the images and another method was required. It was based on the fact that the distribution of transmissions due to the sky only is approximately gaussian, and therefore symmetrical about the maximum point. If there are images present in the region, the distribution will show an excess at low transmissions which has to be removed. This was done by an iterative process.

First the average transmission of the background region and the standard deviation were calculated. Then the minimum transmission was found and compared with the value of the average transmission minus the standard deviation multiplied by a factor. (The factor was chosen for each plate, and will be discussed below.) If the minimum transmission was less than this value, denoted by w, this point was assumed to be the centre of an image. Next the background was scanned to find all the points connected to the central point whose transmissions

were less than one standard deviation below the mean. These points were counted as being part of the image and were subsequently ignored. The new minimum transmission and the value of w were calculated from the remaining points. If the minimum transmission was less than w and background was scanned again to remove all points of transmission less than the average minus one standard deviation, which were connected to the second minimum transmission or to the points surrounding the first minimum transmission. This process was repeated until the minimum transmission was greater than w, i.e. until there were no more images left.

There were two threshold levels used, one, denoted by w, for determining whether or not the minimum transmission was the centre of an image, and the other for deciding whether or not a transmission was to be rejected as belonging to an image. The first threshold was varied from plate to plate by altering the value of the factor, but the second was constant and equalled one standard deviation in transmission below the mean. Both these thresholds were set so that after the image removal process the final distribution of transmissions was symmetrical and approximately gaussian. The method was tested by examining the distributions of background transmissions before and after the removal of the images. An example of the distributions is given in figure 2.9. The factor used in the first threshold level had to be determined from such graphs drawn for a few images on each plate. Values found for the factor were:

plate 329	3.2
plate 330	4.0
plate 950	3.0

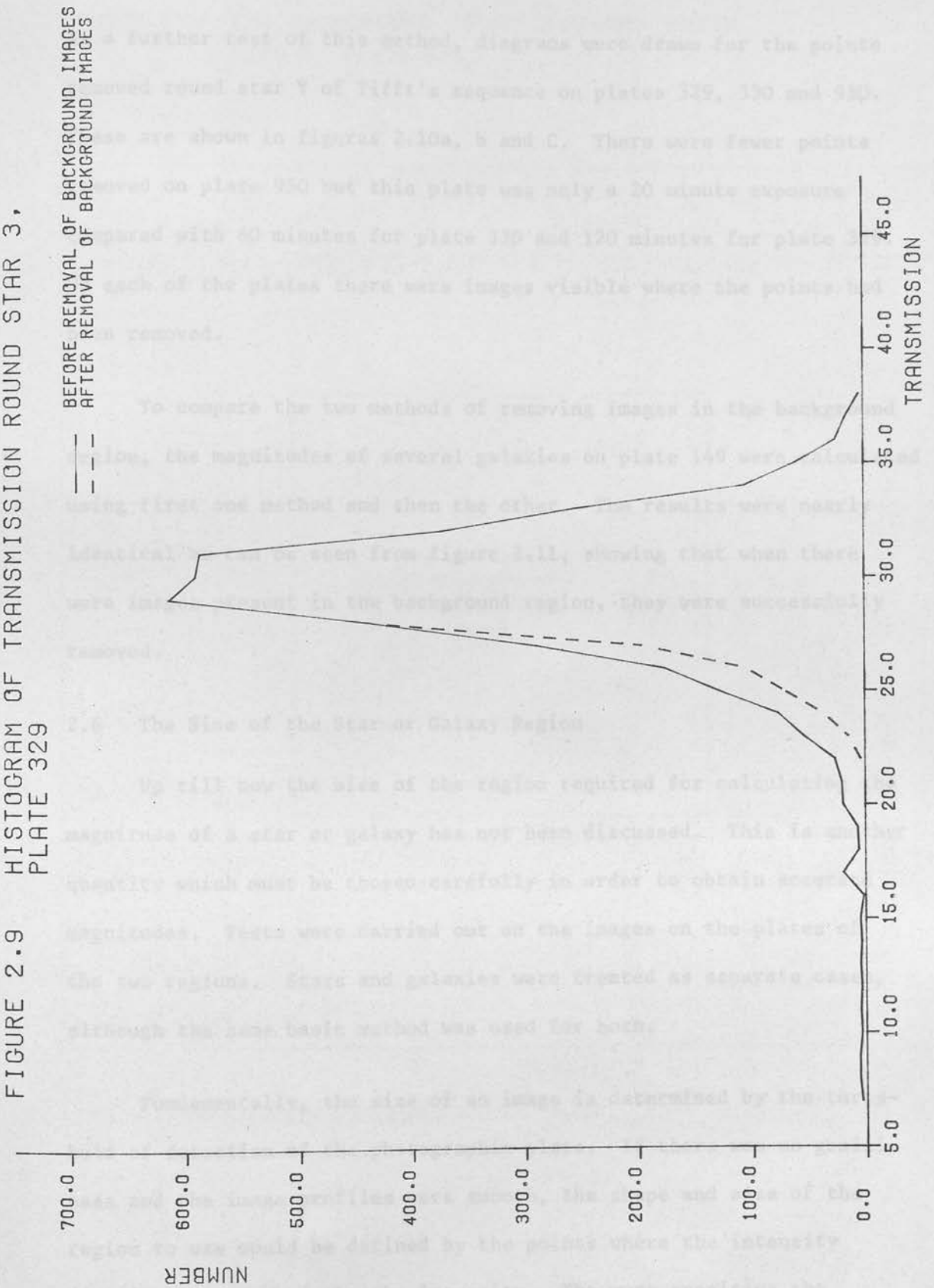

FIGURE 2.9 HISTOGRAM OF TRANSMISSION ROUND STAR 3, PLATE 329

As a further test of this method, diagrams were drawn for the points removed round star Y of Tifft's sequence on plates 329, 330 and 950. These are shown in figures 2.10a, b and C. There were fewer points removed on plate 950 but this plate was only a 20 minute exposure compared with 60 minutes for plate 330 and 120 minutes for plate 329. On each of the plates there were images visible where the points had been removed.

To compare the two methods of removing images in the background region, the magnitudes of several galaxies on plate 149 were calculated using first one method and then the other. The results were nearly identical as can be seen from figure 2.11, showing that when there were images present in the background region, they were successfully removed.

2.6 The Size of the Star or Galaxy Region

Up till now the size of the region required for calculating the magnitude of a star or galaxy has not been discussed. This is another quantity which must be chosen carefully in order to obtain accurate magnitudes. Tests were carried out on the images on the plates of the two regions. Stars and galaxies were treated as separate cases, although the same basic method was used for both.

Fundamentally, the size of an image is determined by the threshold of detection of the photographic plate. If there was no graininess and the image profiles were smooth, the shape and size of the region to use would be defined by the points where the intensity distribution reached the sky intensity. The more sensitive the

FIGURE 2.10A THE BACKGROUND POINTS REMOVED ROUND STAR Y, PLATE 329.

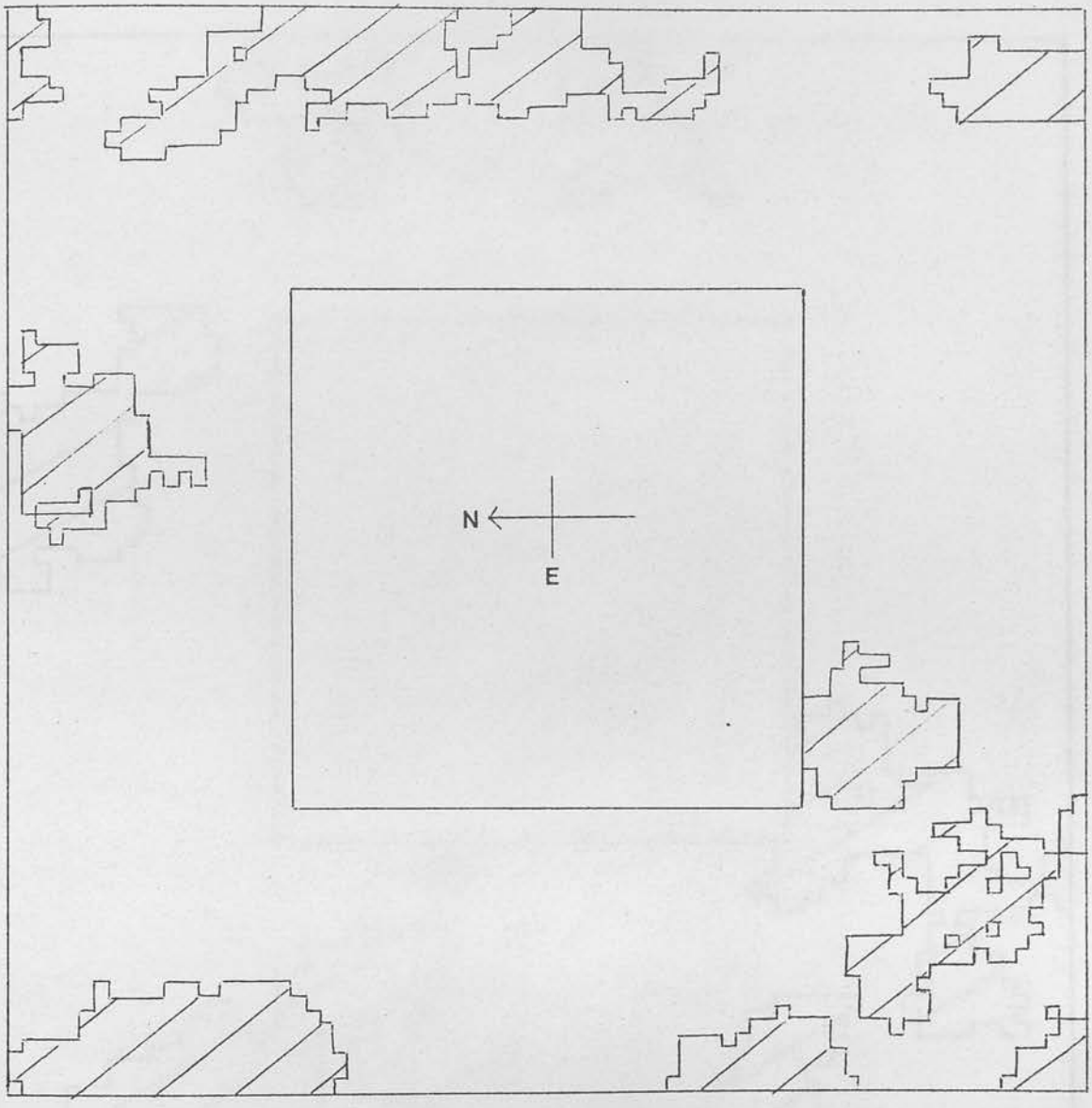

(1 CM REPRESENTS $5 \times (8 \mu M)^2$ ON THE PLATE)

FIGURE 2.10B THE BACKGROUND POINTS REMOVED ROUND STAR Y, PLATE 330.

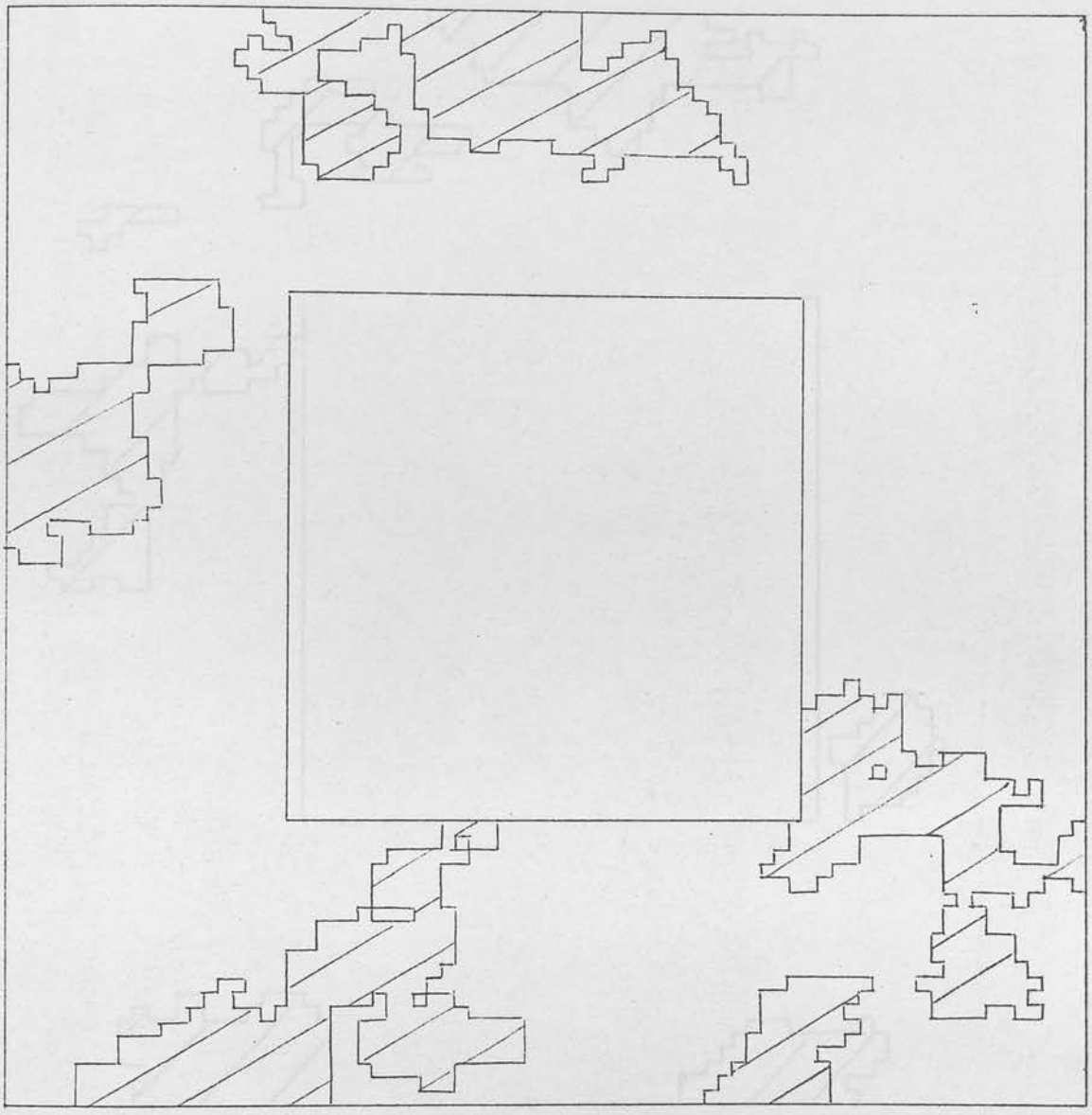

FIGURE 2.10C THE BACKGROUND POINTS REMOVED ROUND STAR Y, PLATE 950.

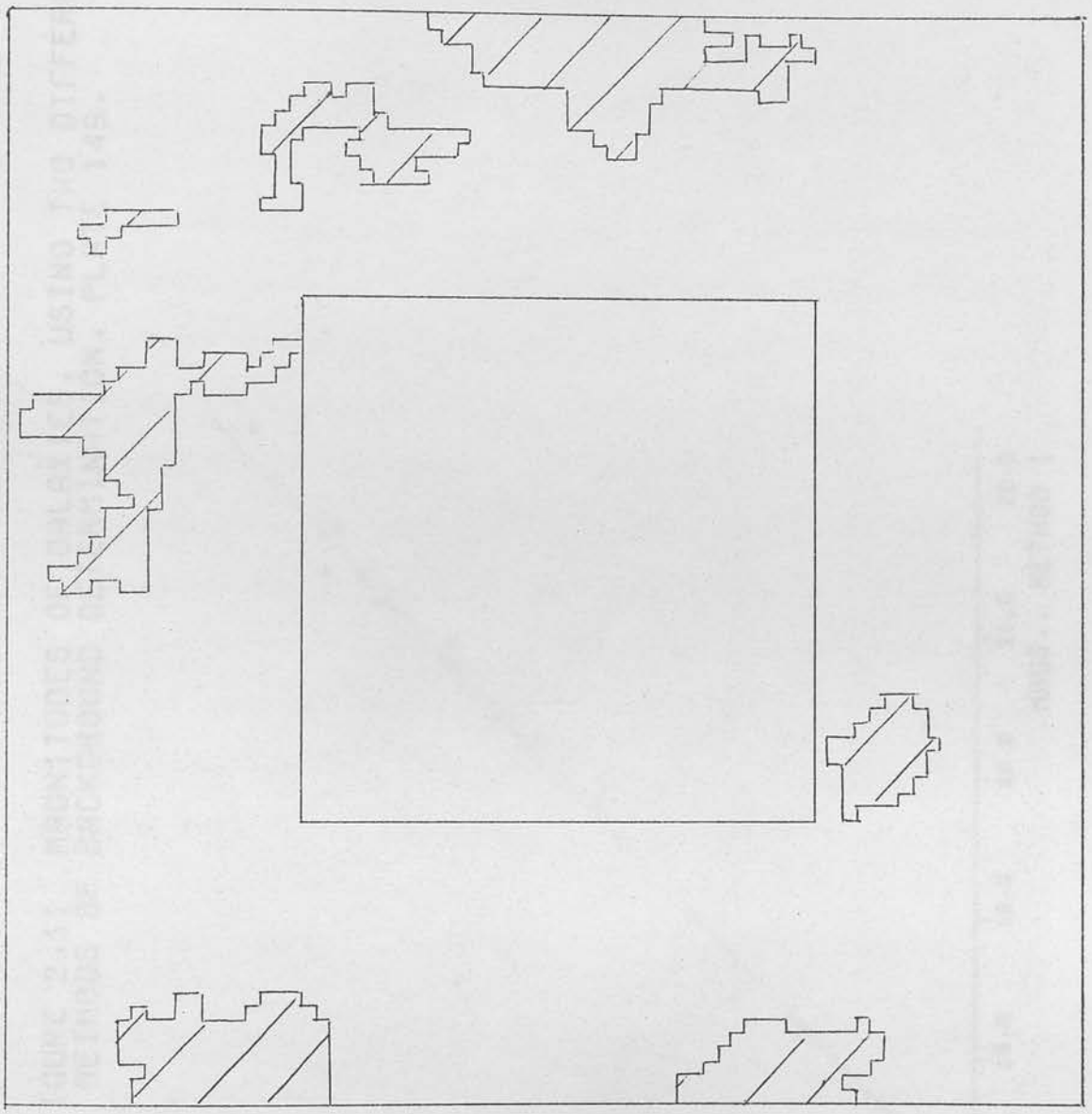

FIGURE 2.11 MAGNITUDES OF GALAXIES, USING TWO DIFFERENT METHODS OF BACKGROUND DETERMINATION, PLATE 149.

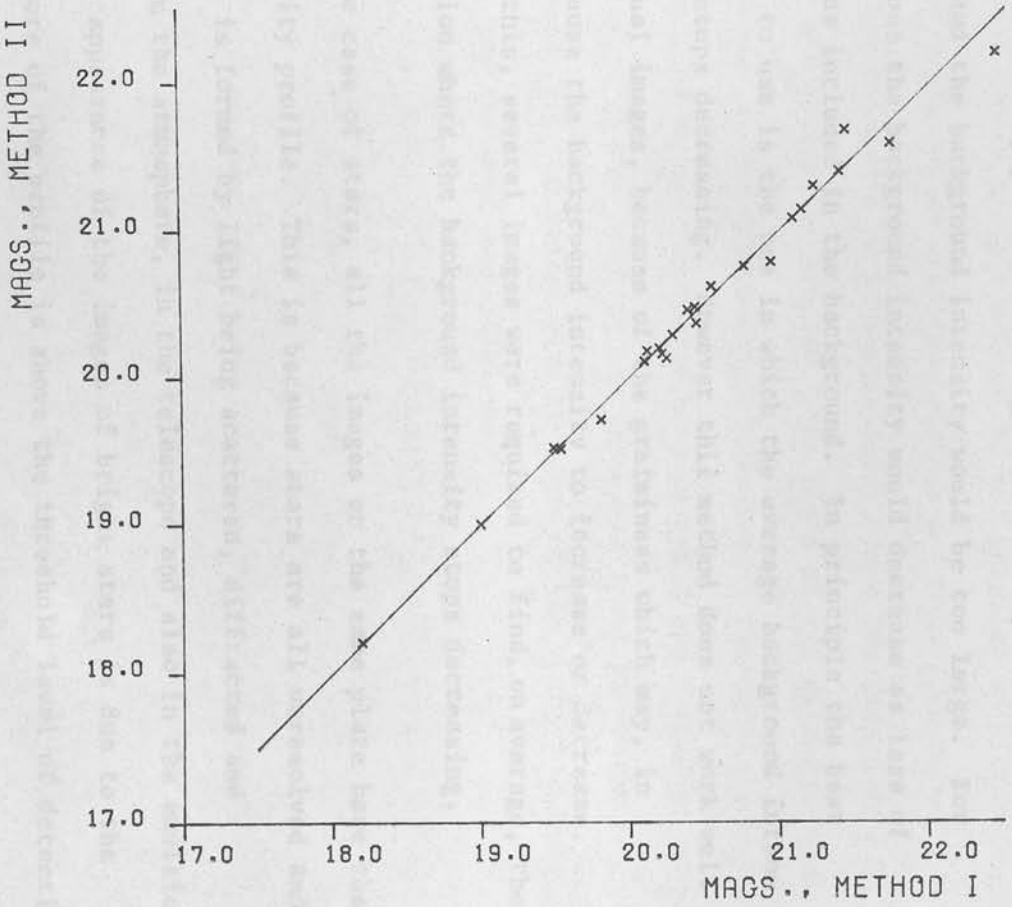

emulsion the larger the region size would be. (There will always be some loss of luminosity from an image due to points of intensity less than the threshold for detection. The consequences of this will be discussed in section 2.15.) Due to the presence of graininess the profiles are not smooth and the size of the region has to be chosen experimentally.

For convenience rectangular regions were used. The average intensity in the background region round the image was calculated for a series of consecutively larger image regions. If the first region was too small, part of the image would be included in the background and the background intensity would be too large. For larger regions the background intensity would decrease as less of the image was included in the background. In principle the best region size to use is the one in which the average background intensity first stops decreasing. However this method does not work well for individual images, because of the graininess which may, in practice, cause the background intensity to increase or decrease. Because of this, several images were required to find, on average, the size of region where the background intensity stops decreasing.

In the case of stars, all the images on the same plate have the same intensity profile. This is because stars are all unresolved and the profile is formed by light being scattered, diffracted and refracted in the atmosphere, in the telescope and also in the emulsion. (The larger appearance of the images of bright stars is due to the fact that more of the profile is above the threshold level of detection.) The same region size includes the same fraction of the total luminosity, and so the region size should be the same for all stars. Table 2.6

shows the values of the average background intensity round some stars on plate 204. From this table a region size of 45 x 8 μm units was chosen. The size of region chosen for the stars on the SMC plates were:

plate 329	37	(in units of 8 μm)
plate 330	37	
plate 950	29	

(A larger region size was required for the stars on plate 204 than on the other plates because the seeing was poorer.)

Different region sizes are required for galaxies of different morphological types and at different distances. This time rectangular instead of square regions were used, since the images of galaxies are not generally circular. The sizes of the galaxy images are already known at the COSMOS coarse measurement threshold level, and it was decided to use the coarse measurement X and Y extents to estimate the size of the image at the threshold level for detection. Several formulae for the region size in terms of the X and Y extents were tested, and the most successful was:

$$X = 2 \times X_{ext} + \text{const}$$

$$Y = 2 \times Y_{ext} + \text{const}$$

The value of the constant was determined using the method described above for stars. The galaxy region sizes found for the S.G.P. plates were:

plate 92	$2 \times X \text{ or } Y_{ext} + 13$	(consts in units of 8 μm)
plate 149	$2 \times X \text{ or } Y_{ext} + 9$	
plate 204	$2 \times X \text{ or } Y_{ext} + 21$	

TABLE 2.6

Average Background Intensity in Arbitrary Units Around Different Sizes of Star Region, Plate 204

No	COSMOS	Region Sizes in units of 8 μm						
	mag.	29	33	37	41	45	49	53
9	18.63	233.2	232.9	232.7	232.6	232.5	232.4	232.2
16	18.57	234.3	234.2	234.0	233.8	233.7	233.7	233.6
17	17.49	234.3	234.1	234.0	234.0	233.9	233.9	233.9
47	-	231.9	232.0	232.1	-	-	-	-
48	19.15	233.1	232.9	232.8	232.7	232.6	232.6	232.6
49	20.17	233.1	233.1	233.1	233.1	233.2	233.2	233.3
50	17.53	234.4	234.1	233.8	233.7	233.6	233.6	233.5
59	19.45	232.2	232.1	232.0	231.9	231.7	231.6	231.5

These formulae were valid for galaxies with a wide range of image sizes.

The size of the background round the stars or galaxies had also to be chosen. The magnitudes were calculated using several sizes of the background region, but this did not have much effect on the results. It was decided to form the background region by adding 20 x 8 μm units to the four sides of the image region, because if a smaller region size was used, the deconvolution discussed in section 2.8 did not work.

2.7 Tests Carried Out on COSMOS

The development of the method as described in the previous sections involved testing the properties of the IIIaJ emulsion but did not check the validity of the COSMOS measurements. In the photometry of Schmidt plates it is very important to use a measuring machine of high precision. The plate scale is small (67.2 arcsec/mm) and the IIIaJ emulsion has a high contrast so, if the measuring machine spot is too large, or if there is scattered light, the detail on the plate will be blurred giving rise to errors. Tests were carried out by the COSMOS staff on the COSMOS cathode ray tube beam.

The size and shape of the spot were measured by scanning across a 'knife edge'. These results showed that the spot was gaussian in shape with a whole width at half height of 25 μm, instead of 8 μm as had been specified in the design of the machine. A step wedge was measured first with masking tape round it, and then without to check for light glow from the tube. The transmissions of the measurement with the masking tape were indeed lower than those of the

other scan, and showed that there was a halo caused by the glow across the face of the cathode ray tube, which consisted of 1% of the total light from the tube, and had a diameter of 6 cm. Finally, scans of a 'saw tooth' pattern showed that there was another halo due to electron flare in the tube which was 6 mm in diameter and accounted for ½% of the light.

Because of the wide measuring spot and the surrounding halos, COSMOS cannot measure the true transmission profile of an image, or a step wedge. The most serious error arises in the measurement of stars and galaxies with the 25 μm spot, because the transmission profiles of the images vary on scales smaller than 25 μm. The measured distribution of an image is a convolution of the true one with the gaussian spot. If there were a linear relationship between intensity and transmission, the integrated magnitude obtained from the measurements would be unaffected. This is because when a two dimensional function (in this case the transmission profile) is convoluted, the volume under the surface remains constant. However, the intensity-transmission relation is of the form:

$$\log I \propto \log (1/T - 1) \quad \text{(the Baker density relation)}.$$

The intensity rises more and more rapidly as the transmission decreases. Therefore the intensity calculated from the convoluted transmission at a point in an image is always less than the true value of the convoluted intensity profile at that point. Consequently, with too large a measuring spot, the luminosity of an image will be underestimated, and the error will increase with increasing luminosity.

The presence of the halos also affects the magnitudes of the stars and galaxies. At any point in an image the measured transmission has a contribution from the surrounding sky background. The transmissions are therefore increased, and the images are again calculated to be too faint.

The step wedge measurements are not affected by the 25 μm spot, but are altered by the halos. Corrections to the step wedge measurements will be discussed after the corrections for the images.

2.8 The Correction of Image Transmission Distributions

a) Deconvolution of Transmissions of the Images

The measured transmission distributions were corrected by deconvolutioning for the 25 μm gaussian spot using a method developed by Jones & Misell (1970). A full description of this method and of its application to the COSMOS measurements is given in appendix II. Basically, a function is derived from the gaussian spot profile which, when convoluted with the observed transmission distribution, gives the deconvoluted distribution.

Tests on the deconvolution were first carried out on star profiles in one dimension. Because there is always noise present in the observed distribution, it is necessary to have a cut-off at high spatial frequencies in order to prevent errors accumulating in the deconvoluted distribution. This cut-off denoted by t^*, should be set so that the variations in the transmissions due to graininess are smoothed, without losing the true structure of the image. However, as can be seen from figure 2.12, the width of the transmission profile

FIGURE 2.12 COMPARISON BETWEEN DECONVOLUTED AND UNDECONVOLUTED TRANSMISSIONS OF STAR B, PLATE 950

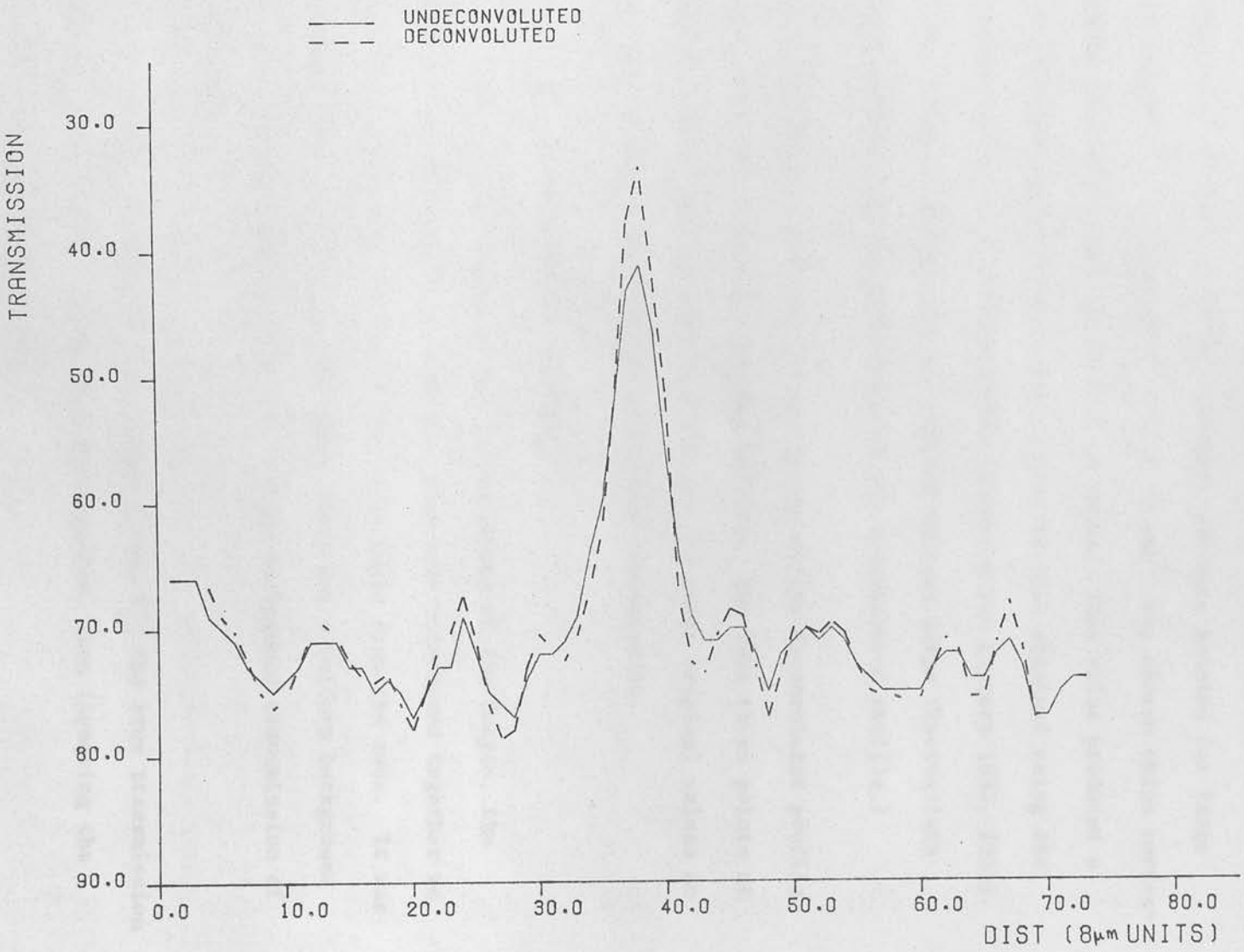

of the star is very small and is of the same order as the scale of the fluctuations due to graininess, making the choice of t^* difficult. A range of values of t^* were tested and it was found that the deconvoluted profile became narrower and more pointed for large values of t^*. A value of $t^* = 0.10\ (8\ \mu m)^{-1}$ was chosen which corresponds to a wavelength of 10 in 8 μm units. This value produced a deconvoluted profile which was similar to that obtained using the iterative method of deconvolution (Burger & Van Cittert 1932, 1933). (The iterative method was not adopted because large fluctuations were produced by the graininess in the deconvoluted profile.)

In figure 2.12 the end few points of the deconvoluted profile had peculiar values due to edge effects. The last three points at either end of the profile were set back to their original values so as not to affect the average background transmission.

b) Correction for the Halo

In the correction of the transmissions of the images, the effects of electron flare and tube glow were considered together as one halo consisting of 1½% of the total light from the tube. It was assumed that surrounding each image there was a uniform background with a transmission equal to the average background transmission of the region.

If T_{obs} is the observed transmission, T_{tr} the true transmission and T_{sky} the average background transmission, then (ignoring the effects of the 25 μm spot),

$$T_{obs} = S \times T_{tr} + H \times T_{sky}$$

where S is the fraction of light from the tube in the spot, and H is the fraction of light in the halo. In this case S = 0.985 and H = 0.015. T_{tr} can be calculated from the formula:

$$T_{tr} = \frac{T_{obs} - H \times T_{sky}}{(1 - H)}$$

When correcting the transmissions of an image for the effects of both the 25 μm spot and the halo, the deconvolution was carried out first, in two dimensions, and then the data was corrected for the halo using the above formula.

2.9 The Correction of the Step Wedge Transmissions

The step wedge consists of 7 steps 6 mm wide and, on average, 3 mm long. (The size of a step depends on its density, the densest steps being larger because of light spread in the emulsion.) Measurements made with a 25 μm spot instead of a 8 μm spot do not affect the results. On the other hand the presence of the halos round the spot do alter the measurements. The diameter of the halo due to electron flare is 6 mm, so the observed transmissions are a convolution of the true ones with the profile of the halo which, in this case, means an averaging over an area of 6 mm in diameter. The halo of 6 cm in diameter due to the tube glow was considered in the same way as the combined halo in the correction of the image transmissions, since its area is much larger than the area of the step wedge. During measurement, the step wedge was surrounded by masking tape of diffuse density 0.8 to 1.0 in order to cut down scattered light. The transmission of the light of the halo was therefore the transmission of the masking tape.

Using a similar notation as before, the equation relating the true transmission to the observed one is:

$$T_{obs} = S \times T_{tr} + F \times T_{cnv} + G \times T_{m}. \qquad (2.1)$$

S is the fraction of light from the tube in the spot and equals 0.985 as before, F is the fraction of light in the halo caused by electron flare which is 0.005, and G is the fraction of light in the halo caused by the tube glow and equals 0.010. T_m is the transmission of the masking tape, and T_{cnv} is the average of the true transmissions over the circular area of 6 mm in diameter covered by the halo due to electron flare. The equation was solved by an iterative method similar to that for deconvolution by Burger & Van Cittert (1932, 1933). First a guess was made at the true transmission profile, i.e. the variation of transmission along the step wedge. This was taken as the observed transmission profile, and used to calculate T_{obs} in equation (2.1). Then an improved approximation to the true transmission profile was formed using the equation:

$$T_{tr\ 1} = T_{tr\ 0} + (T_{obs} - T_{obs}')$$

where $T_{tr\ 0}$ is the previous approximation to T_{tr}, and T_{obs}' is the function obtained by substituting $T_{tr\ 0}$ in (2.1). The process was repeated until a sufficiently small value for the r.m.s. deviation of points in T_{obs}' from T_{obs} was found. In practice only two iterations were required.

The correction for electron flare was larger than the correction for tube glow, so the overall effect was to increase the high transmissions and decrease the low transmissions. This meant that the

slope of the Baker density calibration was decreased. For example, the initial equation for the north step wedge of plate 950 was:

$$\log I = 0.289\Delta + 2.071$$

and after correction the relation was:

$$\log I = 0.283\Delta + 2.888.$$

The correction to the step wedge had an effect on the luminosities of the images opposite to that of the other corrections, but smaller in size.

2.10 The Effect of Binning of Transmissions by COSMOS

The measurements of stars and galaxies are also affected by the binning of transmissions by COSMOS. The voltage between 0 and 10 volts produced by the photomultiplier detecting the transmitted light is converted into 128 levels between 0 and 127 inclusive. Because of this digitisation in transmission there will be an error in the intensity calculated at each point in the image. The errors will be largest at high intensities (low transmissions) where there are larger intervals in intensity between transmission levels. The results will also be affected by the fact that the transmission is only measured at intervals of 8 μm. The integration of the two dimensional intensity profile to give the luminosity is carried out by summing the intensities. This method will only give the correct value for the luminosity if the interval between measurements approaches zero.

Some tests on the errors arising from these effects were carried out using synthesised data. Gaussian intensity distributions were

used to approximate stars. The radial parameter for the gaussians was taken as 2.85 (in 8 μm units) which was the value found for a gaussian fitted to star β of Tifft's sequence in NGC121, plate 950. The intensity-transmission calibration from plate 950 was used and also the value of the average sky background intensity was taken from the measurements of plate 950. To produce stars with a range in luminosities, the central intensity, I_c, was varied. In this model, the graininess of the plate was ignored, and so was the effect of the finite width of the spot.

First the true luminosity and the true intensity distribution were calculated for each image. Then the intensities were converted into transmissions, digitised as in COSMOS, and converted back to intensities and integrated to give the experimental value of the luminosity. Table 2.7 gives true luminosities, the luminosities calculated from digitised transmissions, and the error in magnitude. The error in magnitude can be positive or negative. However the majority of magnitudes are too large, especially for faint images. This is due to the loss of luminosity caused by the fainter outer parts of the images being indistinguishable from the background. The increase in magnitude error for the bright stars is due to the increase in error at high intensities caused by the binning of transmissions. The relationship between the magnitude error, Δm, and $2.5 \log I_c$, (which is proportional to the true magnitude since all the profiles are the same shape), is:

$$\Delta m = -0.003 \times 2.5 \log I_c + 0.021.$$

The systematic error is therefore negligible.

TABLE 2.7

Data for Synthesised Images to Test Effects of Binning on COSMOS

I_c^*	True Luminosity	Luminosity from digitised Transmissions	Δm
10	255.176	252.786	0.010
20	510.352	498.709	0.025
30	765.528	757.086	0.012
40	1020.703	1029.608	-0.009
50	1275.879	1262.408	0.012
75	1913.819	1911.709	0.001
100	2551.759	2545.774	0.003
125	3189.698	3187.743	0.001
150	3827.638	3834.432	-0.002
175	4465.578	4514.914	-0.012
200	5103.517	5065.002	0.008
225	5741.457	5816.468	-0.014
250	6379.397	6293.205	0.015
275	7017.336	6999.705	0.002
300	7655.276	7601.071	0.008

Star profiles are not in fact gaussian. The intensity distribution falls off less rapidly at low light levels (Moffat 1969) so there will be a greater contribution of low intensity light to the luminosity. This means that the systematic error will be slightly larger. However, even if the systematic error is doubled, this error will still be negligible compared with other errors, such as those caused by graininess. In the case of galaxies, though, the error caused by part of the image at low intensities remaining undetected is important, as explained in section 2.15.

Note: At high transmission values the analogue-digital converter on COSMOS favours even numbered transmission values. This will slightly increase the errors caused by binning.

2.11 Measurements of Stars on the Joyce Loebl Microdensitometer

Measurements of the standard stars near NGC121 on plate 330 were also made using a Joyce Loebl microdensitometer. These measurements were made because on the Joyce Loebl machine the measuring slit can be made very small so that the convolution effects arising in the COSMOS machine are reduced. The transmission profiles obtained were therefore more accurate, and the results could be used to check that the correct values for the magnitudes could be obtained using the step wedge to calibrate measurements of stars.

The width of the measuring slit was set so that it corresponded to a size of 8 μm on the plate, and its height was made as small as possible. (The slit height was not calibrated, but it was estimated to be about 8 μm.) Wedge number J45 was used which had a gradient

of 0.199 D/cm, and a useful range of 3.56 in density. A scan of the north step wedge was made using an arm ratio of 10:1, i.e. 1 cm on the plate corresponded to 10 cm on the tracing. The clear plate level was also measured and the height of each step above clear plate was calculated and converted into density and then into Baker density using the formula:

$$\Delta = \log (10^{D} - 1)$$

The calibration was then found by fitting a straight line to the log I - Δ relation. The r.m.s. error in the calibration was $\sigma_{\Delta} = 0.283$, which corresponded to an error in log I of ± 0.065.

The stars were measured using an arm ratio of 100:1 so that 1 mm of the tracing corresponded to 10 μm on the plate. One scan was made though the centre of each star. The height of the tracing was converted into intensity and the background intensity was subtracted. The luminosity was calculated by integrating the profile, assuming circular symmetry, and the magnitudes were found relative to the sky background magnitude, which was set to zero.

A comparison between the results and Tifft's photoelectric measurements is shown in figure 2.13. Stars S, R, and U are obviously saturated. The average regression line fitted through the remaining star magnitudes has the equation:

$$m_{JL} = 0.92 \times m_{pe} - 21.62$$

where m_{JL} is the magnitude calculated from the Joyce Loebl measurements, and m_{pe} is the photoelectric j magnitude.

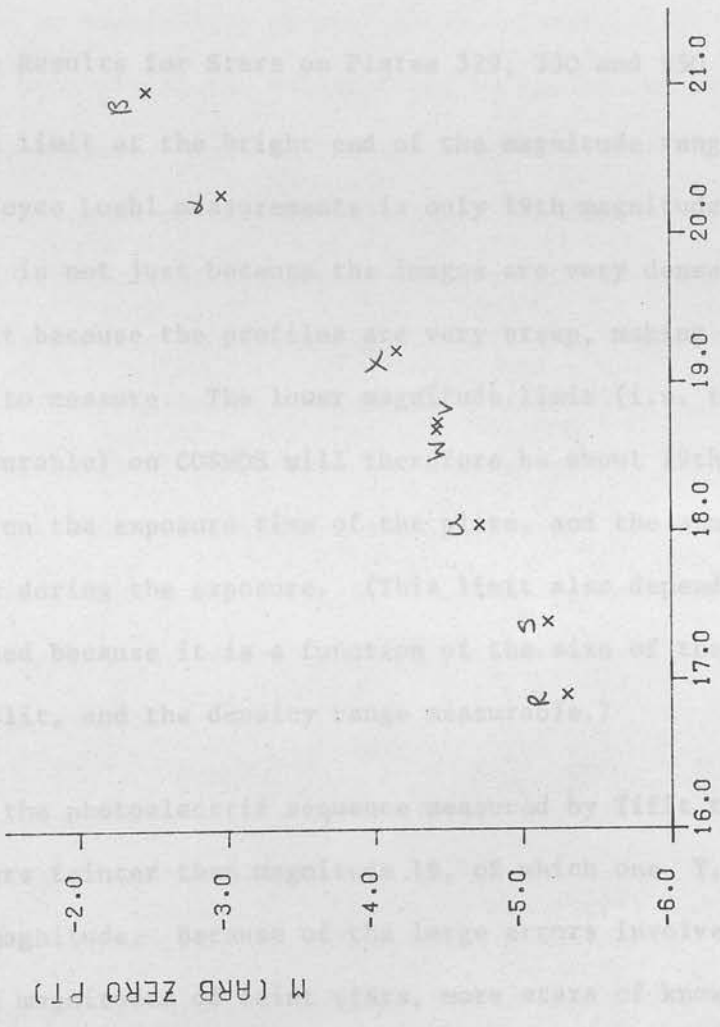

FIGURE 2.13 JOYCE LOEBL MAGNITUDES VS. PHOTOELECTRIC OR PHOTOGRAPHIC MAGNITUDES

If stars W and V are omitted, the equation becomes:

$$m_{JL} = 1.00 \times m_{pe} - 23.33$$

Therefore there is no systematic error in calculating the magnitudes using Joyce Loebl measurements for stars fainter than 19th magnitude. Stars brighter than this become saturated. These results show that it is possible to obtain correct magnitudes from measurements of Schmidt plates and so the COSMOS measurements, if corrected, should produce reasonable magnitudes.

2.12 The Results for Stars on Plates 329, 330 and 950

The limit at the bright end of the magnitude range obtainable from the Joyce Loebl measurements is only 19th magnitude for plate 330. This is not just because the images are very dense in the centre, but because the profiles are very steep, making the centres difficult to measure. The lower magnitude limit (i.e. the brightest stars measurable) on COSMOS will therefore be about 19th magnitude, depending on the exposure time of the plate, and the atmospheric conditions during the exposure. (This limit also depends on the machine used because it is a function of the size of the measuring spot, or slit, and the density range measurable.)

In the photoelectric sequence measured by Tifft there are only 5 stars fainter than magnitude 19, of which one, Y, does not have a B magnitude. Because of the large errors involved in determining the magnitudes of faint stars, more stars of known magnitude were required for comparison with the magnitudes determined from COSMOS mapping. The extra magnitudes were obtained from the coarse

measurement of the region by calibrating the logarithm of the image area against photoelectric magnitude (Dodd et al 1977). Second order polynomials were fitted to the logarithm of the area for stars in the sequence from S (m_j = 17.39) to β (m_j = 20.94). Three separate calibrations were obtained for plates 329, 330 and 950. The average standard deviation of the points from the polynomial was $0^m.2$.

37 stars with estimated magnitudes between 19 and 21 were chosen from an examination of the plates. Their magnitudes were calculated by applying the calibrations to the coarse measurement areas on each plate. Some of the stars were fainter than 21st magnitude and these were later rejected. The results are shown in table 2.8. Frequently, the magnitudes from two of the plates had similar values while the third magnitude differed considerably. When calculating the average magnitude, the result for one plate was rejected if it differed from the average of the other two by more than the difference between the other two. Comparison between the magnitudes from plates 329 and 330, missing out pairs where one star was rejected, and omitting stars fainter than m_j = 21, gave an r.m.s. error of $0^m.1$.

The magnitudes of the extra stars, referred to as photographic magnitudes, and the photoelectric magnitudes were compared with the magnitudes obtained from the COSMOS mapping measurements using the method described in section 2.3. First the magnitudes from the mapping were determined without applying the corrections for the COSMOS spot and halos. The results are shown in figure 2.14. In the case of

TABLE 2.8

Magnitudes of Extra Stars in NGC121

(Values in brackets indicate results which were rejected, as explained in text)

Star Number	Magnitudes			
	Plate 950	Plate 330	Plate 330	Adopted Value
1	-	20.59	-	-
2	20.52	20.33	20.43	20.43
3	-	-	-	-
4	-	19.31	19.14	19.22
5	20.15	20.11	(19.86)	20.12
6	(20.28)	19.72	19.64	19.68
7	-	20.24	20.17	20.20
8	(20.98)	20.55	20.55	20.55
9	21.15	21.23	20.96	(21.19)
10	-	20.06	-	-
11	-	19.09	18.85	18.85
12	(19.93)	19.62	19.46	19.54
13	20.87	(19.72)	20.76	20.81
14	19.45	(20.01)	19.60	19.52
15	(19.40)	18.92	19.04	18.98
16	20.28	(20.01)	20.30	20.29
17	-	21.90	22.42	(22.16)
18	21.20	(20.55)	20.91	(21.05)
19	19.85	(19.52)	19.91	19.88
20	(20.05)	19.67	19.69	19.68

contd...

TABLE 2.8 (contd.)

Star Number	Magnitudes			
	Plate 950	Plate 330	Plate 330	Adopted Value
21	-	21.58	21.90	(21.74)
22	-	-	-	-
23	(20.57)	19.47	19.78	19.62
24	-	21.82	21.90	(21.86)
25	21.10	21.52	(22.12)	(21.31)
26	20.98	21.23	20.88	20.93
27	19.64	19.62	(19.46)	19.63
28	20.01	20.33	20.43	20.38
29	20.63	20.83	20.43	20.63
30	(21.00)	21.83	21.88	(21.85)
31	20.66	20.52	(20.92)	20.58
32	20.15	(19.92)	20.13	20.14
33	20.45	20.46	20.51	20.47
34	20.57	20.51	(20.34)	20.54
35	20.42	20.51	(20.72)	20.46
36	-	20.91	21.07	20.99
37	20.87	20.91	20.96	20.91

FIGURE 2.14A MAGNITUDES FROM COSMOS MAPPING VS. PHOTOELECTRIC OR PHOTOGRAPHIC MAGNITUDES, PLATE 329.

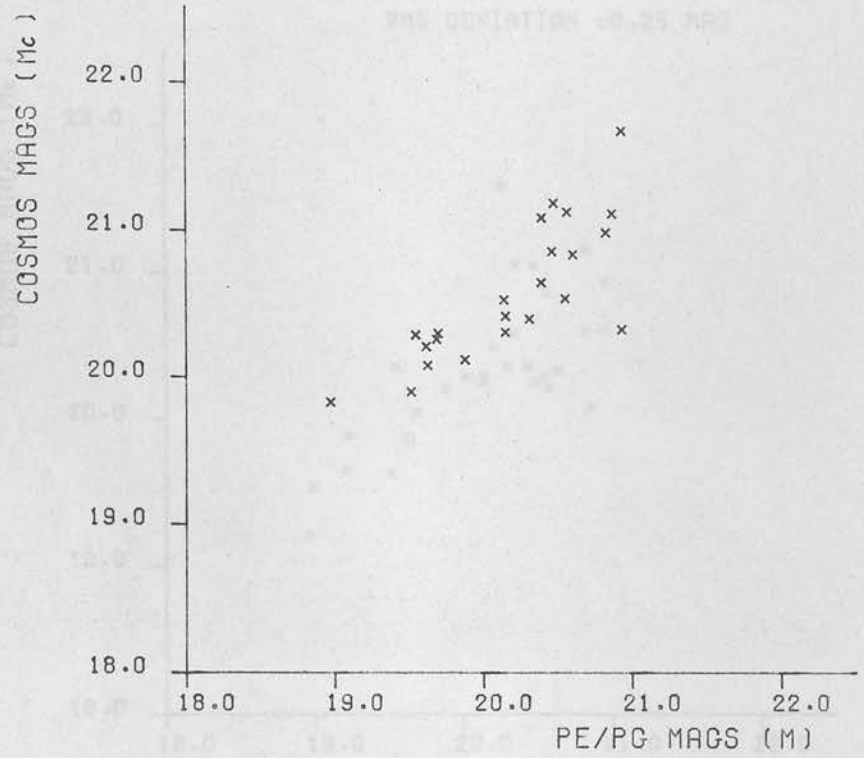

FIGURE 2.14B MAGNITUDES FROM COSMOS MAPPING VS. PHOTOELECTRIC OR PHOTOGRAPHIC MAGNITUDES, PLATE 330.

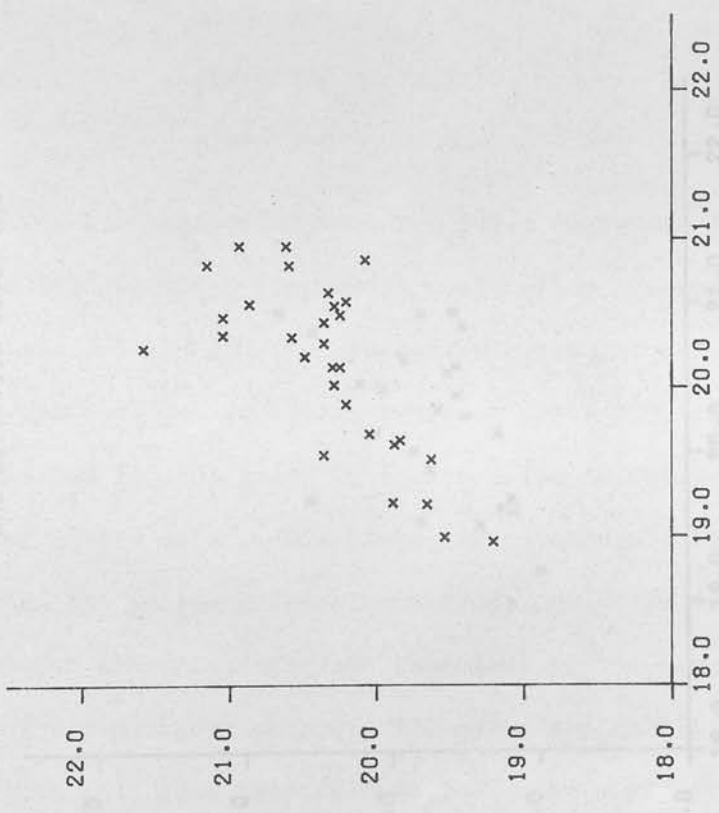

FIGURE 2.14C MAGNITUDES FROM COSMOS MAPPING VS. PHOTOELECTRIC OR PHOTOGRAPHIC MAGNITUDES, PLATE 950.

(SKY BRIGHTNESS SET TO ZERO)

AVE. REGRESSION LINE $M_c = 1.00M + 23.51$

RMS DEVIATION =0.34 MAG

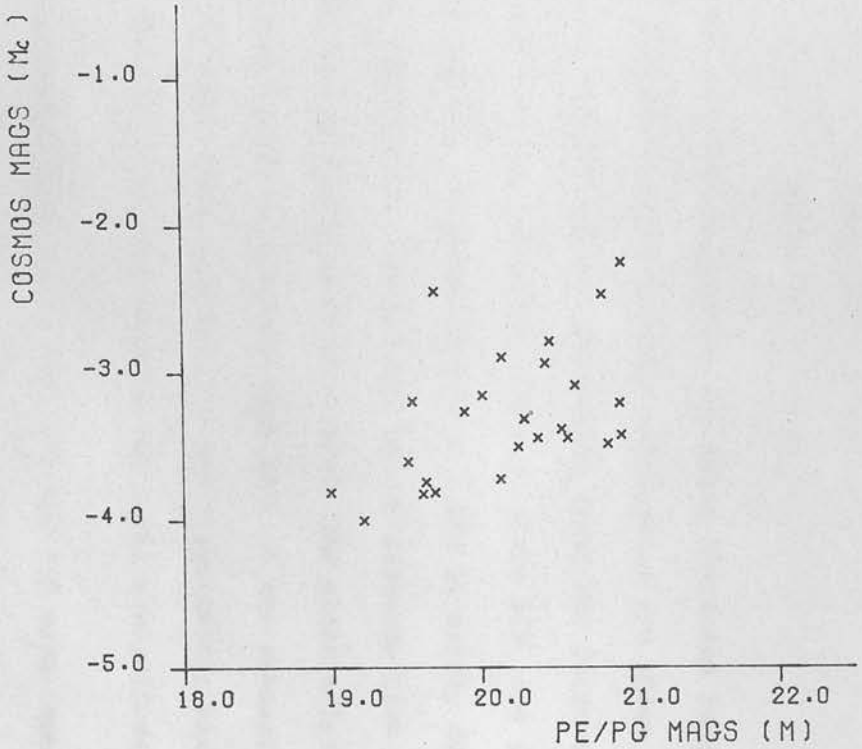

plates 329 and 330 there is a systematic error making the bright stars too faint. For plate 950, which only had a 20 minute exposure, there is no systematic error.

When the results were deconvoluted for the COSMOS spot, one change was made to the computer program. The value of the factor discussed in section 2.5, used in the threshold level for detecting images in the background region, was increased because of the increase in the dispersion of the background transmissions after deconvolution. The new values of the factor, which were obtained using the same method as before, but for deconvoluted transmissions, were:

plate 329	3.4
plate 330	4.3
plate 950	3.3

The results for the magnitudes from the fully corrected image transmissions and the corrected step wedge calibration are shown in figure 2.15. On plate 329 and 330 the systematic error has decreased. However, there are very few remaining stars on plate 329, and the slope of unity obtained for the graph in figure 2.15a is mainly due to the large scatter in the data. This plate had an exposure time of two hours and when the images were deconvoluted, the stars brighter than magnitude 20 had transmissions less than that of the densest step of the wedge. The magnitudes on plate 950 had a systematic error after correction. In this case they covered too large a magnitude range.

The magnitudes from plates 329, 330 and 950 were combined to give the average values, and the results were compared with the photoelectric and photographic magnitudes. In figure 2.16a the magnitudes

FIGURE 2.15A COSMOS MAGNITUDES FROM CORRECTED TRANSMISSIONS VS. PHOTOELECTRIC AND PHOTOGRAPHIC MAGNITUDES, PLATE 329.

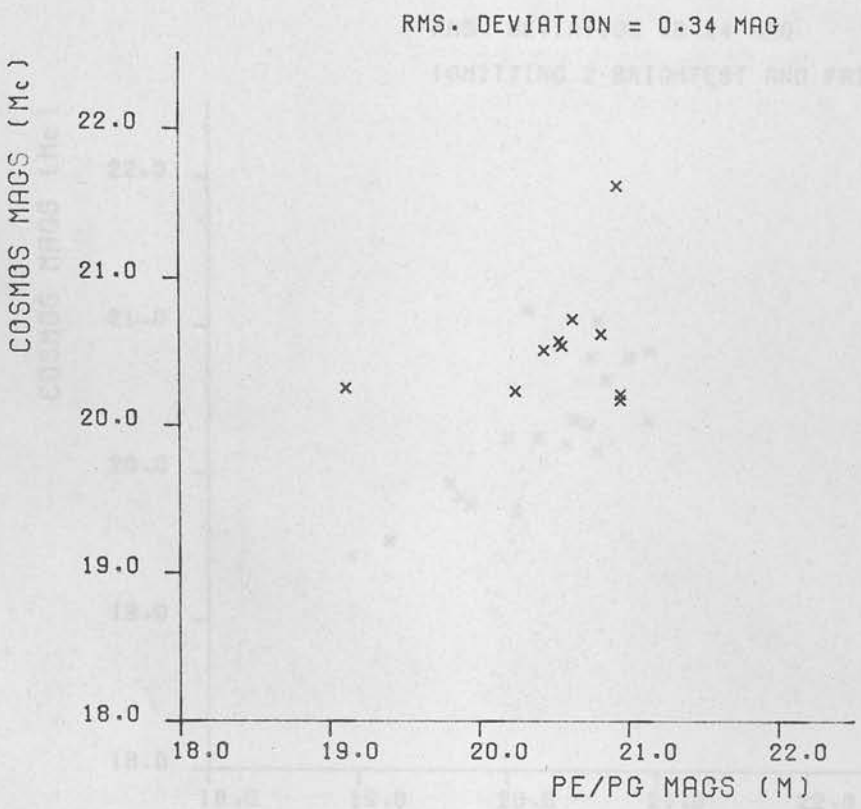

FIGURE 2.15B COSMOS MAGNITUDES FROM CORRECTED TRANSMISSIONS VS. PHOTOELECTRIC AND PHOTOGRAPHIC MAGNITUDES, PLATE 330.

AVE REGRESSION LINE Mc=0.95M+1.06

RMS. DEVIATION =0.24 MAG

(OMITTING 2 BRIGHTEST AND FAINTEST STARS)

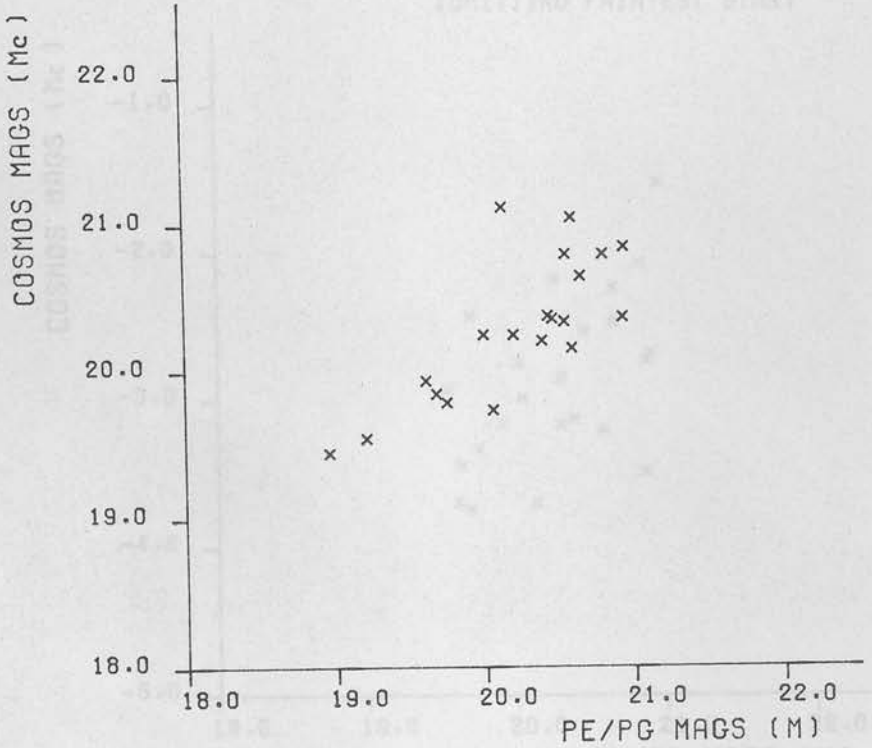

FIGURE 2.15C COSMOS MAGNITUDES FROM CORRECTED TRANSMISSIONS VS. PHOTOELECTRIC OR PHOTOGRAPHIC MAGNITUDES, PLATE 950.

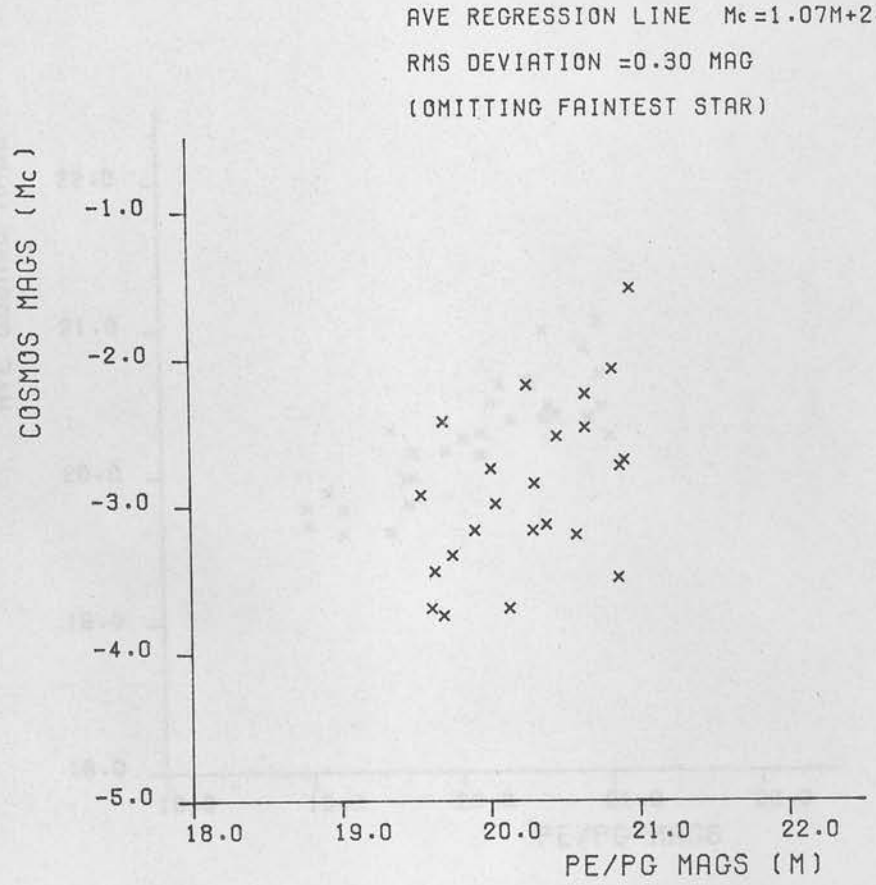

FIGURE 2.16A AVERAGE COSMOS MAGNITUDES FROM UNCORRECTED TRANSMISSIONS VS. PHOTOELECTRIC OR PHOTOGRAPHIC MAGNITUDES.

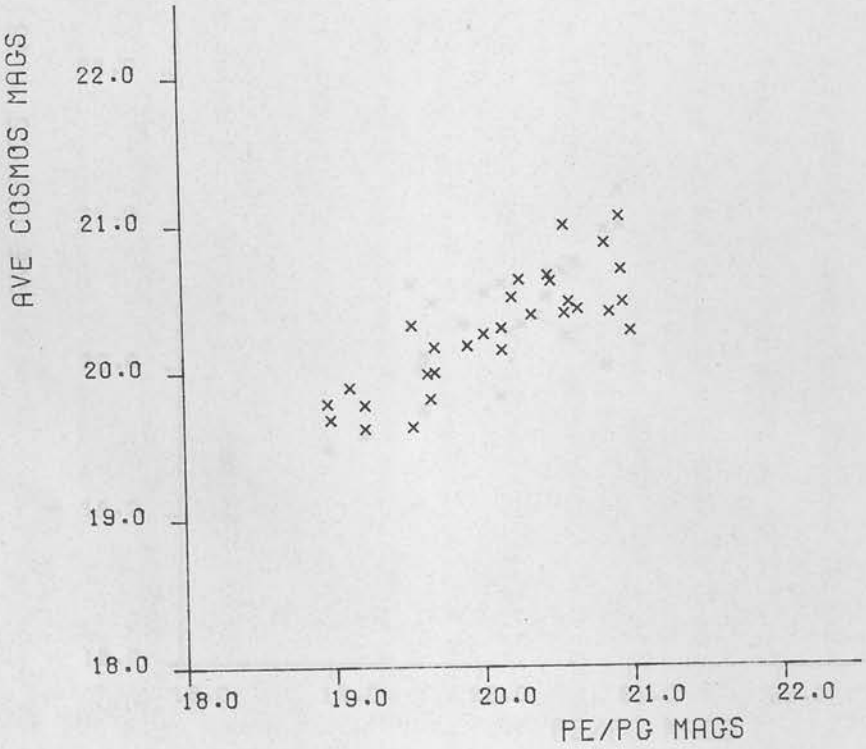

FIGURE 2.16B AVERAGE COSMOS MAGNITUDES FROM CORRECTED TRANSMISSIONS VS. PHOTOELECTRIC OR PHOTOGRAPHIC MAGNITUDES

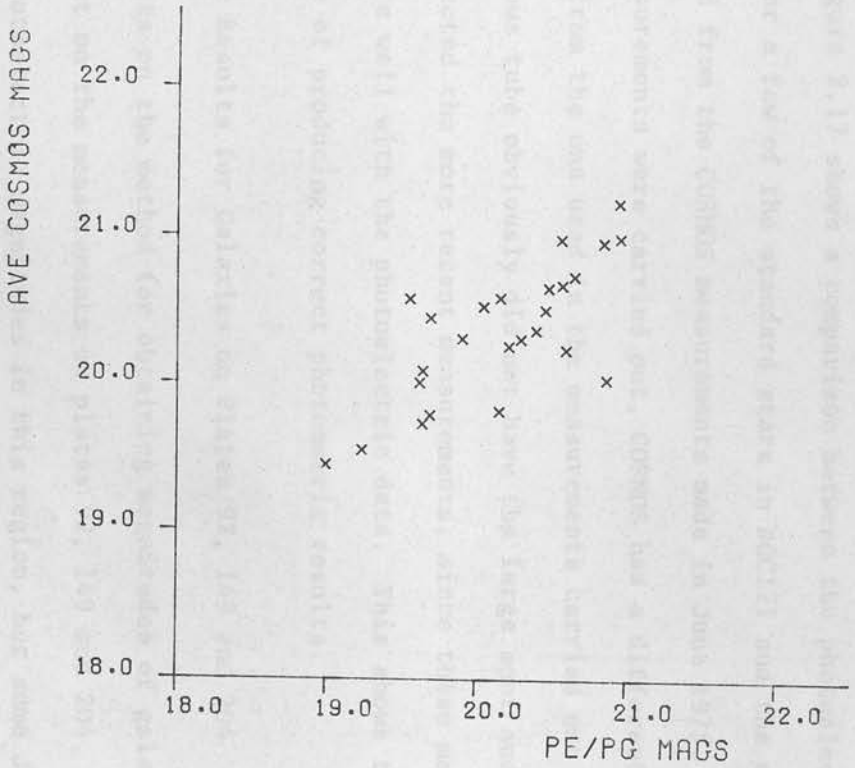

for the uncorrected tranwmissions show a definite systematic error, the slope of the average regression line being 0.67. The results for the corrected transmissions, (figure 2.16b) still show a slight systematic error according to the average regression line fitted through the points from magnitudes 19 to 21, which has a slope of 0.89. However, from an inspection of the graph, there is no systematic error between magnitudes 19.5 and 21.0. The larger scatter in this diagram is partly due to the fact that some star magnitudes could not be determined on all three plates. A few of the points are the results of one plate only and show the individual plate variations.

Figure 2.17 shows a comparison between the photoelectric magnitudes for a few of the standard stars in NGC121 and the magnitudes calculated from the COSMOS measurements made in June 1975. When these measurements were carried out, COSMOS had a different cathode ray tube from the one used in the measurements carried out in 1976. The previous tube obviously did not have the large spot and halos which affected the more recent measurements, since these magnitudes agree quite well with the photoelectric data. This shows that COSMOS is capable of producing correct photometric results.

2.13 The Results for Galaxies on Plates 92, 149 and 204

Tests on the method for obtaining magnitudes of galaxies were carried out on the measurements on plates 92, 149 and 204. There were no photoelectric magnitudes in this region, but some Joyce Loebl measurements were made of both stars and galaxies on plate 92 to compare with the COSMOS data. The Joyce Loebl measurements were

FIGURE 2.17 MAGNITUDES FROM COSMOS MEASUREMENTS MADE IN 1975 VS. PHOTOELECTRIC MAGNITUDES.

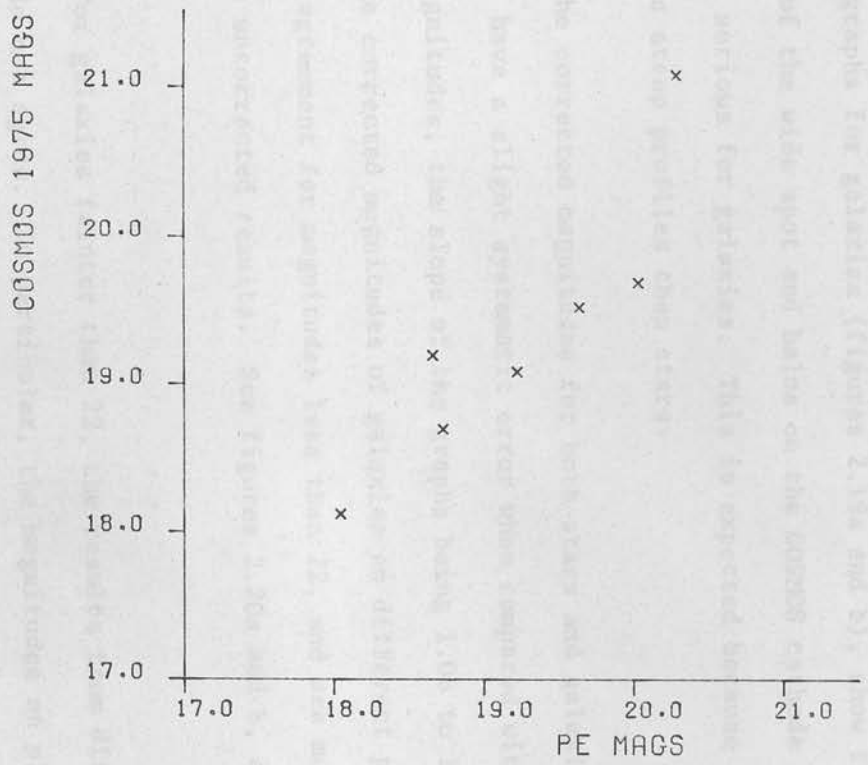

carried out in the same way as those for stars in NGC121, as described in section 2.11. Circular galaxies were chosen to be measured so that the luminosity could be calculated from one scan through the centre of each galaxy.

Figures 2.18a and b show a comparison between the magnitudes from the COSMOS data for the stars on plate 92 and the magnitudes from the Joyce Loebl measurements. As found previously, there is a large systematic error in the magnitudes from the uncorrected COSMOS transmissions, which is reduced in the corrected version. Similar graphs for galaxies (figures 2.19a and b), show that the effects of the wide spot and halos on the COSMOS cathode ray tube are less serious for galaxies. This is expected because galaxies have less steep profiles than stars.

The corrected magnitudes for both stars and galaxies on plate 92 have a slight systematic error when compared with the Joyce Loebl magnitudes, the slope of the graphs being 1.06 to 1.07. However, the corrected magnitudes of galaxies on different plates are in good agreement for magnitudes less than 22, and are much better than the uncorrected results. See figures 2.20a and b, and 2.21a and b.

For galaxies fainter than 22, the results from different plates do not agree. In particular, the magnitudes on plates 92 and 204 are fainter than those on plate 149. This can be explained by the fact that plate 149 had a longer exposure time (120 min) than plates 94 and 204 (90 min and 60 min respectively), and so on plate 149 galaxies were recorded to a lower limit in surface brightness than on the other plates.

FIGURE 2.18A UNCORRECTED COSMOS MAGNITUDES OF STARS ON PLATE 92 VS. JOYCE LOEBL MAGNITUDES.

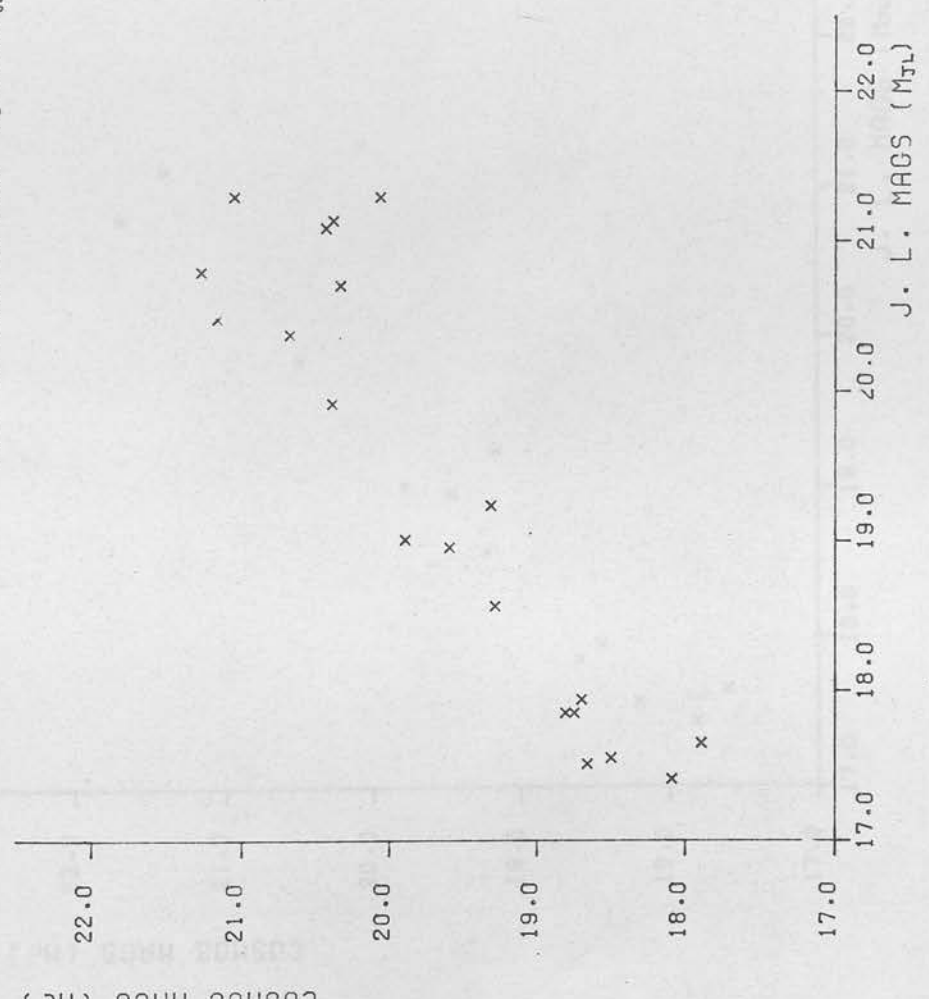

FIGURE 2.18B CORRECTED COSMOS MAGNITUDES OF STARS ON PLATE 92 VS. JOYCE LOEBL MAGNITUDES

AVE REGRESSION LINE $M_c = 1.07 M_{JL} - 0.87$

(OMITTING ONE STAR)

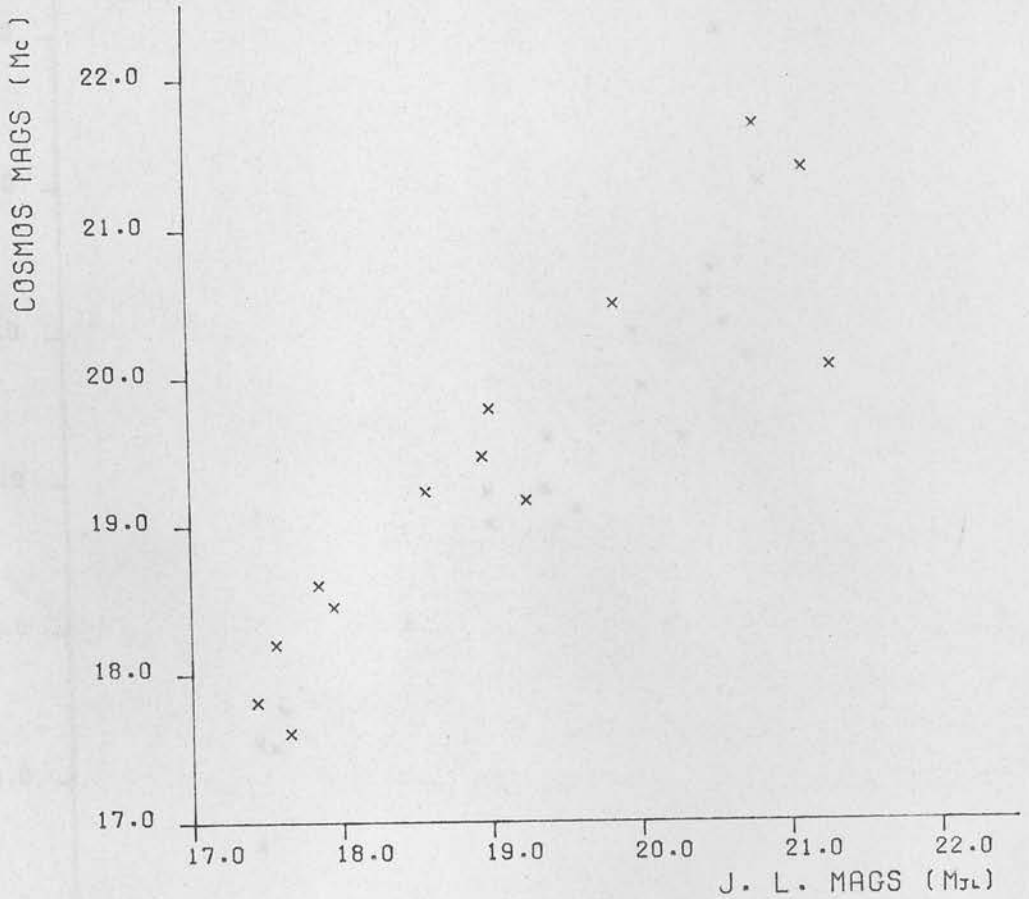

FIGURE 2.19A UNCORRECTED COSMOS MAGNITUDES OF GALAXIES ON PLATE 92 VS. JOYCE LOEBL MAGNITUDES.

AVE. REGRESSION LINE $M_c = 1.00 M_{JL} - 0.16$

(OMITTING BRIGHTEST AND FAINTEST STARS)

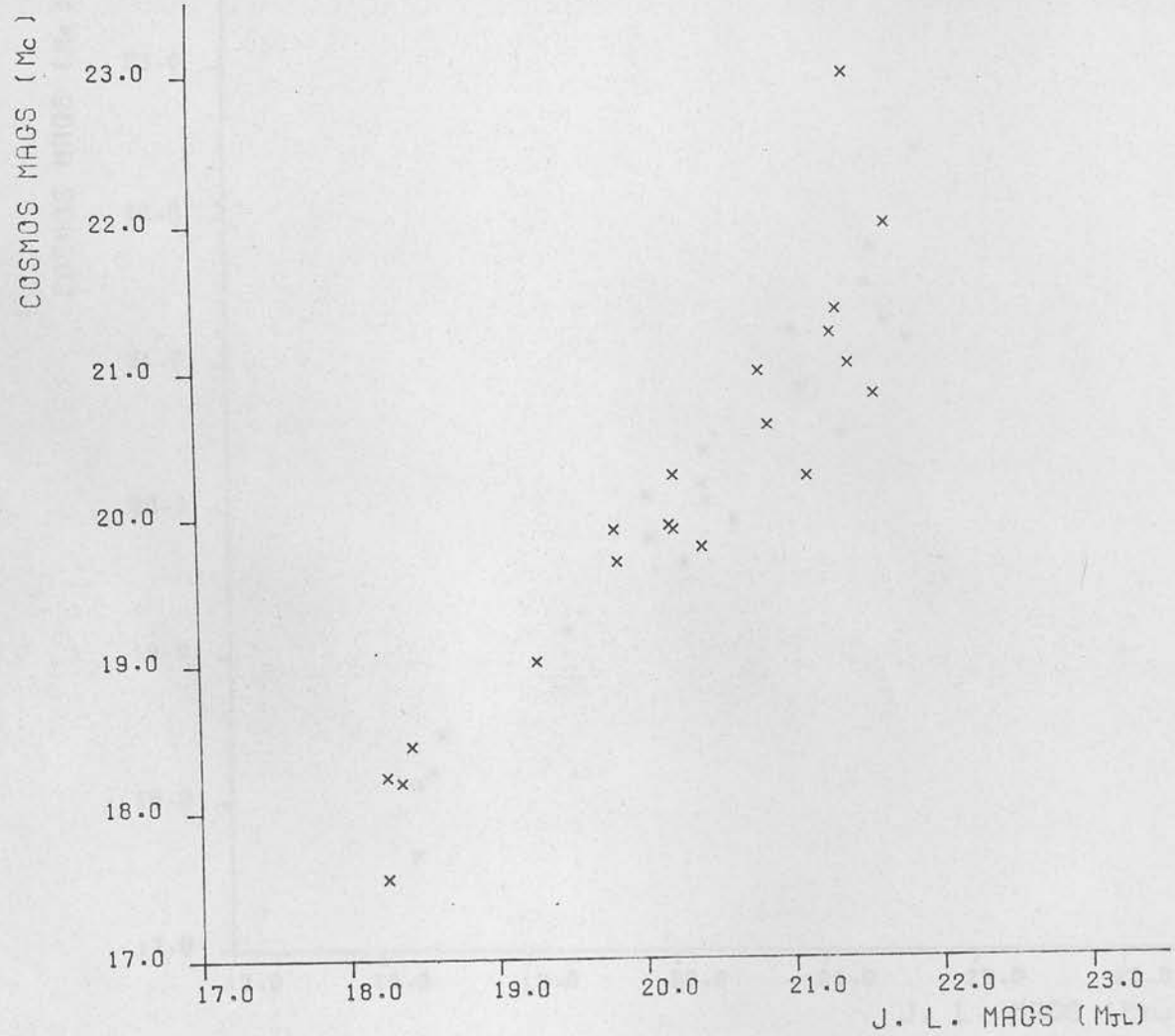

FIGURE 2.19B CORRECTED COSMOS MAGNITUDES OF GALAXIES ON PLATE 92 VS. JOYCE LOEBL MAGNITUDES.

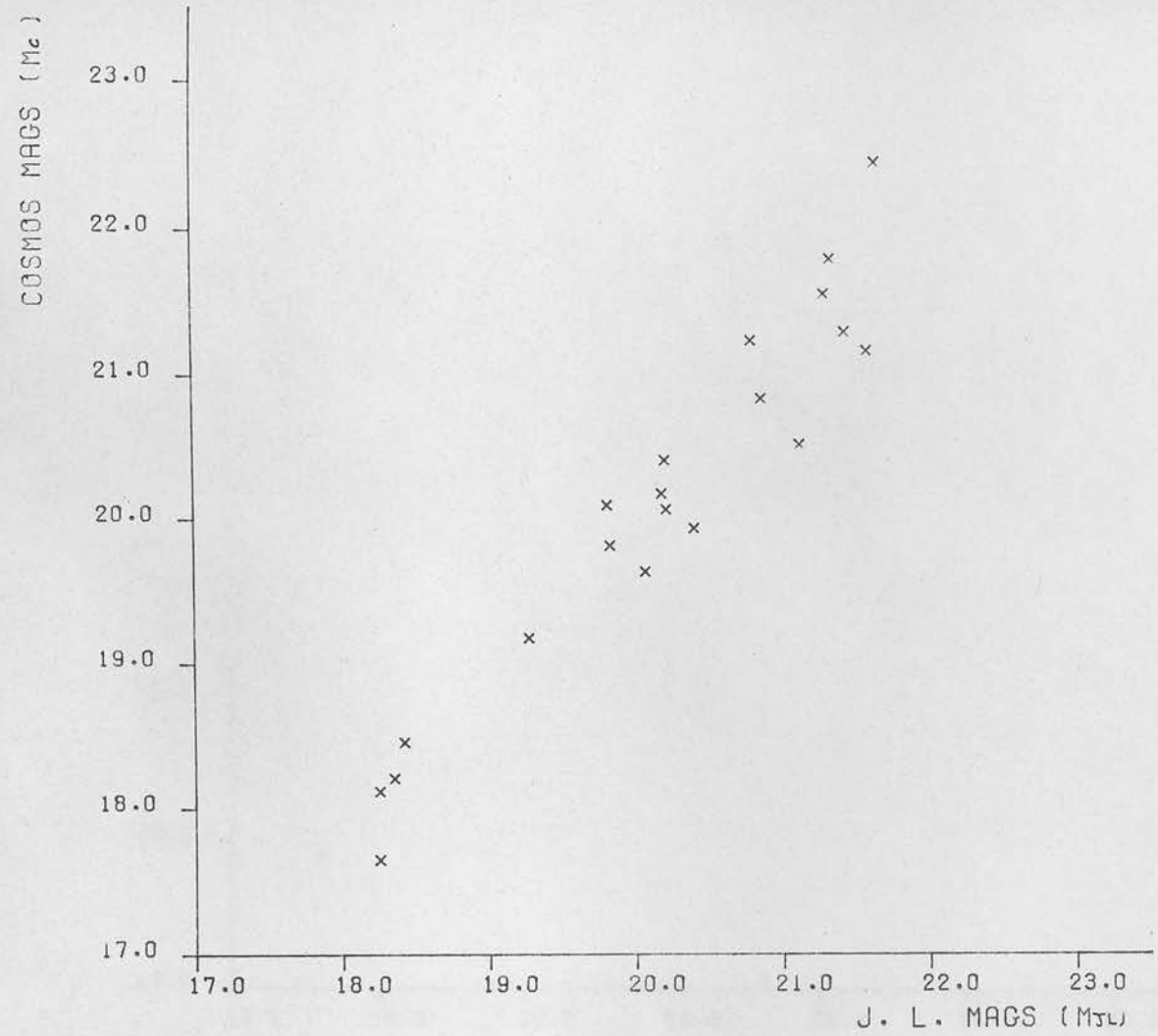

FIGURE 2.20A COMPARISON OF UNCORRECTED MAGNITUDES OF GALAXIES ON PLATES 92 AND 149.

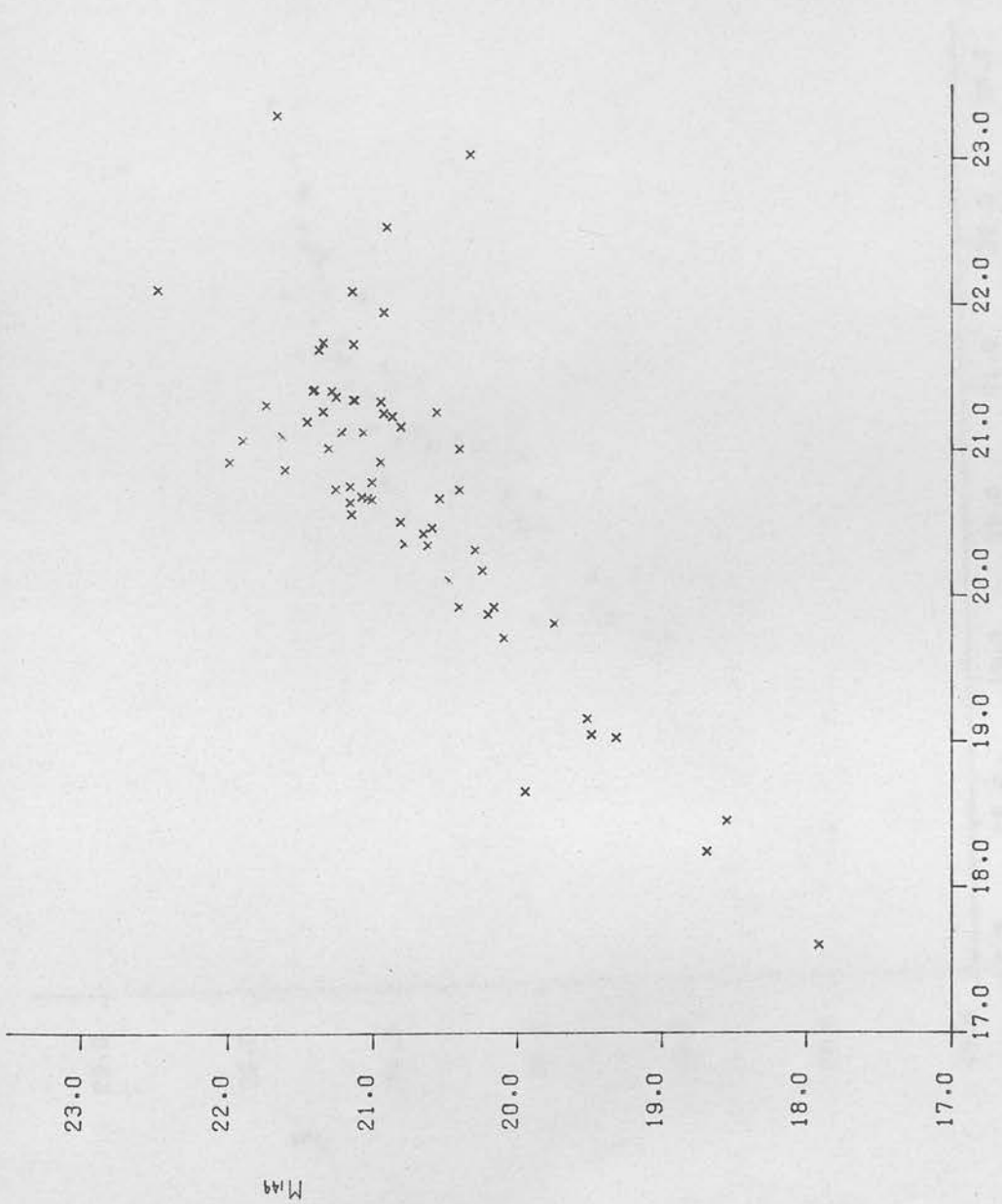

FIGURE 2·20B COMPARISON OF CORRECTED MAGNITUDES OF GALAXIES ON PLATES 92 AND 149.

AVE REGRESSION LINE $M_{149}=0.94M_{92}+1.22$

(OMITTING GALAXIES WITH M >22)

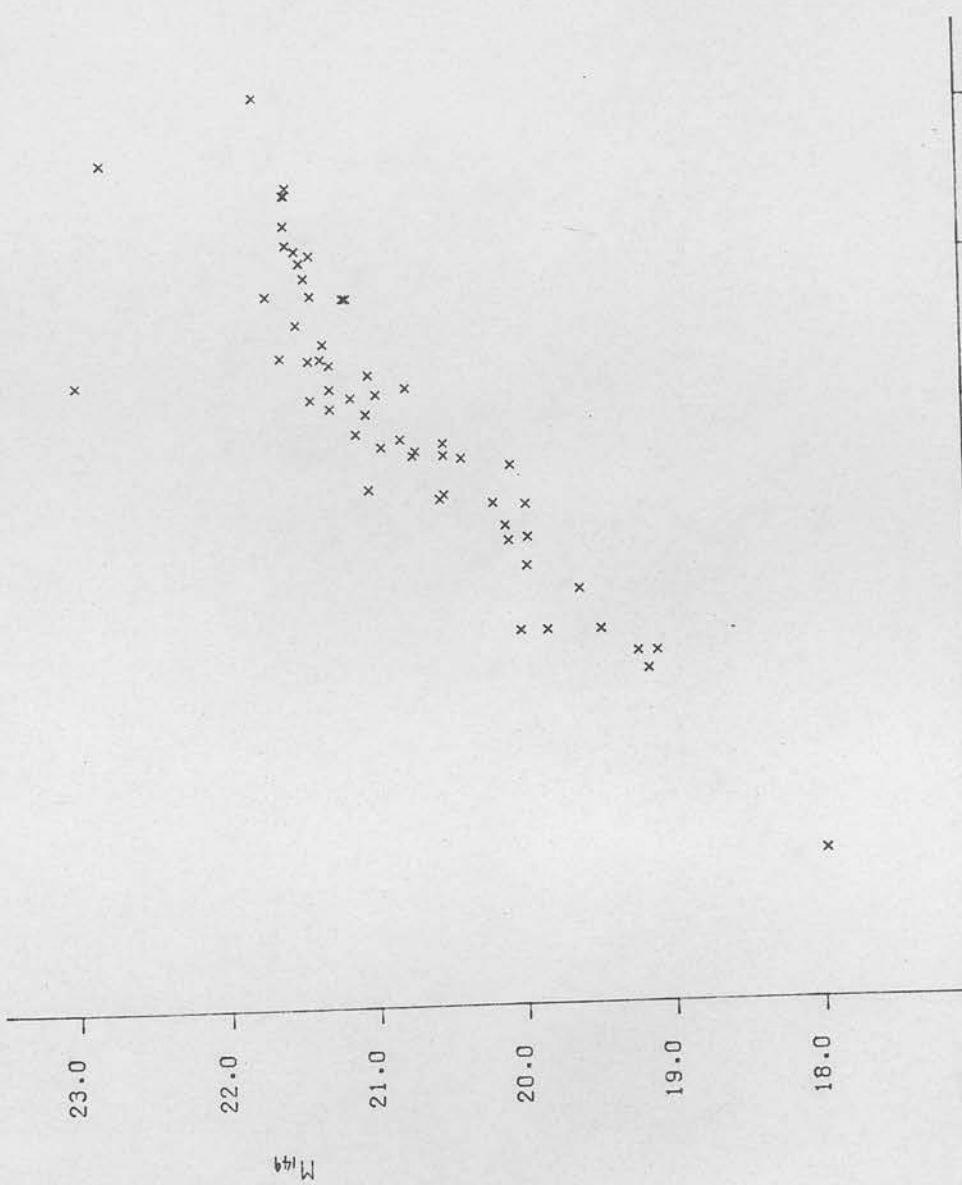

FIGURE 2.21B COMPARISON OF CORRECTED MAGNITUDES OF GALAXIES ON PLATES 92 AND 204.

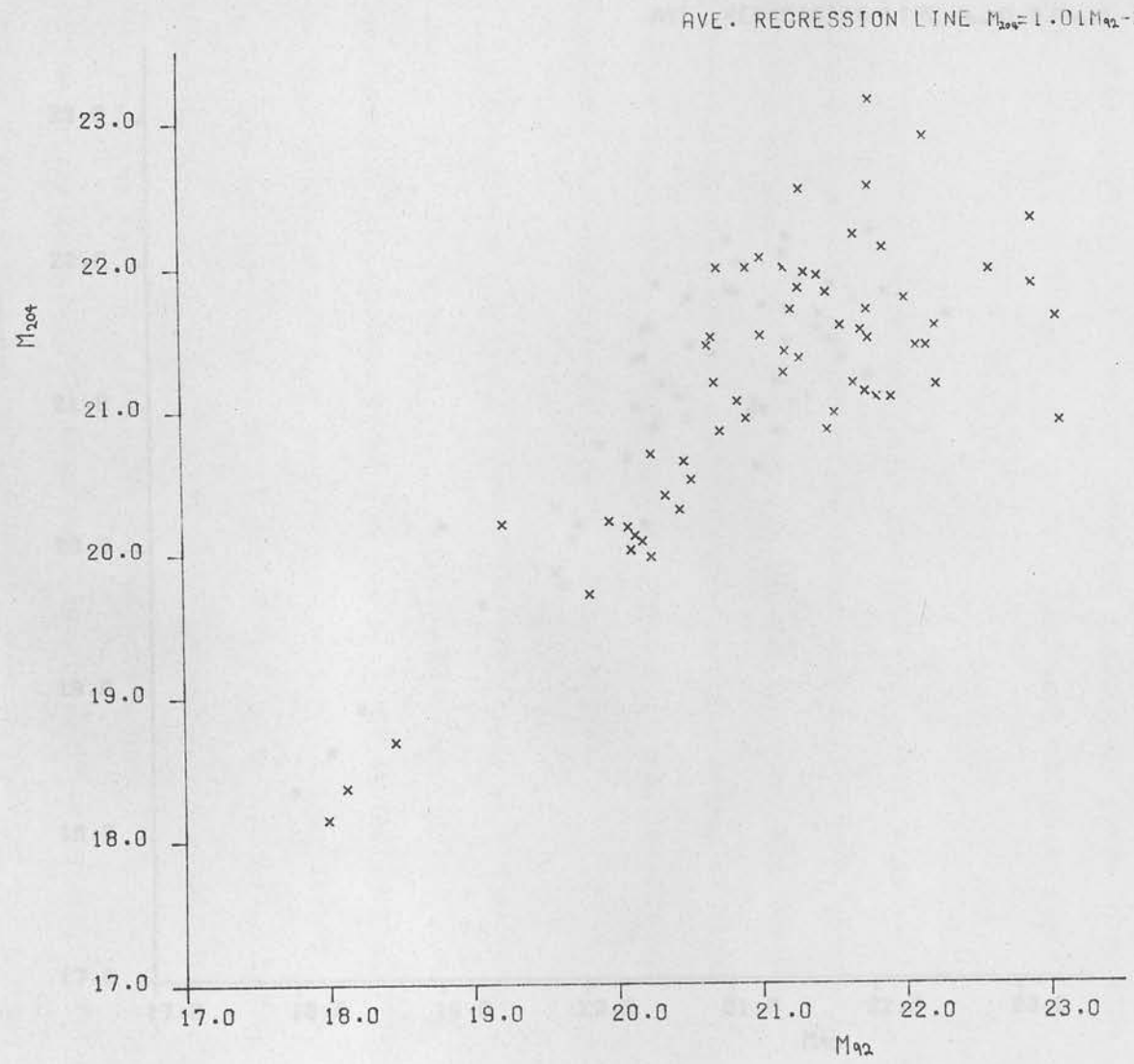

FIGURE 2.21A COMPARISON OF UNCORRECTED MAGNITUDES OF GALAXIES ON PLATES 92 AND 204.

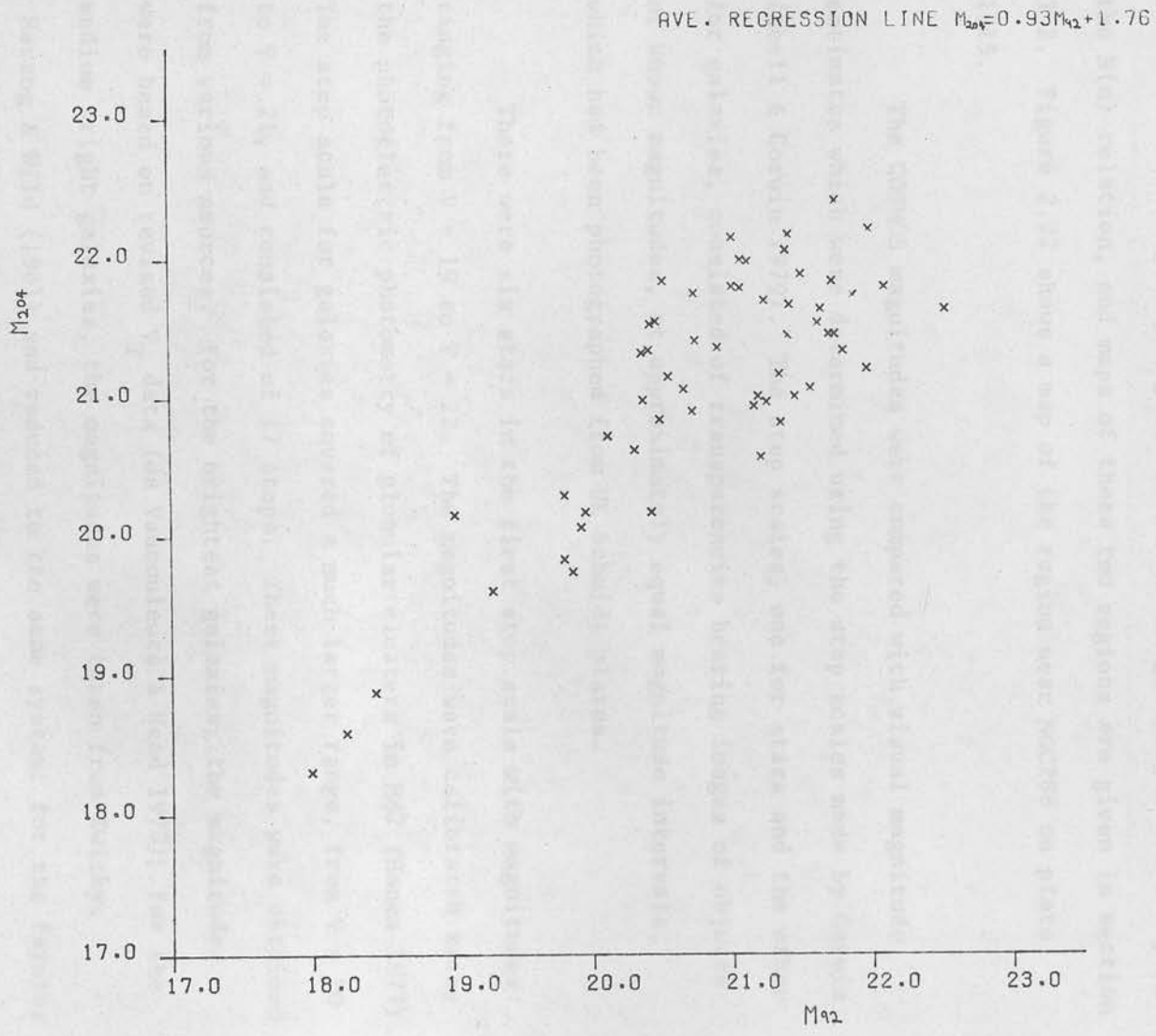

2.14 The Results for Plates 1915 and 1920

Further tests were carried out on some stars on plates 1915 and 1920, and also on some galaxies on plate 1920 (field II). The COSMOS mapping data from the regions on plate 1920 was later used to calibrate the galaxy magnitudes in the larger fields for studying the N(m) relation, and maps of these two regions are given in section 3.2. Figure 2.22 shows a map of the region near NGC288 on plate 1915.

The COSMOS magnitudes were compared with visual magnitude estimates which were determined using the step scales made by Corwin (Abell & Corwin 1979). The step scales, one for stars and the other for galaxies, consisted of transparencies bearing images of objects of known magnitudes, at approximately equal magnitude intervals, which had been photographed from UK Schmidt plates.

There were six stars in the first step scale with magnitudes ranging from V = 19 to V = 22. The magnitudes were calibrated using the photoelectric photometry of globular clusters in M87 (Hanes 1977). The step scale for galaxies covered a much larger range, from V = 10 to V = 21, and consisted of 17 steps. These magnitudes were obtained from various sources. For the brightest galaxies, the magnitudes were based on revised V_T data (de Vaucouleurs & Head 1978); for the medium bright galaxies, the magnitudes were taken from Zwicky, Herzog & Wild (1961) and reduced to the same system; for the fainter galaxies, the magnitudes were derived from 'astrophotometer' scans or iris diaphragm photometry (Eastmond 1977); and for the faintest galaxies, the magnitudes came from photoelectric photometry made by Sandage (1972) and the globular cluster photometry by Hanes (1977).

FIGURE 2.22 MAP OF THE STARS NEAR NGC288.

R. $A._{1950} = 00^h\ 50.2^m$ $DEC._{1950} = -26^\circ\ 52'$

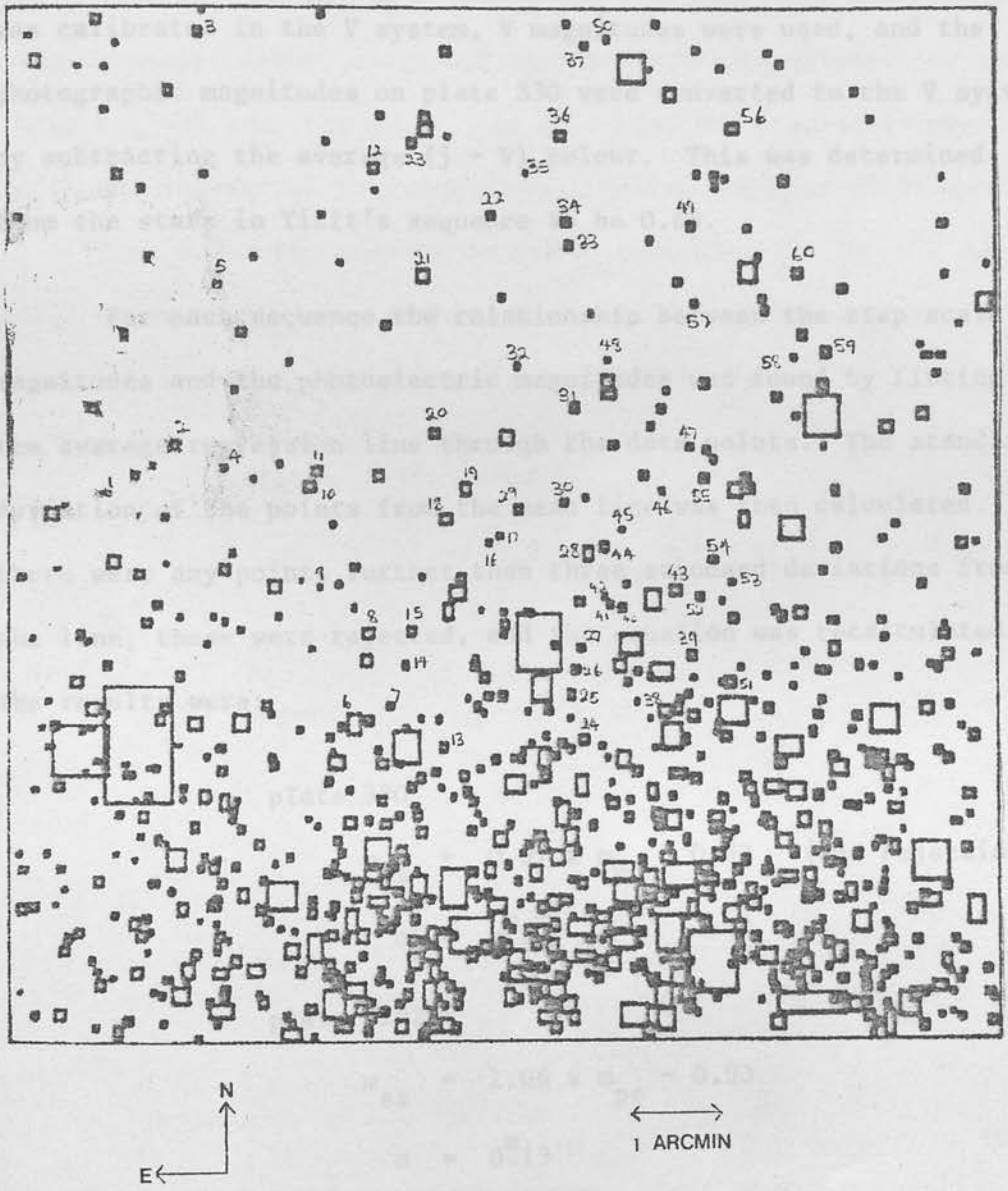

The first scale for stars was tested using two Schmidt plates on which there were faint photoelectric sequences: Tifft's (1963) sequence in NGC121 on plate 330, augmented by the photographic magnitudes obtained from COSMOS coarse measurement, and photometry by Arp (1962) in M5 on plate 3192. Since the step scale was calibrated in the V system, V magnitudes were used, and the photographic magnitudes on plate 330 were converted to the V system by subtracting the average (j - V) colour. This was determined from the stars in Tifft's sequence to be 0.66.

For each sequence the relationship between the step scale magnitudes and the photoelectric magnitudes was found by fitting the average regression line through the data points. The standard deviation of the points from the mean line was then calculated. If there were any points further than three standard deviations from the line, these were rejected, and the equation was recalculated. The results were:

plate 330

$$m_{ss} = 0.97 \times m_{pe} + 0.83 \quad \text{(one rejection)}$$

$$\sigma = 0^m.19$$

plate 3192

$$m_{ss} = 1.06 \times m_{pe} - 0.93$$

$$\sigma = 0^m.13$$

(m_{ss} is step scale magnitude and m_{pe} is photoelectric magnitude.)

In both cases the step scale magnitudes are about $0^m.2$ fainter than the photoelectric magnitudes. This could be caused by a calibration

error in the step scale. The standard deviations, which include the errors in the photoelectric photometry as well as photographic errors and errors in the visual estimates, are small, indicating that the step scale method is accurate.

Tables 2.9a, b and c show a comparison between the COSMOS mapping magnitudes of stars and the step scale magnitudes for the three regions near the S.G.P. In this case the step scale magnitudes were converted to j magnitudes, taking the average value for (j - V) as 0.7. The results were also corrected for the $0^m.2$ zero point error in the step scale calibration. The mean regression line and the standard deviation were calculated as before.

plate 1920 (field I)

$$m_{cos} = 0.97 \times m_{ss} + 0.54 \quad \text{(two rejections)}$$

$$\sigma = 0^m.26$$

plate 1920 (field II)

$$m_{cos} = 1.07 \times m_{ss} - 1.42$$

$$\sigma = 0^m.27$$

plate 1915 (field III)

$$m_{cos} = 1.05 \times m_{ss} - 0.85 \quad \text{(one rejection)}$$

$$\sigma = 0^m.23$$

This indicates a good agreement between the step scale results and the COSMOS measurements.

It is more difficult to make visual estimates of galaxies because of the variety of different types of galaxy. The galaxies

TABLE 2.9a

Comparison between Step Scale and COSMOS Magnitudes
Plate 1920 Field I

Image No *	m_{ss}	m_{cos}
19	21.28	20.69
85	20.75	20.26
104	20.07	19.92
169	20.93	21.29
173	21.10	21.34
220	20.70	20.52
239	19.65	19.46
268	21.05	20.91
(311	20.55	19.39)
317	19.30	19.26
342	19.02	19.01
352	20.20	20.07
358	20.40	20.51
359	21.50	20.68
390	20.06	19.60
392	20.45	21.30
407	19.00	18.99
436	21.50	20.71
466	20.14	20.18
481	20.00	20.09
507	19.28	19.07
(519	20.40	19.06)
532	20.20	20.77
543	20.25	20.00
620	19.28	19.63
638	19.80	20.06
647	20.06	20.09
660	19.60	19.51
690	20.30	20.30
699	20.30	20.04
724	20.55	20.87
726	20.10	20.12

* See figure 3.2a

Note: The stars in brackets were rejected.

TABLE 2.9b

Comparison between Step Scale and COSMOS Magnitudes
Plate 1920 Field II

Image No *	m_{ss}	m_{cos}
11	21.05	20.91
13	20.98	20.99
16	21.50	22.03
30	19.85	20.08
31	19.85	20.22
36	20.65	20.07
43	20.55	20.06
45	21.28	21.62
48	21.40	21.23
52	20.80	21.78
54	21.05	21.40
60	20.55	20.64
64	21.31	21.00
65	21.95	21.57
74	19.80	19.78
75	19.44	19.29
78	20.80	20.36
84	21.31	21.45
95	21.28	21.77
113	21.19	21.10
141	19.54	19.48
155	19.54	19.45
158	21.75	21.74
162	20.55	21.24
174	20.40	20.61
276	19.80	19.65
304	21.12	21.17
346	20.30	20.95

* See figure 3.2b

TABLE 2.9c

Comparison between Step Scale and COSMOS Magnitudes
Plate 1915 Field III

Image No*	m_{ss}	m_{cos}
1	20.94	21.05
5	20.94	21.58
16	21.32	21.38
17	20.80	20.87
20	19.74	19.83
22	20.50	20.88
23	19.74	20.23
28	20.50	20.09
31	19.74	20.16
32	20.94	20.93
33	19.95	20.14
34	19.80	20.13
35	21.98	21.76
36	19.43	19.36
37	20.35	20.87
40	20.64	20.16
41	20.55	20.00
45	21.31	21.44
46	21.98	21.56
47	20.80	21.03
49	20.26	20.13
50	20.90	20.92
51	19.00	19.32
52	20.15	20.60
53	21.08	21.24
57	21.05	21.59

* See figure 2.22

TABLE 2.10

Comparison between Step Scale and COSMOS Magnitudes of Galaxies, Plate 1920 Field II

Image No *	m_{ss}	m_{cos}
(1	23	20.18)
10	22	22.11
22	22	21.57
25	21.25	20.54
28	20.10	20.12
31	19.80	20.22
37	22	22.36
47	21.25	21.62
49	21.24	21.07
51	20.10	19.93
57	19.80	19.69
61	20.70	22.03
66	20.70	21.45
72	21.25	21.39
91	21.25	21.20
98	20.10	20.93
105	20.10	20.39
109	20.70	20.71
111	20.70	21.93
118	22	22.21
136	20.10	19.70
140	21.25	21.88
160	18.30	19.05
(194	20.70	22.91)
234	20.70	20.86
338	20.10	19.49
378	19.80	19.49
473	19.20	19.27

* See figure 3.2b

in the step scale are all early type galaxies, and the majority are face-on. Due to the problems in making the visual estimates, the step scale magnitudes of the faintest galaxies are uncertain. Table 2.10 gives a list of the results. The relationship between the COSMOS magnitudes and the step scale magnitudes was:

$$m_{cos} = 1.09 \times m_{ss} - 1.66 \quad \text{(two rejections)}$$

$$\sigma = 0^{m}.36$$

2.15 The Limiting Isophote

As explained in chapter 1, it is impossible to measure the total magnitude of a galaxy because of the extensive, low intensity halo. Instead an isophotal magnitude can be calculated from the luminosity within a limiting isophote. In the case of the magnitudes determined from COSMOS measurements, extra tests had to be carried out to determine the limiting isophote.

First, the profile of the galaxy NGC7144, plate 2520, was examined. This galaxy is morphological type E_1, with nearly circular isophotes, and the magnitude out to the isophote of 26 mag arcsec^{-2} is V = 11.12 (Sandage 1975). This galaxy was mapped using COSMOS and the N-S cross-section through the centre is shown in figure 2.23a. The nucleus of the galaxy is saturated, but the envelope can be detected at large distances from the nucleus. In fact the outer limits of the galaxy are not reached in the region mapped which is approximately 9 arcmin square. It can be seen that on the outskirts of the galaxy, the difference between the intensity of the galaxy and the sky intensity is less than the fluctuations in intensity due

FIGURE 2.23A N-S CROSS-SECTION THROUGH NGC7144.

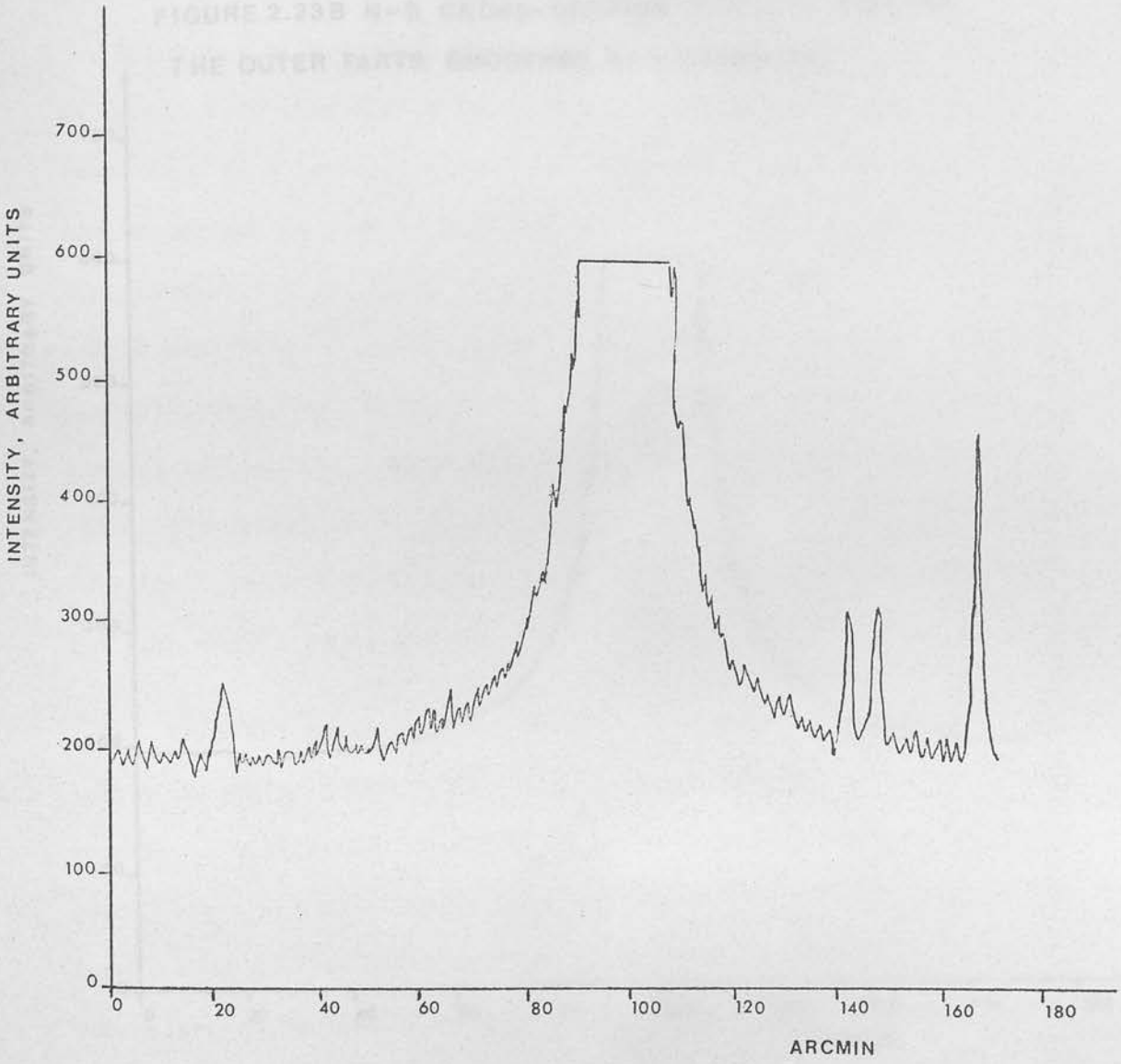

FIGURE 2.23B N-S CROSS-SECTION THROUGH NGC7144, THE OUTER PARTS SMOOTHED BY A GAUSSIAN.

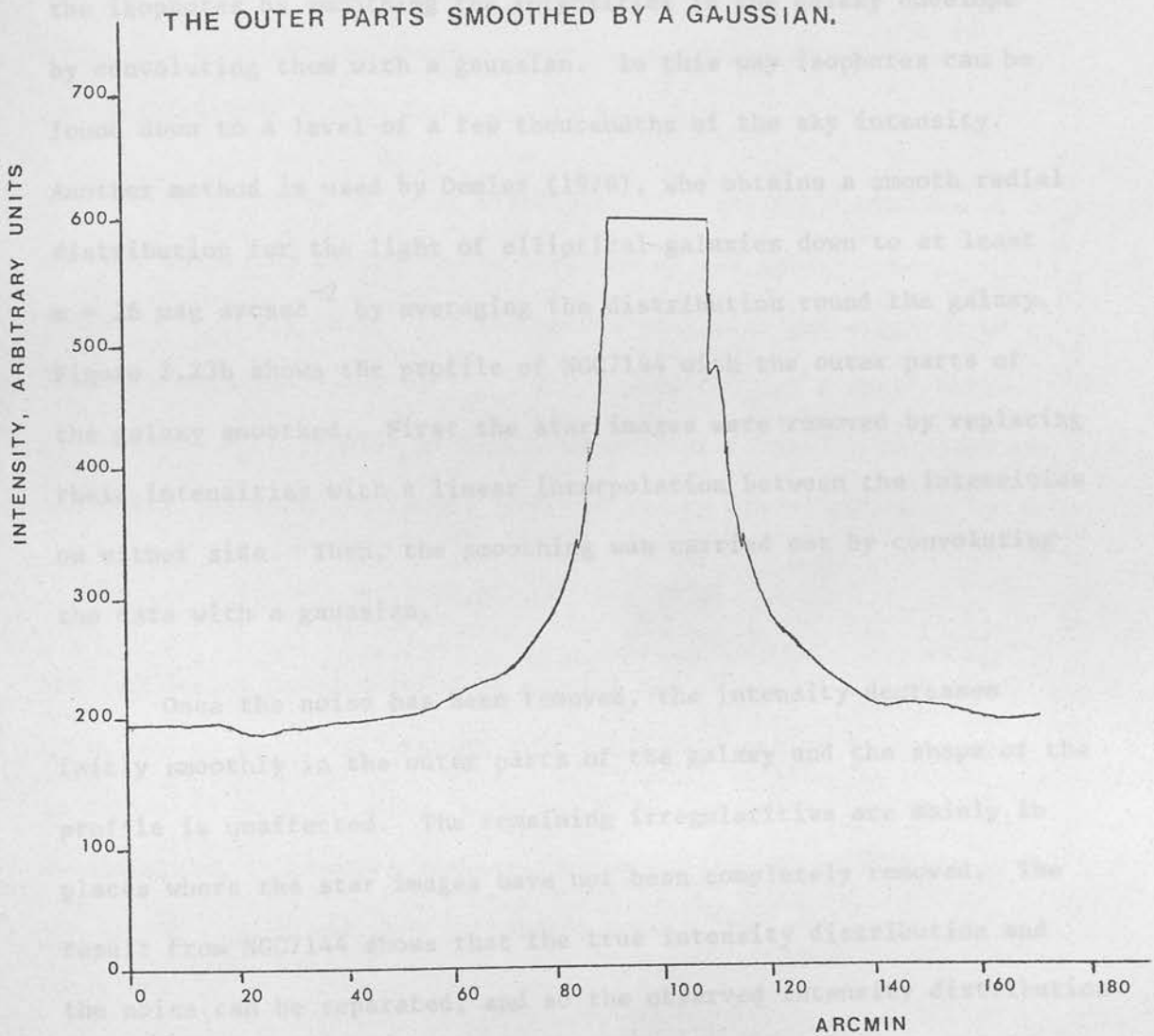

to the graininess. Closed isophotes can only be drawn for intensities above the noise level, i.e. intensities greater than a few percent of the night sky. De Vaucouleurs in his method of galaxy photometry, (Obitts, Gallet, Jones & de Vaucouleurs 1967), extends the isophotes by smoothing the intensities in the galaxy envelope by convoluting them with a gaussian. In this way isophotes can be found down to a level of a few thousandths of the sky intensity. Another method is used by Oemler (1976), who obtains a smooth radial distribution for the light of elliptical galaxies down to at least $m = 26$ mag arcsec^{-2} by averaging the distribution round the galaxy. Figure 2.23b shows the profile of NGC7144 with the outer parts of the galaxy smoothed. First the star images were removed by replacing their intensities with a linear interpolation between the intensities on either side. Then, the smoothing was carried out by convoluting the data with a gaussian.

Once the noise has been removed, the intensity decreases fairly smoothly in the outer parts of the galaxy and the shape of the profile is unaffected. The remaining irregularities are mainly in places where the star images have not been completely removed. The result from NGC7144 shows that the true intensity distribution and the noise can be separated, and so the observed intensity distribution in the galaxy image can be represented by the following formula:

$$I(x,y) = I_g(x,y) + I_{sky} + I_n(x,y)$$

where I_g is the true intensity distribution in the galaxy, I_n describes the random fluctuations about the zero point due to the graininess of the emulsion and the gradual variation due to local errors.

In the absence of photographic noise, the observed intensity distribution would decrease in a series of steps corresponding to the transmission levels on COSMOS. The light of the galaxy could be detected to intensity ΔI, corresponding to the interval between the average sky transmission and one transmission below this. In this case, the magnitude calculated from the summation of the intensities is the magnitude within the isophote ΔI.

The presence of noise firstly affects the determination of the sky intensity in the region surrounding the galaxy. Here, $I(x,y) = I_{sky} + I_n(x,y)$, and the values of $I(x,y)$ are averaged to find the measured value of I_{sky}, which will contain a small error, ε_1, because $I_n(x,y)$ will probably not average to zero. Once the sky intensity has been subtracted from the galaxy distribution,

$$I(x,y) = I_g(x,y) - \varepsilon_1 + I_n(x,y).$$

The luminosity is calculated by summing the values of $I(x,y)$ every 8 μm, and so the error arising from the determination of the sky intensity is multiplied by the area, A, of the galaxy region. A second error, ε_2, occurs because the sum of the values of $I_n(x,y)$ in the galaxy region will not be exactly zero. The total error is therefore

$$\varepsilon = \varepsilon_1 \times A + \varepsilon_2.$$

The noise causes errors in the luminosity, it does not affect the lowest intensity level above the sky background detected by COSMOS.

The galaxies considered in this survey are much more distant

than NGC7144, and there are two factors affecting the profiles of galaxies at different distances. More distant galaxies have smaller angular sizes, and for the faint galaxies observed on the Schmidt plates, their sizes are comparable to the width of the 'seeing disk' i.e. the size of the images of stars whose light has been spread out by atmospheric turbulence. For nearby galaxies, the effect of atmospheric turbulence on the profile is negligible, except in the nucleus. However, in the case of distant galaxies, the true profiles are spread out and altered considerably. In particular, light from the centre of images is scattered to the edges, and the more distant the galaxy, the larger the fraction of the total luminosity which lies below the threshold of detection. This means that the outer envelope of distant galaxies cannot be detected. Figures 2.24a and b show the intensity profiles of two galaxies on plate 149 which have corrected magnitudes of 19.31 and 20.76 respectively. (The profiles were plotted from uncorrected transmissions.) Although the profiles of these images are different from that of NGC7144, the intensity distribution can still be considered in three parts: contributions from the galaxy and from the sky, on which the noise is superimposed. The threshold of detection by COSMOS will still be ΔI as defined above. However, the decreased signal to noise ratio for the fainter images will cause larger errors in the magnitudes.

2.16 Analysis of Errors

The root mean square errors in the data found when comparing the COSMOS magnitudes of stars with standard magnitudes arise from both photographic and photoelectric errors. A series of tests was

FIGURE 2.24A INTENSITY PROFILE OF A GALAXY OF MAGNITUDE 19.31, PLATE 149.

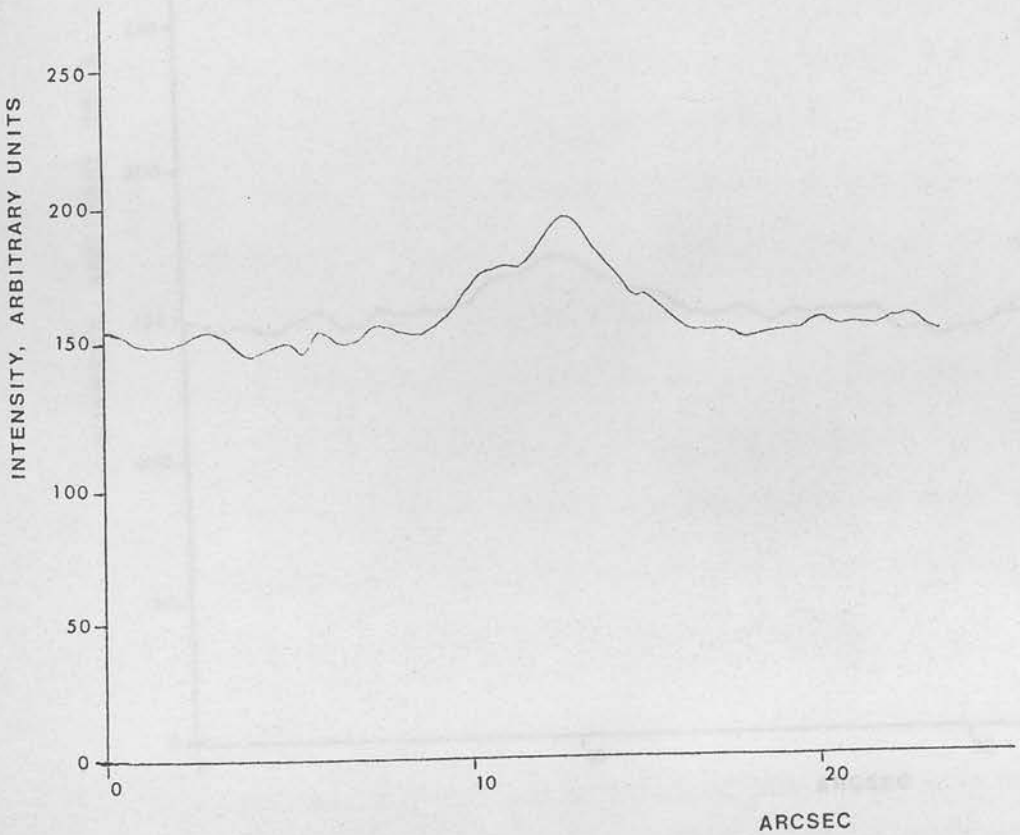

FIGURE 2.24B INTENSITY PROFILE OF A GALAXY OF MAGNITUDE 20.76, PLATE 149.

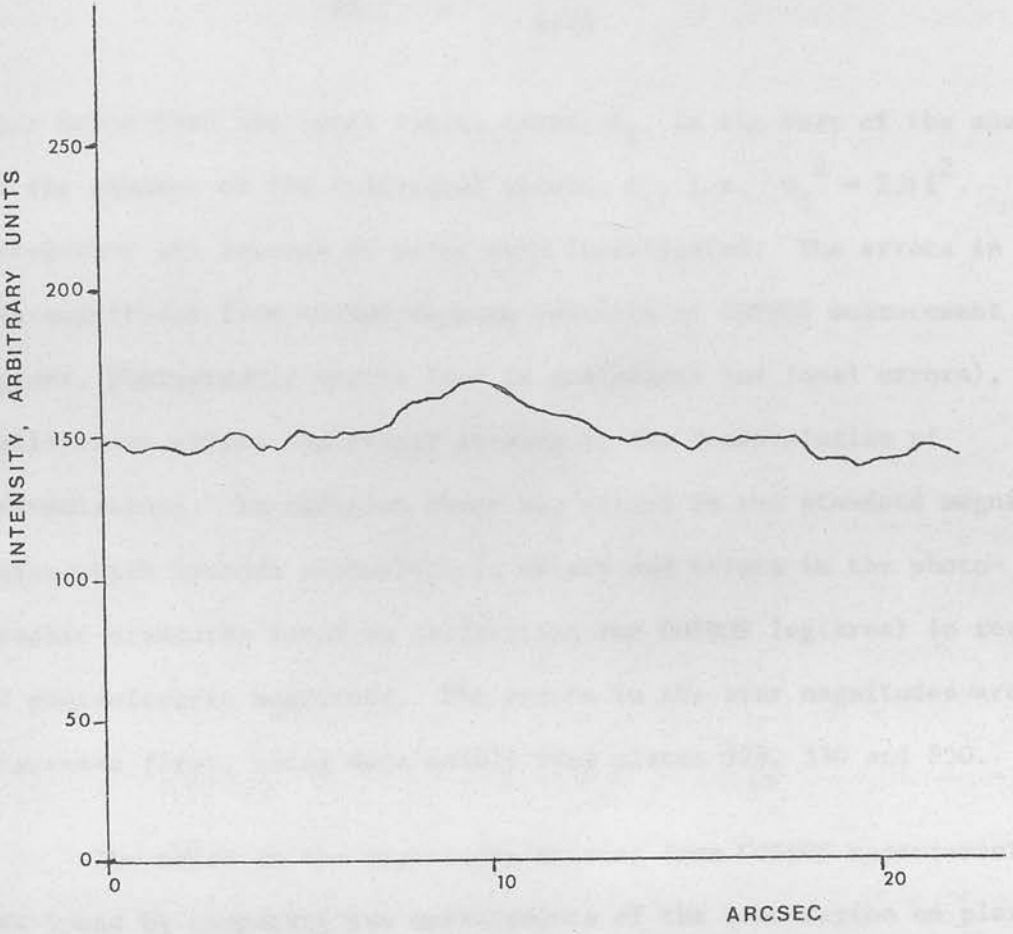

performed to determine the contribution of each source of error to the total error. It was assumed that all types of error had a normal distribution so that for an r.m.s. error, σ, the fraction of points with an error ε is

$$N(\varepsilon) = \frac{1}{\sigma\sqrt{2\pi}} e^{-\frac{\varepsilon^2}{2\sigma^2}}$$

This means that the total r.m.s. error, σ_T, is the root of the sum of the squares of the individual errors, σ_i, i.e. $\sigma_T^2 = \Sigma \sigma i^2$. Altogether six sources of error were investigated. The errors in the magnitudes from COSMOS mapping consists of COSMOS measurement errors, photographic errors (due to graininess and local errors), calibration errors and errors arising in the deconvolution of transmissions. In addition there are errors in the standard magnitudes which include photoelectric errors and errors in the photographic standards found by calibrating the COSMOS log(area) in terms of photoelectric magnitude. The errors in the star magnitudes are discussed first, using data mainly from plates 329, 330 and 950.

The error in the magnitudes arising from COSMOS measurement was found by comparing two measurements of the same region on plate 1920. The relation between the two sets of transmissions was

$$T_2 = T_1 \times 0.98 + 1.12,$$

and the r.m.s. deviation from this relation for a region of the sky background was $\sigma_T = 2.751$, where $\sigma_T^2 = \sigma_{T1}^2 + \sigma_{T2}^2$. Since the slope of the relation between the sets of transmissions is almost unity,

$$\sigma_{T1} = \sigma_{T2} = 1.945.$$

The main cause of error in the magnitudes is the error in determining the average sky background intensity. An error ε_1 in the calculated sky intensity will produce the same error in each of the intensity points in the image when the sky is subtracted. Therefore as mentioned in the previous section, the error in the luminosity will consist of the error in the sky intensity multiplied by the area of the image, plus a contribution from the error in transmissions of the image. Since the latter error is much smaller than the former one, it was neglected. The errors σ_{T1} and σ_{T2} are the r.m.s. errors in the transmissions of individual points. If the transmissions are averaged over an area A, the r.m.s. error in the result will be decreased. For a random distribution the standard deviation decreases with the square root of the size of the measuring sample, and in this case $\sigma \propto 1/\sqrt{A}$. However, in section 2.4 it was shown that this relation does not hold on these scales in the case of the photographic plate because of local errors. An empirical relation found from the data in table 2.4 is $\sigma \propto A^{-0.33}$. In determining the magnitudes from COSMOS mapping, the area used for the star region was about 30 x 30 x $(8\ \mu m)^2$ units, while the total area for the image plus the background region was 70 x 70 x $(8\ \mu m)^2$ units. Therefore the area of the background region was 4000 $(8\ \mu m)^2$ units, giving the r.m.s. error in calibrating the background transmission of $\sigma_{T1}' = \sigma_{T2}' = 0.126$.

This error can be converted into intensity using the slope of the Baker density-transmission to give σ_Δ, and the slope of the Baker density-log(intensity) relation to give $\sigma_{\log I}$. Then the

r.m.s. error in the intensity of the sky background is:

$$\sigma_I = \sigma_{\log I} \times I_{sky}$$

The error in the luminosity was calculated as follows:

$$\sigma_L = A \times \sigma_I$$

$$= A \times \sigma_{\log I} \times I_{sky}$$

$$\sigma_{\log L} = \frac{\sigma_L}{L}$$

$$= \frac{\sigma_L}{A \times \overline{S}}$$

$$= \frac{I_{sky}}{\overline{S}} \times \sigma_{\log I}$$

A is the image area and $\overline{S}$ is the average surface brightness of the image, i.e. the average value of the intensities after the sky background has been subtracted. The error in the magnitude is:

$$\sigma_m = 2.5 \times \frac{I_{sky}}{\overline{S}} \times \sigma_{\log I}$$

The ratio $I_{sky}/\overline{S}$ was determined from the stars on several plates. It increased exponentially with magnitude, and is of the form $I_{sky}/\overline{S} = 10^{0.4(m - \text{const})}$. The value of the constant depends on the width of the stellar intensity profile and the sky background magnitude, and therefore varies slightly from plate to plate. For plate 330 the constant equals 15.81 and this value was adopted throughout the reduction of the star data. Since the error in magnitude depends critically on magnitude, all the errors are given for a star of magnitude 20 in the first instance. For plate 1920, $\sigma_{\log I} = 0.00068$

and for a star of magnitude 20, the error due to COSMOS measurements is $\sigma = 0^m.082$.

A similar method was used for finding the error due to the graininess and the local errors of the photographic plate. The transmission values of the same region on two photographic plates were compared. Plates 329 and 330 were used. The mean relation between the transmissions was:

$$T_{330} = T_{329} \times 1.45 + 1.37$$

$$\sigma_{T330} = \sigma_{T329} \times 1.45$$

The errors are larger for plate 330 because the sky transmission is larger. It was found that the r.m.s. deviation from the mean relation was

$$\sigma_T = 1.969$$

Therefore the r.m.s. scatter in the transmissions on each plate is

$$\sigma_{T329} = 1.118$$

$$\sigma_{T330} = 1.621$$

This gives the error in the magnitude of a star with m = 20 of

$$\sigma_{329} = 0^m.076 \qquad \sigma_{330} = 0^m.111$$

These errors are the combined COSMOS and photographic errors, and have to be compared with the COSMOS error from plate 1920 to find the photographic error alone. However the scale of the errors differs from plate to plate, and before the comparison can be made the errors have to be reduced to a standard system. The r.m.s.

scatter in the transmissions of the sky background depends on two factors. As shown in section 2.4, the ratio σ_T/T increases with decreasing T. This is because the graininess increases with density. The densities of the sky background on the plates varies from 0.4 to 1.2, and in this range σ_T/T increases very slowly and almost linearly with decreasing T. An average relation was found by examining the variation of σ_T/T along several step wedges.

$$\frac{\sigma_T}{T} = -0.00013 \times T + 0.062$$

The second effect arises because the E.H.T. voltage for the photomultiplier on COSMOS can be raised or lowered to increase or decrease the transmission values. For one step of a step wedge, measured at different E.H.T. settings, the relation between σ_T/T and T was:

$$\frac{\sigma_T}{T} = 0.00014 \times T + 0.037.$$

Most of the variation in the average sky transmission from plate to plate is due to different background densities. All the errors arising in the photographic emulsion were reduced to values corresponding to a sky transmission of T = 50, which is equivalent to a density of 0.9. The average sky transmissions of plates 329 and 330 were 30.0 and 44.5 respectively, so the errors were increased. On plate 1920, however, the background transmissions are high (T = 78.2), while the background plate density is approximately 1.1. This was due to the E.H.T. voltage on COSMOS being increased. The r.m.s. error on this plate was scaled to give the error in the COSMOS measurement corresponding to T = 50.

The reduced errors are:

$$\sigma_{1920} = 0^m.052$$

$$\sigma_{329} = 0^m.121$$

$$\sigma_{330} = 0^m.123$$

The average of the combined COSMOS and photographic errors is $0^m.122$. The error in the magnitude due to COSMOS measurement only is $\sigma_{cos} = 0^m.052$, so the error from photographic effects for a star with m = 20 is $\sigma_{pg} = 0^m.110$. (A complete set of results is given in table 2.11.)

In a plot of COSMOS magnitudes of one plate against the magnitudes of another, the scatter of points is due to COSMOS errors, photographic errors, calibration errors and deconvolution errors. The calibration errors were estimated by finding the r.m.s. errors in the magnitudes from undeconvoluted transmissions for plates 329, 330 and 950. The errors in the magnitudes of pairs of plates were:

$$\sigma_{329,\ 330} = 0^m.21$$

$$\sigma_{329,\ 950} = 0^m.29$$

$$\sigma_{330,\ 950} = 0^m.35$$

From these relations, it was found that:

$$\sigma_{329} = 0^m.110$$

$$\sigma_{330} = 0^m.179$$

$$\sigma_{950} = 0^m.301$$

Reducing the errors to those for a star with m = 20, with T_{sky} = 50,

$$\sigma_{329} = 0^{m}.107$$

$$\sigma_{330} = 0^{m}.164$$

$$\sigma_{950} = 0^{m}.154$$

Taking the average, $\sigma = 0^{m}.142$, which gives the calibration error $\sigma_{cal} = 0^{m}.073$

This process was repeated for the magnitudes from deconvoluted transmissions. For plate 329 the errors were larger after deconvolution. However, this was because only a few stars remained unsaturated after deconvolution and larger errors are expected in a fainter sample. The combined r.m.s. error in the magnitudes of plates 330 and 950 was $0^{m}.01$ smaller after deconvolution. From these results it was concluded that there is a negligible error due to deconvolution, and any apparent change in the error is due to the fact that a different sample was examined. (Some stars had to be rejected during deconvolution either because the minimum transmission became too small to be converted into intensity, or because the luminosity because negative due to the effects of surrounding images.)

Since there is no increase in the error due to deconvolution, the error in the standard magnitudes was calculated using magnitudes from uncorrected transmissions, (so that a larger sample could be used). The mean relations and standard deviations are given in figures 2.14a, b and c. As the errors in the COSMOS magnitudes were known, the error in the standard magnitudes (both photoelectric and

photographic) could be found from the combined error. From plates 329, 330 and 950, the errors calculated for the standard star magnitudes at m = 20 and T_{sky} = 50 were $0^m.137$, $0^m.138$ and $0^m.111$ respectively. The average error of $\sigma_{st} = 0^m.129$ was taken.

The error in the photographic standards from the coarse measurement data was found by comparing those magnitudes calculated from plates 329 and 330, omitting the values which had been rejected as explained in section 2.12. It was found that the combined error was $0^m.100$ which corresponds to an error of $0^m.054$ for one plate for a star of magnitude 20. Therefore the error in the photographic standards is $\sigma_{ps} = 0^m.054$. This gives an r.m.s. error in the photoelectric standards of $\sigma_{pe} = 0^m.117$.

Table 2.11 gives the errors for star magnitudes in the range m = 19 to 22. The errors in the COSMOS magnitudes are all given for T_{sky} = 50. If the average sky background transmission is not 50, the approximate error can be found by multiplying the value in the table by the ratio of the actual transmission to the value 50.

The errors in the galaxy magnitudes were analysed using the results from plates 92, 149 and 204. In the case of galaxies, the errors are more difficult to reduce to a standard system. Galaxy images are different shapes and sizes, and different region sizes were used for calculating the magnitudes depending on the coarse measurement x and y extents. Smaller areas were used for smaller images, and so the ratio $I_{sky}/\overline{S}$ did not increase as fast as $10^{0.4m}$. For plate 149 the mean relation was:

$$\frac{I_{sky}}{\overline{S}} = 10^{0.205m - 2.676}$$

TABLE 2.11

Errors in the Magnitudes of Stars

mag.	σ_{cos}	σ_{pg}	σ_{cal}	σ_{cm}	σ_{ps}	σ_{pe}	σ_{st}	σ_{t}
19.0	0.020	0.044	0.029	0.057	0.021	0.047	0.051	0.076
19.5	0.033	0.069	0.046	0.090	0.034	0.074	0.081	0.120
20.0	0.052	0.110	0.073	0.142	0.054	0.117	0.129	0.191
20.5	0.083	0.174	0.116	0.225	0.086	0.185	0.204	0.302
21.0	0.131	0.276	0.183	0.357	0.136	0.294	0.324	0.480
21.5	0.207	0.438	0.291	0.565	0.215	0.466	0.415	0.760
22.0	0.328	0.693	0.461	0.896	0.341	0.738	0.814	1.205

All the errors are given in magnitudes.

σ_{cos} = r.m.s. error due to COSMOS

σ_{pg} = r.m.s. photographic errors (due to graininess and local errors)

σ_{cal} = r.m.s. error in calibration

σ_{cm} = total r.m.s. error in magnitudes obtained from COSMOS

σ_{ps} = r.m.s. error in photographic standards

σ_{pe} = r.m.s. error in photoelectric standards

σ_{st} = combined r.m.s. error in standards

σ_{t} = total r.m.s. error found when comparing COSMOS magnitudes with standard magnitudes

and for the other two plates the coefficient in m was even smaller. The total errors in the magnitudes for each plate were calculated from the r.m.s. scatter of points about the mean relation between the magnitudes for pairs of plates.

$$\sigma_{92,\ 204} = 0^m.312$$
$$\sigma_{92,\ 149} = 0^m.239$$
$$\sigma_{149,\ 204} = 0^m.330$$

This gives:

$$\sigma_{92} = 0^m.151$$
$$\sigma_{149} = 0^m.185$$
$$\sigma_{204} = 0^m.273$$

The errors were reduced to those for a galaxy of magnitude 20, and $T_{sky} = 50$, using the relation $I_{sky}/\overline{S}$ found for each plate. The reduced errors are:

$$\sigma_{92} = 0^m.099$$
$$\sigma_{149} = 0^m.165$$
$$\sigma_{204} = 0^m.170$$

The average error for galaxy magnitudes is therefore $\sigma_{cm} = 0^m.145$.

This value is similar to the error found for stars. However, the error in plate 92 is much smaller than the other errors for the other plates. If plate 92 is ignored the average error from the other two plates is $\sigma = 0^m.167$. This error is larger than the error for stars, which is expected because galaxy images are larger than star images of the same magnitude. Another factor which may cause an increase in the

TABLE 2.12

Errors in the Magnitudes of Galaxies

mag.	σ_{cos}	σ_{pg}	σ_{cal}	σ_{cm}
19.0	0.035	0.090	0.033	0.102
19.5	0.045	0.114	0.040	0.129
20.0	0.056	0.146	0.053	0.165
20.5	0.072	0.184	0.071	0.210
21.0	0.091	0.233	0.090	0.266
21.5	0.115	0.297	0.116	0.339
22.0	0.147	0.376	0.159	0.434

dispersion of galaxy magnitudes when comparing plates of different exposure times, is that galaxies have a range of surface brightnesses and a larger fraction of the total luminosity of some galaxies may be recorded on one plate than on another. This effect causes disagreement between the magnitudes of galaxies fainter than m = 22 on plates 149, 92 and 204.

The reason for plate 92 having such low errors is uncertain, but is probably due to the fact that plate 92 was exposed under good atmospheric conditions and the images are of very good quality.

Table 2.12 shows the errors in the magnitudes of galaxies on plate 149 for magnitudes ranging from 19 to 22, and reduced to $T_{sky} = 50$, so that a comparison can be made between the errors for stars and galaxies. The actual errors for plate 149 were smaller by a factor of 0.78 because $T_{sky} = 38$. For faint images, the errors for galaxies are smaller than the errors for stars. This is because smaller region sizes were used in calculating the magnitudes of faint galaxies. The error in faint star magnitudes could be reduced by using smaller region sizes. Provided the areas were large enough to include all the image above the COSMOS threshold for detection, no systematic error would arise.

2.17 Conclusion

The results of the previous sections show that it is possible to obtain magnitudes of faint galaxies and also stars from Schmidt plates measured by COSMOS. A simple method was adopted because the galaxies are all distant and very little of their structure is

detected. Their angular sizes are small so that the convolution by the atmospheric turbulence smooths and spreads out the profiles considerably. Galaxies of the same morphological type at different distances have differently shaped profiles. For this reason no attempt was made to fit a standard curve to the intensity distribution and so it was not possible to extrapolate the distribution to zero intensity (an infinite distance from the centre) to obtain total magnitudes. The magnitudes are isophotal, the limiting isophote depending on the limiting threshold of detection above the sky background. The smallness of the galaxy images also made it unnecessary to fit a polynomial to the sky background transmissions, because the local errors are unimportant over the size of regions used.

Because of the simplicity of the method, the computer program can be used to calculate the magnitudes of many galaxies at a time, once the initial tests in each field have been carried out. The region chosen for measurement on plates 92, 149 and 204 was about 2 cm square (about 2 arcmin square) and the COSMOS mapping data for this region filled one magnetic tape. From the coarse measurement data there were 625 images detected on plate 149, 768 on plate 204 and 867 on plate 92. (The number of images detected should have been greatest on plate 149 because this plate had the longest exposure time, but the threshold level was set at a greater distance from the background on this plate.) On plate 204, 561 of the images were galaxies and the computer program, omitting the part which deconvolutes the transmissions, calculated the magnitudes of 235 galaxies in 17 min. When the correction to the transmissions were included, the program

took 80 min to run, and calculated 229 magnitudes. The other galaxies were rejected, mainly because they were overlapping with other images. (This plate was taken under poor conditions and the images were large.) Some bright galaxies were rejected because they were saturated in the centre, and a few faint galaxies were rejected because the luminosity became negative, due to an increase in the background intensity surrounding them.

The lower magnitude limit (i.e. the brighter luminosity limit) is determined by the measuring machine, depending on its ability to measure low transmissions. (This limit should depend on the saturation point of the emulsion. However the IIIaJ emulsion saturates at very high densities, which are not measurable on most machines.) It occurs at about magnitude 19 for stars, and for galaxies depends on the morphological type, being at least magnitude 18. The upper magnitude limit depends on the exposure time for the plate and the sensitivity of the emulsion, a measure of which is the contrast, the slope of the linear part of the characteristic curve. However, the images of coarse measurement area less than a certain value were rejected because these images were hardly visible to the naked eye, and many of the images below the limit were caused by graininess. The lower area limit was chosen to be 10 in $(8\ \mu m)^2$ units. This cut-off in area will not produce a uniform upper limit in magnitude, but it is approximately at $m = 22$.

The main source of error is the graininess of the emulsion. Apart from distorting the profiles, it produces errors in the determination of the sky background intensity, which give rise to errors

in the luminosity. Macrofluctuations do not create problems in using the step wedge at the edge of the plate to calibrate a region in the centre of the plate. On plates 92 and 149 the north wedge was measured, while on plate 204 the east wedge was measured because the north edge of the plate was completely blacked out. However, the results on plate 204 agree with those on the other two plates.

The COSMOS measuring machine produces systematic errors due to the spot being too large and the presence of halos round it. However the transmission can be corrected for these errors and the remaining errors due to the binning of transmissions are negligible.

The error in magnitude, determined from the comparison of the same galaxies on different plates depends on magnitude, being larger for fainter galaxies, where there is a lower signal to noise ratio. Over a range in magnitudes from 19 to 22 the average error is $0^{m}.3$.

3. THE OBSERVED N(m) RELATION

3.1 Introduction

The method for calculating galaxy magnitudes from COSMOS mapping measurements, as described in chapter 2, is not suitable for obtaining the magnitudes of a large sample of galaxies which is required for determining the N(m) relation. This is partly due to the fact that mapping measurements produce large quantities of data (the transmission measurements from a square of size 2.5 cm fill one magnetic tape), and also because the computing time necessary to calculate the magnitudes of large numbers of galaxies from such data is prohibitive.

The coarse measurement mode of operation on COSMOS was however designed to detect and measure a limited number of parameters for large numbers of images. As explained in section 2.2, images are detected when they have transmissions lower than a specified threshold level. For each image ten parameters are output, including the x and y coordinates of the centre of the image on the plate, the area of the image at the threshold, and the minimum transmission. In each region in which the N(m) relation was to be found, the whole area was measured using the coarse measurement mode, and a small region of about 2 cm square and the step wedge were mapped. Once the magnitudes of several hundred galaxies had been calculated from the mapping data, a polynomial was fitted to the empirical relationship between magnitude and the logarithm of the coarse measurement area of these galaxies. The magnitudes of the galaxies in the rest

of the region were then calculated from the coarse measurement data using the polynomial.

This chapter describes the method used for determining the N(m) relation for galaxies in three regions near the south galactic pole. In the next section the regions chosen are described, and in subsequent sections a more detailed account of the separation of stars from galaxies is given, and the method for calibrating magnitudes in terms of coarse measurement area is explained. Finally, the observed N(m) relation is given for each region.

3.2 A Description of the Areas Used

Of the three regions chosen, two are on plate 1920 and one is on plate 1915. All the fields are situated within 10^{o} of the south galactic pole, (see figure 3.1), where the effects of selective galactic absorption are minimised. Details of plates 1920 and 1915 are given in table 2.2, section 2.3. The regions have been designated fields I to III. Field I is of size 10 cm by 15 cm and is on plate 1920, to the north of the centre of the plate, while field II is to the south of the centre and is of size 10 cm by 10 cm. Field III, on plate 1915, includes part of the globular cluster NGC288 and is 5 cm by 15 cm, being bound on the north side by the galaxy NGC253.

These regions were originally chosen because there is a sequence of star magnitudes determined by electronography in each

FIGURE 3.1 MAP OF THE THREE FIELDS INVESTIGATED.

(THE CROSSES MARK THE POSITIONS OF THE CALIBRATION REGIONS)

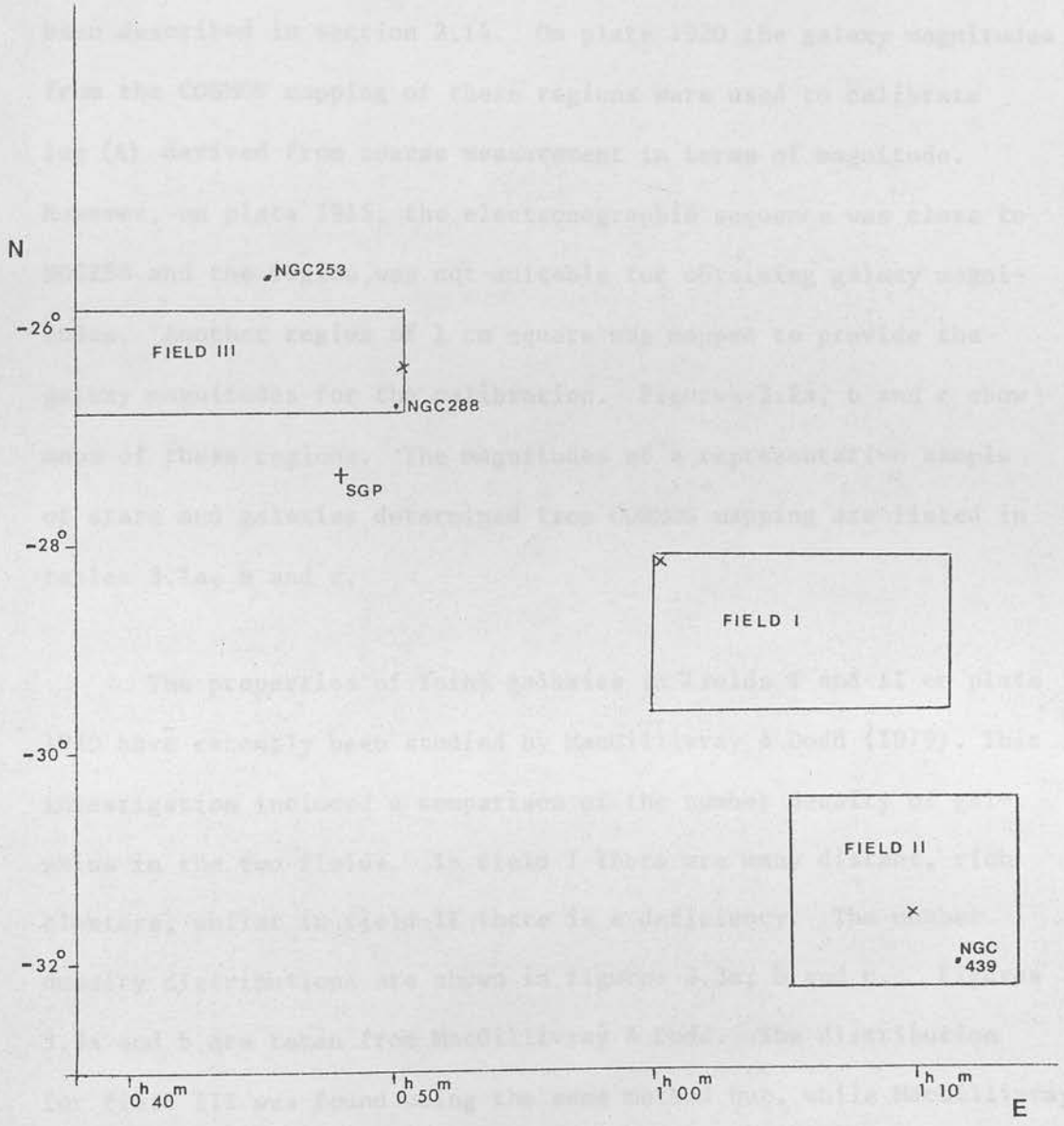

(unpublished). Areas of about 2 cm square coinciding with the sequences were mapped by COSMOS. However, the electronographic magnitudes were found to be unreliable and these magnitudes were not used to check the COSMOS magnitudes. Instead the step scale method was used to check the star magnitudes, and the results have been described in section 2.14. On plate 1920 the galaxy magnitudes from the COSMOS mapping of these regions were used to calibrate log (A) derived from coarse measurement in terms of magnitude. However, on plate 1915, the electronographic sequence was close to NGC288 and the region was not suitable for obtaining galaxy magnitudes. Another region of 1 cm square was mapped to provide the galaxy magnitudes for the calibration. Figures 3.2a, b and c show maps of these regions. The magnitudes of a representative sample of stars and galaxies determined from COSMOS mapping are listed in tables 3.1a, b and c.

The properties of faint galaxies in fields I and II on plate 1920 have recently been studied by MacGillivray & Dodd (1979). This investigation included a comparison of the number density of galaxies in the two fields. In field I there are many distant, rich clusters, whilst in field II there is a deficiency. The number density distributions are shown in figures 3.3a, b and c. Figures 3.3a and b are taken from MacGillivray & Dodd. The distribution for field III was found using the same method but, while MacGillivray & Dodd used a limiting image area of 8.0 arcsec^2, the present sample had a limiting image area of 3.5 arcsec^2. Although the graph for

FIGURE 3.2A MAP OF CALIBRATION REGION FOR FIELD I.

R. A.$_{1950}$= 01^{h} 00.5^{m} DEC.$_{1950}$= - 27° 53′.

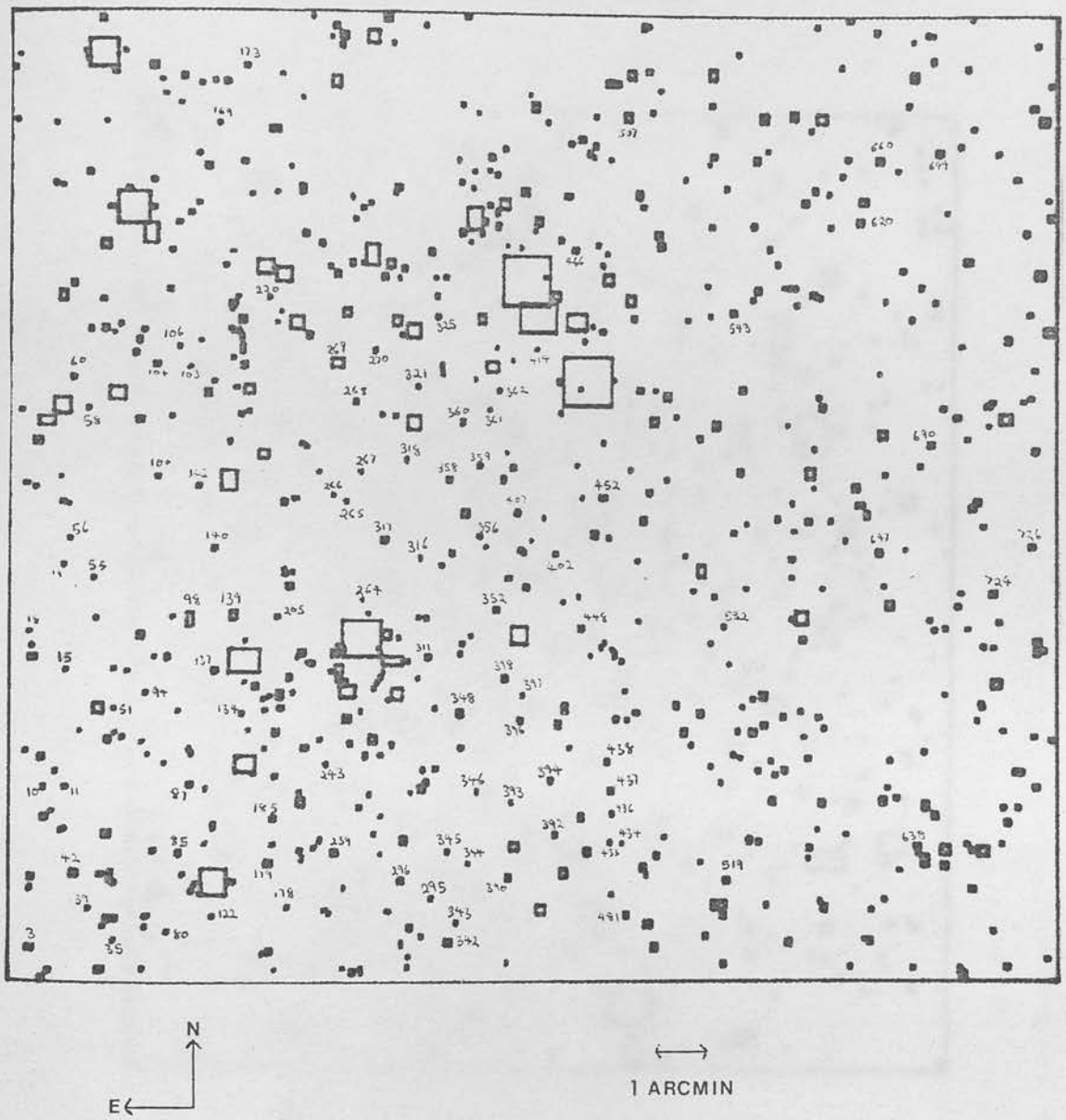

FIGURE 3.2B MAP OF CALIBRATION REGION FOR FIELD II.

R. A.$_{1950}$= $01^h\ 09^m$ DEC.$_{1950}$= $-31^\circ\ 39'$.

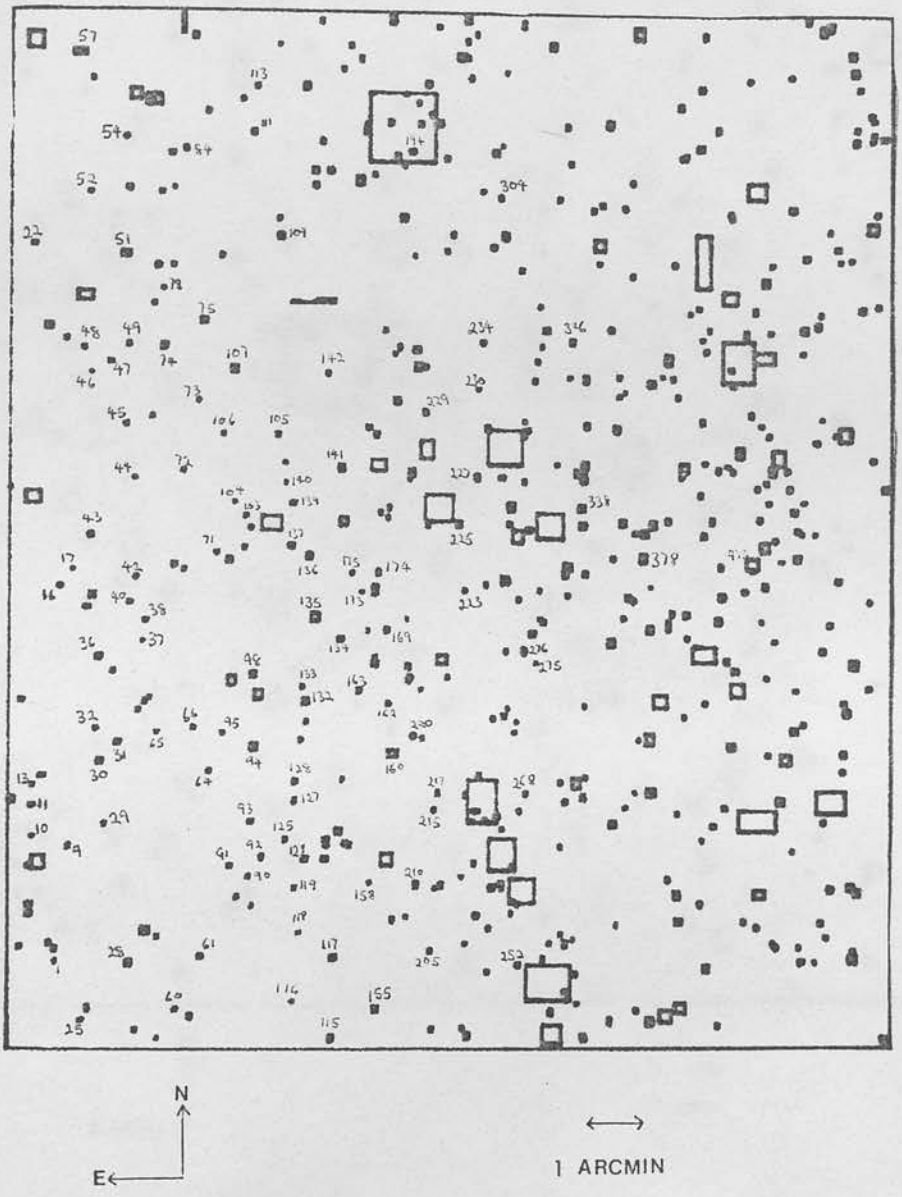

FIGURE 3.2C MAP OF CALIBRATION REGION FOR FIELD III.

R. A.$_{1950}$= 00^{h} 52.8^{m} DEC.$_{1950}$= -26° $18.^{\prime}$

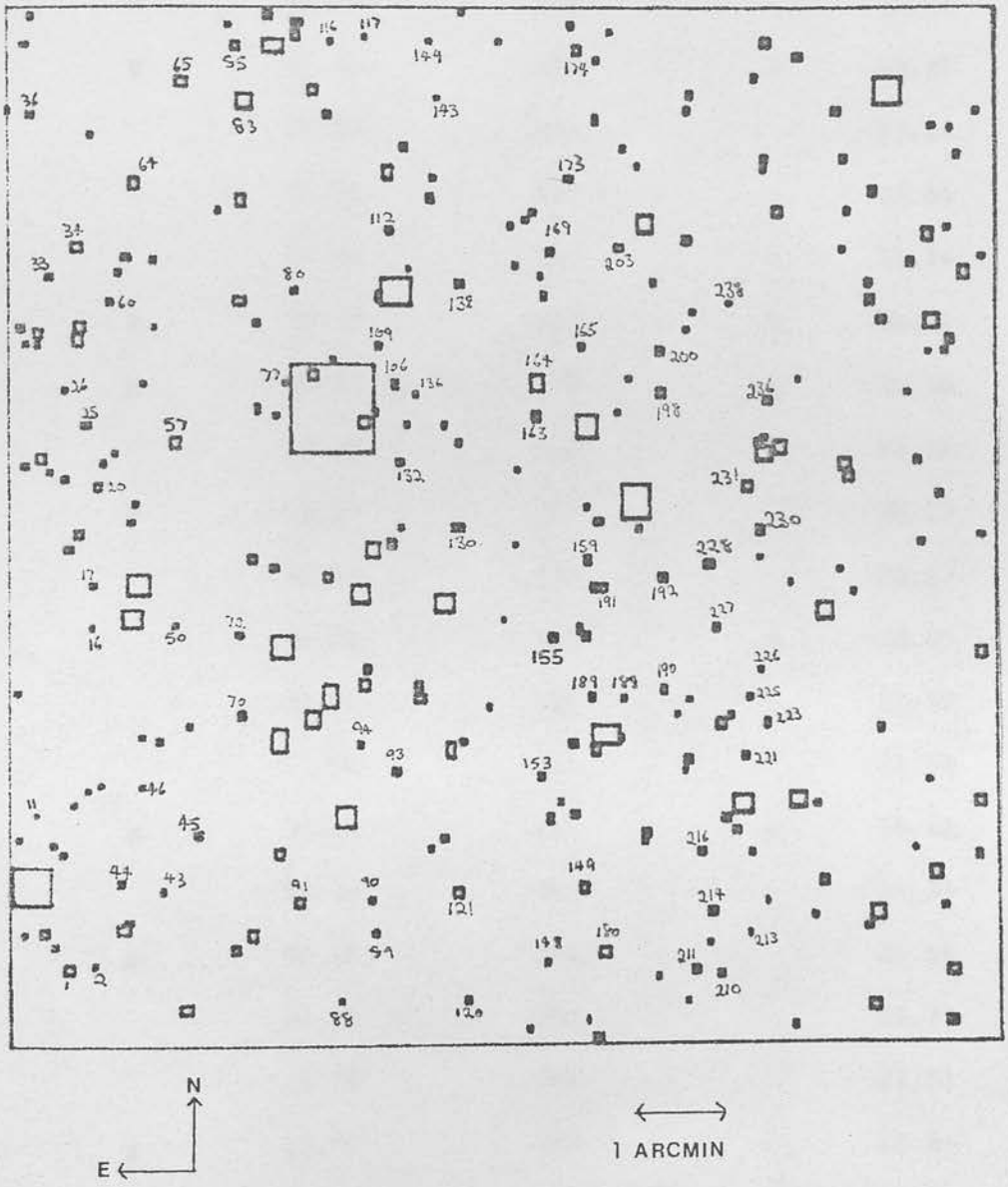

TABLE 3.1a

Magnitudes of Stars and Galaxies in Field I, plate 1920

Image Number	Image Type	Magnitude	Image Number	Image Type	Magnitude
3	s	18.94	103		21.25
10	g	21.00	104	s	19.92
11		20.92	106		21.14
15		21.85	122		20.64
18		21.01	134		21.74
19	g	20.69	137	g	20.81
35	g	20.47	139	g	19.56
39		20.91	140		22.22
42	s	18.87	142		20.72
51		22.12	178		20.87
55		21.94	179	g	20.85
56		21.23	185		21.68
58		21.80	205		21.59
60	g	21.14	239	s	19.46
80		21.31	243		21.35
85	g	20.26	264		21.66
87		21.17	265		22.75
94		21.78	266		21.01
98	g	18.97	267		22.85
100	g	20.87	268		20.91

contd...

TABLE 3.1a (contd.)

Image Number	Image Type	Magnitude	Image Number	Image Type	Magnitude
269	g	18.22	361		21.47
270		20.73	362		21.36
295		21.61	390	s	19.60
296		21.72	392		21.30
316		22.16	393		21.72
317	s	19.26	394		20.71
318		21.21	396	g	20.83
321		22.04	397		20.36
325		21.56	398	g	19.76
342	g	19.01	402		20.84
343	g	21.56	407	s	18.99
344		22.36	414		22.41
345		22.54	433		22.10
346		22.41	434		21.37
348	g	19.77	435	g	20.47
352	s	20.07	436		20.71
356		20.70	437	g	20.88
358	g	20.51	438	g	20.55
359		20.68	448	g	20.58
360	g	20.77	452	g	20.27

TABLE 3.1b

Magnitudes of Stars and Galaxies in Field II, plate 1920

Image Number	Image Type	Magnitude	Image Number	Image Type	Magnitude
1	g	20.18	46		22.69
9		22.67	47	g	21.13
10		22.11	64		21.00
11	g	20.91	65		21.57
16		22.03	66	g	21.45
17		22.46	71		22.65
25		20.54	72		21.39
28	g	20.12	73		22.52
29		22.23	74	s	19.78
30	s	20.08	90		21.09
31	s	20.22	91		21.20
32		21.84	92		21.56
36	s	20.07	93		21.17
37		22.36	94	s	19.07
38		21.13	95		21.77
40		21.00	98	g	20.93
42		22.36	103		21.52
43	s	20.06	104		21.55
44		22.75	105	s	20.39
45		21.62	106		22.33

contd....

TABLE 3.1b (contd.)

Image Number	Image Type	Magnitude	Image Number	Image Type	Magnitude
107	g	19.62	158		21.74
116		22.18	160	g	19.05
117	g	20.65	162	g	21.24
118		22.21	163	g	20.44
119		21.45	169	g	20.94
121	g	20.25	173		20.64
125		21.36	175		22.33
127		21.70	205		22.31
128		20.65	210	g	20.25
132	g	20.85	215		21.82
133		21.30	217		20.72
134	g	20.66	220	s	20.58
135	g	18.58	223		21.60
136	g	19.70	225	g	22.70
137	g	20.43	227	g	20.75
139	g	20.57	229	g	20.87
140		21.33	230		21.86
141	s	19.48	252		21.82
142	g	21.04	268		21.87
155	s	19.45	275		21.64

TABLE 3.1c

Magnitudes of Stars and Galaxies in Field III, plate 1915

Image Number	Image Type	Magnitude	Image Number	Image Type	Magnitude
1	s	19.21	70	g	20.81
2		21.61	72		21.84
11		21.67	77		21.82
16		21.34	80		22.08
17	g	20.07	83	g	18.15
20	g	19.59	85	g	19.80
25	g	21.45	88		21.51
26		22.35	89		21.23
33		21.59	90		21.41
34	g	20.08	91	s	19.41
36		21.08	93	s	20.74
43		21.42	94	g	21.59
44		20.67	106	g	19.82
45		20.73	109		21.48
46		20.98	112		22.39
50		20.29	116		20.89
57	s	19.09	117		21.64
60		20.87	120		21.18
64	s	19.15	121	s	19.60
65	g	19.63	130	g	20.28

contd....

TABLE 3.1c (contd.)

Image Number	Image Type	Magnitude	Image Number	Image Type	Magnitude
132	g	20.77	191	g	20.09
136		21.68	192	g	21.05
138	g	20.17	198	s	19.92
143		22.65	200		21.29
144		21.52	203	g	20.07
148		21.12	210		20.86
149	s	20.09	211	g	20.34
153		20.91	213		21.31
155	g	19.89	214		20.43
159	g	20.03	216		20.03
163	s	20.32	221		21.91
164	g	18.80	223		22.34
165		22.32	225		20.33
169	s	20.37	226		22.81
173		20.84	227		20.91
174	g	22.15	228		20.84
180	s	19.02	230		21.21
188		22.00	231	g	19.68
189	g	20.84	236		20.32
190		21.92	238		22.12

FIGURE 3.3A THE DISTRIBUTION OF GALAXIES, FIELD I.

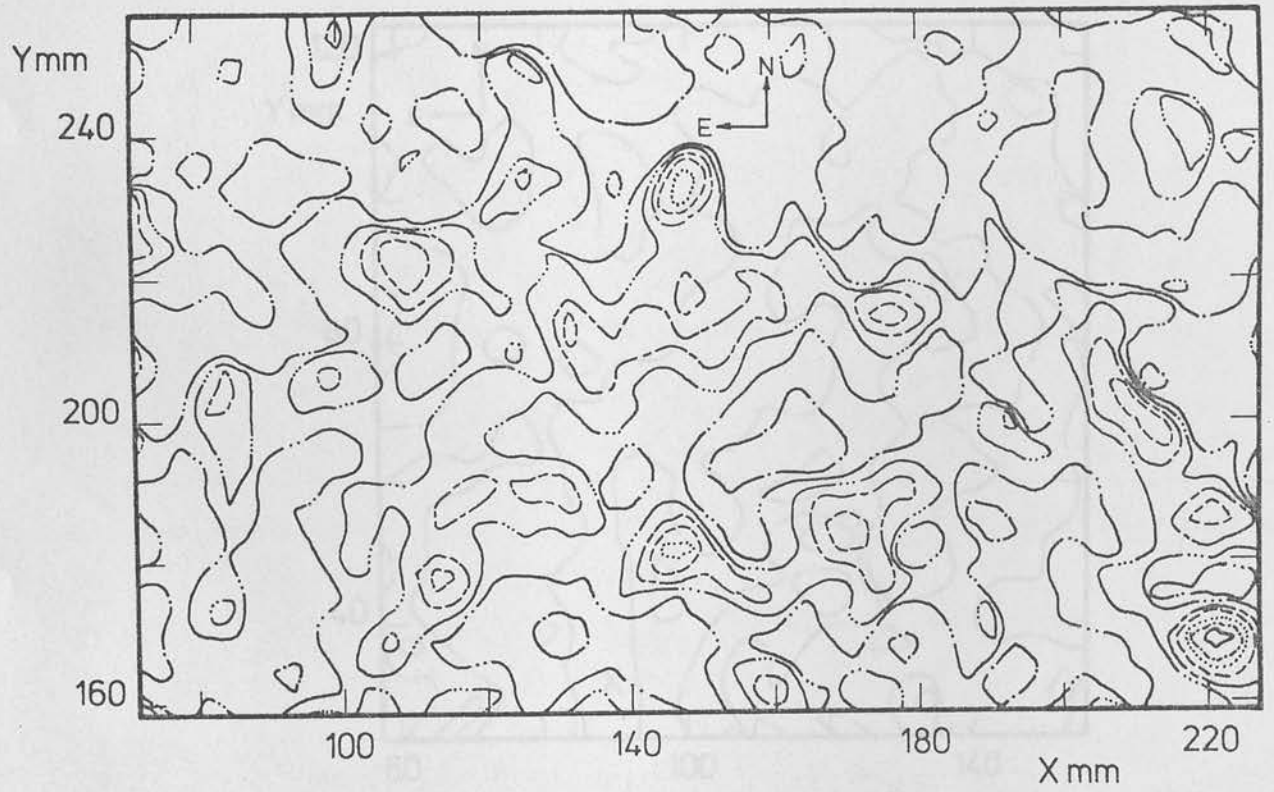

NO. OF GALAXIES/SQ. MM.

—·—	1.0
—·—·—	1.3
—·—·—·—	1.6
— — —	1.8
- - - -	2.0
·····	2.2
—·—·—	2.4
———	2.7

(FROM MACGILLIVRAY AND DODD, 1979)

FIGURE 3.3B THE DISTRIBUTION OF GALAXIES, FIELD II.

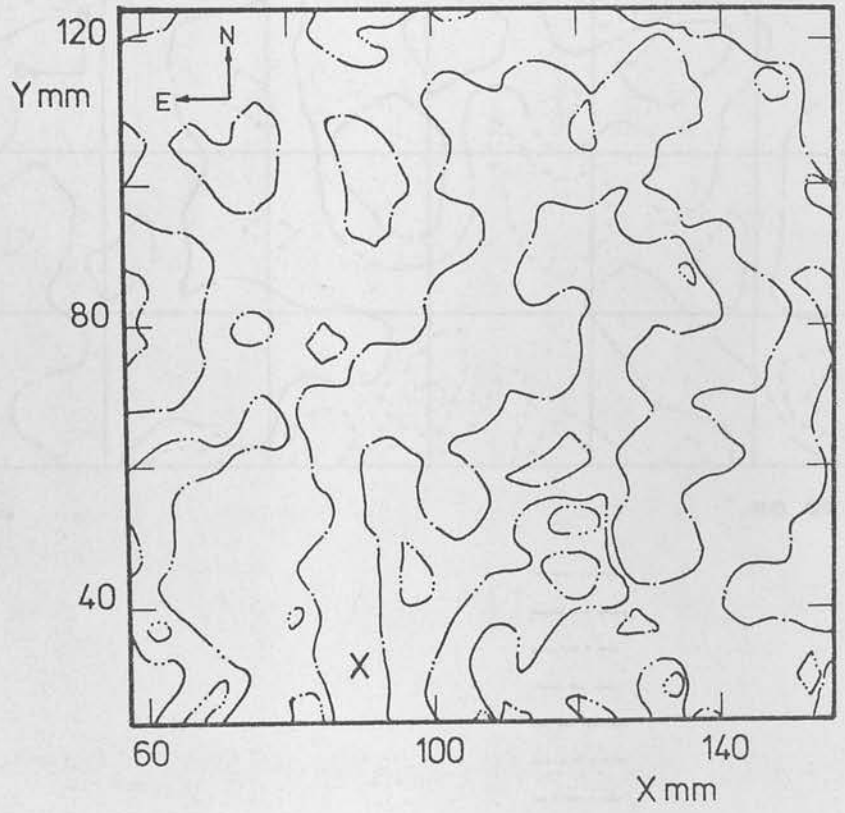

(FROM MACGILLIVRAY AND DODD, 1979.

SEE KEY TO FIGURE 3.3A)

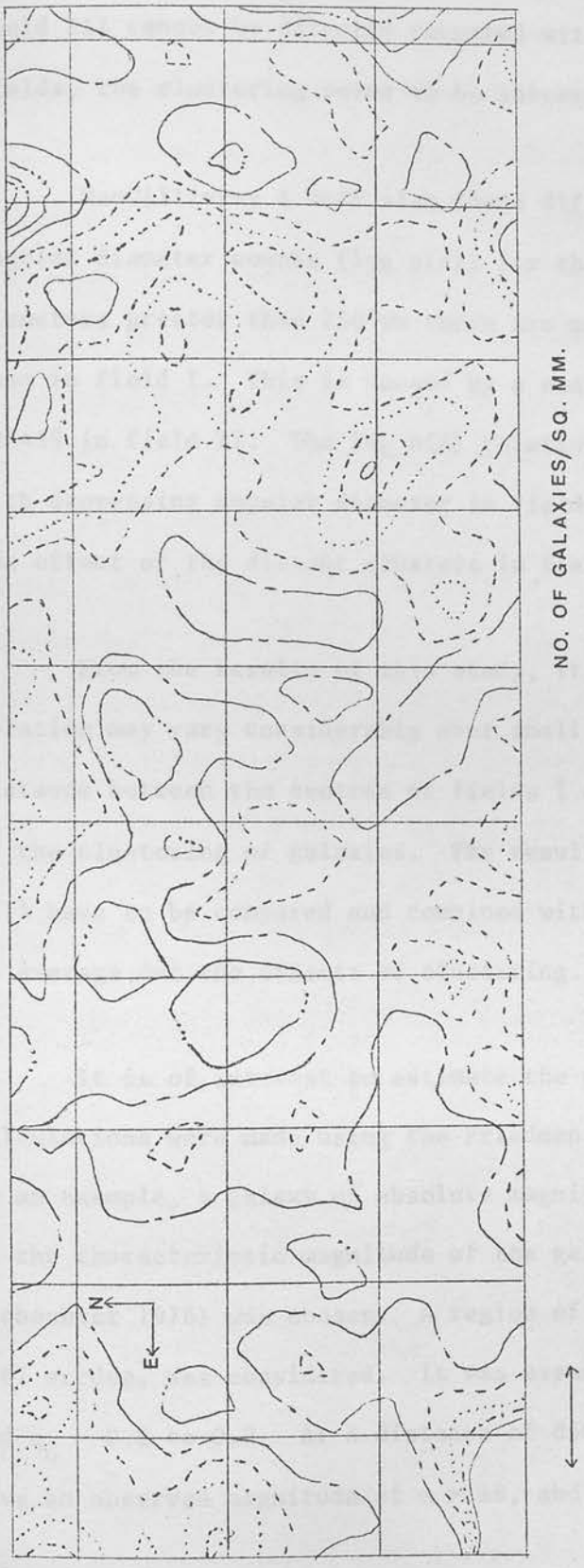

FIGURE 3.3C THE DISTRIBUTION OF GALAXIES, FIELD III.

field III cannot be directly compared with that for the other fields, the clustering seems to be intermediate.

MacGillivray & Dodd also found differences in the cumulative angular diameter counts (log n(d)) for the regions. For angular diameters greater than 256 μm there are more galaxies in field II than in field I. This is caused by a nearby cluster centred on NGC439 in field II. The log n(d) relation increases more rapidly with decreasing angular diameter in field I than in field II due to the effect of the distant clusters in field I.

From the results of this study, it is expected that the N(m) relation may vary considerably over small angular distances, (the distance between the centres of fields I and II is about 3^{o}), due to the clustering of galaxies. The results from one part of the sky will have to be compared and combined with those from other directions to average out the effects of clustering.

It is of interest to estimate the physical sizes of the regions. Calculations were made using the Friedman equations (Appendix I). As an example, a galaxy of absolute magnitude M = -21, which is near to the characteristic magnitude of the galaxy luminosity function (Schechter 1976) was chosen. A region of 10 cm on the plate, or 1.87 arcdeg, was considered. It was assumed that H_o = 50 km $s^{-1}Mpc^{-1}$ and q_o = 0.0 to 0.2. At a distance of 850 Mpc, this galaxy will have an observed magnitude of m = 19, and the region size will

correspond to 25 Mpc across; at a distance of 2050 Mpc, the galaxy will have an observed magnitude of m = 22, and the region size will be 50 Mpc. If H_o = 100 km $s^{-1}Mpc^{-1}$, the values for the distance and region size will be approximately the same for the same magnitudes, but not exactly so because the redshifts will be different in the two cases, and so the K-correction will differ. The angular distance spanned by the three fields from the south-east corner of field II to the north-west corner of field III is 10^o. This corresponds to a region size of 125 Mpc across at a distance of 850 Mpc, and to a region size of 250 Mpc at a distance of 2050 Mpc. The average size of a supercluster, as measured by Abell (1961), is 70 Mpc, for H_o = 50 km $s^{-1}Mpc^{-1}$. Therefore the effects of superclustering should be smoothed by combining the data from the three regions.

3.3 The Coarse Measurement Data

The coarse measurement data for the three fields used for determining the N(m) relation was obtained by a different method from that described in section 2.2, because the COSMOS coarse measurement mode was temporarily out of action. Each region was mapped at an increment of 16 μm, the data from 5 cm square being stored on one magnetic tape. (The 8 μm increment used for measuring small regions of a few cm square produces too much data when larger regions are measured.) The reduction of the mapping data to coarse measurement data was carried out by MacGillivray using the method of MacGillivray & Dodd (1979) which is described as follows.

Initially, the average background transmission corresponding to the sky intensity was determined in cells of size 2.048 mm, the width of a lane of mapping data. This was done by examining the frequency distribution of transmissions in each cell and taking the transmission corresponding to the maximum of the distribution. In cells affected by bright stars, the background transmission was replaced by the average of the values in the four surrounding cells. Polynomials, typically of 15th order, were then fitted along each lane of mapping data. From these polynomials the transmission corresponding to the night sky could be determined at each point in the region. The transmissions were converted to intensities using the step wedge calibration and the threshold level for detection of images was set at 7% of the night sky. Since the sky surface brightness at the time of exposure was B = 22.11 mag arcsec^{-2} for plate 1920, and B = 22.06 mag arcsec^{-2} for plate 1915, the threshold level corresponds approximately to m_j = 25 mag arcsec^{-2}. The error in the threshold level was estimated at ±1.5% of the night sky, where 0.5% comes from the error in the polynomial fitting (which includes the error due to graininess) and 1% arises from the error in the step wedge calibration. All the points with intensities greater than the threshold were selected and adjacent points, (in the horizontal, vertical and diagonal directions), were joined up to form the images. Large images straddling lanes or different magnetic tapes were later recombined. The parameters stored on magnetic tape for each image were the x and y coordinates, the x and y extents, the area at the

threshold, the minimum transmission, the sky transmission and the threshold transmission. Images with areas less than 3 x $(16\ \mu m)^2$ on the plate, or 3.5 $arcsec^2$ were rejected as being too affected by noise.

The accuracy of the coarse measurement data was assessed by comparing the images detected with those observed by a visual examination of the plate, and it was found that a small percentage of the images were not real. The spurious images arose from various sources, the most common being the increase in the emulsion density round bright stars and galaxies which was not taken into account in the determination of the threshold level, and which gave rise to a surfeit of faint images surrounding bright images. Also parts of the diffraction spikes and halos round stars were sometimes detected as separate images.

At the edges of a region the coarse measurement threshold level was not always determined correctly due to 'ringing' of the polynomial fitted to the background transmissions. This caused too many or too few images to be detected. Other sources of error were faults in the emulsion such as marks or scratches which were picked up as images, and on plate 1915 there were two satellite trails which were detected as a series of images.

The first set of checks on the data were made using maps of the images such as that shown in figure 3.4a covering an area of

2.5 cm square on the plate. Areas on the maps where there were no corresponding images on the photographic plate were marked, and their positions measured. A computer program was written to reject all the images in these regions. The numbers of bright stars and galaxies which were also rejected by this process were noted (see table 3.2). Figure 3.4b shows a sample of data after the corrections had been made. The total area removed from each field was 1 to 2%.

Further tests were carried out to check the faint images more thoroughly in case some were caused by graininess in the emulsion due to the threshold being set too low in some regions. For each field an area of 1 cm square on the plate was examined visually through a microscope, and the images were classified as those which were definitely real, and those which could possibly be due to graininess. The criterion for classifying images as being perhaps due to graininess was that they were very faint and did not look significantly different from the clumps of grains in the surrounding background. These images all had COSMOS areas of less than or equal to 10 x $(16\ \mu m)^2$ ($11.5\ arcsec^2$), and the numbers increased from a few percent at area A = 10 to about 20% at A = 3 ($3.5\ arcsec^2$) with a large increase at low areas. This indicates that either the images were caused by graininess, or the smaller images were more difficult to see. This test was repeated on a small area in field I which had been photographed on plates 1916 and 1921 as well as plate 1920. The results were compared for two plates at a time. About half the images were classified as being perhaps due to graininess on both plates and,

FIGURE 3.4A IMAGES DETECTED BY COSMOS COARSE MEASUREMENT, BEFORE CORRECTION.

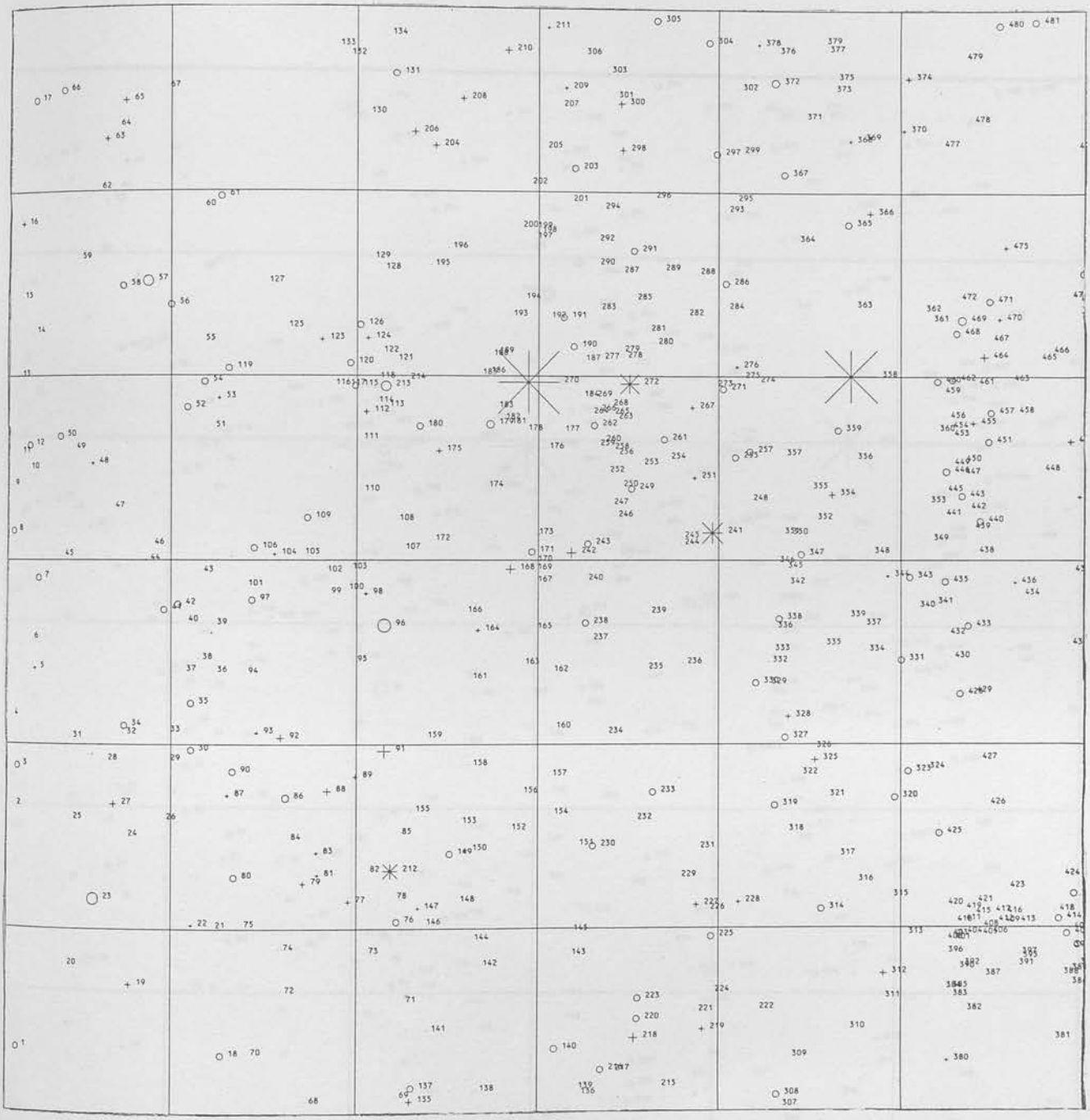

+ STAR

* VERY LARGE IMAGE

O GALAXY

. VERY SMALL IMAGE

FIGURE 3.4B IMAGES DETECTED BY COSMOS COARSE MEASUREMENT, AFTER CORRECTION.

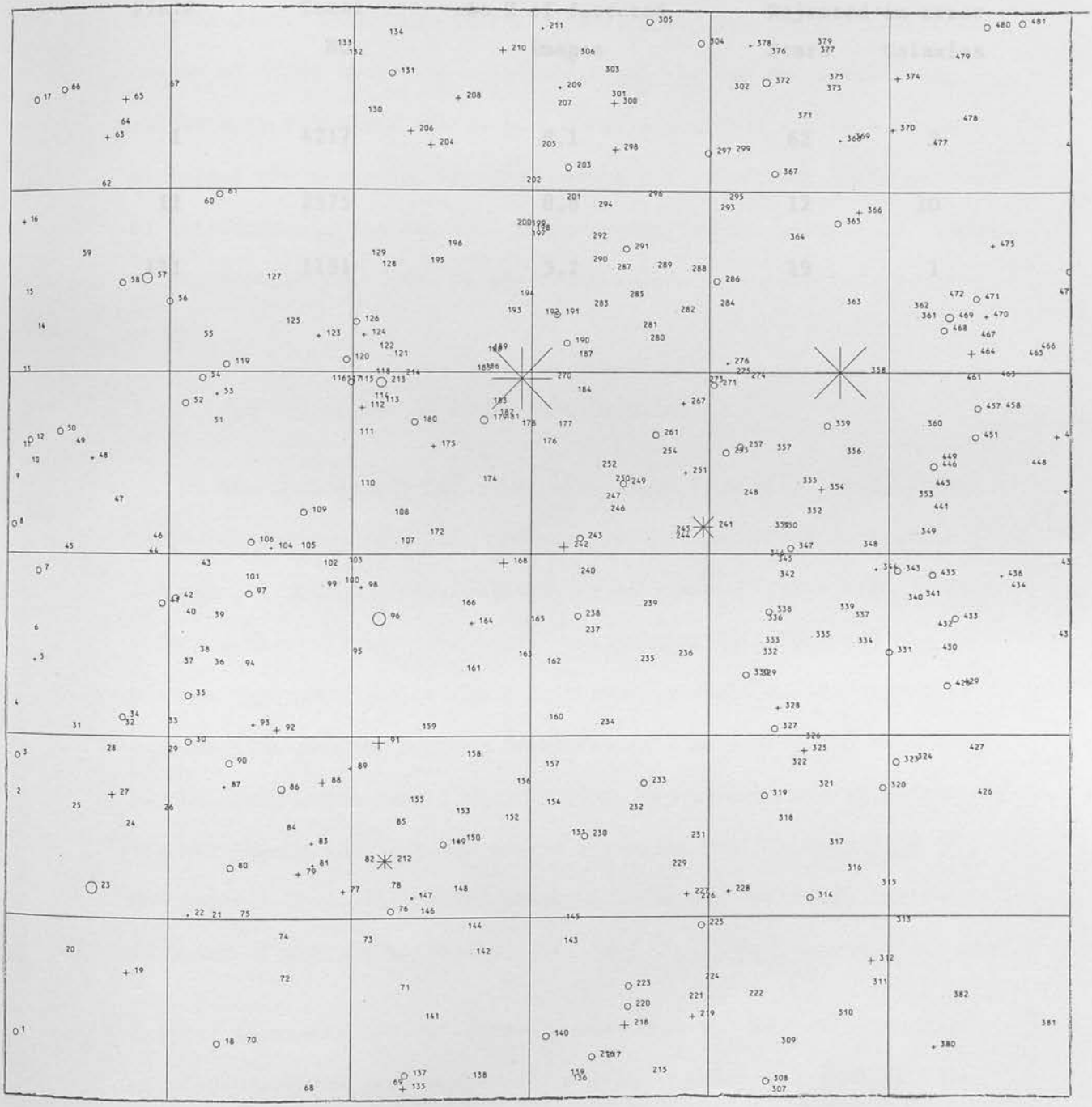

(SEE KEY TO FIGURE 3.4A)

TABLE 3.2

Rejected Images

Field	Total No	As % of detected images	Rejected in error	
			Stars	Galaxies
I	4217	8.1	62	2
II	2575	8.8	12	10
III	1151	5.2	19	1

of the remaining half, equal numbers were classified as real images on one plate and graininess on the other and vice versa. In nearly all cases a density enhancement was visible at the point where an image had been detected by COSMOS, so the correlation of images between plates indicates that they are real. However the classification of faint images is a difficult process and the results may not be very reliable. In general the images with A = 4 (4.6 arcsec^2) or larger are real, but of those with A = 3, about 20% could be due to graininess in the emulsion and/or errors in the polynomial fitting to the background. None of the faint images were rejected at this stage.

3.4 The Separation of Stars from Galaxies

The method used for separating stars from galaxies in these large regions was basically the same as that described in section 2.3 and the method of MacGillivray et al (1976). There were however slight modifications. The coarse measurement data included the average sky transmission round each image as well as the threshold transmission and the minimum transmission. As before the logarithm of the coarse measurement area, log(A), was used as one parameter for the separation, but the second parameter was the logarithm of the central intensity of the image with the sky intensity subtracted, in units of the sky intensity, i.e. $\log\left(\frac{I_c - I_{sky}}{I_{sky}}\right)$, where I_c is the central intensity derived from the coarse measurement minimum transmission using the step wedge calibration, and I_{sky} is the sky intensity calculated from the average sky transmission.

When reducing data in areas as large as 10 cm across on the plate, it is necessary to take account of macroscopic errors, or local errors in the emulsion. These cause variations in the sky transmission over the region, and similar variations in the minimum transmissions of the images. Using central intensities in terms of the sky intensities, these macroscopic errors are taken into account (de Vaucouleurs 1948b).

In each of the fields, three small regions of 1 cm square, (one in the middle of the field and two in diagonally opposite corners) were examined by eye, and the images were classified as stars or galaxies. Graphs of $\log \frac{I_c - I_{sky}}{I_{sky}}$ vs. log(A) were drawn for each of the sample regions. It was found that there was no dependence on position of the separation criteria for stars and galaxies across a field, and combined graphs were formed for each field. The graph for plate 1920, field II is shown in figure 3.5. From the graphs, the coordinates at intervals along the curve forming the boundary between stars and galaxies were noted, and these were used in the computer program to separate all the stars and galaxies in the field. (Linear interpolation was used to determine the position of the boundary between known coordinates.) The error in determining where the boundary should be was estimated for each region. Images which were within a distance, d, on the graph from the boundary were classified as uncertain. The values of d are given in table 3.3.

This method for separating stars from galaxies cannot be used for all images, but is suitable for images in the magnitude range 17

FIGURE 3.5 THE SEPARATION OF STARS FROM GALAXIES, FIELD II PLATE 1920.

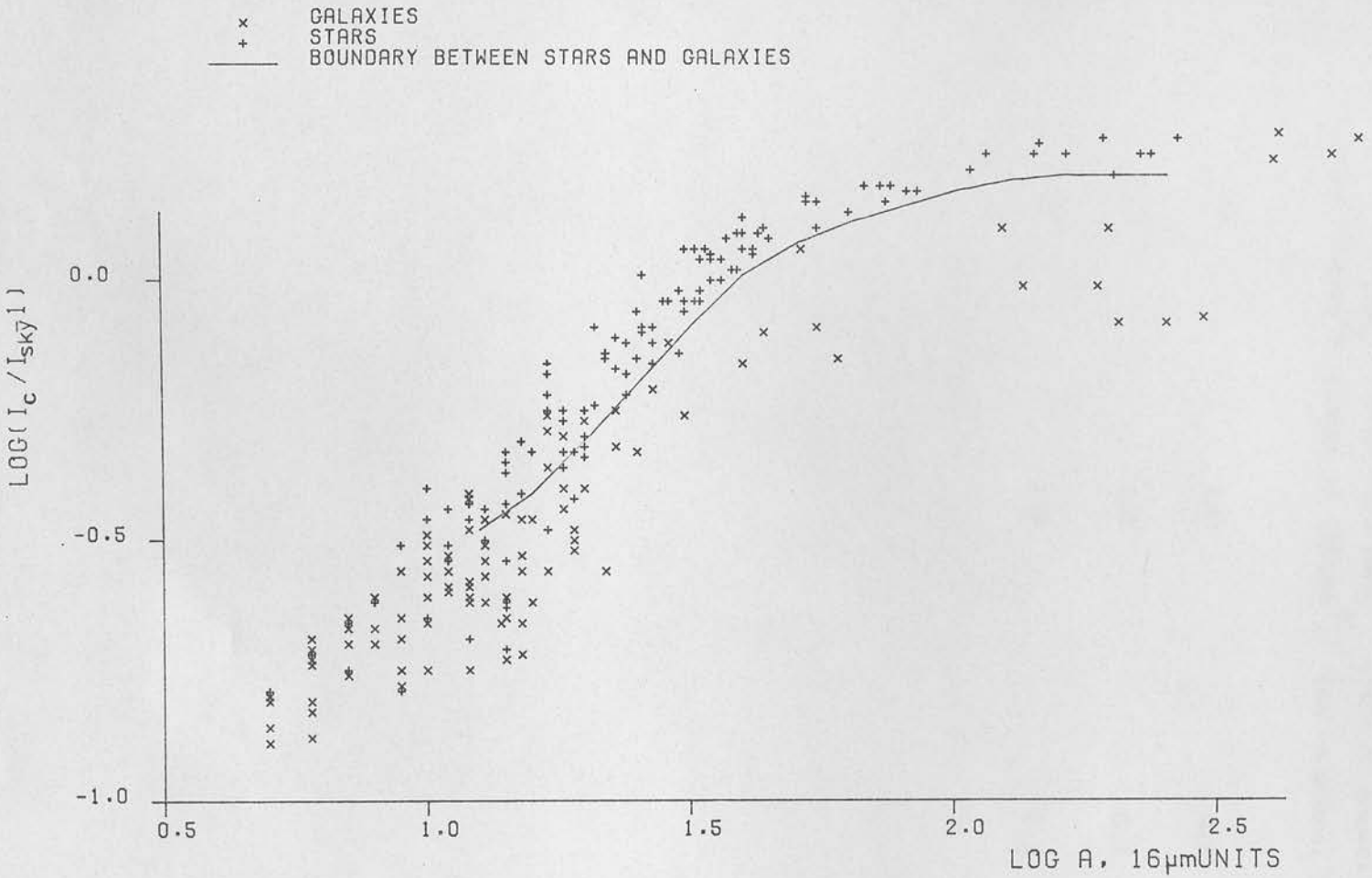

TABLE 3.3

Limiting Areas and Uncertainty in the Separation of Stars from Galaxies

Field	Lower Area Limit (units of $(16\,\mu m)^2$)	Upper Area Limit (units of $(16\,\mu m)^2$)	Width of Uncertainty Zone (cm on graph, fig. 3.5)
I	10	250	0.2
II	13	250	0.2
III	10	250	0.3

to 21. Fainter than 21st magnitude, the visual distinction between stars and galaxies becomes difficult because star images cease to have dense cores. At the bright limit the images become saturated, so that the measured central intensity is the same for stars and galaxies and the criterion for separation no longer holds. The lower and upper limits of the areas of the images used in the separation are given in table 3.3.

There are several types of error affecting this method. Random errors arise from visual misidentification and from the effects of the graininess of the emulsion on the area and minimum transmission of the images. There may also be an error in determining the boundary for separating stars and galaxies depending on factors such as the plate exposure time and the atmospheric seeing.

The error due to misidentification was found by determining the number of images which were classified differently during two different inspections of a region. This was estimated as 2%. The error arising from the graininess of the plate was calculated by comparing the results of the computer separation with the visual separation. It was found that there was an error of 8.6% on plate 1920 (the average of the two fields), and an error of 11.0% on plate 1915. (These errors include the 2% error due to misidentification.)

The error in determining the position of the boundary between star and galaxy images may be more serious. For images brighter than $m_j = 20$, it is fairly easy to distinguish stars from galaxies, although compact galaxies and quasars may be wrongly classified as stars. For fainter images, the results become more subjective and may be

affected by the atmospheric seeing or the exposure time of the plate. Bad seeing and a longer exposure time both increase the width of images as seen on a photographic plate.

The dependence of the results on atmospheric seeing and exposure time was checked by comparing the classifications given for stars and galaxies in the test region on plates 92, 149 and 204. For each pair of plates there was 86 to 89% agreement on the classification (i.e. an error of 8 to 10% for each plate). The disagreement was largely due to the affect of graininess on the coarse measurement since the numbers of images classified as galaxies on the first plate and stars on the second was about equal to the number of images classified as stars on the first plate and galaxies on the second. On plate 92 there were 2.8% more stars than on plate 149, and on plate 204 there were 1% more stars than on plate 149. As can be seen from table 2.2, plate 204 has the shortest exposure time of 60 min, plate 92 has an exposure time of 90 min, and plate 149 an exposure time of 120 min. The atmospheric seeing, assessed from the quality of the images was good when plates 92 and 149 were exposed but not so good when plate 204 was exposed. The widths of several star images on the three plates were measured. It was found that the images were largest on plate 149, on account of the long exposure time, and smallest on plate 92 because of the good atmospheric seeing. The number of images classified as stars or galaxies is therefore correlated with the size of the images, either because when the images are small some galaxies are classified as stars, or when the images are large some stars are classified as galaxies.

TABLE 3.4

Results of Separation of Stars from Galaxies

Field	Stars*	Galaxies	Uncertain Stars	Uncertain Galaxies	Too Bright	Too Faint	Total No of images
I	8.9	17.5	2.3	3.2	0.4	67.7	47,802
II	11.1	23.7	3.1	4.9	1.1	56.1	26,801
III	11.0	20.4	5.1	8.7	1.0	53.8	21,085

* Percentages of total

However, this effect is not very important because the errors it causes are small compared with the errors due to graininess. It is unlikely that there are large errors in the total numbers of images classified as stars or galaxies by this method.

The results of the separation are shown in table 3.4. In each region, the proportions of images of different types were approximately the same. Over half the images were too faint to be classified. Of the separable images, about a third were stars. There was a larger number of images in the uncertainty category on plate 1915, for which the width of the uncertainty zone was larger. The atmospheric seeing was less good when this plate was exposed.

3.5 The Determination of Magnitudes from the COSMOS Coarse Measurement Mode

In section 2.12 it was shown that the magnitudes of stars can be represented by a second order function of log(A). Only one variable is necessary to calculate the magnitudes of stars because stellar intensity profiles are all the same shape, since stars are unresolved. Neglecting the effects of atmospheric seeing on the profiles, two parameters should be necessary to calculate the magnitudes of galaxies of one morphological type, e.g. $\log I_c$ and $\log A$. The first parameter accounts for the range in intrinsic luminosities, and the other accounts for the range in the widths of the profiles due to differing distances. When calculating the magnitudes of galaxies of differing morphological types more parameters should be used. However, the galaxies studied in this project were in the magnitude range 18 to 22 and their diameters were comparable to the

diameter of the atmospheric seeing disk, so that the profiles were spread out by the seeing, making the profiles of different types of galaxy more similar.

Two types of expression for representing the magnitudes of galaxies were tested. Firstly the magnitudes were calibrated in terms of the two parameters derived from coarse measurement, $\log A$ and $\log \frac{I_c - I_{sky}}{I_{sky}}$. It was found that this did not give a good fit, the standard deviation of points from the curve being about $0^m.5$. The magnitudes depend more on $\log A$ than on $\log \frac{I_c - I_{sky}}{I_{sky}}$, and the central intensities are affected by grain noise in the emulsion. Next, the magnitudes were calibrated against $\log A$ only using the same method as for stars. The standard deviation decreased for fields II and III and increased slightly for field I. Since there is no advantage in using a two parameter calibration, a one parameter relation was used.

Figure 3.6 shows the magnitude from COSMOS mapping measurements versus $\log A$ from COSMOS coarse measurement for galaxies in field I, plate 1920. Similar results were obtained for the other two fields. There is an approximately linear relation between magnitude and $\log A$ for galaxies brighter than $m_j = 21$. Extra magnitude determinations were made for bright galaxies using Corwin's step scale, described in section 2.14. These measurements confirm that there is a linear relationship over a large magnitude range, (see figure 3.7). The slope for the relationship between step scale magnitude and $\log A$ is greater than that for the relationship between

FIGURE 3.6
MAGNITUDE VS. LOG (COSMOS AREA) PLATE 1920 FIELD I

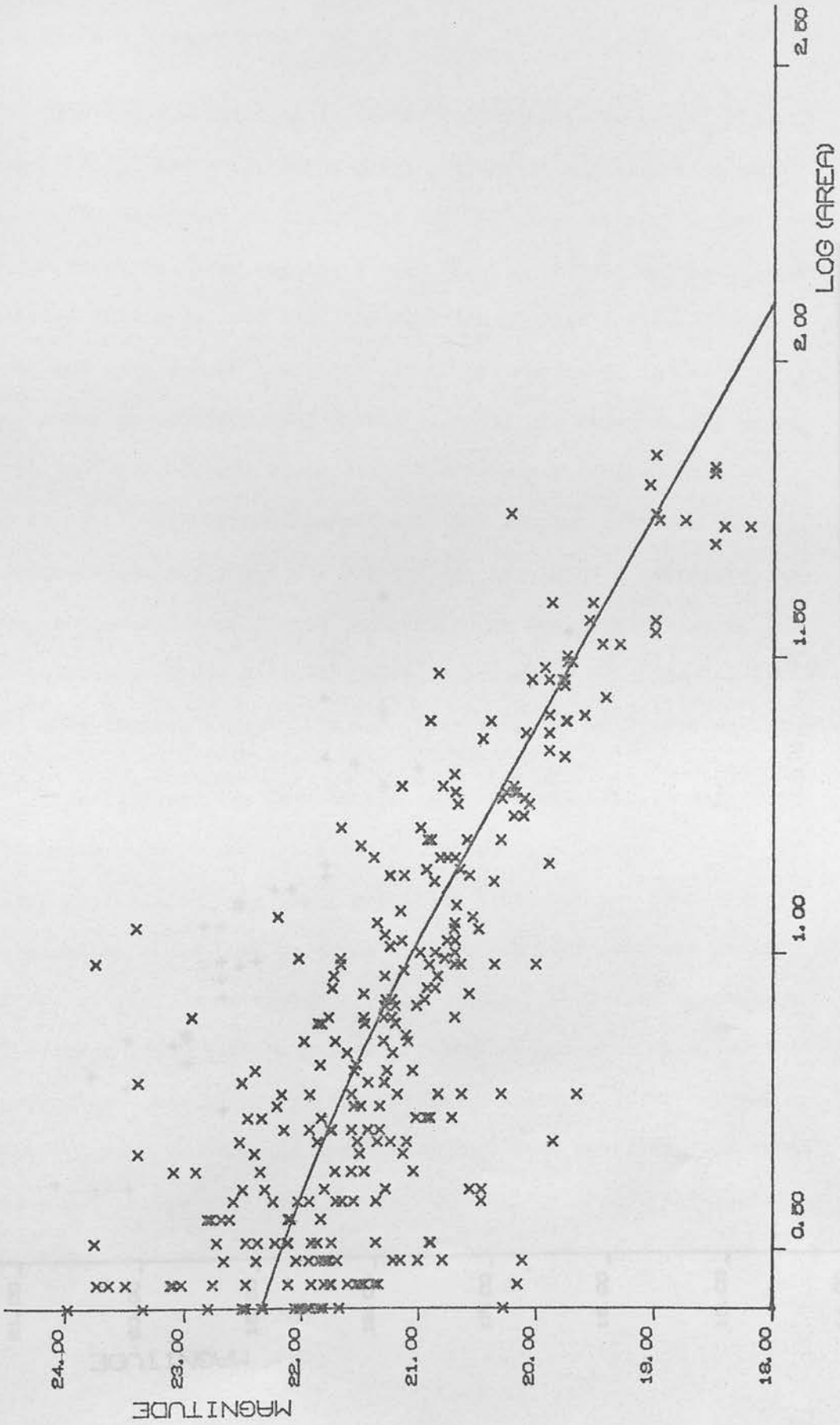

FIGURE 3.7
STEP SCALE MAGNITUDES VS. LOG (COSMOS AREA), PLATE 1920 FIELD I

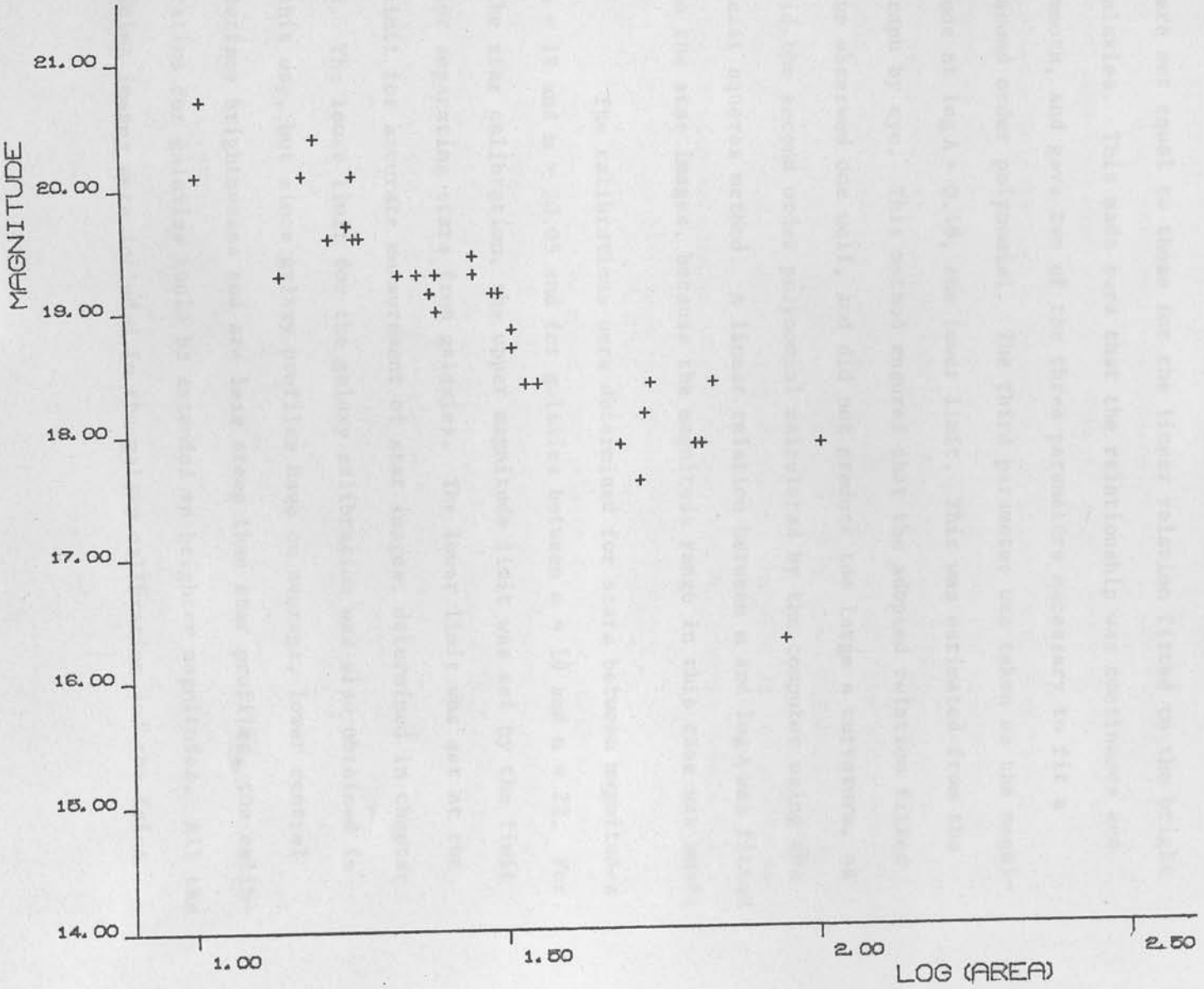

COSMOS mapping magnitude and $\log A$, and there is a zero point difference. However, this could be caused by the fact that the step scale magnitudes are V magnitudes.

The $m(\log A)$ relation is curved for faint galaxies ($m_j > 21$, or $\log A < 1.1$), and so a second order polynomial was fitted in this region. The magnitude at $\log A = 1.1$ and the slope at this point, were set equal to those for the linear relation fitted to the bright galaxies. This made sure that the relationship was continuous and smooth, and gave two of the three parameters necessary to fit a second order polynomial. The third parameter was taken as the magnitude at $\log A = 0.48$, the lower limit. This was estimated from the graph by eye. This method ensured that the adopted relation fitted the observed one well, and did not produce too large a curvature, as did the second order polynomial calculated by the computer using the least squares method. A linear relation between m and $\log A$ was fitted to the star images, because the magnitude range in this case was small.

The calibrations were determined for stars between magnitudes m = 19 and m = 20.05 and for galaxies between m = 18 and m = 22. For the star calibration, the upper magnitude limit was set by the limit for separating stars from galaxies. The lower limit was set at the limit for accurate measurement of star images, determined in chapter 2. The lower limit for the galaxy calibration was also obtained in this way, but since galaxy profiles have on average, lower central surface brightnesses and are less steep than star profiles, the calibration for galaxies could be extended to brighter magnitudes. All the faint images were included in the galaxy calibration and the faint

limit is the magnitude corresponding to area A = 3 x $(16\ \mu m)^2$, the smallest image area.

The errors in the magnitudes obtained from these calibrations depend on the error in the magnitudes from COSMOS mapping measurement, the error arising from the calibration and the error in log A.

Assuming the distribution of errors is gaussian, the error in the calibration obtained from n galaxies due to the errors in the magnitudes from COSMOS mapping mode is $\frac{\sigma_m}{\sqrt{n}}$, where σ_m is the average error in magnitude. The errors in galaxy magnitudes were discussed in section 2.16, where it was found that the errors depend on the magnitude, the density of the plate, and to a lesser extent the COSMOS E.H.T. setting. Using the method described, the errors for the magnitudes were calculated for m_J = 18 to 22 in intervals of one magnitude, and the results were divided by the root of the number of galaxies with magnitudes in that interval. The average errors for the three fields are given in table 3.6a.

The error in the magnitudes arising from the calibration is the r.m.s. deviation of points from the fitted curve, which is given in table 3.5. This error also depends on magnitude and the errors were calculated in magnitude intervals as above.

The error in the logarithm of the image area, log A, was found by comparing two sets of coarse measurement data of the same region. The region used was that from which the galaxy magnitudes were obtained on plate 1915. It was found that the r.m.s. error in log A decreased almost linearly with increasing log A, from 0.3 at

TABLE 3.5

Polynomials Fitted to Magnitudes in Terms of Log A

Field I

Stars	$m = 24.356 - 3.605 \log A$	
Galaxies	$m = 22.849 - 0.912 \log A - 0.861 (\log A)^2$	$\log A \leq 1.1$
	$m = 23.889 - 2.803 \log A$	$\log A \geq 1.1$

Field II

Stars	$m = 24.131 - 3.391 \log A$	
Galaxies	$m = 22.829 - 0.850 \log A - 0.884 (\log A)^2$	$\log A \leq 1.1$
	$m = 23.893 - 2.790 \log A$	$\log A \geq 1.1$

Field III

Stars	$m = 24.143 - 3.340 \log A$	
Galaxies	$m = 22.239 + 0.398 \log A - 1.565 (\log A)^2$	$\log A \leq 1.1$
	$m = 24.130 - 3.038 \log A$	$\log A \geq 1.1$

TABLE 3.6

The Average Errors in the Magnitudes Obtained from the Calibrations

a) Galaxies

Magnitude	σ_1	σ_2	σ_3	σ_T
18.0	0.054	0.035	0.028	0.070
19.0	0.070	0.180	0.049	0.199
20.0	0.061	0.326	0.066	0.338
21.0	0.051	0.472	0.077	0.481
22.0	0.086	0.618	0.074	0.628

b) Stars

Magnitude	σ_1	σ_2	σ_3	σ_T
19.0	0.033	0.113	0.099	0.154
19.5	0.052	0.167	0.120	0.212
20.0	0.086	0.221	0.142	0.276
20.5	0.159	0.274	0.164	0.357

σ_1 = r.m.s. error in the calibration resulting from errors in the magnitudes from mapping.

σ_2 = r.m.s. deviation of points from the fitted curve.

σ_3 = r.m.s. error in the magnitudes resulting from errors in log A.

σ_T = combined error.

$\log A = 0.5$ (m = 22) to 0.05 at $\log A = 1.9$ (m = 18). To obtain the errors in the magnitudes, these errors were multiplied by the slope of the m($\log A$) calibration. The total error in the magnitudes derived from the calibration was found from the root ~~mean~~ square sum of the individual errors. The errors in the star magnitudes were calculated in a similar manner, and are listed in table 3.6b.

It was stated in section 2.15 that the galaxy magnitudes obtained from COSMOS mapping measurements are isophotal magnitudes, the limiting isophote being one intensity increment as measured by COSMOS above the average sky intensity. An attempt was made to verify this value of the limiting isophote for the galaxies in the three fields under investigation. One method of obtaining an independent value for the limiting isophote is to assume a standard profile for a galaxy and to compare the luminosity calculated from COSMOS measurements with the calculated luminosity within a particular isophote. Several relatively bright elliptical galaxies (m = 18 to 19) were chosen from each field. Their intensity profiles, except in the centres obeyed the de Vaucouleurs $\exp(-r^{\frac{1}{4}})$ law (de Vaucouleurs 1962).

If $\overline{I}$ is the average intensity of two isophotes, ΔI is the difference between them and ΔA is the area of the image lying between the isophotes, then, following de Vaucouleurs (1977), a quantity Q may be defined as:

$$Q = \frac{\overline{I}\,\Delta A}{\Delta I}$$

Q represents the change in luminosity per intensity isophote, and has units of area. A graph of $\log Q$ vs. $\log \bar{I}$ for successive isophotes is a straight line, as shown in figure 3.8, and an extrapolation of this graph can be used to obtain the total luminosity of the galaxy, or the luminosity within a faint isophote. For each of the selected galaxies $\log Q$ and $\log \bar{I}$ were determined out to an isophote of about 24.8 mag arcsec^{-2} which is above the noise level due to graininess of the emulsion. The luminosity within this isophote was also calculated and compared with the luminosity corresponding to the COSMOS magnitude (obtained from mapping measurements). From the $\log Q (\log \bar{I})$ relation the isophote which gives rise to the COSMOS magnitudes can be found.

For each galaxy the ratio of the limiting isophote to the expected value of the limiting isophote, i.e. one intensity increment, was calculated. The average of this ratio was found to be 1.48 with a satndard deviation of 1.22. (One galaxy was rejected because the ratio was greater than three standard deviations from the mean.) Since the limiting isophote is close to the expected value, considering the large errors, it was assumed that the limiting isophote can be correctly obtained from the smallest intensity increment. The values for the three fields, calculated from the smallest intensity increment are:

plate 1920, field I	27.96 mag arcsec^{-2}
plate 1920, field II	28.33 mag arcsec^{-2}
plate 1915, field III	28.01 mag arcsec^{-2}

The magnitudes calculated from COSMOS coarse measurement will also be

FIGURE 3.8 LOG Q VS. LOG $\bar{I}$ FOR A GALAXY ON PLATE 1915.

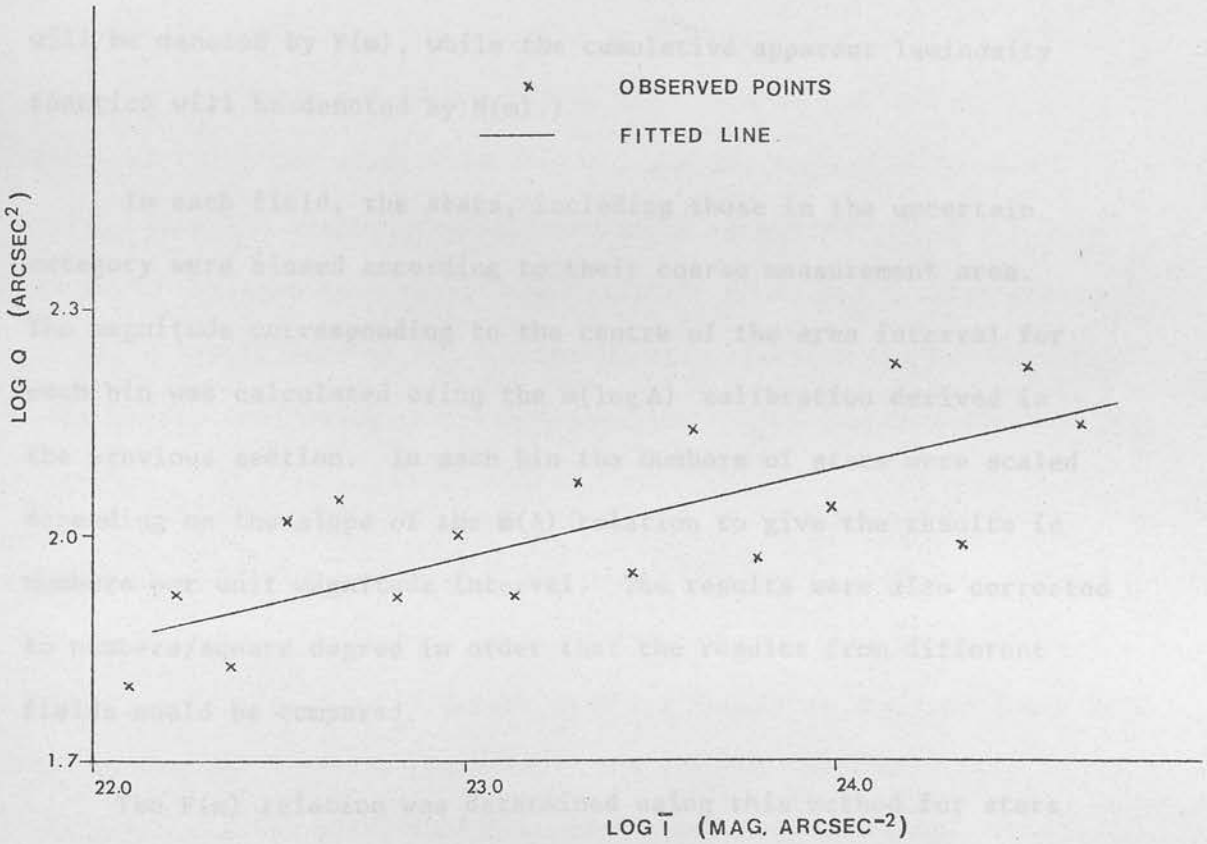

isophotal magnitudes with the limiting isophotes as above, because they were determined by calibrating image agea against the magnitudes from COSMOS mapping measurements.

3.6 The F(m) Relation for Stars

Although the aim of this project was to study the N(m) relation for galaxies, the results for stars were also examined in the form of the numbers of stars in a given magnitude interval, or the F(m) relation. (The differential apparent luminosity function will be denoted by F(m), while the cumulative apparent luminosity function will be denoted by N(m).)

In each field, the stars, including those in the uncertain category were binned according to their coarse measurement area. The magnitude corresponding to the centre of the area interval for each bin was calculated using the m(log A) calibration derived in the previous section. In each bin the numbers of stars were scaled depending on the slope of the m(A) relation to give the results in numbers per unit magnitude interval. The results were also corrected to numbers/square degree in order that the results from different fields could be compared.

The F(m) relation was determined using this method for stars fainter than m = 19, which is the brighter magnitude limit of the calibration. The faint limit was set by the limit of the separation of stars from galaxies. This limit was m = 20.34 for field I, m = 20.74 for field II and m = 20.80 for field III. (The limit for field I is lower because the lower area for the separation of stars

from galaxies was set to image area A = 13 instead of A = 10 as in the other fields.) Figure 3.9 shows the graph of log F vs. m for plate 1920, field II. The relation was similar for all fields. There was a gradual increase in the numbers of stars from m = 19 to m = 20, and then fainter than m = 20 the numbers start to decrease.

The errors in log F were estimated from the numbers of images classified as uncertain stars or galaxies. Log F was recalculated first using only the stars in the definite category, and then including all the stars plus the galaxies in the uncertain category. For stars in the range m = 19.0 to 19.9, this gave an average error in log F of ± 0.05 for plate 1920 fields I and II, and ± 0.08 for plate 1915. Then the errors gradually increased to about ± 0.1 at m = 20.0 to 20.4. Fainter than this, nearly all the stars and a large portion of the galaxies were in the uncertain categories and the errors were very large, indicating that the separation was no longer accurate.

For images brighter than m = 20, it is fairly easy to distinguish stars from galaxies. The most plausible explanation for the decrease in the numbers of stars fainter than this is that the stars become less easy to detect as their images become less dense in the centre and look like galaxies. The fainter the images, the larger the proportion of stars that are misclassified as galaxies. This interpretation of the log F(m) relation was favoured because it is unlikely that the true luminosity function for stars would decrease in this way. If the number of bright distant stars tends to zero because the outer extremities of the galaxy have been reached, this should not affect the log F(m) relation significantly, because there are relatively few very luminous stars.

FIGURE 3.9 LOG F(M) VS. MAGNITUDE FOR STARS ON PLATE 1920, FIELD II.

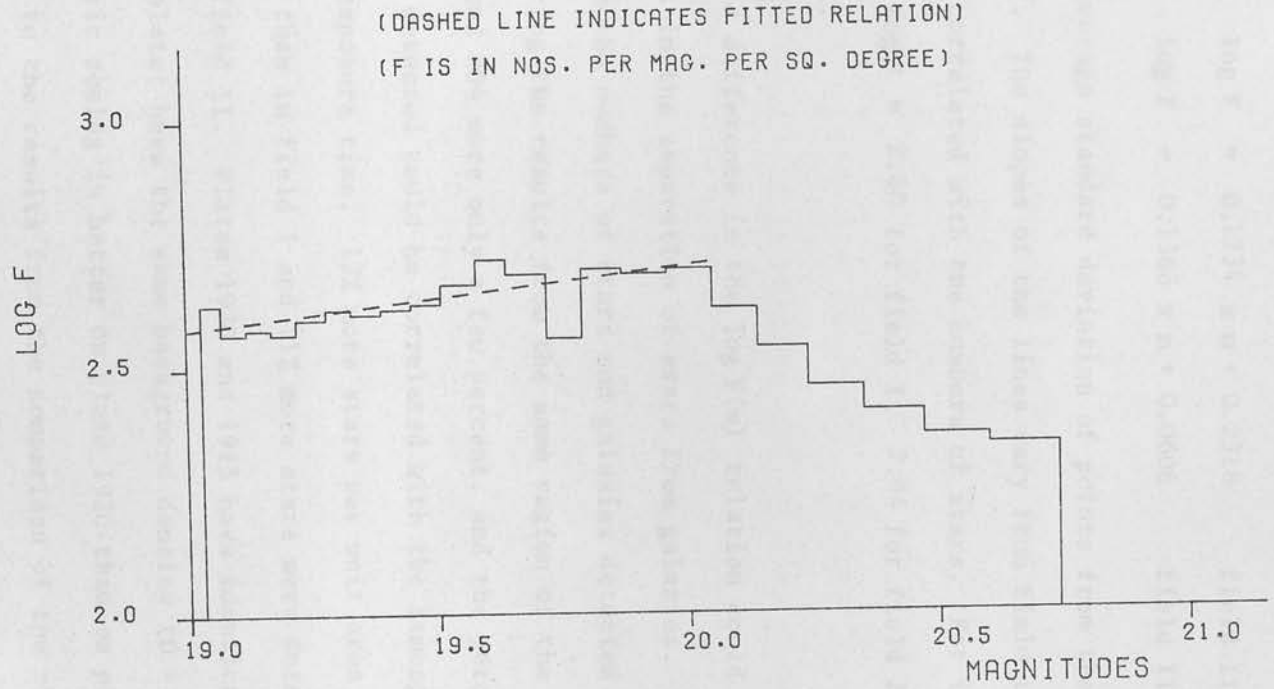

A straight line was fitted to $\log F(m)$ between $m = 19$ and $m = 20$ using the least squares method, minimising the residuals in $\log F$. The results were:

$$\log F = 0.0709 \times m + 1.2192 \qquad \text{field I}$$

$$\log F = 0.1234 \times m + 0.2318 \qquad \text{field II}$$

$$\log F = 0.1368 \times m + 0.0606 \qquad \text{field III}$$

and the average standard deviation of points from the lines was $\sigma = 0.047$. The slopes of the lines vary from field to field and the slope is correlated with the numbers of stars. For instance, at $m = 19.5$ $\log F = 2.60$ for field I, 2.64 for field II, and 2.72 for field III.

The difference in the $\log F(m)$ relation could be partly due to errors in the separation of stars from galaxies. However, the errors in the numbers of stars and galaxies detected in section 3.4 by comparing the results from the same region of the sky on plates 92, 149 and 204 were only a few percent, and the percentage of galaxies detected could be correlated with the atmospheric seeing and the exposure time. 12% more stars per unit area were detected in field II than in field I and 11% more stars were detected in field III than in field II. Plates 1920 and 1915 have identical exposure times and the plates have the same background density ($D = 1.08$). The atmospheric seeing is better on plate 1920 than on plate 1915, but contrary to the results from the comparison of the numbers of stars detected on plates 92, 149 and 204, a larger percentage of stars were detected on plate 1915. The fact that field III (plate 1915) contains NGC288, a globular cluster, did not affect the results which were the same if the region surrounding NGC288 was omitted.

Another possibility is that the variation from field to field in the log F(m) relation could be caused by an error in the magnitude calibration. The log m (log A) relation was similar for the three fields, but not identical, the slopes of the calibration being -3.605, -3.391 and -3.340 for fields I, II and III respectively. Some difference in slope is expected from plate to plate because the isophotal areas of images of the same magnitude depend on the atmospheric seeing. The fact that the slope for field I is larger could partly account for the slope of the log F(m) relation for field I being so low. However, altering the calibration is not enough to make the slope of the log F(m) relation the same as that for the other two fields. It seems likely therefore that the differences in the log F(m) relations are partly real.

The average log F(m) relation was taken as:

$$\log F(m) = 0.1183 \times m + 0.3608 \qquad (3.1)$$

giving half weight to the result of field I.

This was compared with the expected apparent luminosity function calculated from theoretical models. Two recent determinations of the distribution of mass in the galaxy indicate that the density, ρ, varies as a power law with the radius, R. Sanders & Lowinger (1972) used the infrared observations of the nucleus of the Galaxy by Becklin & Neugebauer (1968) to give $\rho \propto R^{-1.8}$ for the nucleus. A study of RR Lyrae variables in the Galaxy by Oort and Plaut (1975) gave $\rho \propto R^{-3.0}$.

It was assumed that the number density of stars as a function of distance, r, from the Sun in the direction of the south galactic pole

is given by $n(r) = k r^{-\alpha}$ where k and α are constants. The number of stars at a distance r in a solid angle Ω is

$$dF = \Omega r^2 n(r)\, dr$$

and the number of stars of apparent magnitude m and absolute magnitude M is

$$dF(m) = \Omega r^2 n(r)\, \phi(M)\, dr$$

where $\phi(M)$ is the fraction of stars with absolute magnitude M. Using $m - M = 5 \times \log r - 5$,

$$dF(m) = -\Omega r^2 n(r)\, \phi(M)\, r \frac{dM}{5 \log_{10} e}$$

or, substituting for r in terms of m and using $n(r) = k r^{-\alpha}$

$$dF(m) = \frac{k\Omega}{5 \log_{10} e} 10^{(0.6 - 0.2\alpha)(m - M + 5)} \phi(M)\, dM$$

Integrating over all absolute magnitudes:

$$F(m) = +\frac{k\Omega}{5 \log_{10} e} 10^{(0.6 - 0.2\alpha)(m + 5)} \int_{M_f}^{M_b} 10^{(0.6 - 0.2\alpha)(-M)} \phi(M)\, dM$$

Since the integral is independent of m, it is a constant,

and $F(m) \propto 10^{(0.6 - 0.2\alpha)(m + 5)}$

or $\log F(m) = \text{const} + (0.6 - 0.2\alpha)\, m$

From equation (3.1) the value of α obtained is 2.41 with a standard deviation of ± 0.08, i.e. using the number counts of stars between m = 19 and m = 20, the number density of stars decreases as $r^{-2.41}$ with height above the plane of the galaxy. This result cannot be compared directly with the other two values of α given above, because

the distances were measured from the Sun instead of the centre of the galaxy. However it is interesting to note that the value of α obtained is intermediate between the other two.

3.7 The N(m) Relation for Galaxies

First the F(m) relation for galaxies was determined using the same method as that for the stars. Initially all the images which were too faint to be separated into stars and galaxies were included in the counts, supposing that they were galaxies. As before, the images were binned according to coarse measurement area, and the magnitudes corresponding to the centre of the area interval were calculated using the m(log A) relation for galaxies. For areas larger than $A = 28 \times (16\ \mu m)^2$, the galaxies were binned according to log A in intervals of 0.03. The numbers were again scaled to give the results in numbers per unit magnitude interval per square degree.

Because of the uncertainty in determining the numbers of faint stars, two different methods were used to correct the numbers of faint galaxies. The first method assumed that the eye can correctly distinguish faint stars from galaxies by examining the images, although there is no separation of the two types of image in the $\log \left(\frac{I_c}{I_{sky}} - 1\right)$ vs. log A diagram due to the effects of grain noise on the central surface brightness.

For each field, the numbers of faint stars detected visually in each of the calibration regions were counted as a function of image size, and the average linear relation between the numbers of stars and the image area was found. These numbers were then scaled to give an

estimate of the numbers of stars over the whole field.

The second method assumed that the eye is incapable of recognising faint star images, but that the numbers of faint stars could be obtained by extrapolating the results for brighter stars. As mentioned in the previous section the numbers of stars increased to about m = 20 and then decreased at fainter magnitudes. It is probable that the number of faint stars was not complete, because of the difficulty in detecting faint stars. The log F(A) relation, i.e. the number of stars with image area A, is approximately linear and increase for images with $30 \geq A \geq 15$ ($19 \leq m \leq 20$). A straight line was fitted to the log F(A) relation for each field, and the average relation was extrapolated to obtain the numbers of stars with small image areas.

The numbers of stars estimated by these two methods is shown in table 3.7. These results probably show the extremes; it is likely that the numbers of stars lie between the two relations. The estimated numbers of stars with each image area was subtracted from the F(A) relation for galaxies. This method for correcting the numbers of faint galaxies should not affect the magnitude calibration, i.e. m(log A) relation, even though all the images too faint to be classified were included in the calibration for galaxies. The profiles of faint stars and galaxies are alike, and therefore the function m(log A) is similar for stars and galaxies.

The resulting log F(m) graphs are shown in figures 3.10a, b and c. Figures 3.11a, b and c show the corresponding log N(m) relations,

TABLE 3.7

The Average Numbers of Faint Stars (per arcdeg^2), Estimated Using Methods 1 and 2

Area ((16 μm)^2)	No derived from method 1	No derived from method 2
3	0.0	80.2
4	0.0	75.9
5	1.6	71.9
6	8.1	68.2
7	14.2	64.6
8	19.2	61.2
9	22.5	57.9

FIGURE 3.10A FREQUENCY DISTRIBUTION OF GALAXY MAGNITUDES, PLATE 1920, FIELD I.

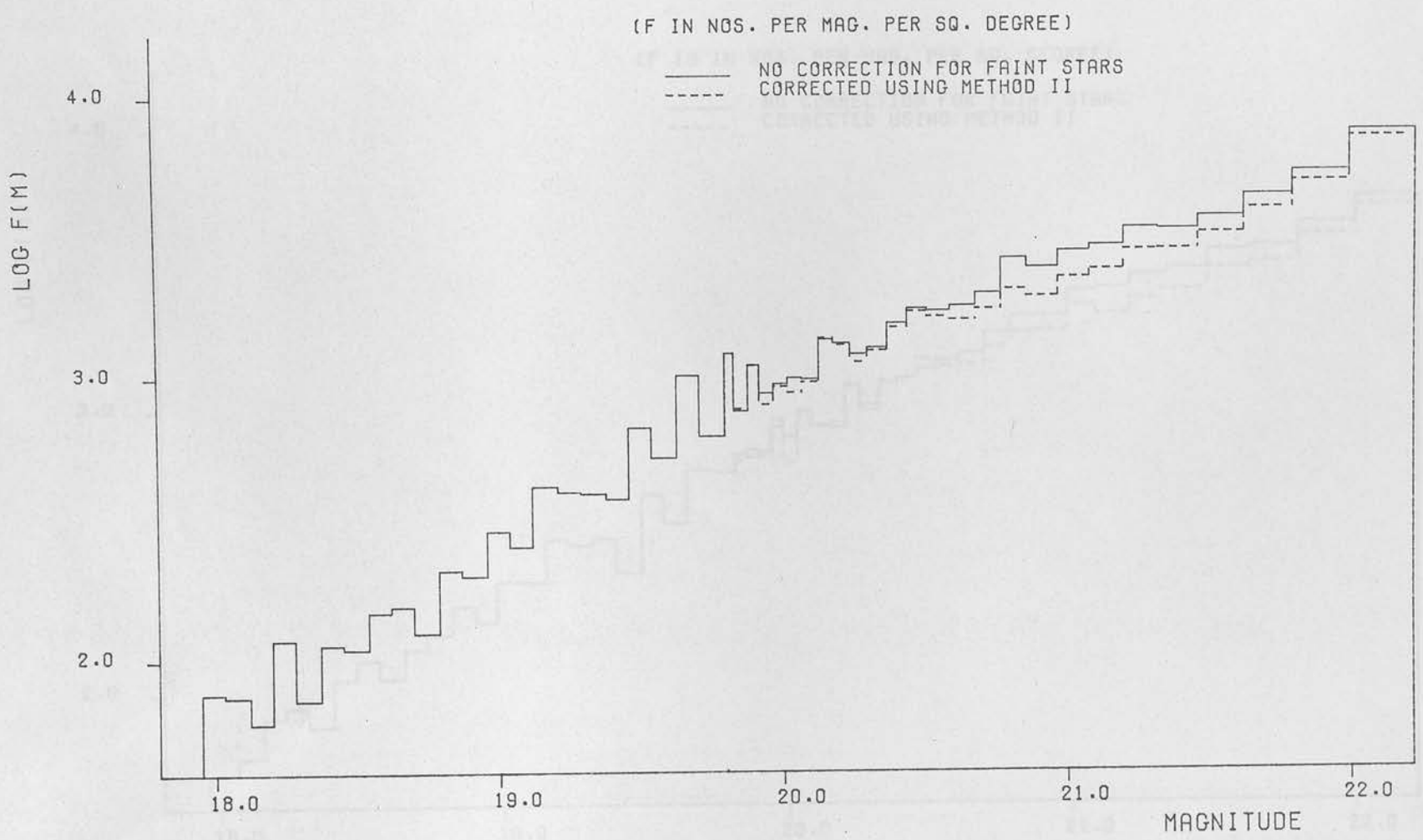

FIGURE 3.10B FREQUENCY DISTRIBUTION OF GALAXY MAGNITUDES, PLATE 1920 FIELD II.

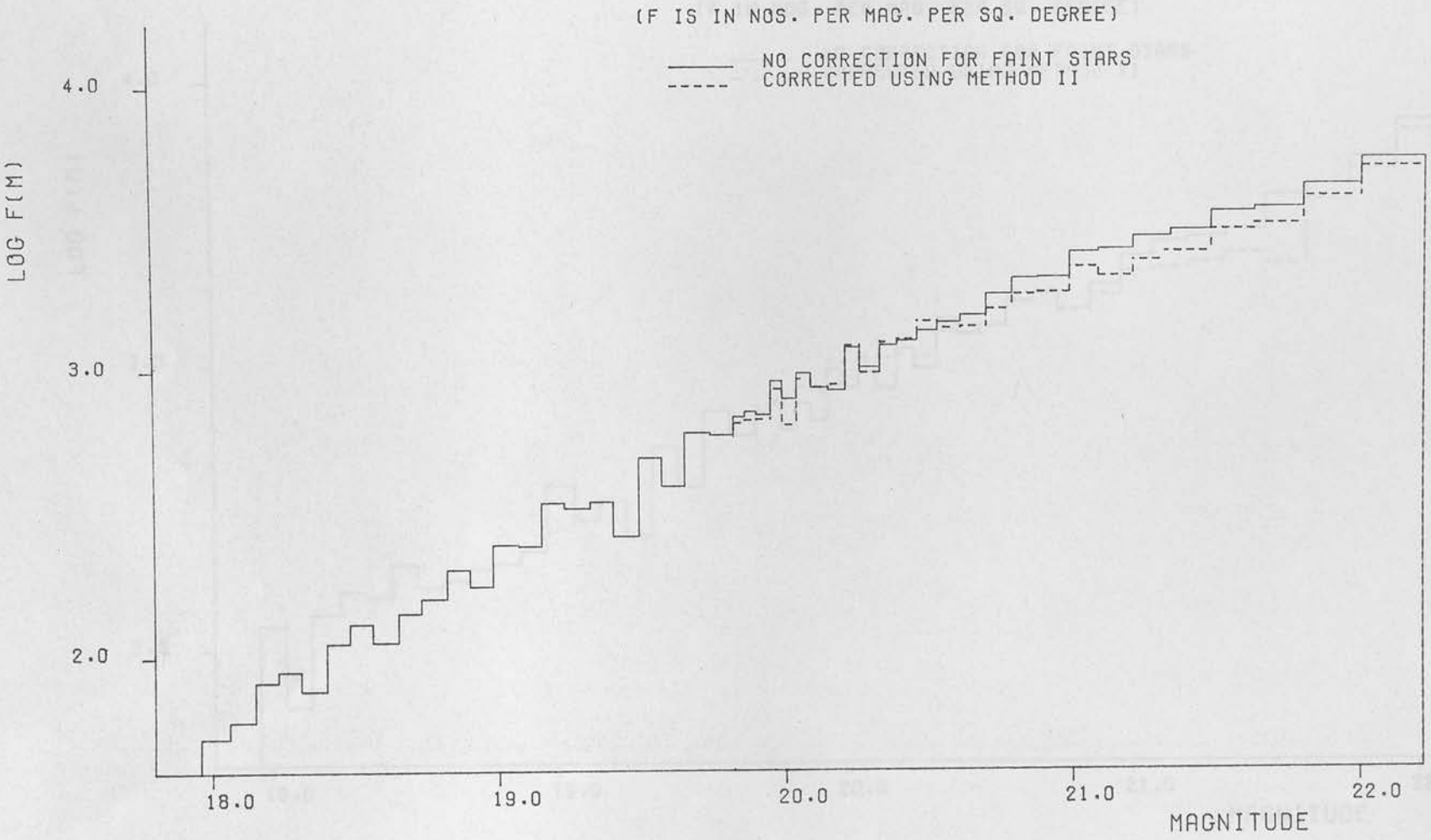

FIGURE 3.10C FREQUENCY DISTRIBUTION OF GALAXY MAGNITUDES, PLATE 1920 FIELD III.

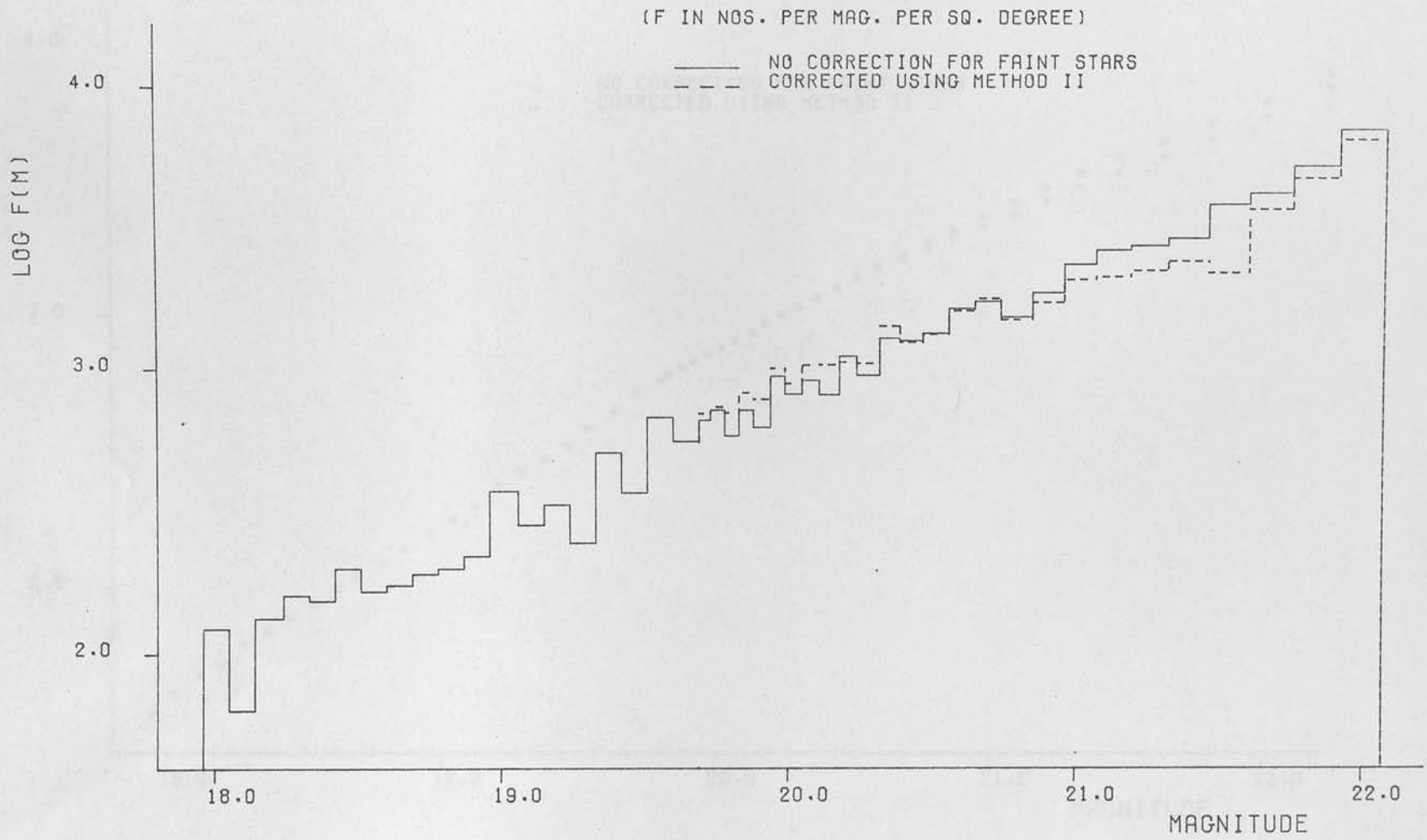

FIGURE 3.11A CUMULATIVE DISTRIBUTION OF GALAXY MAGNITUDES, PLATE 1920 FIELD I.

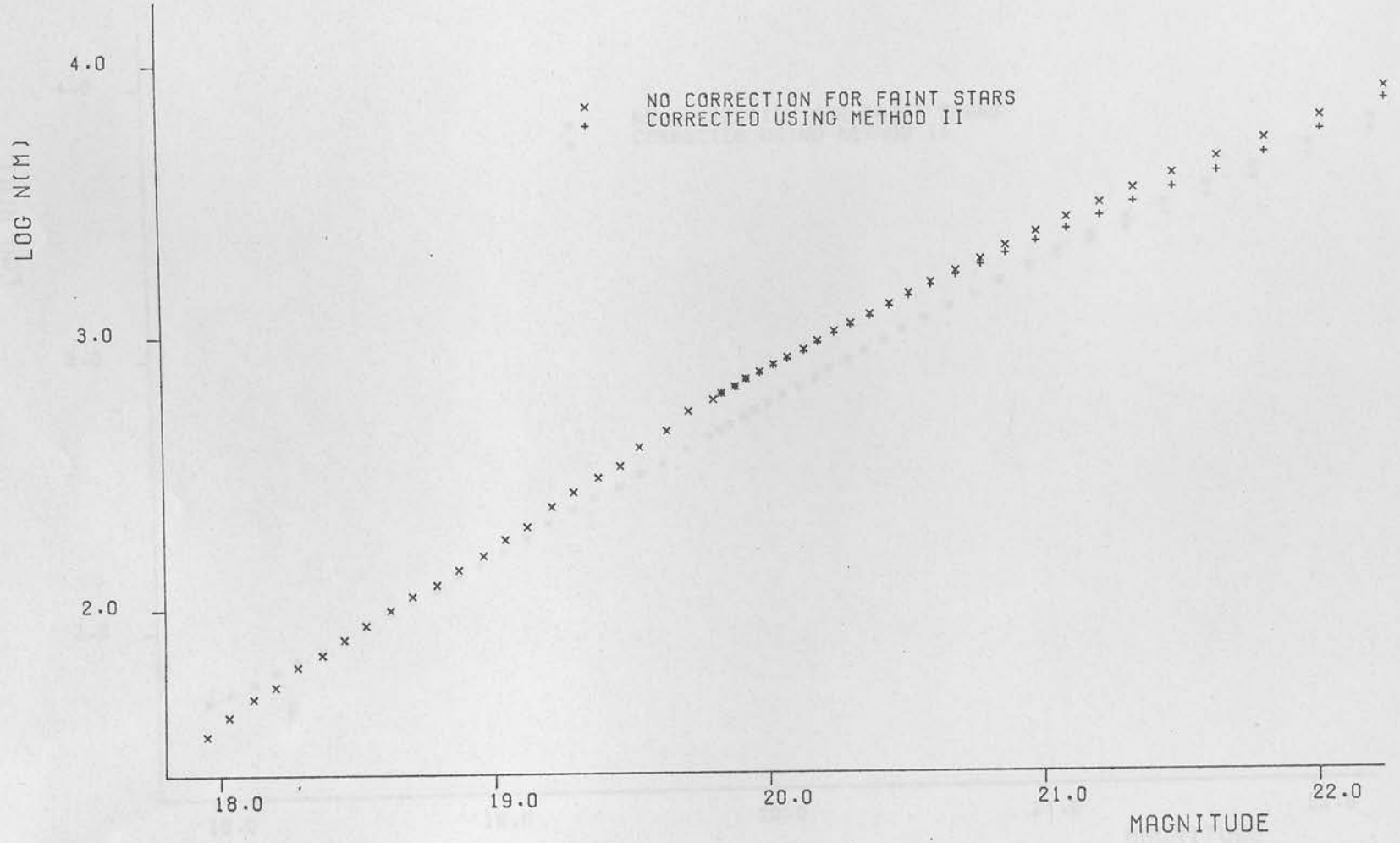

FIGURE 3.11B CUMULATIVE DISTRIBUTION OF GALAXY MAGNITUDES, PLATE 1920 FIELD II.

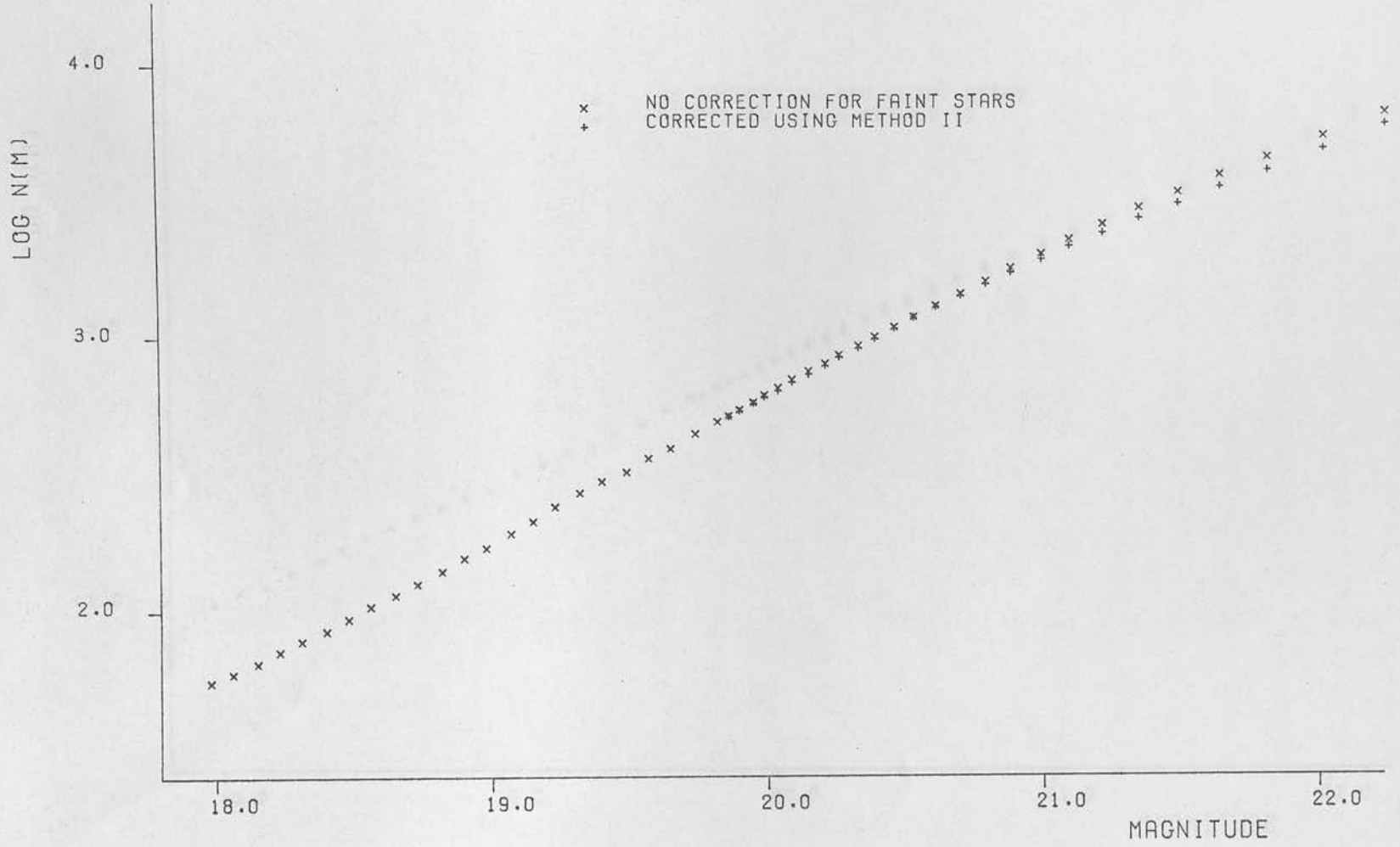

FIGURE 3.11C CUMULATIVE DISTRIBUTION OF GALAXY MAGNITUDES, PLATE 1915 FIELD III.

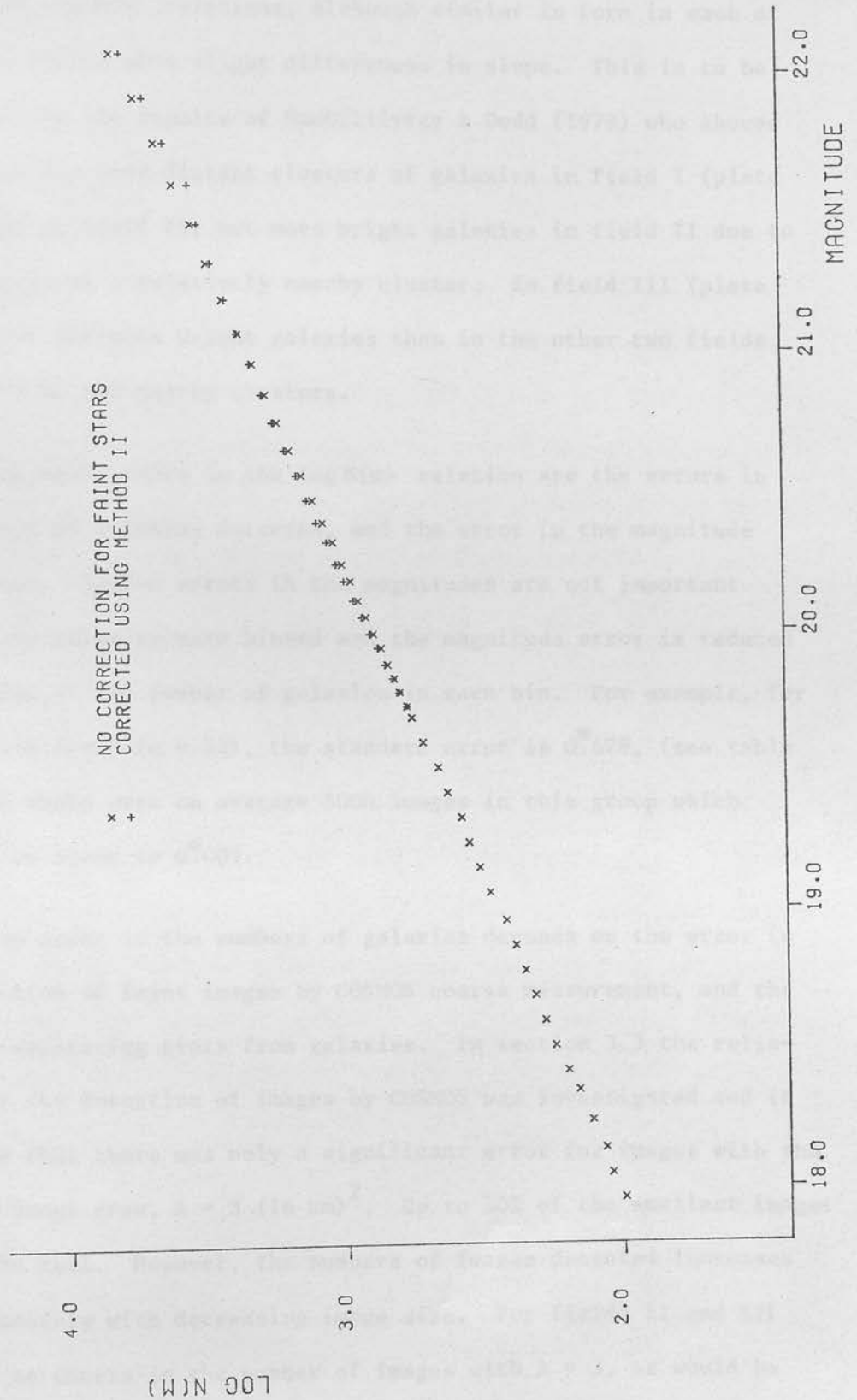

which are the cumulative counts.

The log N(m) relations, although similar in form in each of the three fields show slight differences in slope. This is to be expected from the results of MacGillivray & Dodd (1979) who showed that there are more distant clusters of galaxies in field I (plate 1920) than in field II, but more bright galaxies in field II due to the presence of a relatively nearby cluster. In field III (plate 1915) there are more bright galaxies than in the other two fields, on account of two nearby clusters.

The main errors in the log N(m) relation are the errors in the numbers of galaxies detected, and the error in the magnitude calibration. Random errors in the magnitudes are not important because the galaxies were binned and the magnitude error is reduced by the root of the number of galaxies in each bin. For example, for images with A = 3 (m = 22), the standard error is $0^{m}.628$, (see table 3.6), but there were on average 5000 images in this group which reduces the error to $0^{m}.009$.

The error in the numbers of galaxies depends on the error in the detection of faint images by COSMOS coarse measurement, and the error in separating stars from galaxies. In section 3.3 the reliability of the detection of images by COSMOS was investigated and it was found that there was only a significant error for images with the smallest image area, A = 3 (16 μm)^{2}. Up to 20% of the smallest images may not be real. However, the numbers of images detected increases fairly smoothly with decreasing image size. For fields II and III there is no excess in the number of images with A = 3, as would be

expected if some of the images were due to the affects of grain noise. In the case of field I, there is a slight excess of images with A = 3. This could either be due to very faint clusters of galaxies or to grain noise, but should not affect the overall results.

The error due to the separation of stars from galaxies is only important for m > 21. Figures 3.10a, b and c and 3.11a, b and c show the log F(m) and log N(m) relations without correction for faint stars, and then corrected using method two. If the error in log N is half the difference between log N with no correction and log N corrected using method two, the average error over the three fields increases from 0.009 at m = 21 to 0.02 at m = 22.

The error arising from the magnitude calibration is again only serious for faint galaxies. The m(log A) calibration is well established in the linear part of the curve, from m = 18 to m = 21. For $m \geq 21.5$ the r.m.s. magnitude error is 0.628 and there were on average about 80 galaxies in each calibration region with $m \geq 21.5$. This gives rise to an error of $\pm 0^{m}.07$ for faint galaxies, and since the slope of the log N(m) relation is approximately 0.5, the error in log N for faint galaxies is ±0.035. The combined error from the separation of stars from galaxies and the magnitudes calibration is ±0.04.

The observed log N(m) at m = 22 is 3.81, 3.75 and 3.79 in the three fields respectively. Although these values lie within the estimated errors, the differences are to a large extent real, as can

be seen by inspecting the plates under a microscope. The variation in the number of faint galaxies is caused by clustering or super-clustering.

3.8 The Completeness of the Sample of Galaxies

The criterion for including galaxies in the sample was that they should have image areas of at least 3 x $(16\ \mu m)^2$ on the plate, or 3.5 $arcsec^2$, within the threshold isophote for COSMOS coarse measurement of 25 mag $arcsec^{-2}$. In section 3.4 it was shown that galaxy magnitudes can be calibrated adequately in terms of log A, ignoring the dispersion in the central surface brightness. If magnitudes were dependent only on the image area, the sample would be complete to $m \doteq 22$, the magnitude corresponding to the limiting area. However, the dispersion in surface brightness is important in determining the completeness of the sample, because if low surface brightness galaxies are not detected the sample is not complete to a given magnitude limit.

The completeness of the sample was checked by a method similar to that used by Oemler (1974), who divided the galaxies in his sample into magnitude intervals and then examined the distribution of the central opacities of the images in each group. The distributions were found to be almost gaussian in form, but at fainter magnitudes they were truncated due to the fact that low surface brightness images had not been detected. Assuming that the distributions should have been symmetrical, the incompleteness of the sample was calculated as a function of magnitude.

In this case the images were divided according to image area and the distribution of the central surface brightness (obtained from T_{min} of COSMOS coarse measurement) in each area interval was examined. Both stars and galaxies were included in the study, and the distributions were found for each field, using all the images in the field. These were also approximately gaussian as can be seen from figures 3.12a to e. (The form of the distributions is discussed below.) The results were approximately the same for each field. For images with areas above the limit for separating stars from galaxies, the stars are indicated by the shaded regions of the diagrams, and it can be seen that at an image area of 40 (46.1 arcsec^2) the stars form a separate distribution from the galaxies. As the image area decreases, the surface brightness distributions for stars and galaxies merge as the galaxies become less well resolved. There is no definite cut-off in the numbers at a certain surface brightness in any of the distributions, but for images with areas less than 10 x (16 μm)^2 or 11.5 arcsec^2 the slope of the distributions is steeper on the low surface brightness side. This could be caused by the failure to detect all the low surface brightness images, or it could be due to the fact that stars were included in the diagrams and they may have affected the distributions by extending them to higher surface brightnesses. The distribution also becomes narrower, which could be caused partly by the loss of low surface brightness galaxies and partly because the distributions for stars and galaxies merge.

The fraction of faint images which are stars was estimated by two methods in section 3.7. Using the first method which assumed

FIGURE 3.12 DISTRIBUTIONS OF CENTRAL SURFACE BRIGHTNESS (S.B.) OF IMAGES, PLATE 1920 FIELD II.

A) IMAGES WITH AREAS OF 46.1 (ARCSEC)^2

THE SHADED AREA REPRESENTS STAR IMAGES

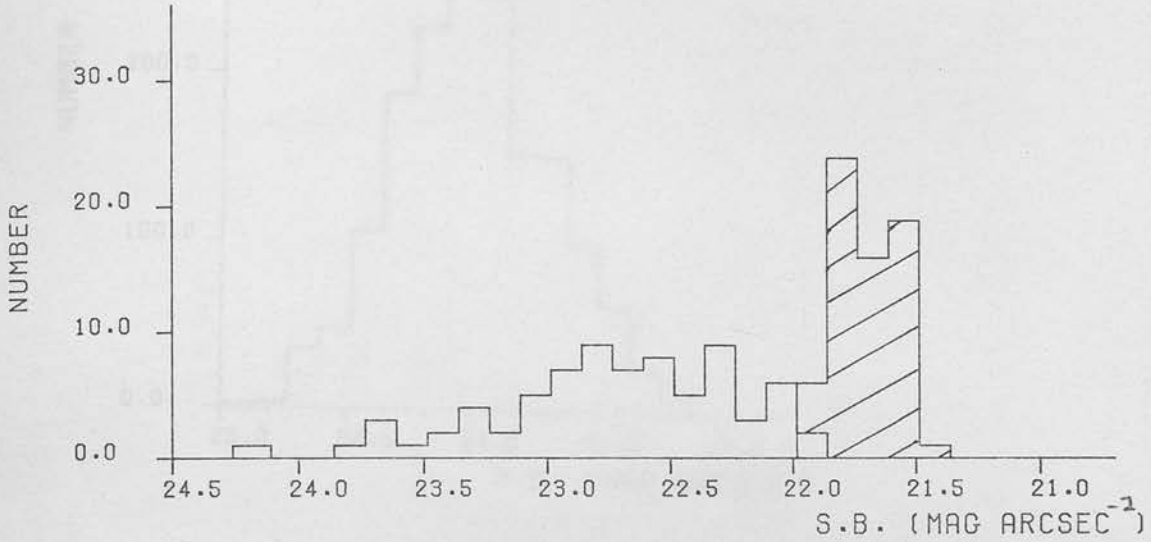

B) IMAGES WITH AREAS OF 23.1 ARCSEC^2

THE SHADED AREA REPRESENTS STAR IMAGES

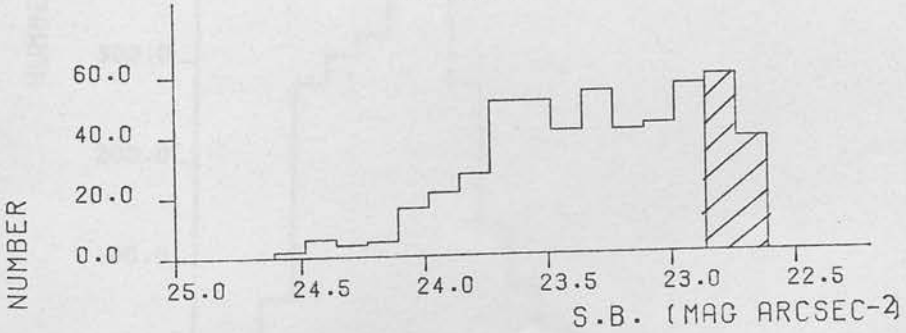

C) IMAGES WITH AREAS OF 11.5 ARCSEC^2

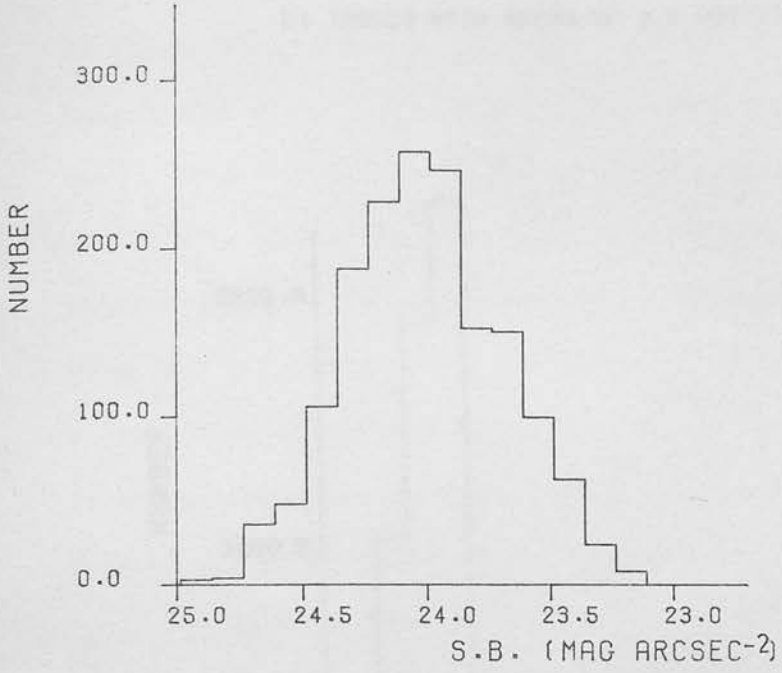

D) IMAGES WITH AREAS OF 8.1 ARCSEC^2

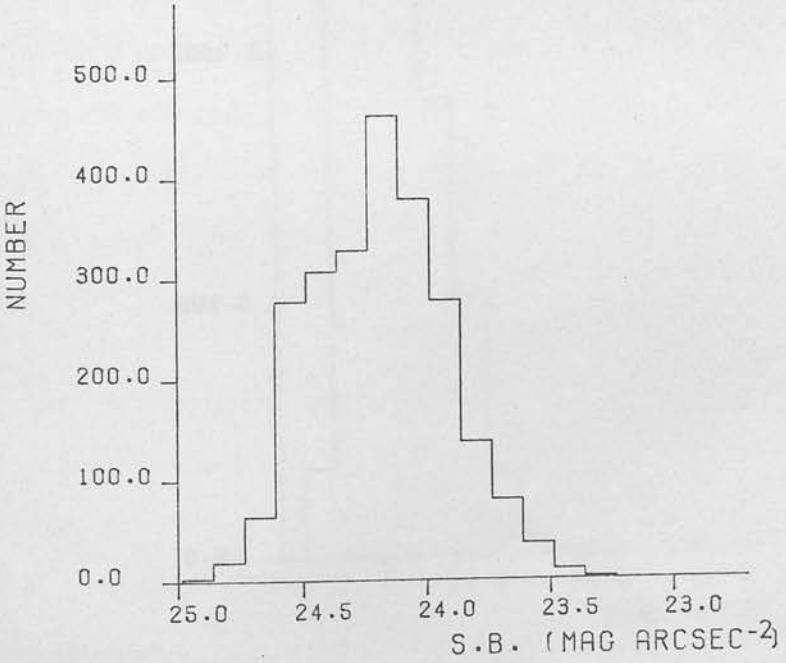

E) IMAGES WITH AREAS OF 3.5 ARCSEC^2

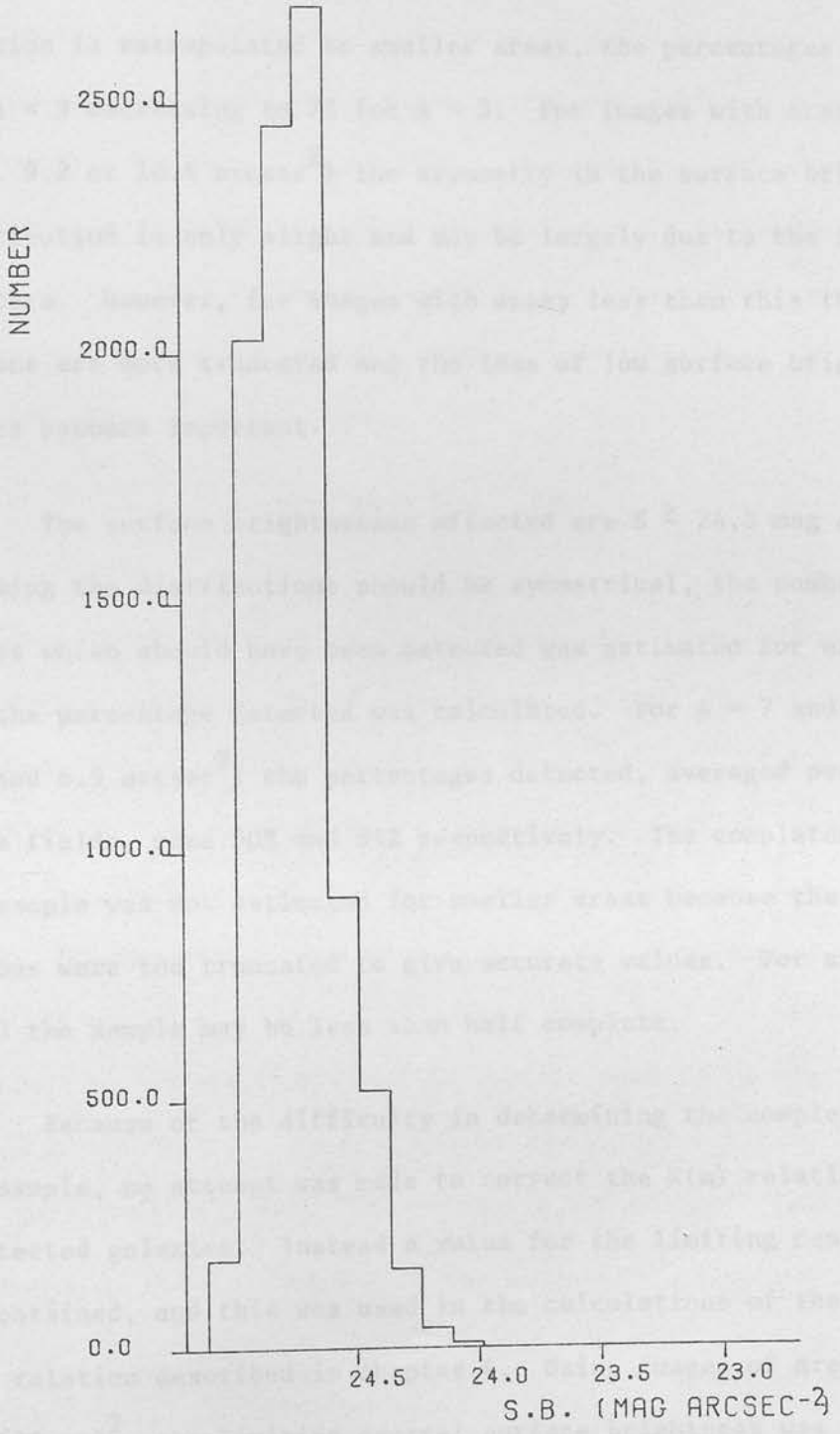

that the eye could distinguish accurately between faint stars and galaxies, the percentage of stars should decrease from about 7% for images with A = 9 (10.4 arcsec^2) to zero for images with areas less than 5 or 5.8 arcsec^2. If the second method is used and the log F(A) relation is extrapolated to smaller areas, the percentages are 19% for A = 9 decreasing to 7% for A = 3. For images with areas 8 or 9 (i.e. 9.2 or 10.4 arcsec^2) the asymmetry in the surface brightness distribution is only slight and may be largely due to the inclusion of stars. However, for images with areas less than this the distributions are more truncated and the loss of low surface brightness images becomes important.

The surface brightnesses affected are $S \geq 24.5$ mag arcsec^{-2}. Assuming the distributions should be symmetrical, the number of images which should have been detected was estimated for each area, and the percentage detected was calculated. For A = 7 and 6 (i.e. 8.1 and 6.9 arcsec^2) the percentages detected, averaged over the three fields, were 90% and 84% respectively. The completeness of the sample was not estimated for smaller areas because the distributions were too truncated to give accurate values. For areas of A = 3 the sample may be less than half complete.

Because of the difficulty in determining the completeness of the sample, no attempt was made to correct the N(m) relation for undetected galaxies. Instead a value for the limiting central surface was obtained, and this was used in the calculations of the theoretical N(m) relation described in chapter 4. Using images of areas 6 and 7 x (16 μm)^2, the limiting central surface brightness was found to be 24.8 mag arcsec^{-2}.

So far it has been assumed that the true central surface brightness distribution of galaxies with a given isophotal area is symmetrical and approximately gaussian. If the central surface brightness of galaxies depends on the total luminosity, the numbers of galaxies with low surface brightnesses would be expected to increase since the number of galaxies decreases with decreasing luminosity. However, Freeman (1970) studied the central surface brightnesses of galaxies and found that there is little variation in the central surface brightnesses of galaxies. He measured the intensity profiles of the disk component of spiral and lenticular galaxies which is of the form

$$\log \left(\frac{I}{I_o}\right) = -\left(\frac{r}{\alpha}\right) \qquad (3.2)$$

(de Vaucouleurs 1962), where I_o is the central intensity and α the scale size. He found that I_o was almost constant for all the galaxies studied, and equalled 21.64 B mag arcsec^{-2} with a standard deviation of 0.30 mag arcsec^{-2}. Freeman also used the results of Fish (1964) to show that elliptical galaxies have the same central surface brightnesses. Fish investigated the relationship between potential energy and mass of elliptical galaxies. He assumed that the ratio of surface brightness to surface density is constant, i.e. $M = kL$, where M is the mass, L is the luminosity and k is the constant of proportionality. Then the expression for the potential energy becomes $\Omega = \frac{k^2 L^2}{R_e}$, where Ω is the potential energy and R_e the effective radius, i.e. the radius containing half the total luminosity. The masses for the majority of the galaxies were calculated from the

average mass/luminosity ratio. Fish found that $\Omega \propto M^{3/2}$ which implies that $L \propto R_e^2$ and therefore that the central surface brightness is constant, assuming that all the galaxies have the same intensity profiles. (The quantities which Fish measured were L and R_e for each galaxy, and his results, as explained by Disney (1976), show that $L \propto R_e^2$ regardless of the relation between potential energy and mass). The average central surface brightness for elliptical galaxies is 14.8 ± 0.9 B mag arcsec^{-2} as calculated by Disney.

If it is true that the central surface brightness of galaxies of a given type is approximately constant, the observed surface brightness from Schmidt plates can be explained without invoking further selection effects. The average surface brightness decreases with the area of the image (see figure 3.12) but this is because the galaxy profiles are convoluted by the atmospheric seeing. The more distant a galaxy, the smaller the angular diameter compared with the size of the seeing disk, and the more its central surface brightness is decreased. The convolution also explains why the range in the surface brightness at a given image area is only two magnitudes instead of about seven magnitudes which is the difference between the central surface brightnesses for ellipticals and the disks of spirals. The intensity distribution for ellipticals and the spheroidal component of spirals is

$$\log \frac{I}{I_o} = - \frac{r}{\alpha}^{\frac{1}{4}} \qquad (3.3)$$

(de Vaucouleurs 1948) and is more peaked in the centre than the distribution for the disk component of spirals which follows equation

(3.2). Therefore the smoothing due to the atmospheric seeing will have more effect on the intensity profiles of ellipticals and early type spirals where the spheroidal component dominates, and the high central surface brightnesses will not be observed.

However, Disney (1976) claims that the results of Freeman and Fish are due to selection effects. He used the de Vaucouleurs' intensity profiles (equations (3.2) and (3.3) above) and assumed that the constants I_o and α are independent, i.e. for any I_o a range of values of α can be found. Then he calculated the apparent angular sizes of elliptical and spiral galaxies at an isophote of 24 B mag arcsec^{-2} as a function of central surface brightness, for a given total luminosity. He found that the distribution reached a maximum at 21.83 B mag arcsec^{-2} for spirals and 15.31 B mag arcsec^{-2} for ellipticals. Since these values are very close to the values obtained by Freeman and Fish, Disney believes that their results are the consequence of selecting the galaxies whose images look largest on photographic plates.

If Disney is correct, the central surface brightness distribution for galaxies with image areas larger than 11.5 arcsec^{-2} may after all be altered by selection effects. In this case, the completeness of the sample cannot be determined by Oemler's method.

The relation between surface brightness and absolute luminosity of elliptical galaxies was studied by Strom & Strom (1978). In the range $-24 \leq M_V \leq -18$ they found that the surface brightness is higher in intrinsically faint galaxies, which indicates that selection effects

dependent on surface brightness should not arise for elliptical galaxies with $M \leq 18$. Christensen (1975) investigated the luminosity function for different types of field galaxies, and discovered that there are no elliptical galaxies with $-18 \leq M_B \leq -16$. This implies that there are two types of elliptical galaxies: giants and dwarfs. The dwarf category includes galaxies such as M32, NGC205 and the Sculptor galaxy which has a very low surface brightness of 25 B mag arcsec^{-2}. He also found that there are no faint early type spirals with $M_B \geq 17.5$. For simplicity, it was assumed that galaxies could be classified as either giants or dwarfs, and that the dwarf galaxies ($M_B > -17$) could not be detected in the present survey. This cut-off in the absolute magnitude was applied in addition to the surface brightness cut-off of 24.8 mag arcsec^{-2}. Tinsley (1977) and Ellis, Fong & Phillipps (1977) also used $M_B = -17$ as a low luminosity cut-off.

The selection function $\phi(z)$ for galaxies on the UK Schmidt plates has been estimated by Ellis, Fong & Phillipps (1977) by comparing the observed angular diameter frequency distribution, obtained from COSMOS measurements, with theoretical models. The results depended on the amount of luminosity evolution incorporated in the model, on the width of the atmospheric seeing disk, and on the threshold isophote for coarse measurement data. They found that $\log \phi(z) = 1$ for $z \lesssim 0.1$ and then, if a liberal model for luminosity evolution was used, (the redshift of galaxy formation, $z_F = 3.5$), $\log \phi(z)$ decreased almost linearly with a constant of proportionality of about -3.5. The decrease was more rapid if the conservative model for evolution was used, ($z_F = 6.2$).

$\phi(z)$ cannot be compared directly with the selectivity as a function of angular diameter, or isophotal area, because of the variety of sizes of galaxies. However, it can be shown that this form of selection function holds for the data in the present sample by considering the magnitude limit alone. Assuming $H_o = 50\,km\,s^{-1}\,Mpc^{-1}$ and $q_o = 0.02$, (the values used by Ellis, Fong & Phillipps), and using the standard Mattig (1958) m(z) relation, a galaxy of absolute magnitude $M_B = -17$, which is the faint limit, will have an observed magnitude of m = 22.31 at z = 0.1. This is too faint to be included in the sample. (The K-correction was taken from Pence (1976), the last column of table 12, and the luminosity evolution was ignored.) This is why log $\phi(z)$ starts to decrease just before z = 0.1. The rate of decrease of log $\phi(z)$ will depend on the slope of the luminosity function at the faint end, and the slope of the m(z) relation. From Arakelyan & Kelloglyan (1970), the slope of the luminosity function is 0.324 for faint galaxies. The slope of the m(z) relation varies with redshift, but the average slope between z = 0.1 and z = 0.6 is about 10. This means that if the log $\phi(z)$ relation is formed by losing all galaxies with observed magnitudes fainter than m = 22, the log $\phi(z)$ vs. z graph should have a slope of about -3.2 which is close to that found by Ellis, Fong & Phillipps.

To conclude, the completeness of the sample can be expressed as a function of several parameters. Firstly, there is a limit on the isophotal area of the images. This is 3.5 $arcsec^2$, (although, as pointed out in section 3.2, some of the smallest images may not be real). The limiting central surface brightness is S = 24.8 mag $arcsec^{-2}$,

and is the limit on the apparent central surface brightness which is measured after the intensity profile of the galaxy has been convoluted by the atmospheric seeing. Thirdly, if there are further selection effects acting on the data, which cannot be detected by Oemler's method, a limit on the absolute magnitude may be applied. This limit is less well defined than the other two, but was initially chosen as $M_B = -17^m.0$.

3.9 Comparison with Other Magnitude Counts of Galaxies

Before analysing the log N(m) relation, the data was compared with magnitude counts from other sources. Brown (1974) investigated the apparent luminosity function of galaxies in a region centred on the north galactic pole. He obtained a series of photographic plates with different exposure times and hence different limiting magnitudes. The number of galaxies on each plate was counted and then the limiting magnitude for each exposure was derived using photoelectric photometry to determine the log N(m) relation. Brown combined his results with data from various sources, such as Hubble (1934) and Shapley (1957) and the mean values for the log N(m) relation were presented in table 22 of his thesis.

Brown converted the magnitudes he used to the standard B waveband. In order to compare his data with the present results, the magnitudes were converted to the j system using the colour equation obtained for stars by Kontizas, given in section 2.3. The relation between the B and j colour bands depends on the spectrum of the source, and so there will be a small error in applying the colour equation obtained for stars to galaxies. At present, no colour equation for the

B and j bands is available for galaxies. (Oemler (1974) obtained a relationship between magnitudes of galaxies photographed on IIIaJ emulsion and the standard V band, but his system utilised a Wratten 4 filter instead of a Schott GG395 filter.)

The (B - V) colour of galaxies varies from 0.9 for early type galaxies to 0.4 for late type galaxies (de Vaucouleurs 1974). Since in a survey of distant galaxies the low surface brightness irregular galaxies will not be detected so easily as the earlier type galaxies, the average value of (B - V) was taken as 0.7. This gives $m_j = B - 0.14$.

In converting from the B to the j magnitude system, the fact that galaxies are redshifted must be taken into account. The K-corrections are different in the two bands, being larger in the B band. The K-corrections for the B band were obtained from Pence (1976) and those for the j band were calculated using the galaxy spectra obtained by Pence as described in chapter 4. The difference in the K-correction as a function of B magnitude was calculated for Sbc galaxies (assuming that these galaxies have average properties) and applied to the B magnitudes. The corrections were $0^m.6$ or less.

Figure 3.13 shows a comparison of the results in the present study with Brown's data, the B magnitudes having been converted to j magnitudes. Either there is a magnitude discrepancy and/or there is a discrepancy in log N. Brown's results are for the north galactic pole, whereas the present survey is near the south galactic pole, and the magnitudes and numbers may be affected by the Local Supercluster, the centre of which is towards the north galactic pole.

FIGURE 3.13 A COMPARISON OF THE DATA WITH BROWN'S RESULTS.

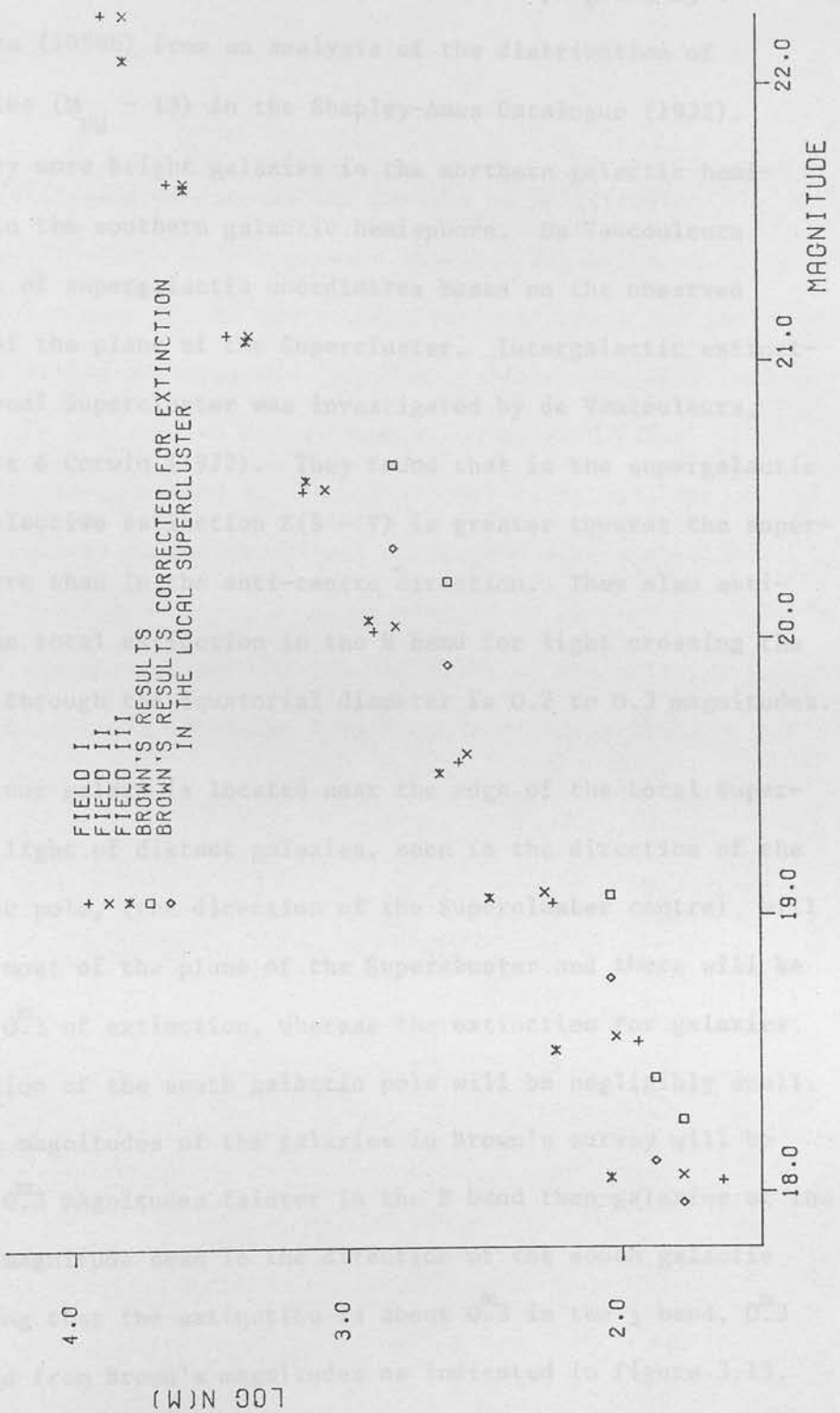

The presence of the Local Supercluster was proposed by de Vaucouleurs (1958b) from an analysis of the distribution of bright galaxies ($M_{pg} - 13$) in the Shapley-Ames Catalogue (1932). There are many more bright galaxies in the northern galactic hemisphere than in the southern galactic hemisphere. De Vaucouleurs defined a set of supergalactic coordinates based on the observed orientation of the plane of the Supercluster. Intergalactic extinction in the Local Supercluster was investigated by de Vaucouleurs, de Vaucouleurs & Corwin (1972). They found that in the supergalactic plane, the selective extinction E(B - V) is greater towards the supergalactic centre than in the anti-centre direction. They also estimated that the total extinction in the B band for light crossing the Supercluster through the equatorial diameter is 0.2 to 0.3 magnitudes.

Since our galaxy is located near the edge of the Local Supercluster, the light of distant galaxies, seen in the direction of the north galactic pole, (the direction of the Supercluster centre), will pass through most of the plane of the Supercluster and there will be about $0^m.2$ to $0^m.3$ of extinction, whereas the extinction for galaxies in the direction of the south galactic pole will be negligibly small. Therefore the magnitudes of the galaxies in Brown's survey will be about $0^m.2$ to $0^m.3$ magnitudes fainter in the B band than galaxies of the same absolute magnitude seen in the direction of the south galactic pole. Assuming that the extinction is about $0^m.3$ in the j band, $0^m.3$ was subtracted from Brown's magnitudes as indicated in figure 3.13. This gave closer agreement between his results and the present results. The remaining difference can be explained in several ways. The value

for extinction in the supergalactic plane may be larger than $0^m.3$ or, there may be an error in the equation used to convert the B magnitudes to j magnitudes.

It is difficult to compare the numbers of galaxies in Brown's data with those in the present sample. The types of photographic emulsion used in the two studies were different and the method of detecting galaxies was different. Brown used IIaO emulsion and counted the galaxies by visual inspection of each plate. The selection effects operating on the samples are different, and so the two sets of numbers do not completely correspond with each other. Apart from these factors, log N is expected to be smaller for Brown's data because the extinction will dim the light of the galaxies so that some, which would otherwise have been recorded, are below the threshold of detection.

4. THE ANALYSIS OF THE N(m) RELATION

4.1 Introduction

The most common method of interpreting the N(m) relation is by comparison with a theoretical relationship using a model universe. As mentioned in chapter 1, the N(m) relation, which measures the volume of space contained within successive radii, depends on the curvature of space which is determined by the density of matter in the universe. In theory it should be possible to determine the deceleration parameter, q_o, from the observed N(m) relationship, but it has been shown by Sandage (1961) and by Brown & Tinsley (1974) that N(m) is not very sensitive to the cosmological model. However, advantage can be taken of this fact and the N(m) relation can be used to investigate other effects such as the luminosity evolution of galaxies, if the cosmological model is derived from other sources.

The 'big bang' model of the universe was chosen since this model fits most of the observational evidence at present. It can explain the redshift-distance relation observed for nearly all galaxies. (The discrepant redshifts discovered by Arp seem to occur in isolated cases, (Field, Arp & Bahcall 1973).) Also, the 2.7^{o} K microwave background radiation can be explained as the cooled-down remains of the radiation which ceased to interact with matter at recombination. Friedman (1922) derived equations for an expanding universe, and in Appendix I, the N(m) relation is derived from the two equations of state.

In this model, as in the majority of cosmological models, it

is assumed that the universe is homogeneous and isotropic (the cosmological principle). It is obvious from the difference in the N(m) relations in the three fields studied that the universe is not homogeneous over scales of less than a few hundred megaparsecs. However, if inhomogeneities are included in the equations, an extra parameter would be required and there is not enough data to determine both the amount of inhomogeneity of the universe and the luminosity evolution of galaxies. Instead, the results of the three fields have to be combined to smooth out the effects of inhomogeneities.

While deriving the theoretical N(m) relation it was assumed that the cosmological constant, Λ, was zero. The cosmological constant describes the curvature of the universe in the absence of matter, and the main reason for assuming $\Lambda = 0$ was again because there is not enough data to study luminosity evolution and to determine the value of Λ. Since N(m) is relatively insensitive to the cosmological model, varying Λ in a model will have a much smaller effect than varying the rate of luminosity evolution.

The model N(m) relations were calculated using the ICL4130 computer at the Royal Observatory Edinburgh. Initially a simple model was chosen in which luminosity evolution was ignored in order to investigate the sensitivity of the model to errors in the K-correction and the luminosity function. The model for calculating N(m) was as follows. For a given value of the deceleration parameter q_o, the m(z) and the log N(z) relations were calculated. The m(z) relation (equation A1.12 in Appendix I) was determined for one value of the absolute magnitude, which was chosen to be the 'characteristic'

magnitude of the luminosity function (see section 4.3). The value of the Hubble constant, H_o, cancels in the equation for m(z), because the luminosity function depends on H_o, (due to the fact that the absolute magnitudes of galaxies whose distances were determined from their redshifts depend on H_o). The K-correction which is a function of redshift was included in the m(z) relation, so that m(z) represented the observed magnitude as a function of redshift. The log N(z) relation was calculated using equations A1.11 and A1.13 in Appendix I. The two relations were then combined and the log N(m) relation was interpolated at regular magnitude intervals by fitting a low order polynomial. The N(m) relation (not the logarithmic form) was convoluted with the luminosity function $\phi(M)$, and the log N(m) relation was recalculated. Finally, the numbers were scaled by comparing the log N(m) values with the average observed log N(m) relation for the five brightest magnitude classes.

4.2 The K-correction for the j Magnitude Band

As explained in chapter 1, the K-correction is the difference between the magnitude measured for a galaxy at a given redshift and the magnitude for an identical galaxy with zero redshift. K-corrections, $K_j(z)$ for the j magnitude band were calculated using the formula given by Oke and Sandage (1968):

$$K_j(z) = 2.5 \log(1+z) + 2.5 \log \{ \int_o^\infty F(\lambda)\, S_j(\lambda)\, d\lambda \Big/ \int_o^\infty F\left[\frac{\lambda}{1+z}\right] S_j(\lambda)\, d\lambda \}$$

where $F(\lambda)$ is the spectral flux of the galaxy and $S_j(\lambda)$ is the spectral response of the detecting system for the j band.

The relative spectral sensitivity was obtained by combining the spectral response of the Kodak IIIaJ emulsion with the spectral response of the Schott GG395 filter. Pence (1976) found the mean energy distribution from λ = 1500 nm to λ = 800 nm for galaxies of five different morphological types: E-SO, Sab, Sbc, Scd and Sdm-Im. The spectra in the ultraviolet were obtained from the OAO-2 satellite photoelectric photometry, and most of the rest of the data was obtained by Wells (1972) using a scanning spectrophotometer. The spectra were corrected by Pence for galactic extinction using $A_B = 0^m.23$ at the galactic pole.

The values of the K-correction as a function of redshift for each morphological type are shown in table 4.1. (The values shown in brackets for E-SO galaxies were extrapolated.) The K-corrections for the j magnitude band are similar to those for the B band. It can be seen that there is a marked difference between the K-correction for the E-SO galaxies and the spiral galaxies. The K-correction for E-SO galaxies increases rapidly with increasing redshift, while that for the spiral and irregular galaxies increases to a maximum and then decreases. This decrease in the K-correction for late-type galaxies is due to the fact that the spectral flux starts to increase at wavelengths below λ = 200 to 300 nm. In the case of E-SO galaxies the spectrum decreases rapidly with wavelength down to λ = 200 nm. At smaller wavelengths the spectrum is uncertain, so Pence did not extend the spectrum for E-SO galaxies below λ = 200 nm. Because of this the K-corrections for E-SO galaxies could not be found for $z > 0.88$. According to the preliminary results from the OAO-2 satellite the spectrum increases rapidly below λ = 200 nm. However, these

results are very uncertain. Tinsley (1977) argues that the spectral energy distribution for elliptical galaxies should continue to decrease at wavelengths smaller than λ = 200 nm, if star formation in elliptical galaxies takes place in a single burst. The K-corrections for E-S0 galaxies in table 4.1 were extrapolated assuming that the spectrum continues to decrease at low wavelengths.

The error in the K-corrections for the B band for E-S0 galaxies was estimated by Pence to be $\Delta K_B/K_B = \pm 0.00$ for $z = 0.2$, ± 0.06 for $z = 0.4$, ± 0.10 for $z = 0.6$ and ± 0.11 for $z = 0.8$. In the case of the other types of galaxies the errors are smaller because the flux is larger. Since the values of the K-corrections for the j band are similar to those from the B band, the errors will be approximately the same size.

The effect of the K-correction on the model log N(m) relation for galaxies of different types was assessed by calculating log N(m) for each type of galaxy separately. It was assumed that the spectrum of a galaxy does not change with time. An arbitrary value of $q_o = 0.0$ was used, and the same absolute magnitude of -21.2 (H_o = 50 km $s^{-1} Mpc^{-1}$) was taken for each calculation. The results were not convoluted with the luminosity function at this stage. As can be seen in figure 4.1 the log N(m) relation increases more rapidly with m for late type galaxies, because the K-correction is smaller.

4.3 The Luminosity Function

The log N(m) relation for galaxies of all absolute magnitudes was found by convoluting the relation obtained for galaxies of one

TABLE 4.1

The K-corrections for Different Galaxy Types

z	E-SO	Sab	Sbc	Scd	Sdm-Im
0.02	0.073	0.055	0.034	0.024	0.011
0.04	0.145	0.111	0.070	0.051	0.025
0.08	0.297	0.231	0.153	0.122	0.078
0.12	0.461	0.358	0.245	0.199	0.136
0.16	0.635	0.495	0.342	0.274	0.185
0.20	0.810	0.634	0.442	0.350	0.233
0.24	0.980	0.771	0.540	0.422	0.276
0.28	1.144	0.900	0.638	0.493	0.317
0.32	1.302	1.222	0.732	0.558	0.351
0.36	1.458	1.143	0.823	0.621	0.387
0.40	1.579	1.240	0.901	0.670	0.411
0.44	1.698	1.331	0.970	0.711	0.433
0.48	1.824	1.412	1.028	0.741	0.446
0.52	1.954	1.489	1.078	0.761	0.450
0.56	2.091	1.566	1.121	0.777	0.451
0.60	2.237	1.638	1.160	0.789	0.450
0.64	2.390	1.701	1.193	0.798	0.447
0.68	2.547	1.755	1.223	0.804	0.443
0.72	2.703	1.802	1.248	0.807	0.438
0.76	2.856	1.844	1.269	0.808	0.431
0.80	3.002	1.879	1.285	0.807	0.422
0.84	3.138	1.909	1.297	0.804	0.411
0.88	3.267	1.933	1.306	0.798	0.398

contd...

TABLE 4.1 (contd.)

z	E-SO	Sab	Sbc	Scd	Sdm-Im
0.92	(3.39)	1.951	1.311	0.791	0.382
0.96	(3.51)	1.964	1.312	0.781	0.364
1.00	(3.62)	1.972	1.310	0.769	0.344
1.04	(3.74)	1.974	1.303	0.753	0.322
1.08	(3.86)	1.972	1.292	0.734	0.298
1.12	(3.97)	1.966	1.278	0.712	0.273
1.16	(4.08)	1.957	1.261	0.688	0.247
1.20	(4.18)	1.944	1.241	0.661	0.220
1.24	(4.29)	1.929	1.219	0.631	0.192
1.28	(4.40)	1.911	1.194	0.599	0.162
1.32	(4.50)	1.890	1.167	0.566	0.130
1.36	(4.60)	1.867	1.138	0.531	0.096
1.40	(4.70)	1.842	1.107	0.495	0.059
1.44	(4.80)	1.816	1.076	0.458	0.020
1.48	(4.92)	1.787	1.042	0.419	-0.023
1.52	(5.02)	1.757	1.007	0.379	-0.068
1.56	(5.11)	1.725	0.971	0.339	-0.115

FIGURE 4.1
THE LOG N (M) RELATION FOR DIFFERENT TYPES OF GALAXY

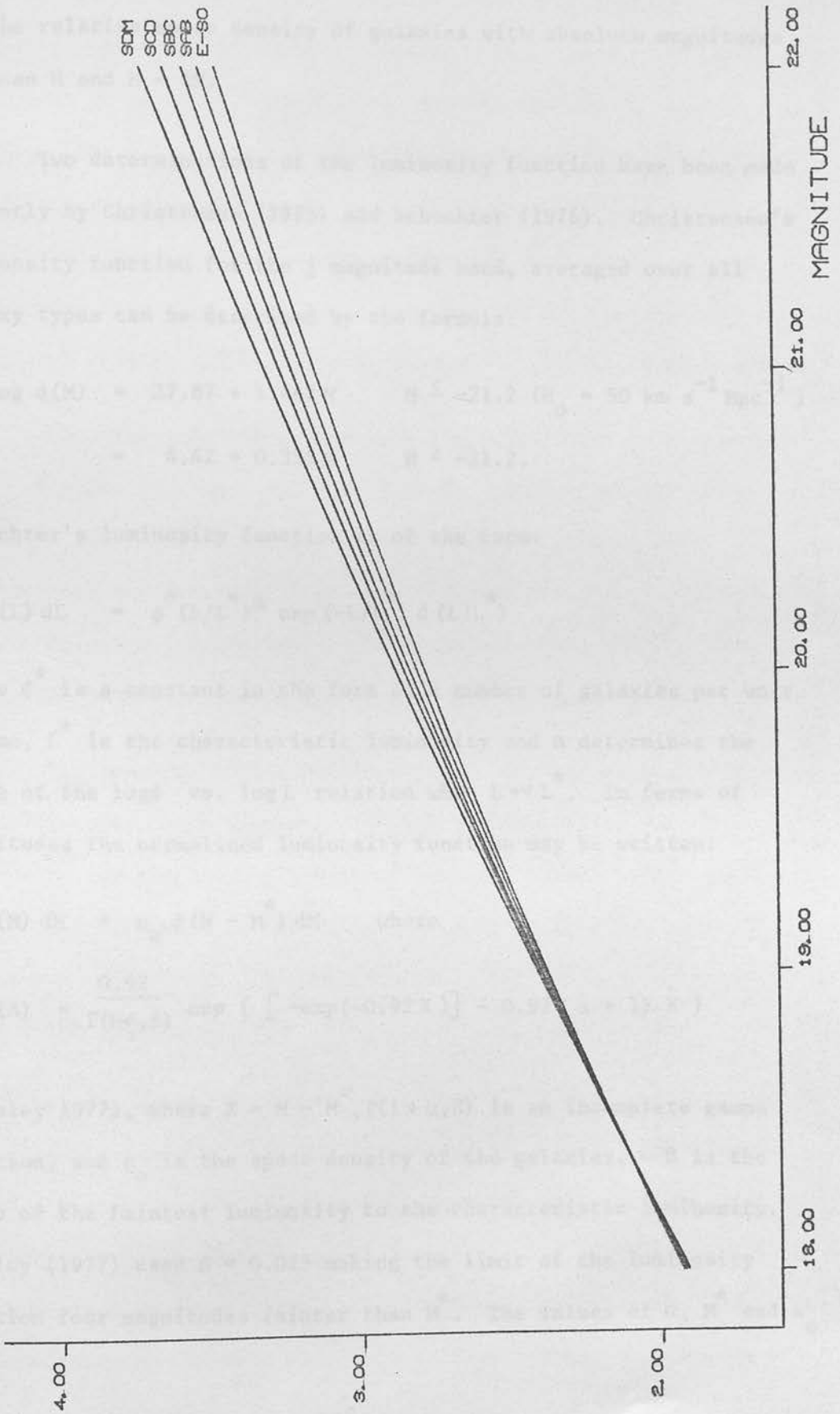

absolute magnitude with the luminosity function $\phi(M)$, where $\phi(M)\,dM$ is the relative space density of galaxies with absolute magnitudes between M and M + dM.

Two determinations of the luminosity function have been made recently by Christensen (1975) and Schechter (1976). Christensen's luminosity function for the j magnitude band, averaged over all galaxy types can be described by the formula:

$$\log \phi(M) = 27.87 + 1.462\,M \qquad M \leq -21.2 \quad (H_o = 50 \text{ km s}^{-1} \text{ Mpc}^{-1})$$

$$= 4.42 + 0.355\,M \qquad M \geq -21.2.$$

Schechter's luminosity function is of the form:

$$\phi(L)\,dL = \phi^*(L/L^*)^{\alpha} \exp(-L/L^*)\,d(L/L^*)$$

where ϕ^* is a constant in the form of a number of galaxies per unit volume, L^* is the characteristic luminosity and α determines the slope of the $\log\phi$ vs. $\log L$ relation when $L \ll L^*$. In terms of magnitudes the normalised luminosity function may be written:

$$\phi(M)\,dM = n_o\,F(M - M^*)\,dM \qquad \text{where}$$

$$F(X) = \frac{0.92}{\Gamma(1+\alpha,\beta)} \exp\{\left[-\exp(-0.92\,X)\right] - 0.92\,(\alpha + 1)\,X\}$$

(Tinsley 1977), where $X = M - M^*$, $\Gamma(1+\alpha,\beta)$ is an incomplete gamma function, and n_o is the space density of the galaxies. β is the ratio of the faintest luminosity to the characteristic luminosity. Tinsley (1977) used $\beta = 0.025$ making the limit of the luminosity function four magnitudes fainter than M^*. The values of α, M^* and n_o

used are given in table 4.2. They are taken from Tinsley (1977) table I, with the magnitudes converted to the j band, and the space densities of galaxies converted to relative instead of absolute values. The relative space densities which were calculated from Christensen (1975) are for $\beta = 0.025$, and the values of n_o have to be altered if β is altered. The reason for the relatively large numbers of late type galaxies is that the luminosity function increases rapidly with decreasing luminosity for late type galaxies.

Christensen's and Schechter's luminosity functions are very similar apart from near the bright limit, where there are more galaxies according to Christensen's formula. (In fact both Christensen and Schechter used data from the Reference Catalogue of Bright Galaxies (de Vaucouleurs & de Vaucouleurs 1964). In both cases the number of very bright galaxies is relatively small.

The theoretical $\log N(m)$ relations derived using both luminosity functions were compared. It was arbitrarily assumed that $q_o = 0.0$, and the average K-corrections were calculated using the relative frequencies of the different types of galaxies given in table 4.2. The upper limit of the luminosity functions was taken as $M = -24.0$.

It was found that there was a negligible difference in $\log N(m)$ calculated using the different luminosity functions. Schechter's formula was chosen for investigating the effects of varying β on the $\log N(m)$ relation. Two values of β were tested, 0.010 and 0.063, corresponding to 5 and 3 magnitudes respectively below the characteristic magnitude. In each case the relative numbers of galaxies of

TABLE 4.2

The Data Used for Calculating the Luminosity Function

	E-SO	Sab	Sbc	Scd	Sdm-Im
$M_j^* - 5\log(H_o/100)$	-21.2	-21.2	-21.2	-20.6	-20.6
α	1.25	1.25	1.25	1.00	1.00
n_o	0.069	0.0345	0.0345	0.431	0.431

FIGURE 4.2
THE LOG N (M) RELATION FOR DIFFERENT LOWER LIMITS OF THE LUMINOSITY FN.

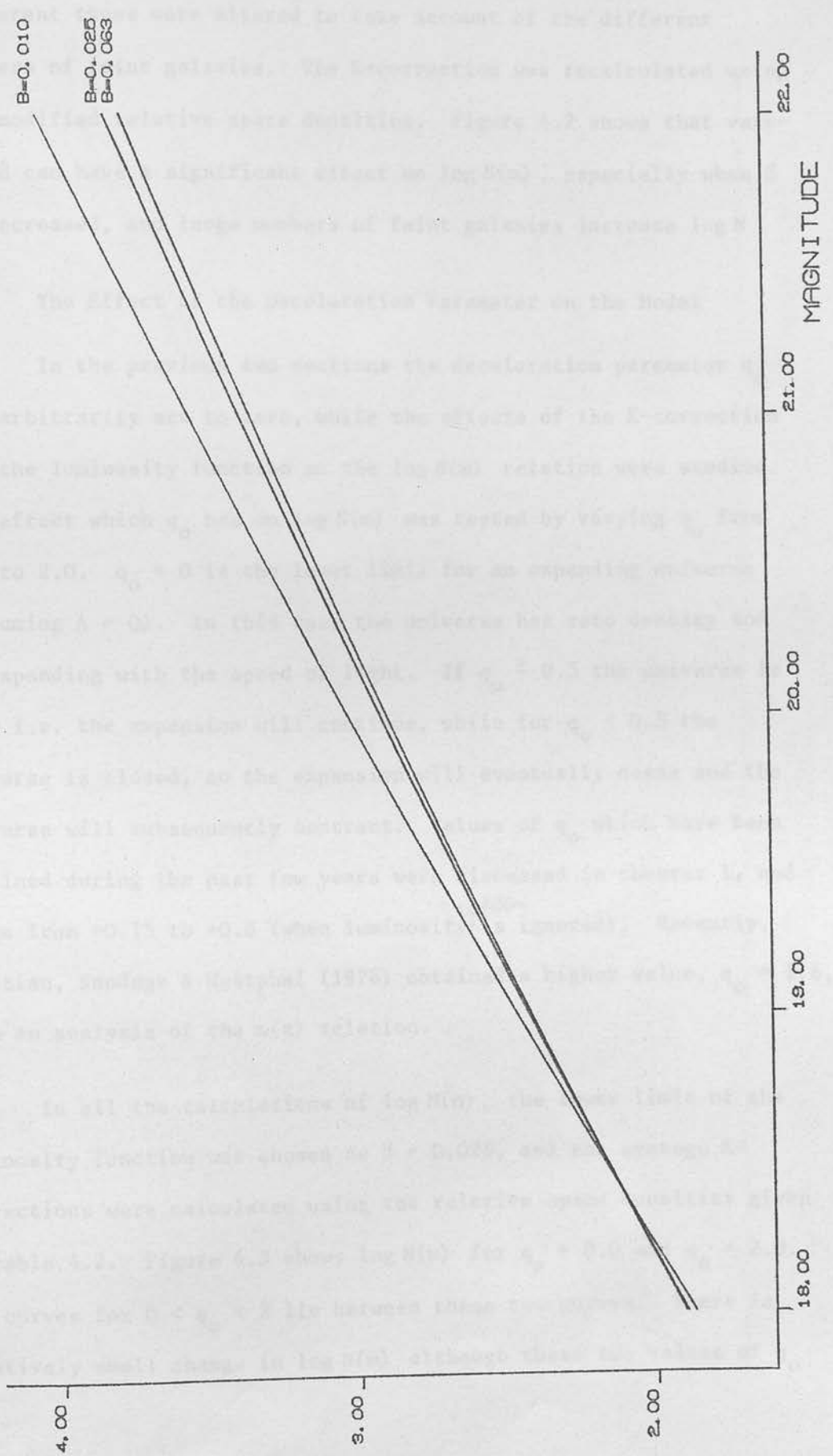

different types were altered to take account of the different numbers of faint galaxies. The K-correction was recalculated using the modified relative space densities. Figure 4.2 shows that varying β can have a significant effect on $\log N(m)$, especially when β is decreased, and large numbers of faint galaxies increase $\log N$.

4.4 The Effect of the Deceleration Parameter on the Model

In the previous two sections the deceleration parameter q_o was arbitrarily set to zero, while the effects of the K-correction and the luminosity function on the $\log N(m)$ relation were studied. The effect which q_o has on $\log N(m)$ was tested by varying q_o from 0.0 to 2.0. $q_o = 0$ is the lower limit for an expanding universe (assuming $\Lambda = 0$). In this case the universe has zero density and is expanding with the speed of light. If $q_o \geq 0.5$ the universe is open i.e. the expansion will continue, while for $q_o < 0.5$ the universe is closed, so the expansion will eventually cease and the universe will subsequently contract. Values of q_o which have been obtained during the past few years were discussed in chapter 1, and range from -0.15 to +0.8 (when luminosity evolution is ignored). Recently, Kristian, Sandage & Westphal (1978) obtained a higher value, $q_o = 1.6$, from an analysis of the m(z) relation.

In all the calculations of $\log N(m)$, the lower limit of the luminosity function was chosen as $\beta = 0.025$, and the average K-corrections were calculated using the relative space densities given in table 4.2. Figure 4.3 shows $\log N(m)$ for $q_o = 0.0$ and $q_o = 2.0$. The curves for $0 < q_o < 2$ lie between these two curves. There is relatively small change in $\log N(m)$ although these two values of q_o

FIGURE 4.3
THE LOG N (M) RELATION FOR DIFFERENT VALUES OF THE DECELERATION PARAMETER

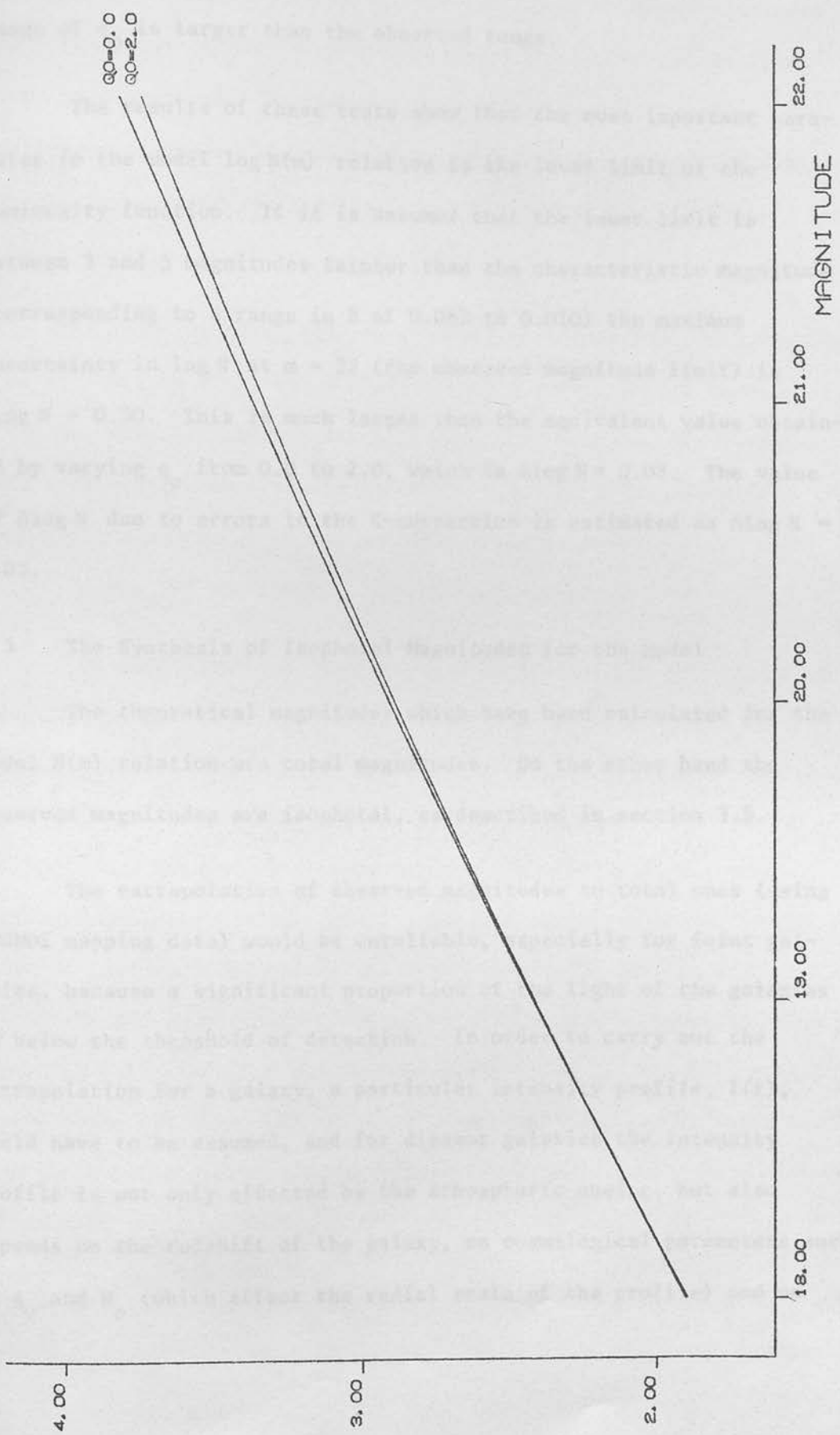

represent completely different models of the universe, and this range of q_o is larger than the observed range.

The results of these tests show that the most important parameter in the model log N(m) relation is the lower limit of the luminosity function. If it is assumed that the lower limit is between 3 and 5 magnitudes fainter than the characteristic magnitude (corresponding to a range in β of 0.063 to 0.010) the maximum uncertainty in log N at m = 22 (the observed magnitude limit) is $\Delta \log N = 0.30$. This is much larger than the equivalent value obtained by varying q_o from 0.0 to 2.0, which is $\Delta \log N = 0.08$. The value of $\Delta \log N$ due to errors in the K-correction is estimated as $\Delta \log N = 0.03$.

4.5 The Synthesis of Isophotal Magnitudes for the Model

The theoretical magnitudes which have been calculated for the model N(m) relation are total magnitudes. On the other hand the observed magnitudes are isophotal, as described in section 3.5.

The extrapolation of observed magnitudes to total ones (using COSMOS mapping data) would be unreliable, especially for faint galaxies, because a significant proportion of the light of the galaxies is below the threshold of detection. In order to carry out the extrapolation for a galaxy, a particular intensity profile, I(r), would have to be assumed, and for distant galaxies the intensity profile is not only affected by the atmospheric seeing, but also depends on the redshift of the galaxy, on cosmological parameters such as q_o and H_o (which affect the radial scale of the profile) and on

luminosity evolution. Since neither the redshift nor the distance of a galaxy is known, the true profile cannot be determined from Schmidt plate data. Furthermore, the profiles of galaxies at different distances are affected to different degrees by the seeing, so the correction from isophotal to total magnitude is different for each galaxy.

Instead of attempting to extrapolate the observed magnitudes, the theoretical N(m) relation was computed for isophotal magnitudes. This was done by assuming standard intensity profiles for galaxies and synthesising what should be observed for each field studied, using the atmospheric seeing spread function, determined for each plate below, and the limiting isophotes found in section 3.5.

De Vaucouleurs' formulae were used to describe the intensity profiles of galaxies. These two formulae have already been given in section 1.1. The profile for elliptical galaxies can be described by the $\exp(-r^{\frac{1}{4}})$ formula, and that for late-type spirals (from Scd onwards) and irregulars follows the $\exp(-r)$ law. Early-type spiral galaxies consist of a spheroidal component, with a profile similar to that of elliptical galaxies, and a disk component with an exponential profile. The importance of the spheroidal component decreases from Sa to Sc galaxies. The calculations were performed for five galaxy types E-S0, Sab, Sbc, Scd and Sdm-Im corresponding to the types used for the K-corrections. It was assumed that the galaxies were circular (face-on).

There are two free parameters in these formulae: the effective radius r_e, which is the radius containing half of the total luminosity

of the galaxy, and the effective intensity μ_e (in mag arcsec^{-2}), which is the intensity at this radius. The correlation between the effective radius and the absolute magnitude of elliptical galaxies has been studied by Strom & Strom (1978). They found that the more luminous galaxies have larger effective radii and lower effective intensities. Also, however, elliptical galaxies in regions of high galaxy density (i.e. near the centres of rich clusters) tend to have smaller effective radii than those in regions of lower galaxy density. This is supposed to be due to tidal stripping in the high density regions. The three clusters studied by Strom & Strom were the Coma cluster, Abell 426 (the Perseus cluster) and Abell 1367. Abell 1367 is a spiral rich cluster which has a lower galaxy density than the other two clusters. The results for this cluster were used in the computations because they are more suitable for the fields studied which contain both field and cluster galaxies. This relationship is:

$$\log r_e = -1.95 - 0.2654\, M_V$$

for r_e in pc, assuming $H_o = 50$ km s^{-1}Mpc^{-1}. M_V is the absolute magnitude in the V band. If the absolute magnitudes are expressed in the j magnitude system the formula becomes:

$$\log r_e = -1.76 - 0.2654\, M_j$$

If the absolute magnitude of a galaxy is specified in the model, the effective radius can be calculated from the above formula, and the effective intensity can be determined from the total luminosity and the effective radius using equation (1.1) in section 1.1. This formula was also used for the spheroidal component of spiral galaxies.

Freeman (1970) fitted exponential curves to the disks of spiral galaxies and determined the central surface brightness of the disks by extrapolation. The majority of galaxies studied had the same central surface brightness of 21.65 mag arcsec^{-2}. This discovery was investigated by Disney (1976) and Kormendy (1978). As mentioned in section 3.8, Disney suggested that the constant central surface brightness was a result of selecting galaxies with the largest apparent diameters in any magnitude interval. Kormendy criticised the method used by Freeman, who fitted the exponential to the galaxy profile as it was observed. At large radii the $\exp(-r^{\frac{1}{4}})$ formula is similar to the $\exp(-r)$ formula, and the exponential curves determined by Freeman included a contribution from the spheroidal component. Kormendy showed that the constant central surface brightness found by Freeman is largely due to the spheroidal component of the galaxies, and that real disks can be much fainter. In most of the present calculations the central surface brightness for the disk component was set to 21.64 mag arcsec^{-2}, giving an effective intensity of μ_e = 23.47 mag arcsec^{-2}. (The small difference between the B and the j magnitude systems was ignored here.) However, in case Freeman's result is not valid, different values for the central surface brightness were also tried.

De Vaucouleurs (1958a) found that the contribution of the spheroidal component to the total luminosity is 76% for M31, an Sab galaxy. For M33 and NGC300 (both type Scd) the exponential component accounts for 80 to 90% of the total luminosity, while in the Large and Small Magellanic Clouds (types Sm and Im respectively) the exponential

component makes up almost 100% of the luminosity. In the computer models the ratio of the luminosity in the spheroidal component to that in the disk was set to 3:1 for Sab, 1:1 for Sbc and 1:3 for Scd.

The galaxy profiles were convoluted with the seeing spread function which was determined from star profiles. Brown (1974) showed that stellar intensity profiles can be represented by the sum of several gaussians in the form:

$$I(r) = k_1 e^{\frac{-r^2}{a_1^2}} + k_2 e^{\frac{-r^2}{a_2^2}} + k_3 e^{\frac{-r^2}{a_3^2}}$$

where k_1, k_2, k_3 and a_1, a_2 and a_3 are constants. He found that the ratios $a_1:a_2$ and $a_2:a_3$ were both approximately equal to 3, and that the constants k_2 and k_3 were approximately equal. The contribution to the total luminosity from each gaussian was set to 86.2%, 6.9% and 6.9% respectively.

A formula of this type was tested on the star profiles from Schmidt plates. The star transmission profiles were first deconvoluted for the COSMOS spot, since the galaxy magnitudes had been determined from deconvoluted transmissions. It was found that the stellar intensity profiles could be described by two gaussians, contributing equally to the total luminosity with one gaussian about 10 times the width of the other, i.e.

$$I(r) = k \left(e^{\frac{-r^2}{b^2}} + 0.1\, e^{\frac{-r^2}{10b^2}} \right).$$

(If there is a third gaussian in the profile, its contribution to the

total luminosity must be very small, and it can be ignored.) The constant b was determined by the least squares method from several star profiles on each plate. For plate 1920 b = 1.213 arcsec, and for plate 1915 b = 1.356 arcsec. The constant k depends on the stellar luminosity, but for convolution the spread function should be normalised, so k was chosen to give a total luminosity of unity.

The differences between isophotal and total magnitudes of the model galaxies were calculated as a function of redshift using Friedman cosmology. It was assumed that the de Vaucouleurs formulae for the profiles held for redshifted galaxies. This assumption may not be valid, because the light observed for redshifted galaxies was emitted at shorter wavelengths and different parts of a galaxy may have different spectra. This is most likely to affect spiral galaxies where the disk is bluer than the nucleus.

Because surface brightness decreases with $(1 + z)^4$, the effective intensity of a galaxy at redshift z becomes:

$$\mu_e(z) = \mu_e(0) + 10 \log (1 + z) + K(z)$$

where K(z) is the K-correction and $\mu_e(0)$ is the effective intensity at zero redshift. The effective radius (in seconds of arc) of a galaxy at redshift z is:

$$\theta_{eff}(z) = \frac{r_{eff}(1 + z)}{R_o \, \sigma(u)}$$

The factor (1 + z) is due to the expansion of the universe. $R_o \, \sigma(u)$ is the distance of the galaxy, R_o describing the present distance

scale of the universe, and u being the metric distance (dimensionless) travelled by light from the galaxy.

$$\sigma(u) = \sin u \quad \text{if the universe is closed}$$
$$= u \quad \text{if the universe is open and Euclidean}$$
$$= \sinh u \quad \text{if the universe is open and hyperbolic.}$$

$R_o\,\sigma(u)$ can be expressed in terms of z, q_o and H_o. The formula is given in equation A1.11 of Appendix I.

The galaxy profiles were convoluted ~~for~~ with the atmospheric seeing function, and integrated within the limiting isophote. The differences between the isophotal and total magnitudes were then calculated. Figures 4.4 and 4.5 show the magnitude differences for E-S0 and Sdm-Im galaxies of different absolute magnitudes, using the limiting isophote and seeing spread function for field I. The Hubble constant was taken as $H_o = 50$ km $s^{-1}Mpc^{-1}$, and the deceleration parameter as $q_o = 0$. Each curve stops when the galaxy becomes too faint, or has too low a surface brightness to be detected by COSMOS on the Schmidt plates. On the whole, the results for Sab, Sbc, and Scd galaxies lay between those for E-S0 and Sdm-Im galaxies, although some of the magnitude differences for Scd galaxies were slightly lower than those for Sdm-Im galaxies.

The results for field III were identical to those for field I, since the broader seeing profile compensated for the lower limiting isophote. For field II, the magnitude differences were slightly smaller because the width of the seeing profile was the same as that for field I but the limiting isophote was lower.

FIGURE 4.4 ISOPHOTAL MINUS TOTAL MAGNITUDE VS. REDSHIFT FOR E GALAXIES.

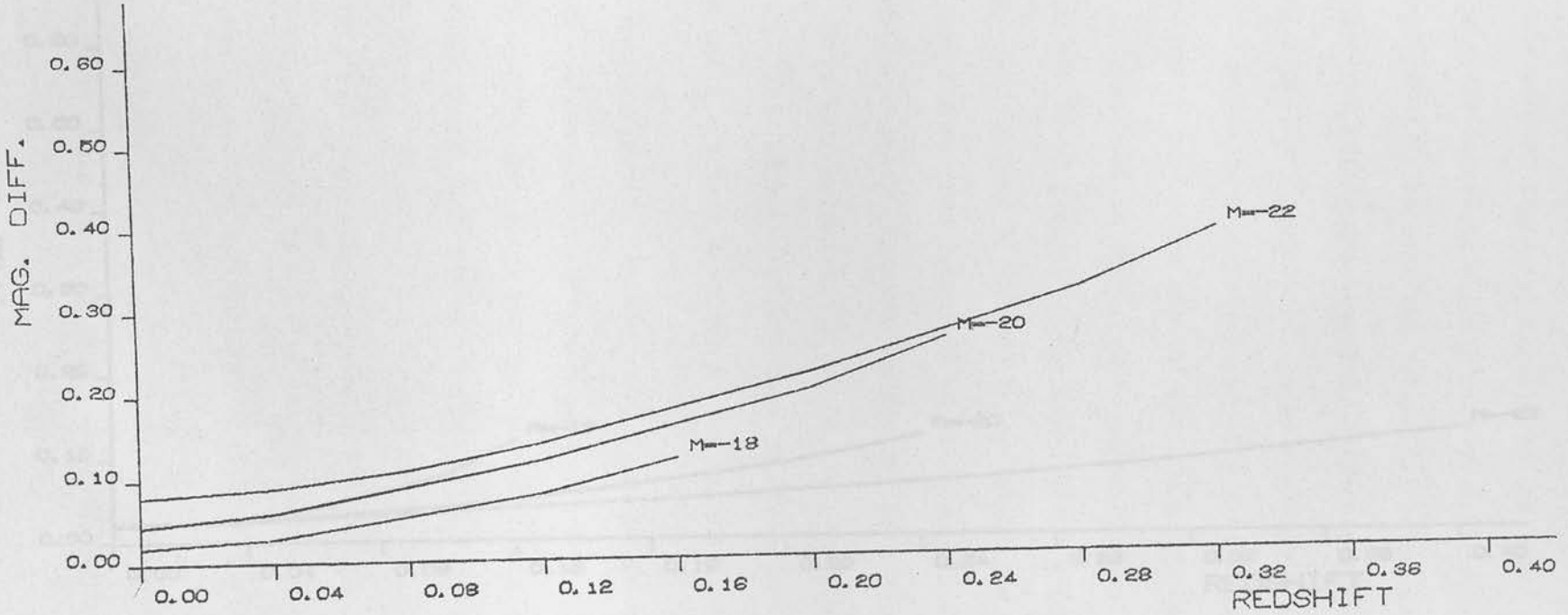

FIGURE 4.5 ISOPHOTAL MINUS TOTAL MAGNITUDE VS. REDSHIFT FOR SDM GALAXIES.

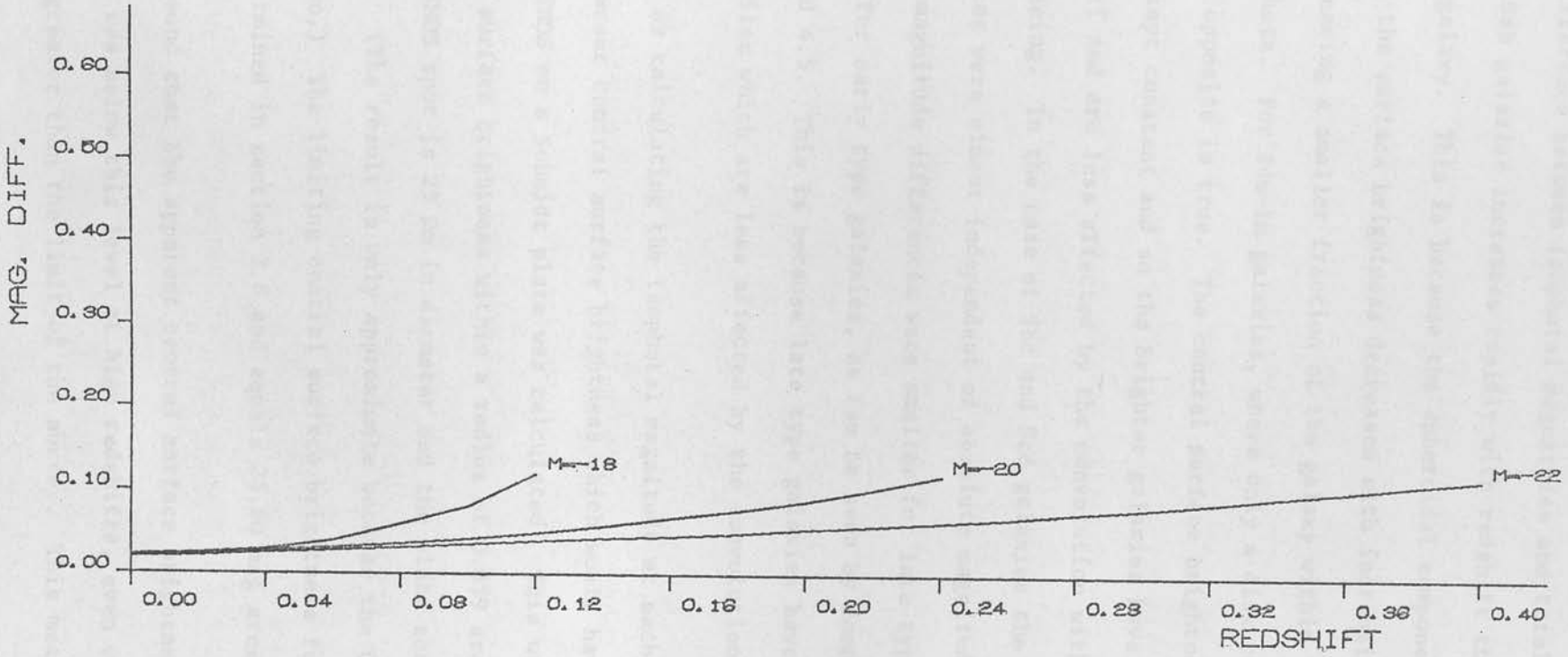

The difference between isophotal magnitudes and total ones for E-S0 and Sab galaxies increases rapidly with redshift the more luminous the galaxy. This is because the spheroidal component dominates and the surface brightness decreases with increasing luminosity, leaving a smaller fraction of the galaxy within the limiting isophote. For Sdm-Im galaxies, where only a disk component was used, the opposite is true. The central surface brightness of the disk was kept constant and so the brighter galaxies have larger effective radii and are less affected by the convolution with the atmospheric seeing. In the case of Sbc and Scd galaxies the magnitude differences were almost independent of absolute magnitude. On the whole the magnitude differences were smaller for late type galaxies than for early type galaxies, as can be seen by comparing figures 4.4 and 4.5. This is because late type galaxies have shallower profiles which are less affected by the convolution.

As well as calculating the isophotal magnitude at each redshift, the apparent central surface brightness which would have been detected by COSMOS on a Schmidt plate was calculated. This was taken as the average surface brightness within a radius of 0.839 arcsec, because the COSMOS spot is 25 μm in diameter and the plate scale is 67.2 arcsec/mm. (The result is only approximate because the COSMOS spot is gaussian.) The limiting central surface brightness for the survey was determined in section 3.8 and equals 24.80 mag arcsec^{-2}.

It was found that the apparent central surface brightness of Sdm-Im galaxies was below this level at high redshifts, even when the luminosity was greater than the limit of the survey. This means that

in surveys such as the present one, distant late-type galaxies may not be detected, although they are within the magnitude limit. The redshift limit for detecting an Sdm-Im galaxy depends on the absolute magnitude, and is shown in figure 4.6. This effect did not occur for the other types of galaxy which had spheroidal components. However, the results for spirals with combined profiles may not be accurate. Firstly, the spheroidal component is redder than the disk, and so the spheroid will become fainter relative to the disk as the redshift increases, and the central surface brightness will be decreased. Because of this, other types of spiral galaxies may not be detected. Also, the use of Strom & Strom's relationship between absolute magnitude and effective radius may not be valid for the spheroidal component of spiral galaxies. This relationship gives rise to very bright nuclei in the model spiral galaxies.

Because of the uncertainty in some of the parameters used, the calculations were repeated using different values. The intrinsic central surface brightness of the Sdm-Im galaxies was varied by half a magnitude on either side of the average value of S = 21.65 mag arcsec^{-2} found by Freeman. The resulting magnitude differences were altered by only a few hundredths of a magnitude. However, the largest redshift at which a galaxy can be detected was changed. For example, if the central surface brightness is S = 21.65 mag arcsec^{-2}, a galaxy of M = -22 can be detected at z = 0.40, while if S = 21.15 mag arcsec^{-2}, the limiting redshift is z = 0.50, and if S = 22.15, z = 0.30.

Increasing the deceleration parameter had very little effect on

FIGURE 4.6
LIMITING REDSHIFT VS. ABSOLUTE MAGNITUDE FOR SDM-IM GALAXIES

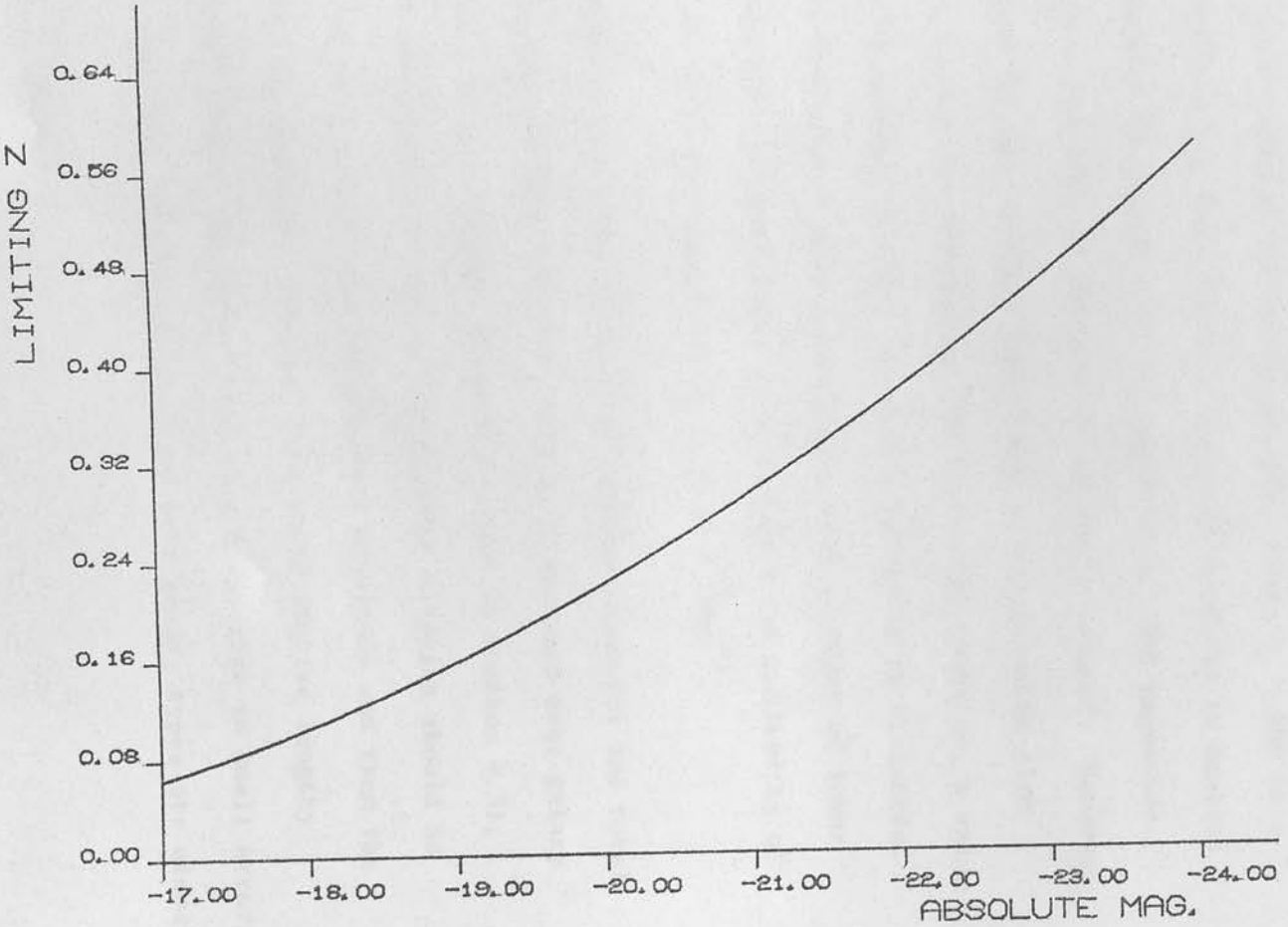

the results. This is because a galaxy at a given redshift is nearer if q_o is larger. The effective radius will be larger and so both the total and isophotal luminosities will be greater. Therefore the difference between isophotal and total magnitudes is hardly changed.

Since the relationship between the effective radius and the absolute magnitude for elliptical galaxies depends on the Hubble constant, the results for E-S0 galaxies are independent of H_o. The calculations were repeated for Sdm-Im galaxies using H_o = 100 km s^{-1} Mpc^{-1}. By doubling H_o, the effective radius of a galaxy is doubled and the luminosity is increased by 1.5 magnitudes. The magnitude differences as a function of redshift are slightly reduced. However, the values used for the absolute magnitudes of the galaxies also depend on H_o, because in determining the luminosity function, a value of H_o has to be assumed in order to convert redshifts to distances. The magnitude differences were recalculated with galaxies of lower absolute luminosity and were found to be within a few hundredths of a magnitude of those determined for H_o = 50 km s^{-1} Mpc^{-1}.

In order to apply the differences between isophotal and total magnitudes to the log N(m) relation, they were averaged over galaxy type, (weighted by the relative frequencies used in section 4.3), and absolute magnitude. In theory the log N(m) relation should be calculated for each galaxy type and absolute magnitude and then the results should be combined. However, this would involve lengthy computer calculations. The method used only gives rise to small errors, because the magnitude differences averaged over galaxy types are almost

independent of absolute magnitude, due to the fact that early and late type galaxies are affected in opposite ways.

As mentioned above, the magnitude differences for Sab, Sbc and Scd galaxies which have combined profiles may be unreliable and in fact were probably underestimated. Instead of using the calculated values, it was assumed that the magnitude differences for Sab, Sbc and Scd galaxies lay a quarter, a half and three-quarters respectively between those for E-S0 and Sdm-Im galaxies. (The reason for using these ratios was that the profiles for these galaxy types were interpolated from the profiles of E-S0 and Scd-Im galaxies using these ratios.)

A second order polynomial was fitted through the average magnitude differences, giving:

$$\Delta m = 0.027 + 0.083\ z + 1.721\ z^2 \quad \text{for fields I and III}$$

and $$\Delta m = 0.019 + 0.016\ z + 1.387\ z^2 \quad \text{for field II.}$$

These differences were added to the magnitudes calculated using the m(z) relation, at the same time as the K-correction.

The calculation of $\log N(m)$ was also modified to take account of the fact that some galaxies may not be detected because of their low surface brightness. The relationship between absolute magnitude and limiting redshift for Sdm-Im galaxies shown in figure 4.6 was used, and it was assumed that 43% of the galaxies were in the Sdm-Im class. (See table 4.2).

Instead of calculating $\log N(m)$ for one absolute magnitude and

convoluting it with the luminosity function as was done previously, the frequency distribution F(m) was calculated at redshift intervals of 0.005. F(m) was derived from the m(z) relation, the luminosity function, and the volume of space between redshifts z - 0.005 and z. At each redshift the luminosity function was modified for galaxies fainter than the limiting absolute magnitude for Sdm-Im galaxies. The distributions were combined to give the log N(m) relation, and the results were scaled to fit the observations at the bright end. This method is equivalent to the previous method when it is assumed that all galaxies are detected. The only disadvantage of this method is that the resulting curve contains a series of bumps due to the sharp cut-off at the faint end of the luminosity function. To overcome this problem the luminosity function was tapered at the faint end by reducing the last three values.

Figures 4.7a, b and c show the observed log N(m) relation and three theoretical models. The curve labelled A is log N(m) for total magnitudes (the original model), curve B is log N(m) for isophotal magnitudes, and curve C is log N(m) for isophotal magnitudes altered to take account of the failure to detect low surface brightness galaxies as described above.

All the theoretical curves were derived for $q_o = 0$. The effect of increasing q_o is to lower the values of log N(m) at faint magnitudes (see figure 4.3). The observed curves were corrected for faint stars using the visual method described in section 3.4.

F(m) for theoretical model C shows a decrease in the numbers of faint

FIGURE 4.7A THE LOG N(M) RELATION,
PLATE 1920 FIELD I.

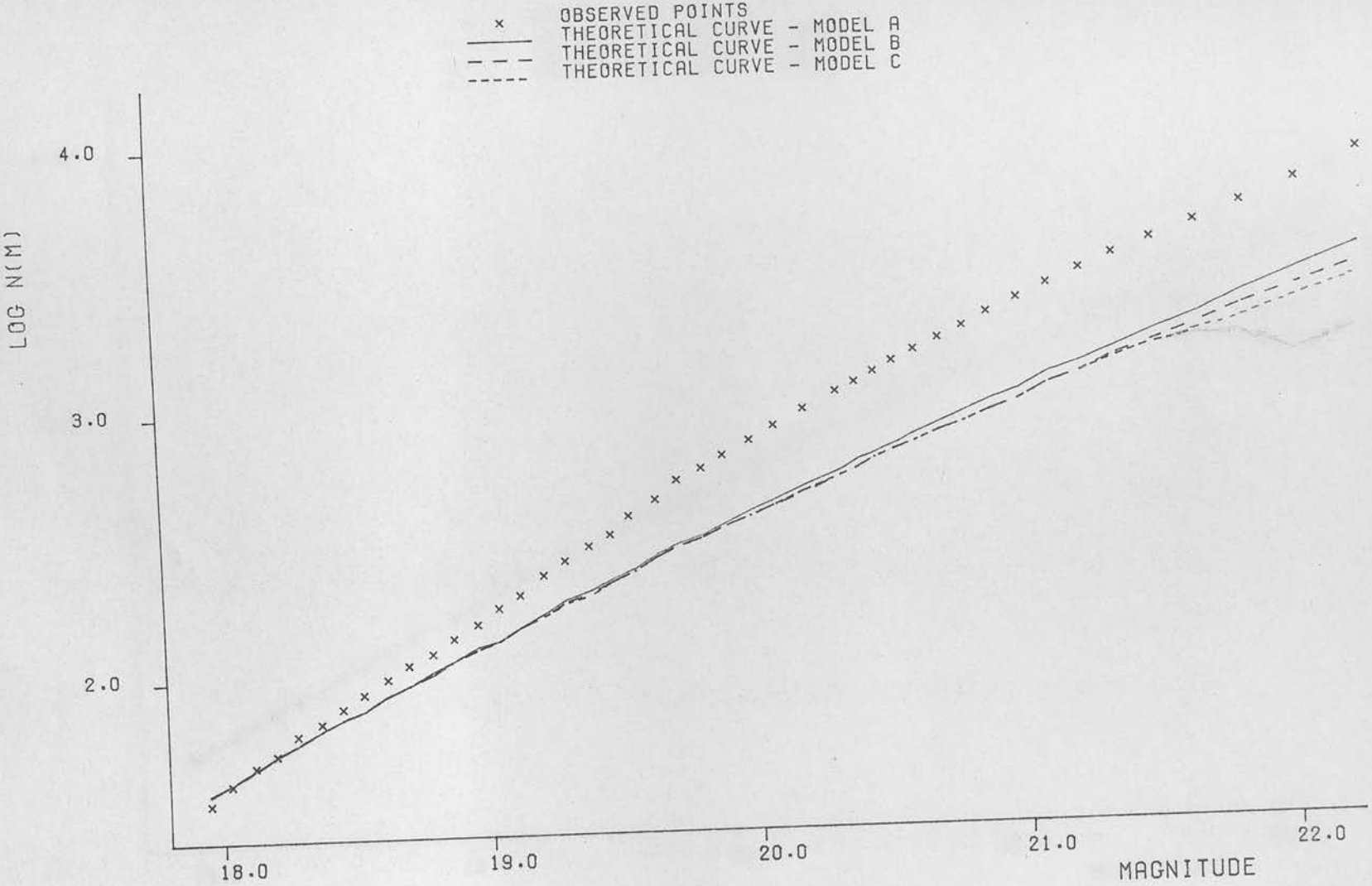

FIGURE 4.7B THE LOG N(M) RELATION,
PLATE 1920 FIELD II.

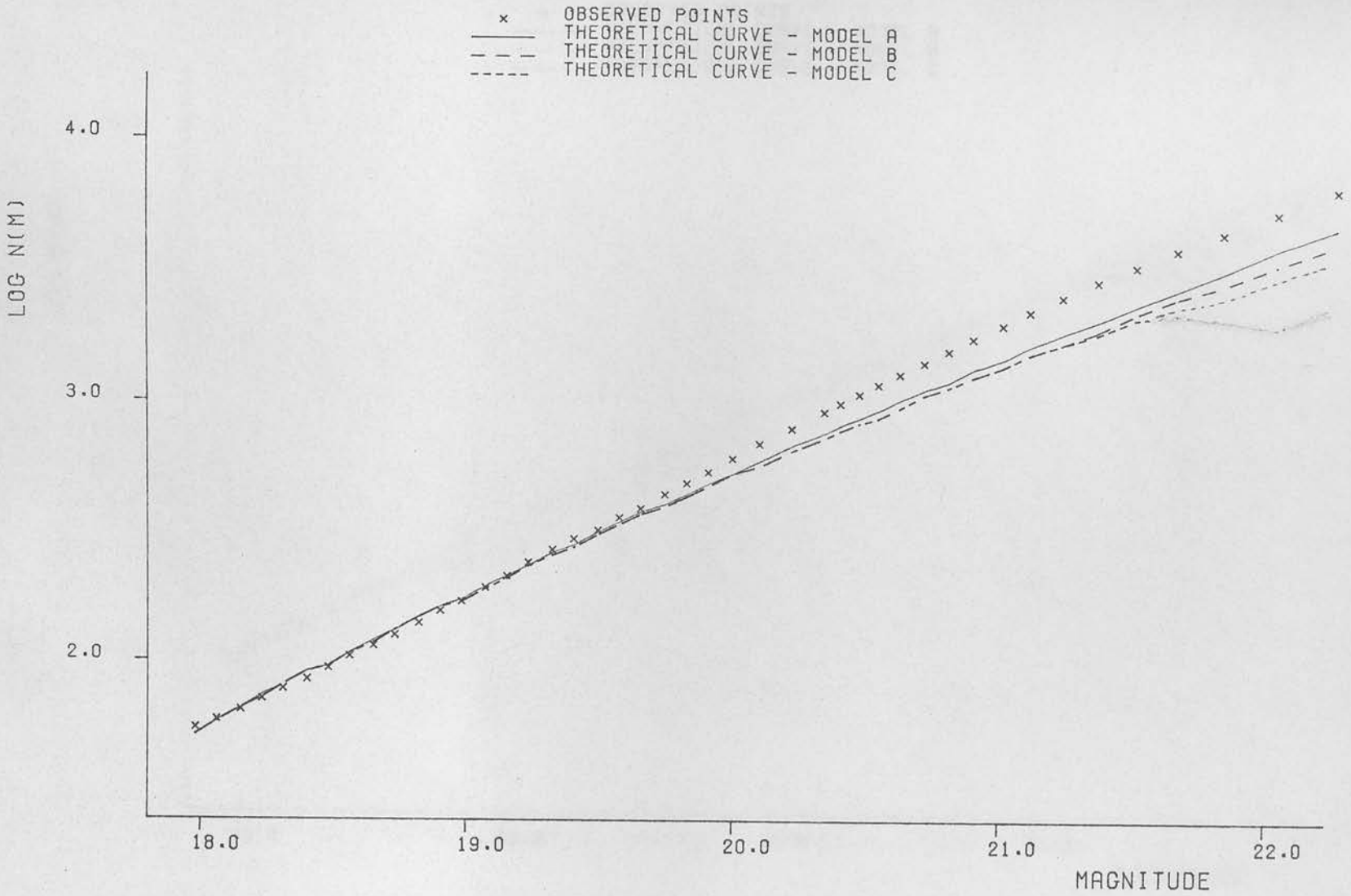

FIGURE 4.7C THE LOG N(M) RELATION,
PLATE 1915 FIELD III.

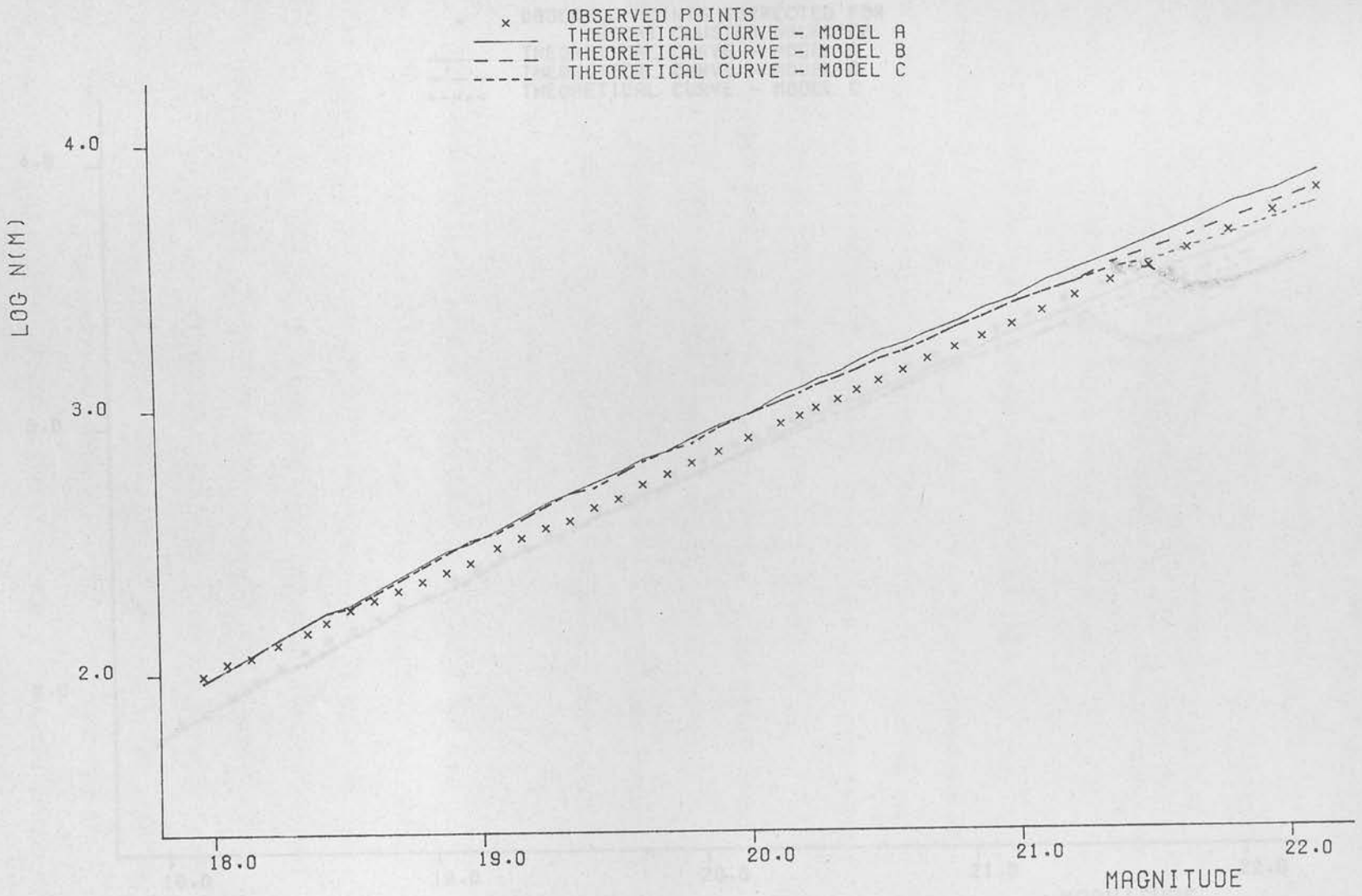

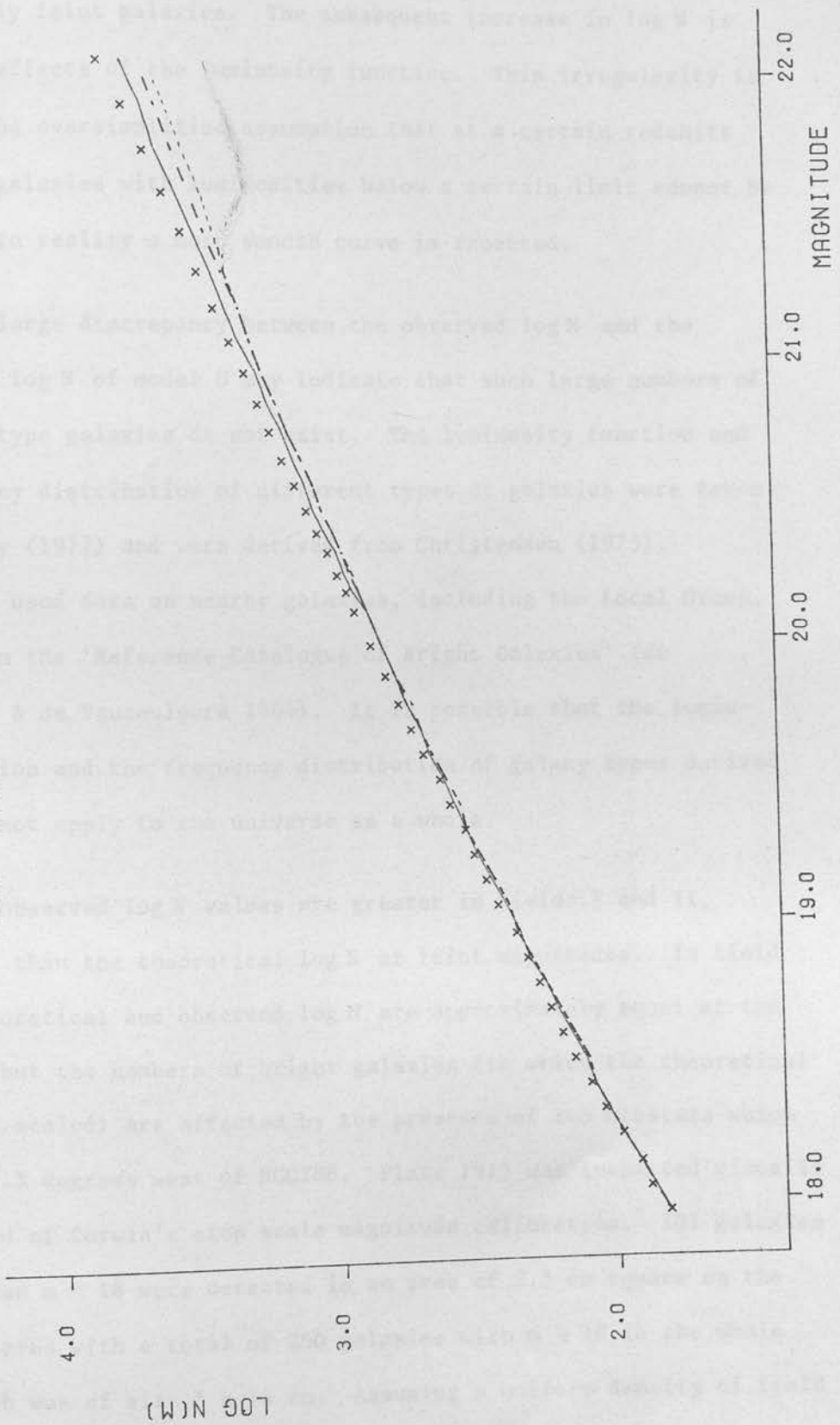

FIGURE 4.7D THE LOG N(M) RELATION, PLATE 1915 FIELD III, CORRECTED FOR BRIGHT CLUSTER GALAXIES.

galaxies at m $\sim$ 22. It is caused mainly by the rejection of nearby intrinsically faint galaxies. The subsequent increase in log N is due to the effects of the luminosity function. This irregularity is caused by the oversimplified assumption that at a certain redshift all Sdm-Im galaxies with luminosities below a certain limit cannot be detected. In reality a more smooth curve is expected.

The large discrepancy between the observed log N and the theoretical log N of model C may indicate that such large numbers of faint late type galaxies do not exist. The luminosity function and the frequency distribution of different types of galaxies were taken from Tinsley (1977) and were derived from Christensen (1975). Christensen used data on nearby galaxies, including the Local Group, published in the 'Reference Catalogue of Bright Galaxies' (de Vaucouleurs & de Vaucouleurs 1964). It is possible that the luminosity function and the frequency distribution of galaxy types derived locally do not apply to the universe as a whole.

The observed log N values are greater in fields I and II, plate 1920, than the theoretical log N at faint magnitudes. In field III the theoretical and observed log N are approximately equal at the faint end, but the numbers of bright galaxies (to which the theoretical results are scaled) are affected by the presence of two clusters which lie about 1.5 degrees west of NGC288. Plate 1915 was inspected visually with the aid of Corwin's step scale magnitude calibration. 101 galaxies brighter than m = 18 were detected in an area of 2.5 cm square on the plate, compared with a total of 260 galaxies with m < 18 in the whole field, which was of size 5 x 15 cm. Assuming a uniform density of field

galaxies, there should be 14.45 galaxies in the area covered by the clusters. This gives an excess of 86.55 due to the clusters, or an excess of 32.9 galaxies per square degree on the N(m) relation. Figure 4.7d shows the log N(m) relation for field III corrected for the cluster galaxies. When the theoretical models were scaled to fit the corrected observations at the bright end, there is an excess of observed galaxies over the theoretical numbers at the faint end, as in fields I and II.

The remaining differences in log N(m) for the three fields are probably due to clustering or superclustering. Patchy galactic extinction can be ruled out because this would affect all the galaxies in one field in the same way. Field I, however, has the lowest number density of bright galaxies and the highest number density of faint galaxies. It is possible that the differences in the log N(m) relation for faint galaxies could be caused by irregular extragalactic extinction.

The discrepancy between the observed numbers and the theoretical ones can be interpreted in several different ways. Firstly, galaxy evolution has so far been ignored. If it is assumed that galaxies were brighter in the past, they should be detected at higher redshifts. This means that a larger volume of space is being sampled, which will increase the counts of galaxies at faint magnitudes.

Another explanation could be that larger numbers of intrinsically faint galaxies have been detected. It is generally assumed that low luminosity galaxies are not detected on account of their low

surface brightness (e.g. Pence 1976). However, figure 4.2 shows that lowering the faint limit of the luminosity function has quite a large effect. The theoretical values could be increased at the faint end by decreasing the lower limit in model A from $4^m.0$ below the characteristic magnitude M^* to $4^m.5$ or $5^m.0$ below M^*.

The log N(m) relation would also be increased at the faint end if q_o were negative. For 'big bang' models with the cosmological constant $\Lambda = 0$, the lower limit for q_o is zero, in which case the universe has zero density and expands with the speed of light. For steady state theory $q_o = -1$. Evolving models with negative q_o are permissible if Λ which measures the intrinsic curvature of the universe is positive (Gunn & Tinsley 1975). Since many astronomers have obtained positive values of q_o using different techniques, this is an unlikely explanation for the large log N values observed at faint magnitudes.

Finally, there could be a higher number density of distant galaxies in the direction observed due to superclustering. The log F(m) relation for galaxies (figures 3.10a, b and c) gives no indication of an increase in the number density at a particular distance. Variations of this kind may be smoothed out by the luminosity function, but this could indicate that there are very large scale inhomogeneities in the universe. If this is the case, standard Friedman cosmology no longer applies; the universe does not have a uniform curvature and the observed value of q_o will depend on direction. Because of the problems of constructing models with large scale variations in the number density of galaxies, the consequences of an inhomogeneous universe were not pursued further.

4.6 Luminosity Evolution

There is much evidence indicating that galaxies were brighter in the past. Schmidt (1963) showed that in order to explain the present day luminosity function in the solar neighbourhood, the rate of formation of stars of one solar mass must have been three times greater in the past. He also showed by studying the distribution of ultraviolet excess in G stars that relatively more bright stars were formed in the past.

Many astronomers have investigated the time variation in the rate of star formation and the stellar mass function required to produce the present day properties of galaxies, such as the colour, the mass-luminosity ratio, the ratio of the mass of gas to the mass of stars and the heavy element abundance.

Larson & Tinsley (1974) suggested that there was an initial burst of star formation in elliptical galaxies producing a variation in the absolute magnitude with time of

$$\frac{dM_v}{d\ln t} = 0.87$$

For spiral galaxies they found that a more continuous rate of star formation is required to fit the present observed proerties.

Reddish (1975) investigated the rate of star formation assuming that stars form when clouds fragment due to the condensation of hydrogen molecules on interstellar grains. The rate of star formation depends on the temperature of the grains. Reddish's calculations show that initially supermassive objects ($M \sim 10^{10} M_\odot$) form. In this

model the temperature of the grains in the proto-galactic cloud determines whether an elliptical or a spiral galaxy forms. The cooler the grains, the more the star formation overshoots producing a higher bulge:disk ratio.

Tinsley (1977) calculated log N(m) using Friedman cosmology and models for galaxy evolution and compared the numbers with those for a static Euclidean universe, i.e.

$$\log N_o = 0.6\ m + \text{const.}$$

Without evolution a graph of log (N/N_o) decreases towards faint magnitudes. This is due to the fact that fewer photons are received in an expanding universe and that they have less energy. There is also the effect of the K-correction. When evolution is included, the graph of log (N/N_o) has a maximum at $m \sim 20$ which is produced by large numbers of luminous young galaxies with this apparent magnitude. The exact position of the maximum and its size depend on the time or redshift assumed for the formation of the galaxies, and the value of q_o. In all models, however, the counts at limiting magnitudes greater than 20 are increased by a factor of 3 or more by evolution.

The observed log N(m) in the present study shows only a slight excess of faint galaxies when compared with model galaxy counts which ignore evolution. There is no maximum at $m \sim 20$ when the results are plotted in the form of log (N/N_o) vs. m. This indicates that the large numbers of very luminous young galaxies predicted in Tinsley's model have not been detected. However, Tinsley suggested that primeval galaxies may not be as bright as expected, either due to obscuration by

dust, or due to optical thickness if z_F is large enough for wavelengths below the Lyman limit to be shifted into the observers passband ($z_F > 3$ for the j band).

The theoretical model described in sections 4.1 to 4.5 was altered to allow for a time variation in the absolute magnitude. The simple assumption was made that

$$\Delta M = -\varepsilon \times H_o \times \Delta t$$

where ΔM is the change in absolute magnitude (which was assumed to be the same for all galaxies), Δt is the light travel time from a galaxy, H_o is the Hubble constant and ε is a parameter which was varied to give the lowest standard deviation of the theoretical $\log N(m)$ from the observed values. Δt can be calculated as a function of q_o and z, and the equations are given in Appendix I, part 2.

This formula for ΔM does not agree with the formula given by Larson & Tinsley for elliptical galaxies (see above), but it is assumed that there are both spiral and elliptical galaxies amongst the distant galaxies detected, and the evolution has less effect on spiral galaxies. Also the observed log N show a much smaller excess of faint galaxies than the models produced by Tinsley (1977).

It was assumed that in the past the distribution of galaxy types was the same as in the present, i.e. all galaxies have the same ages (Sandage, Freeman & Stokes 1970), and do not evolve from one type to another. (The second assumption was made mainly for simplification.)

If the star formation rate was greater in the past, the spectra and therefore the colours of distant galaxies will differ from those of present day galaxies. In particular, distant elliptical and SO galaxies are expected to appear much bluer due to large numbers of young stars. The K-corrections for E-SO galaxies should be altered to take account of this. The effect is not important though when the calculation of log N(m) is averaged over all types of galaxy types. The average K-corrections contain a significant contribution from Scd and Sdm-Im galaxies, whose spectra are dominated by young stars and are probably similar to those of young ellipticals.

It is necessary to re-evaluate the corrections to log N(m) for isophotal magnitudes and the failure to detect low surface brightness galaxies when evolution is considered. Both these corrections depend on the profiles of the galaxies which will probably change as the galaxies evolve. It has been suggested that quasars are galaxies in the early stages of evolution (Field 1964, and other references given in section 1.6) and it is assumed that quasars appear stellar because their nuclei are very bright compared with the surrounding galaxy. If galaxies are 'quasi-stellar' in the early stages, the corrections for isophotal magnitudes and loss of low surface brightness galaxies become unnecessary.

Because of the uncertainties involved in calculating these corrections when evolution is included in the model, log N(m) was calculated as before for 3 models: A (total magnitudes), B (isophotal magnitudes) and C (isophotal magnitudes with the numbers corrected for low surface brightness galaxies).

The dimensionless evolutionary parameter ε was varied from 2 to 8 in the computer calculations, and the deceleration parameter was varied from 0 to 2.

Table 4.3 shows the values of the standard deviation of theoretical values for log N of model A from the observed values. In general the standard deviations are small indicating that the model fits the data well, although in some cases there is an excess of observed galaxies over the theoretical counts at $m \sim 20$. The value of ε giving the best fit increases from 3 at $q_o = 0$ to 6 at $q_o = 2$. This is partly because as q_o is increased the light travel time from a galaxy at redshift z decreases, and also because log N(m) increases less rapidly as q_o is increased so more evolution is required to compensate. Figure 4.8 shows the observed curve compared with the theoretical model for $\varepsilon = 5$ and $q_o = 1.5$, which gave the lowest standard deviation.

If the theoretical models B and C are used, the value of ε has to be increased. For model B the standard deviation was 0.01 for $q_o = 0$ and $\varepsilon = 5$, which represents a good fit. However, when ε was increased to determine the best fit for larger values of q_o, it was found that log N(m) increased too steeply at the bright end. When model C was used ε had to be increased to 8 in order to raise log N(m) for faint galaxies, but again this made the numbers increase too rapidly at the bright end. The reason models B and C with evolution do not fit well is either that the corrections applied in these models are not important if galaxies were brighter in the past, or that it becomes too difficult to calculate the corrections accurately when evolution is included.

TABLE 4.3

The Standard Deviation of Theoretical log N(m) from the Observations

ε \ q_o	0.0	0.5	1.0	1.5	2.0
2.5	0.028	0.045	0.061	0.083	0.210
3.0	0.023	0.027	0.044	0.068	0.090
3.5	0.041	0.018	0.028	0.054	0.078
4.0	0.071	0.031	0.015	0.039	0.066
4.5	0.107	0.054	0.021	0.024	0.053
5.0	0.146	0.081	0.039	0.010	0.041
5.5	0.192	0.108	0.059	0.012	0.030
6.0	0.239	0.136	0.080	0.026	0.021

FIGURE 4.8
THEORETICAL LOG N (M) WITH QO=1.5 AND E=5 COMPARED TO OBSERVED VALUES (CROSSES)

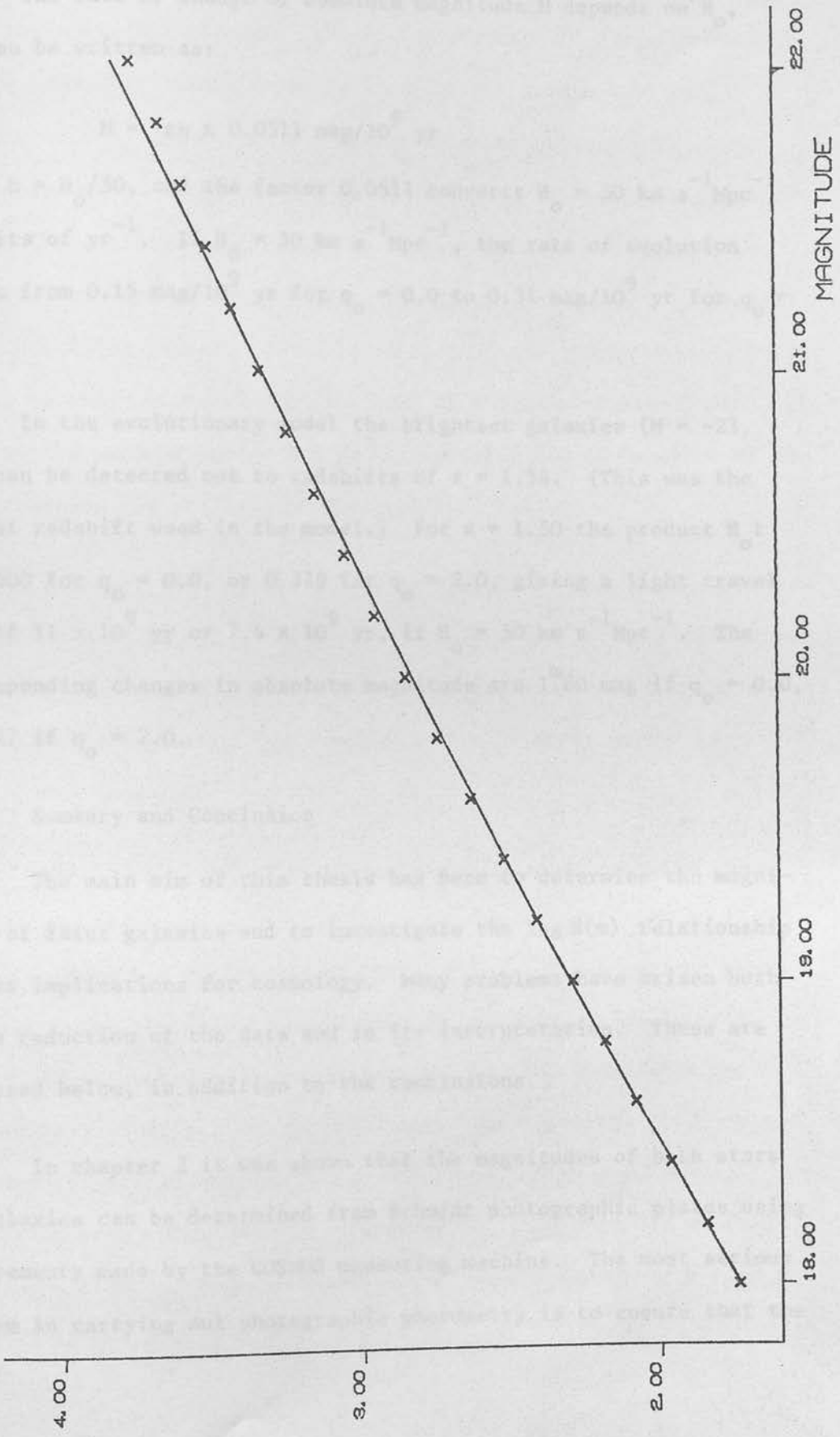

The rate of change of absolute magnitude M depends on H_o, and can be written as:

$$\dot{M} = \varepsilon h \times 0.0511 \text{ mag}/10^9 \text{ yr}$$

where $h = H_o/50$, and the factor 0.0511 converts $H_o = 50$ km $s^{-1}Mpc^{-1}$ to units of yr^{-1}. If $H_o = 50$ km $s^{-1}Mpc^{-1}$, the rate of evolution varies from 0.15 mag/10^9 yr for $q_o = 0.0$ to 0.31 mag/10^9 yr for $q_o = 2.0$.

In the evolutionary model the brightest galaxies (M = -23, -24) can be detected out to redshifts of z = 1.56. (This was the largest redshift used in the model.) For z = 1.50 the product $H_o t$ is 0.600 for $q_o = 0.0$, or 0.379 for $q_o = 2.0$, giving a light travel time of 11 x 10^9 yr or 7.4 x 10^9 yr, if $H_o = 50$ km $s^{-1}Mpc^{-1}$. The corresponding changes in absolute magnitude are $1^m.80$ mag if $q_o = 0.0$, or $2^m.27$ if $q_o = 2.0$.

4.7 Summary and Conclusion

The main aim of this thesis has been to determine the magnitudes of faint galaxies and to investigate the log N(m) relationship and its implications for cosmology. Many problems have arisen both in the reduction of the data and in its interpretation. These are discussed below, in addition to the conclusions.

In chapter 2 it was shown that the magnitudes of both stars and galaxies can be determined from Schmidt photographic plates using measurements made by the COSMOS measuring machine. The most serious problem in carrying out photographic photometry is to ensure that the

beam of light in the microdensitometer is very small ($\sim$ 8 μm) and that there is no scattered light in the system. If these conditions do not hold, the transmission profiles of the images will be convoluted and, due to the non-linear relation between photographic transmission and the intensity of light in the telescope image incident on the emulsion, there will be scale errors in the magnitudes. Because the slope of the intensity vs. transmission curve increases with increasing intensity, the luminosity of the bright objects will always be underestimated. At the time of measurement, the COSMOS spot was 25 μm in diameter and so this problem had to be overcome by deconvoluting the profiles of the images.

The root mean square errors in the magnitudes of the galaxies range from 0.08 at m = 18 to 0.43 at m = 22. They are a combination of errors in the COSMOS measurements, the graininess of the emulsion and calibration errors. The largest source of error is the graininess of the emulsion.

The log N(m) relation was determined for galaxies in three fields near the south galactic pole, covering a total area of 11.3 square degrees and containing 83,000 galaxies. These regions were measured using the COSMOS coarse mode of operation which detects images and outputs various parameters such as the image area and the minimum transmission level in the image. The logarithm of the image area was calibrated against galaxy magnitude, using magnitudes calculated from COSMOS mapping measurements. The accuracy of the magnitudes from coarse measurement varies from σ = 0.07 at m = 18 to σ = 0.63 at m = 22.

The galaxies were binned according to image area or log (image area) depending on image size, and using the magnitude calibration, the frequency distribution log F(m) and the cumulative distribution log N(m) were calculated. The bright magnitude limit, at m = 18, was set because more luminous galaxies tend to be saturated. The faint magnitude limit of m = 22 corresponds to an image area of 3.468 arcsec^2 (or 3 x (16 μm)^2 on the plate). 'Images' with smaller areas were detected by COSMOS, but correlating images between plates shows that many of these were caused by grain noise.

The errors in log N(m) include errors in detecting images, errors in separating stars from galaxies, errors in log (image area) arising from COSMOS measurements and grain noise, and errors in the magnitude calibration. At bright magnitudes these errors are negligible. For the faintest galaxies, with m = 22, the combined error in log N was calculated to be ±0.04. The largest source of error at the faint end is the magnitude calibration, because of the scatter in the m vs. log A graph.

The results were compared with the log N(m) relation derived by Brown (1974). At m = 18 the two sets of data agree quite well. However the log N(m) from the present study increased more rapidly towards faint magnitudes. This could reflect a real difference in the numbers of galaxies in the northern and southern galactic hemispheres. However, it is more likely to be caused by the different techniques employed in detecting the images. Brown detected the images by eye, which probably suffers more from selection effects than detection by a machine such as COSMOS. The limiting magnitude of Brown's survey was m = 21.

The differences in the log N(m) relation for the three fields may be attributed to the effects of clustering. There are two nearby clusters of galaxies in field III, which produce an excess of galaxies with $m < 18$. This excess was removed by visual inspection of the plate. MacGillivray & Dodd (1978) noticed that the number of faint galaxies in field I is greater than the number in field II, and interpreted this as being due to superclustering. The number of faint galaxies in field III was intermediate. In the later stages of the data analysis the mean log N(m) relation was calculated to average out the effects of clustering and superclustering.

In order to analyse the results several assumptions have to be made. In cosmology it is usually assumed that the universe is homogeneous and isotropic: the cosmological principle. This implies that the number density of galaxies is the same in all parts of the universe, and that the luminosity function is universal, (since all galaxies will have formed under the same conditions and will have the same properties). If it is also assumed that galaxies do not change with time, the observations of distant galaxies can be compared with those of nearby galaxies to determine the deceleration parameter q_o, and to deduce whether the universe will expand for ever or whether the expansion will cease, and the universe will subsequently contract.

These assumptions were made at the beginning of chapter 4, when the data was compared with standard cosmological models. Although the assumptions simplify the analysis, there are still uncertainties in constructing the models. Firstly, the light from galaxies is red-shifted, so the light detected from distant galaxies originated at

shorter wavelengths. This means that in order to analyse the j magnitudes of galaxies the redshifts of $z \gtrsim 0.3$, it is necessary to know the average ultraviolet spectrum of galaxies. Recently galaxies have been observed in the ultraviolet (Code, Welch & Page 1972), but the results are still uncertain.

The analysis of the results also requires a knowledge of the luminosity function. Many determinations of the luminosity function have been made for both field and cluster galaxies, and it is well established that the frequency of galaxies increases with decreasing luminosity. However galaxies which are intrinsically faint are not likely to be detected and it is important to know how selection has affected the data.

The factors which determine whether or not a galaxy is detected are the apparent luminosity and the apparent surface brightness. When deriving the theoretical $\log N(m)$ it is easy to reject galaxies which are calculated to have luminosities corresponding to $m > 22$, but it is more difficult to take account of selection effects operating on the surface brightness. As a first approximation, a cut-off in the luminosity function was made at $M = -17$, assuming that galaxies fainter than this could not be detected. Later, the procedure for rejecting low surface brightness galaxies was improved as described below.

Another problem is that isophotal magnitudes of galaxies are detected instead of total ones. Since it is difficult to extrapolate the observed galaxy magnitudes, this effect was taken into account by the theoretical calculations. Standard galaxy profiles were used to

calculate the effect of atmospheric seeing on the fraction of the luminosity detected for galaxies of different redshifts. An average correction $\Delta m(z)$ was calculated to convert the model magnitudes to isophotal magnitudes. The convoluted theoretical profiles of Sdm-Im galaxies were found to have predicted central surface brightnesses too low to be detected, so the numbers of model galaxies were also modified as a function of redshift to take this into account.

In all cases the observed log N(m) values for faint galaxies were greater than those of the models, which implies that some of the assumptions made while constructing the model were wrong. In fact the assumptions that the number density of galaxies is constant throughout the universe and that the luminosities of galaxies are constant with time are thought to be invalid. The theoretical log N(m) relation could be made to fit the observations by supposing that either the number density of galaxies increases in the direction observed, or that galaxies were brighter in the past.

The effects of clustering on the log N(m) relation can be seen by comparing the observed curves for the three fields. There were two nearby clusters in field III; once these had been removed, the log N(m) relation was similar in the three fields. However, it is possible that there could be an excess of faint galaxies in all the fields, due to the presence of a supercluster. The frequency distribution of galaxies log F(m), in figures 3.10a, b and c, show no sudden increase in the number density of galaxies. This could indicate that there is a gradual variation of the galaxy density throughout the universe, and therefore the universe can no longer be assumed to be homogeneous and

isotropic. In this case the cosmological equations should be modified to take account of large scale inhomogeneities. There are obviously many problems associated with studying cosmology in an inhomogeneous universe, and the observations from a small area of the sky can no longer be used to draw general conclusions.

The observed log N(m) relation cannot be used to study both the number density of galaxies and the evolution of galaxies without ambiguity. When the data was used to investigate evolution it was assumed that the universe was homogeneous. Models in which the absolute magnitude varies linearly with time were tested. The best fitting models were those for total magnitudes, i.e. without the corrections for isophotal magnitudes and failure to detect low surface brightness galaxies. This is not surprising because these corrections are expected to be reduced when evolution is taken into account. The resulting evolution rates vary from $\dot{M} = 0.15$ mag/10^9 yr for $q_o = 0.0$ to $\dot{M} = 0.31$ mag/10^9 yr for $q_o = 2.0$, assuming $H_o = 50$ km $s^{-1} Mpc^{-1}$.

These rates for the luminosity evolution of galaxies are not as large as that predicted by Larson & Tinsley (1974) and there is no large excess of galaxies with m > 20 as suggested by Tinsley (1977). Young galaxies may not be as bright as Tinsley predicts, or they may be too distant to be detected. It may be wrong to assume that galaxy luminosities decrease monotonically with time. Bailey & Clube (1978) suggest that galaxies undergo periodic brightening due to recurrent nuclear activity.

The conclusions which can be drawn from studying the $\log N(m)$ relation are limited. There are three uncertain factors, namely the deceleration parameter q_o, the large scale distribution of galaxies and the rate of change of the luminosity of galaxies, but their effects on the $\log N(m)$ relation cannot be distinguished. In future, further progress could be made by combining several observed quantities such as magnitudes, colours and redshifts. For example, the $m(z)$ and the $\log N(m)$ relations could be used to distinguish between the effects of galaxy evolution and large scale variations in the number density of galaxies. Nevertheless there is sufficient evidence from the analysis of the $\log N(m)$ relation to show that galaxies were slightly brighter in the past and/or there is a higher number density of galaxies in the direction of the south galactic pole.

APPENDIX I

1. The N(m) Relation for a Friedman Cosmological Model with $\Lambda = 0$.

Assuming that the universe is homogeneous and isotropic, the expression for the space-time interval ds is given by:

$$ds^2 = c^2\,dt^2 - R^2(t)\,du^2 \qquad \text{A1.1}$$

which is the Robertson-Walker metric. R(t) describes the expansion of the universe and has dimensions of distance.

$$du^2 = \frac{dr^2}{1 - kr^2} + r^2(d\theta^2 + \sin^2\theta d\phi^2) \qquad \text{A1.2}$$

where r, θ, and ϕ are dimensionless, co-moving coordinates, i.e. they are independent of time. k is the curvature of space and equals +1 if the universe is closed, 0 if the universe is open and Euclidean, and -1 if it is open and hyperbolic.

Photons move along the null geodesic, i.e. ds = 0, so the metric distance travelled by a photon emitted at time t_1 and detected at time t_o is:

$$u = c\int_{t_1}^{t_o} \frac{dt}{R(t)} = \int_o^r \frac{dr}{\sqrt{1 - kr^2}}$$

$$= \begin{cases} \sin^{-1} r & k = +1 \\ r & k = 0 \\ \sinh^{-1} r & k = -1 \end{cases} \qquad \text{A1.3}$$

or $r = \sigma(u) = \sin u$, u, $\sinh u$ according as k = +1, 0, or -1. The metric distance only equals the coordinate distance for a Euclidean (flat) universe.

The expansion factor R(t) can be found in terms of the density ρ and the pressure p in the universe from Einstein's field equations of general relativity, using the assumptions of isotropy and homogeneity.

$$\frac{\dot{R}^2}{R^2} + \frac{2\ddot{R}}{R} + \frac{8\pi G p}{c^2} = \frac{-kc^2}{R^2} + \Lambda c^2 \qquad \text{A1.4}$$

$$\frac{\dot{R}^2}{R^2} - \frac{8\pi G\rho}{3} = \frac{-kc^2}{R^2} + \frac{\Lambda c^2}{3} \qquad \text{A1.5}$$

The second equation is known as Friedman's differential equation. The cosmological constant will be set to zero, and the pressure is negligible at the present epoch. Equation A1.5 may be rewritten as

$$\dot{R}^2 = \frac{2GM}{R} - kc^2. \qquad \text{A1.5}'$$

The Hubble parameter and the deceleration parameter are defined as:

$$H = \frac{\dot{R}}{R} \quad \text{and} \quad q = \frac{\ddot{R}R}{\dot{R}^2}$$

Using these parameters, and equations A1.4 and A1.5, the following relations may be found:

$$\rho = \frac{3H^2 q}{4\pi G} \qquad \text{A1.6}$$

$$\frac{kc^2}{R^2} = H^2(2q - 1) \qquad \text{A1.7}$$

$$\frac{Rc^2}{GM} = \frac{(2q - 1)}{q}. \qquad \text{A1.8}$$

Suffices zero will be used to denote the present values of quantities, e.g. R_o, H_o, and suffices unity to denote the values when a photon was

emitted from a distant galaxy, e.g. R_1, H_1.

Light emitted at t_1 when the distance scale of the universe was $R_1(t)$ is received at time t_o when the scale factor is $R_o(t)$. Between emission and detection the universe has expanded in the ratio R_o/R_1 and the detected energy of the photon is reduced in the ratio R_1/R_o because of the relative velocities of the two galaxies, so that the wavelength is increased in the ratio $\lambda'/\lambda = (\lambda + \Delta\lambda)/\lambda = 1 + z$, where z is the redshift. It follows that

$$1 + z = \frac{R_o(t)}{R_1(t)} . \qquad \text{A1.9}$$

The bolometric luminosity of a galaxy, the coordinate distance of which is given by r, is:

$$1 = \frac{L}{4\pi R_o^2 \sigma^2(u)(1 + z)^2} .$$

where L is the intrinsic luminosity and $4\pi R_o^2 \sigma^2(u)$ is the area of the radiation wavefront at the time of detection. The factor $1/(1 + z)^2$ is due to the 'energy' and 'number' effects of the expansion of the universe on the photons received. If L_{abs} is the absolute luminosity, then

$$1 = \frac{L_{abs}\, 10^{-5}}{R_o^2 \sigma^2(u)(1 + z)^2}$$

since L_{abs} is the luminosity at a distance of 10^{-5} Mpc.

The distance modulus is therefore:

$$m - M = 5\log\left[R_o \sigma(u)(1 + z)\right] + 25. \qquad \text{A1.10}$$

The factor $R_o\sigma(u)$ may be found by substituting from the Friedman equation A1.5' into A1.1 for the Robertson-Walker metric. (This is the method used by Mattig (1958)).

$$u = c\int_{R_1}^{R_o} \frac{dt}{R(t)}$$

$$= c\int_{R_1}^{R_o} \frac{dR}{R\dot{R}}$$

$$= c\int_{R_1}^{R_o} \frac{dR}{R\sqrt{2GM/R - kc^2}}$$

This can be integrated, and using equations A1.7 and A1.8 gives:

$$\sigma(u) = r = \frac{c}{R_o H_o q_o^2 (1 + z)} \{q_o z + (q_o - 1)\left[\sqrt{1 + 2q_o z} - 1\right]\} \qquad \text{A1.11}$$

which holds for all k, and $q_o > 0$.

If $q_o = 0$, the universe has zero density and expands at the velocity of light. In this case

$$r = \frac{z(1 + z/2)}{(1 + z)} \qquad \text{A1.11'}$$

Substituting these equations into equation A1.10 gives

$$m - M = 5\log\left\{\frac{1}{q_o^2}\left[q_o z + (q_o - 1)\left[\sqrt{1 + 2q_o z} - 1\right]\right]\right\} + 5\log\left(\frac{c}{H_o}\right) + 25$$

A1.12

for $q_o > 0$,

$$\text{or} \quad m - M = 5\log\{ z(1 + z/2) \} + 5\log\left(\frac{c}{H_o}\right) + 25 \qquad \text{A1.12'}$$

for $q_o = 0$.

Equations A1.12 and A1.12' give the m(z) relation. However, the apparent magnitude m has to be corrected for K-dimming first.

$$m = m_{obs} - m_K(z)$$

where m_{obs} is the observed magnitude and $m_K(z)$ is the K-correction.

For the N(m) relation it is necessary to know the volume contained within solid angle ω out to coordinate distance r.

$$V = R_o^3 \omega \int_o^r \frac{r'^2 dr'}{\sqrt{1 - kr'^2}}$$

This is the value of the volume at the present time, and the number of galaxies within r can be found from the present number density of galaxies, n_o, found locally.

$$N = R_o^3 n_o \omega \int_o^r \frac{r'^2\, dr'}{\sqrt{1 - kr'^2}}$$

$$= \begin{cases} \frac{1}{2} n_o R_o^3 (u - \sin u \cos u) & \text{if } k = 1 \\ \frac{1}{3} n_o R_o^3 u^3 & \text{if } k = 0 \\ \frac{1}{2} n_o R_o^3 (\sinh u \cosh u - u) & \text{if } k = -1 \end{cases} \qquad \text{A1.13}$$

where $u = \sin^{-1} r$, r or $\sinh^{-1} r$ for k = +1, 0 or -1.

If u is calculated in terms of z, H_o and q_o from $\sigma(u)$ in equation A1.11 or A1.11', the N(z) relation is found.

The N(m) relation, where m is the observed magnitude, can be calculated by combining the m(z) relation with the N(z) relation. (The

K-corrections as a function of redshift can be found from tables, such as those given by Pence (1976).)

2. The Calculation of the Light Travel Time as a Function of q_o, H_o and z.

The time taken for light to reach an observer from a galaxy at redshift z can be calculated using Friedman's differential equation, in the form:

$$\dot{R}^2 = \frac{\alpha c^2}{R} - kc^2 \qquad \text{A1.14}$$

where $\alpha = \frac{2GM}{c^2}$ and $\frac{2R_o}{\alpha} = \frac{k(2q_o - 1)}{q_o}$. A1.15

Equations A1.14 and A1.15 were derived in part 1 of Appendix I.

From A1.14,

$$\dot{R} = c\sqrt{\alpha/R - k}$$

$$\therefore \int dt = \frac{1}{c}\int \frac{dR}{\sqrt{\alpha/R - k}}$$

Let t_1 and t_o be the times of emission and detection of the light and R_1 and R_o be the distance scales of the universe at those times.

$$\Delta t = t_o - t_1 = \frac{1}{c}\int \frac{dR}{\sqrt{\alpha/R - k}} \qquad \text{A1.16}$$

This equation can be integrated and, using equations A1.9 and A1.7, the following formulae for Δt can be calculated.

i) $q > \frac{1}{2}$, $k = +1$ (use the substitution $\sin\theta = (1 - 2R/\alpha)$)

$$\Delta t = \frac{q_o}{H_o(2q_o - 1)^{3/2}}\left\{\sin^{-1}\left(\frac{q_o z - q_o + 1}{q_o(1+z)}\right) - \sin^{-1}\left(\frac{1 - q_o}{q_o}\right)\right\}$$

$$+ \frac{1}{H_o(2q_o - 1)}\left\{\frac{\sqrt{1 + 2q_o z}}{(1+z)} - 1\right\}$$

ii) $0 < q_o < \frac{1}{2}$, $k = -1$ (use the substitution $\cosh\theta = (1 + 2R/\alpha)$)

$$\Delta t = \frac{1}{H_o(1 - 2q_o)}\left\{1 - \frac{\sqrt{1 + 2q_o z}}{(1+z)}\right\}$$

$$- \frac{1}{H_o(1 - 2q_o)^{3/2}}\left\{\cosh^{-1}\left(\frac{1 - q_o}{q_o}\right) - \cosh^{-1}\left(\frac{q_o z - q_o + 1}{q_o(1+z)}\right)\right\}$$

iii) $q_o = \frac{1}{2}$, $k = 0$

In this case, equation A1.14 becomes

$$\dot{R}^2 = \frac{\alpha c^2}{R}$$

giving:

$$\Delta t = \frac{2}{3H_o}\left[1 - \frac{1}{(1+z)^{3/2}}\right].$$

iv) $q_o = 0$

When q_o is zero, the universe expands with the speed of light, i.e. $\dot{R} = c$. Also $H_o = \frac{\dot{R}_o}{R_o} = \frac{c}{R_o}$.

This gives:

$$\Delta t = \frac{1}{H_o}\left[1 - \frac{1}{(1+z)}\right].$$

A P P E N D I X II

Deconvolution.

In one dimension the formula for the convolution integral is:

$$g(x) = \int_{-\infty}^{+\infty} f(u)\, S(x - u)\, du$$

where f(x) is the true profile, i.e. the true transmission profile of an image in this case; S(x) is the spread function which is the gaussian profile of the COSMOS spot; and g(x) is the convoluted function, or the observed image transmission profile. The aim of deconvolution is to calculate f(x) from g(x) and S(x). There are many problems involved in doing this which are discussed by Jones & Misell (1970).

It is well known that when the functions are fourier transformed, the convolution integral becomes a product,

i.e. $\overline{g}(t) = \overline{f}(t) \times \overline{S}(t)$

where $\overline{g}(t) = \int_{-\infty}^{+\infty} g(x)\, e^{-2\pi i x t} dx$ is the fourier transform of g(x), and $\overline{f}(t)$ and $\overline{S}(t)$ are the fourier transforms of f(x) and S(x) respectively. In this form the equation can be solved easily.

$$\overline{f}(t) = \frac{\overline{g}(t)}{\overline{S}(t)}$$

or $\overline{f}(t) = \overline{g}(t) \times T(t)$ where $T(t) = \dfrac{1}{\overline{S}(t)}$.

If the inverse fourier transform is taken on both sides, the last equation becomes:

$$f(x) = \int_{-\infty}^{+\infty} \bar{g}(t)\ T(t)\ e^{+2\pi i x t}\, dt$$

$$= \int_{t=-\infty}^{\infty} \int_{u=-\infty}^{\infty} g(u)\ e^{-2\pi i u t}\, du\ T(t)\ e^{+2\pi i x t}\, dt$$

$$= \int_{u=-\infty}^{+\infty} g(u) \int_{t=-\infty}^{+\infty} T(t)\ e^{+2\pi i (x-u) t}\, dt\, du$$

$$= \int_{-\infty}^{+\infty} g(u)\ M(x-u)\, du\ .$$

M(x) is the inverse fourier transform of T(t). The true profile, f(x), is a convolution of g(x) with the function M(x). Since the spread function is gaussian in this case, the formula for T(t) may be calculated analytically.

$$S(x) = \frac{1}{a\sqrt{\pi}}\ e^{-x^2/a^2}$$

(S(x) is normalised so that $\int_{-\infty}^{+\infty} S(x)\, dx = 1.$)

Fourier transforming,

$$\bar{S}(t) = e^{-\pi^2 a^2 t^2}$$

$$T(t) = e^{+\pi^2 a^2 t^2}$$

This function tends to infinity as $|t|$ tends to infinity, so the function M(x) cannot be calculated. However, in practice, the total range of t is not used. The observed profile g(x) always contains noise which affects the fourier transform $\bar{g}(t)$. At high values of $|t|$ the contribution to $\bar{g}(t)$ by the noise will always be larger than the true value of $\bar{g}(t)$ and these errors, when multiplied by the exponential function T(t), produce large values of $\bar{f}(t)$ giving rise

to large errors in f(x). Therefore the accuracy of the value of the function f(x) is improved if a cut-off is made at high frequencies. The function R(t) is defined as:

$$R(t) = T(t) \qquad |t| < t_*$$

$$= U(t) \qquad |t| \geq t_*$$

where t_* is the frequency at which the effects of noise become important. U(t) is defined to make R(t) and its first derivative continuous at t_*, and to decrease rapidly at high values of $|t|$.

$$U(t) = \exp\{\pi a^2 [-(|t| - 2t_*)^2 + 2t_*]\}$$

(R(t) is not set to zero at $|t| > t_*$ because a sharp cut-off in frequency gives rise to errors in the fourier transformed function.)

The function M(x) is now given by:

$$M(x) = \int_{-\infty}^{+\infty} R(t)\, e^{+2\pi i x t}\, dt.$$

The deconvolution of images measured by COSMOS has to be carried out in two dimensions. The convolution integral becomes:

$$g(x,y) = \int_{-\infty}^{+\infty}\int_{-\infty}^{+\infty} f(u,v)\; S(x-u, y-v)\, du\, dv$$

and the solution is given by:

$$f(x,y) = \int_{-\infty}^{+\infty}\int_{-\infty}^{+\infty} g(u,v)\; M(x-u, y-v)\, du\, dv\,.$$

Since the spread function is gaussian, it is separable into the product of a function of x with the same function of y.

i.e.

$$S(x,y) = S'(x)\, S'(y)$$

$$= \frac{1}{a\sqrt{\pi}} e^{-x^2/a^2} \quad \frac{1}{a\sqrt{\pi}} e^{-y^2/a^2}$$

The formula for a fourier transform in two dimensions is:

$$S(s,t) = \int_{-\infty}^{+\infty} \int_{-\infty}^{+\infty} S(x,y)\, e^{-2\pi i(sx + ty)} dx\, dy$$

$$= \int_{-\infty}^{+\infty} S'(x)\, e^{-2\pi isx} dx \int_{-\infty}^{+\infty} S'(y)\, e^{-2\pi ity}\, dy$$

$$= \overline{S}'(s)\, \overline{S}'(t).$$

Since the function $\overline{S}(s,t)$ is separable into two equal functions of s and t, so is the function T(s,t), and the function M(x,y). Therefore the deconvoluting function, M, was derived as in the one dimensional case by calculating R(t) from a gaussian and fourier transforming. Then g(x,y) was convoluted with M in the x-direction, and again with M in the y-direction to give f(x,y).

REFERENCES

Abell, G.O., 1961. A. J., 66, 607.

Abell, G.O., 1962. I.A.U. Symposium 15, 'Problems of Extragalactic Research', 213.

Abell, G.O., 1975. 'Stars and Stellar Systems', 9, 'Galaxies and the Universe' ed. Sandage, Sandage & Kristian, (Chicago Univ. Press), p.610.

Abell, G.O. & Corwin, H.G., 1979. In preparation.

Abell, G.O. & Mihalas, D.M., 1966. A. J., 71, 635.

Ables, D.A., 1971. U.S. Naval Obs. Publ. XX, Pt. IV.

Ables, D.A. & Ables, P.G., 1972. A. J., 77, 642.

Alcaino, G., 1974. Astron. and Astrophys. Suppl., 13, 305.

Arakelyan, M.A. & Kalloglyan, A.T., 1970. Soviet Ast. A. J., 13, 953.

Arp, H.C., 1962. Ap. J., 135, 311.

Austin, T.B. & Peach, J.V., 1974. M.N.R.A.S., 167, 437.

Austin, T.B., Godwin, J.G. & Peach, J.V., 1975. M.N.R.A.S., 171, 135.

Bailey, M.E. & Clube, S.M.V., 1978. Nature, 275, 278.

Baldwin, J.A., Burke, W.L., Gaskell, C.M. & Wampler, E.J., 1978. Nature, 273, 431.

Baker, E.A., 1949. Pub. Royal Obs. Edin., Vol. I, No 2, 13.

Barnothy, J.M. & Tinsley, B.M., 1973. Ap. J., 182, 343.

Baum, W., 1957. A. J., 62, 6.

Baum, W.A. & Florentin-Nielsen, R., 1976. Ap. J., 209, 319.

Bautz, L.P. & Morgan, W.W., 1970. Ap. J., 162, L149.

Bautz, L.P. & Abell, G.O., 1973. Ap. J., 184, 709.

Becklin, E.E. & Neugebaur, G., 1968. Ap. J., 151, 145.

Bergh, S. van den, 1960. Ap. J., 131, 215.

Bergh, S. van den, 1961. Z. fur Astrophys., 53, 219.

Bergh, S. van den, 1974. I.A.U. Symposium, 58, 'The Formation and Dynamics of Galaxies' 157.

Bergh, S. van den, 1975. 'Structure and Evolution of Galaxies', D. Reidel Publ. Co., Dordrecht, Holland, 247.

Bernacca, P.L. & Bertola, F., 1969. Contrib. Assiago, No 214.

Bertola, F., 1966. Contrib. Assiago, No 186.

Bertola, F., 1967. Contrib. Assiago, No 197.

Bigay, J.H., 1951. Ann. d'Astrophys., 14, 319.

Bondi, H. & Gold, T., 1948. M.N.R.A.S., 108, 252.

Branch, D., 1977. M.N.R.A.S., 179, 401.

Brown, G.S., 1974. Thesis, Univ. of Texas.

Brown, G.S, & Tinsley, B.M., 1974. Ap. J., 194, 555.

Burger, H.C. & Van Cittert, P.H., 1932. Z. Phys., 79, 722.

Burger, H.C. & Van Cittert, P.H., 1932. Z. Phys., 81, 428.

Chitre, S.M. & Narlikar, J.V., 1976. Astrophys. and Sp. Sci., 44, 101.

Christensen, C.G., 1975. A. J., 80, 282.

Code, A.D., Welch, G.A. & Page, T.L., 1972. 'The Scientific Results from the Orbiting Astronomical Observatory', ed. A.D. Code, N.A.S.A, Washington, p.559.

Corben, P.M., Reddish, V.C. & Sim, M.E., 1974. Nature, 249, 22.

Davis, M. & Wilkinson, D.T., 1974. Ap. J., 192, 251.

Dennison, E., 1954. Thesis, Univ. of Michigan, unpublished.

Disney, M.J., 1976. Nature, 263, 573.

Dodd, R.J., Morgan, D.H., Nandy, K., Reddish, V.C. & Seddon, H., 1975. M.N.R.A.S, 171, 329.

Dodd, R.J., MacGillivray, H.T. & Hilditch, R.W., 1977. M.N.R.A.S., 181, 729.

Eastmond, T.S., 1977. Thesis, Univ. College, Los Angeles, unpublished.

Eberhard, G., 1931. Handbuch der Astrophys., 2, 458.

Eggen, O.J., Lynden-Bell, D. & Sandage, A., 1962. Ap. J., 136, 748.

Eggen, O.J., & Vaucouleurs, G. de, 1956. P.A.S.P., 68, 421.

Ellis, R.S., Fong, R. & Phillipps, S., 1977. M.N.R.A.S., 181, 163.

Elvey, C.T. & Roach, F.E., 1937. Ap. J., 85, 213.

Evans, D.S., 1951. M.N.R.A.S., 111, 526.

Evans, D.S., 1952. M.N.R.A.S., 112, 606.

Field, G.B., 1964. Ap. J., 140, 1434.

Field, G.B., Arp, H.C. & Bahcall, J.N., 1973. 'The Redshift Controversy', Pub. Benjamin, Reading, Mass., London.

Fish, R.A., 1964. Ap. J., 139, 284.

Flandern, T.C. van, 1975. M.N.R.A.S., 170, 333.

Fraser, C.W., 1977. Astron. and Astrophys. Suppl. Ser., 29, 161.

Freeman, K.C., 1970. Ap. J., 160, 811.

Freeman, K.C., 1976. 'Stars and Stellar Systems', 9, 'Galaxies and the Universe' ed. Sandage, Sandage & Kristian, Ch.11.

Friedman, A., 1922. Z fur Phys., 10, 377.

Gamow, G., 1956. Vistas in Astronomy, 2, 1726.

Gott, J.R., 1973. Ap. J., 186, 481.

Gott, J.R., Gunn, J.E., Schramm, D.N. & Tinsley, B.M., 1974. Ap. J., 194, 543.

Gott, J.R. & Thuan, T.X., 1976. Ap. J., 204, 649.

Gross, P.G., 1977. Ap. J., 215, 417.

Gudehus, D.H., 1975. P.A.S.P., 87, 763.

Gunn, J.E. & Gott, J.R., 1972. Ap. J., 176, 1.

Gunn, J.E. & Oke, J.B., 1975. Ap. J., 195, 255.

Gunn, J.E. & Tinsley, B.M., 1975. Nature, 257, 454.

Gunn, J.E. & Tinsley, B.M., 1976. Ap. J., 210, 1.

Guthrie, B.N.G., 1976. Astrophys. and Sp. Sci., 43, 425.

Hanes, D.A., 1977. Mem. R.A.S., 84, 45.

Hawkins, M.R.S. & Martin, R., 1977. Nature, 265, 711.

Hawkins, M.R.S. & Reddish, V.C., 1975. Nature, 257, 722.

Heidman, J., Heidman, N. & Vaucouleurs, G. de, 1972. Mem. R.A.S., 75, 85, 105, 121.

Hinks, A.R., 1911. M.N.R.A.S., 71, 588.

Hodge, P.W., 1963. A.J., 68, 237.

Hoffman, A.A. & Crane, P., 1977. Ap. J., 215, 379.

Holetschek, J., 1907. Annalen der Weiner Sternwarte.

Holmberg, E., 1946. Medd. Lunds Ast. Obs., Ser. II, No 117.

Holmberg, E., 1950. Medd. Lunds Ast. Obs., Ser. II, No 128.

Holmberg, E., 1958. Medd. Lunds Ast. Obs., Ser. II, No 136.

Hopman, J., 1921. A. N., 214, 425.

Houten, C.J. van, 1961. B.A.N., 16, 1.

Houten, C.J. van, Oort, J.H. & Hiltner, W.A., 1954. Ap. J., 120, 439.

Hoyle, F., 1948. M.N.R.A.S., 108, 373.

Hoyle, F. & Narlikar, J.V., 1972. M.N.R.A.S., 155, 323.

Hoyle, F. & Sandage, A., 1956. P.A.S.P., 68, 301.

Humason, M.L., Mayall, N.U. & Sandage, A., 1956. A. J., 61, 97.

Hubble, E.P., 1925. Ap. J., 62, 409.

Hubble, E.P., 1929. Proc. Nat. Acad. Sci., 15, 168.

Hubble, E.P., 1930. Ap. J., 71, 231.

Hubble, E.P., 1934. Ap. J., 79, 8.

Hubble, E.P., 1936a. Ap. J., 84, 158.

Hubble, E.P., 1936b. Ap. J., 84, 270.

Hubble, E.P., 1936c. Ap. J., 84, 517.

Hubble, E.P. & Tolman, R.C., 1935. Ap. J., 82, 302.

Jeans, J., 1928. 'Astronomy and Cosmogony', Cambridge Univ. Press.

Johnson, H.L., 1959. Lowell Obs. Bull., 4, No 98.

Johnson, H.L. & Morgan, W.W., 1953. Ap. J., 117, 313.

Jones, A.F. & Missell, D.L., 1970. J. Phys. A : Gen. Phys., 3, 462.

Jones, W.B., Obitts, D.L., Gallet, R.M. & Vaucouleurs, G. de, 1967.
Pub. Dept. Ast. Univ. of Texas at Austin, Ser. II, Vol 1, No 8.

Kaufman, M. & Thuan, T.X., 1977. Ap. J., 215, 11.

Keenan, P.C., 1935. Ap. J., 82, 62.

Kiang, T., 1961. M.N.R.A.S., 122, 263.

King, E.I. & Hinrichs, E.L., 1967. P.A.S.P., 79, 226.

Kirshner, R.P. & Kwan, J., 1974. Ap. J., 193, 27.

Knapp, G.R., 1975. A.J., 80, 111.

Knapp, G.R. & Kerr, F.J., 1974. Astron. and Astrophys., 35, 361.

Kormendy, J., 1973. A. J., 78, 255.

Kormendy, J., 1978. Ap. J., 217, 406.

Krat, V.A. & Gerlovin, I.L., 1974. Astrophys. and Sp. Sci., 33, 15.

Kristian, J., 1973. Ap. J., 179, L61.

Kristian, J., Sandage, A. & Westphal, J.A., 1978. Ap. J., 221, 383.

Lang, K.R., Lord, S.D., Johanson, J.M. & Savage, P.D., 1975. Ap. J., 202, 583.

Larson, R.B., 1974. M.N.R.A.S., 166, 585.

Larson, R.B., 1975. M.N.R.A.S., 173, 671.

Larson, R.B., 1976. M.N.R.A.S., 176, 31.

Larson, R.B. & Tinsley, B.M., 1974. Ap. J., 192, 293.

Liller, M.H., 1960. Ap. J., 132, 306.

Liller, M.H., 1966. Ap. J., 146, 28.

MacGillivray, H.T. & Dodd, R.J., 1979. M.N.R.A.S., 186, 69.

MacGillivray, H.T., Martin, R., Pratt, N.M., Reddish, V.C., Seddon, H., Alexander, L.W.G., Walker, G.S. & Williams, P.R., 1976. M.N.R.A.S., 176, 265.

Mattig, W., 1958. A. N., 284, 109.

Mattig, W., 1959. A. N., 285, 1.

McMullan, D., Powell, J.R. & Curtis, N.A., 1973. Adv. in Electronics and Electron Phys., 33A, 37.

Mees, C.E.K. & James, T.H., 1966. 'The Theory of the Photography Process', Pub. McMillan, pp.525-530.

Meier, D.L., 1976. Ap. J., 203, L103.

Moffat, A.F.J., 1969. Astron. and Astrophys., 3, 455.

Oemler, A., 1974. Ap. J., 194, 1.

Oemler, A., 1976. Ap. J., 209, 693.

Oke, J.B. & Sandage, A., 1968. Ap. J., 154, 21.

Oort, J.H. & Plaut, L., 1975. Astron. and Astrophys., 41, 71.

Opik, E., 1923. Observatory, 46, 51.

Ostriker, J.P. & Tremaine, S.D., 1975. Ap. J., 202, L113.

Ozernoy, L.M., 1974. I.A.U. Sumposium, 58, 'The Formation and Dynamics of Galaxies' p.85.

Partridge, R.B., 1974. Ap. J., 192, 241.

Peach, J.V., 1970. Ap. J., 159, 753.

Peebles, P.J.E., 1969. Ap. J., 155, 393.

Peebles, P.J.E., 1974. I.A.U. Symposium, 58, 'The Formation and Dynamics of Galaxies', p.55.

Peimbert, M. & Torres-Peimbert, S., 1974. Ap. J., 193, 327.

Pence, W., 1976. Ap. J., 203, 39.

Peterson, B.A., 1970. A. J., 75, 695.

Petrosian, V., 1976. Ap. J., 209, L1.

Pettit, E., 1954. Ap. J., 120, 413.

Pratt, N.M., Martin, R., Alexander, L.W.G., Walker, G.S. & Williams, P.R., 1975. 'Image Processing Techniques in Astronomy', ed. de Jager/ Nieuwenhuijzen, D. Reidel Publ. Co., Dordrecht, Holland, pp.217-222.

Reddish, V.C., 1968. Q.J.R.A.S., 9, 409.

Reddish, V.C., 1975. M.N.R.A.S., 170, 261.

Reinmuth, K., 1926. Veroff Heidelberg, 9.

Redman, R.O., 1936. M.N.R.A.S., 96, 588.

Redman, R.O. & Shirley, E.G., 1937. M.N.R.A.S., 97, 416.

Redman, R.O. & Shirley, E.G., 1938. M.N.R.A.S., 98, 613.

Reynolds, J.H., 1914. M.N.R.A.S., 74, 132.

Reynolds, J.H., 1920. M.N.R.A.S., 81, 129.

Robertson, H.P., 1955. P.A.S.P., 67, 82.

Rogerson, J.B. & York, D.G., 1973. Ap. J., 186, L95.

Rood, H.J. & Baum, W.A., 1968. A. J., 73, 442.

Rowan-Robinson, M., 1976. Nature, 262, 97.

Rubin, V. & Ford, W.K., 1975. Bull. A. A. S., 7, 253.

Rubin, V., Ford, W.K. & Rubin, J., 1973. Ap. J., 183, L111.

Salpeter, E.E., 1955. Ap. J., 121, 161.

Sandage, A., 1958. Ap. J., 127, 513.

Sandage, A., 1961. Ap. J., 133, 355.

Sandage, A., 1972a. Ap. J., 173, 485.

Sandage, A., 1972b. Ap. J., 178, 1.

Sandage, A., 1972c. Ap. J., 178, 25.

Sandage, A., 1973a. Ap. J., 180, 687.

Sandage, A., 1973b. Ap. J., 183, 711.

Sandage, A., 1973c. Ap. J., 183, 731.

Sandage, A., 1975. Ap. J., 202, 563.

Sandage, A. & Hardy, E., 1973. Ap. J., 183, 743.

Sandage, A. & Smith, L.L., 1963. Ap. J., 137, 1057.

Sandage, A. & Tamman, G.A., 1974a. Ap. J., 190, 525.

Sandage, A. & Tamman, G.A., 1974b. Ap. J., 191, 603.

Sandage, A. & Tamman, G.A., 1974c. Ap. J., 194, 223.

Sandage, A. & Tamman, G.A, 1974d. Ap. J., 194, 559.

Sandage, A. & Tamman, G.A., 1975a. Ap. J., 196, 313.

Sandage, A. & Tamman, G.A., 1975b. Ap. J., 197, 265.

Sandage, A. & Tamman, G.A., 1976. Ap. J., 210, 7.

Sandage, A., Freeman, K.C. & Stokes, N.R., 1970. Ap. J., 160, 831.

Sanders, R.H. & Lowinger, T., 1972. A. J., 77, 292.

Schechter, P., 1976. Ap. J., 203, 297.

Schild, R.E. & Oke, J.B., 1971. Ap. J., 169, 209.

Schmidt, M., 1959. Ap. J., 129, 243.

Schmidt, M., 1963. Ap. J., 137, 758.

Seares, F.H., 1922. Ap. J., 56, 97.

Selwyn, E.W.H., 1935. Phot. J., 75, 571.

Sersic, J.L., 1968. Atlas de Galaxias Australes, Astron. Obs., Univ. of Cordoba, Argentina.

Seyfert, C.K., 1935. Circulars of Harvard College, No 403.

Shane, C.D., 1974. 'Stars and Stellar Systems', 9, 'Galaxies and the Universe', ed. Sandage, Sandage & Kristian, (Chicago Univ. Press), p.647.

Shane, C.D. & Wirtanen, C.A., 1954. A. J., 59, 285.

Shane, C.D. & Wirtanen, C.A., 1967. Pub. Lick Obs., Vol 22, Pt. 1.

Shapley, H., 1957. 'The Inner Metagalaxy', Yale Univ. Press, Inc.

Shapley, H. & Ames, A., 1932. Ann. Harvard Coll. Obs., 88, 43 (No 2).

Shobbrook, R.R., 1966. M.N.R.A.S., 131, 351.

Silk, J., 1974. Ap. J., 193, 525.

Stebbins, J. & Whitford, A.E., 1937. Ap. J., 86, 274.

Stebbins, J. & Whitford, A.E., 1948. Ap. J., 108, 413.

Stebbins, J. & Whitford, A.E., 1952. Ap. J., 115, 284.

Stock, J. & Scheuking, E., 1957. A. J., 62, 98.

Strom, K.M. & Strom, S.E., 1978. A. J., 83, 73.

Tamman, G.A., 1973. Proc. I.A.U. Symp. 63, Cracow, p.47.

Tifft, W.G., 1958. Thesis, Cal. Inst. of Technology, unpublished.

Tifft, W.G., 1961. A. J., 66, 390.

Tifft, W.G., 1963a. A. J., 68, 302.

Tifft, W.G., 1963b. M.N.R.A.S., 125, 199.

Tifft, W.G., 1969. A. J., 74, 354.

Tinsley, B.M., 1972a. Ap. J., 173, L93.

Tinsley, B.M., 1972b. Astron. and Astrophys., 20, 383.

Tinsley, B.M., 1973. Ap. J., 186, 35.

Tinsley, B.M., 1976. Ap. J., 210, L49.

Tinsley, B.M., 1977a. Ap. J., 211, 621.

Tinsley, B.M., 1977b. Physics Today, 30, No 6, 32.

Tully, R.B., 1968. A. J., 73. S205.

Tully, R.B., 1972. M.N.R.A.S., 159, 35P.

Tully, R.B. & Fischer, J.R., 1977. Astron. and Astrophys., 54, 661.

Turner, E.L. & Gott, J.R., 1976. Ap. J., 209, 6.

Vaucouleurs, G. de, 1944. Pub. Obs. Houga, No 10.

Vaucouleurs, G. de, 1946. Pub. Inst. Astrophus. Paris, Série B, No 15.

Vaucouleurs, G. de, 1948a. Ann. d'Astrophys., 11, 247.

Vaucouleurs, G. de, 1948b. Contr. de l'Inst. d'Astrophys. Paris, Série A, No 24.

Vaucouleurs, G. de, 1953. A.J., 58, 30.

Vaucouleurs, G. de, 1956. Occ. Notes R.A.S., 3, No 18, 118.

Vaucouleurs, G. de, 1958a. Ap. J., 128, 465.

Vaucouleurs, G. de, 1958b. A. J., 63, 253.

Vaucouleurs, G. de, 1959a. Lowell Obs. Bull., No 97, Vol 4, 105.

Vaucouleurs, G. de, 1959b. A. J., 64, 397.

Vaucouleurs, G. de, 1959c. Ap. J., 130, 728.

Vaucouleurs, G. de, 1961a. Ap. J., 133, 405.

Vaucouleurs, G. de, 1961b. Ap. J. Suppl. 5, 233.

Vaucouleurs, G. de, 1962. I.A.U. Symposium, 15, 'Problems of Extragalactic Research', p.3.

Vaucouleurs, G. de, 1963a. Ap. J., 137, 720.

Vaucouleurs, G. de, 1963b. Ap. J., 138, 934.

Vaucouleurs, G. de, 1963c. Ap. J. Suppl. 8, 31.

Vaucouleurs, G. de, 1964. Ap. J., 139, 899.

Vaucouleurs, G. de, 1969. Astrophys. Letters, 4, 17.

Vaucouleurs, G. de, 1974. I.A.U. Symposium, 58, 'The Formation and Dynamics of Galaxies', p.1.

Vaucouleurs, G. de, 1977. Occasional Reports of the Royal Observatory Edinburgh, No 2 'Topics in Extragalactic Astronomy with special reference to the southern hemisphere', p.9.

Vaucouleurs, G. de & Head, C., 1978. Ap. J. Suppl., 36, 439.

Vaucouleurs, G. de & Malik, G.M., 1969. M.N.R.A.S., 142, 387.

Vaucouleurs, G. de & Page, J., 1962. Ap. J., 136, 107.

Vaucouleurs, G. de & Vaucouleurs, A. de, 1964. 'Reference Catalogue of Bright Galaxies', Univ. of Texas Press, Austin.

Vaucouleurs, G. de & Vaucouleurs, A. de, 1970. Astrophys. Letters, 5, 219.

Vaucouleurs, G. de & Vaucouleurs, A. de, 1972. Mem. R.A.S., 77, 1.

Vaucouleurs, G. de, Vaucouleurs, A. de & Corwin, H.G., 1972. A.J., 77, 285.

Vaucouleurs, G. de, Vaucouleurs, A. de & Corwin, H.G,m 1976. 'Second Reference Catalogue of Bright Galaxies', Univ. of Texas Press, Austin and London.

Vorontsov-Vel 'yaminov, B.A., 1976. 'Stars and Galaxies from Observational Points of View', (Proc. of Third European Astronomical Meeting, ed. Kharadze).

Weedman, D.W., 1976. Ap. J., 208, 30.

Weisacker, C.F. von, 1951. Ap. J., 114, 165.

Wells, D.C., 1972. Thesis, Univ. of Texas.

Westerlund, B.E. & Wall, J.V., 1969. A.J., 74, 335.

Whitford, A.E., 1936. Ap. J., 83, 424.

Whitford, A.E., 1971. Ap. J., 169, 215.

Zwicky, F., 1957. 'Morphological Astronomy', Springer, p.166, p.222.

Zwicky, F., Herzog, E. & Wild, P., 1961. 'Catalogue of Galaxies and Clusters of Galaxies', Vol 1.